Characterisation of a Forkhead Transcription Factor: FOXE1

Martyn Bullock

Submitted for the Degree of Doctor of Philosophy

Centre for Endocrine and Diabetes Sciences and
Department of Dermatology
Cardiff University

Submitted July 2007

ProQuest LLC
789 East Eisenhower Parkway
P.O. Box 1346
Ann Arbor, MI 48106-1346

Form: PG/R/06/09

APPENDIX 1:
Specimen Layout for Thesis Summary and Declaration/Statements page to be included in a Thesis

DECLARATION

This work has not previously been accepted in substance for any degree and is not concurrently submitted in candidature for any degree.

Signed ..... (candidate) Date 03/07/07

STATEMENT 1

This thesis is being submitted in partial fulfillment of the requirements for the degree of PhD (insert MCh, MD, MPhil, PhD etc, as appropriate)

Signed ..... (candidate) Date 03/07/07

STATEMENT 2

This thesis is the result of my own independent work/investigation, except where otherwise stated.
Other sources are acknowledged by explicit references.

Signed ..... (candidate) Date 03/07/07

STATEMENT 3

I hereby give consent for my thesis, if accepted, to be available for photocopying and for inter-library loan, and for the title and summary to be made available to outside organisations.

Signed ..... (candidate) Date 03/07/07

STATEMENT 4 - BAR ON ACCESS APPROVED

I hereby give consent for my thesis, if accepted, to be available for photocopying and for inter-library loans after expiry of a bar on access approved by the Graduate Development Committee.

Signed ..... (candidate) Date .....

Library Loan and Photocopying

I hereby consent for my thesis to be made available for photocopying and for interlibrary loan, and for the title and summary to be made available to outside organisations.

Candidate:

Martyn Bullock BSc (Hons)

Summary

FOXE1, a forkhead transcription factor, plays an essential role in the development of the thyroid and hair follicle. Loss-of-function FOXE1 mutations cause aberrant morphogenesis of both tissues, apparently due to a defect in cell migration.

In the mature thyroid, FOXE1 plays an essential role in the control of thyroid hormone synthesis, modulating both thyroglobulin and thyroid peroxidase gene expression. Several studies have shown there is considerable inter-individual variability in thyroid hormone levels, and this is due at least in part to genetic factors. One of the main features of the FOXE1 protein is a highly polymorphic polyalanine tract that can range in size from 11 to 19-Ala residues (wild-type being 14-Ala residues).

The aims of this thesis were: 1) To determine the precise location of FOXE1 expression within the human hair follicle. 2) To identify genes involved in cell migration that could be potential FOXE1 target genes. 3) To investigate the possible role of FOXE1 polyalanine polymorphisms in thyroid dysfunction.

1) Immunohistochemical analysis confirmed previous observations that FOXE1 was expressed in human epidermis and hair follicle outer root sheath. However, technical difficulties prevented more detailed analyses (e.g. colocalisation with hair-specific proteins). 2) Bioinformatics yielded several potential FOXE1 target genes. Subsequent QPCR-based expression profiling and siRNA-based gene knockdown experiments suggested TIMP3 as a likely direct downstream target. Thus, FOXE1 may have a direct role in the modulation of ECM architecture by migratory cells. 3) The genotyping of a small cohort of subclinical hypothyroid subjects, showed there to be an increased incidence of the 16-Ala allele compared with the control group. Luciferase assays revealed the transcriptional activity of the 16-Ala allele to be significantly reduced compared with wild-type. This provides the first evidence that polymorphic variation can affect the transcriptional activity of FOXE1, and be a possible contributing factor in the sub-optimal thyroid function.

For my Mam and Dad

Acknowledgements

Firstly I would like to express my deepest gratitude to Dr Marian Ludgate and Dr Paul Bowden for all of their help and support throughout the past 4 years.

I would also like to give many thanks to Professor Andrew Finlay and Professor Scanlon for giving me the opportunity to study in their departments.

A big thankyou to all my friends and collegues, in both the department of dermatology and the centre for endocrine and diabetes science for their support and help throughout this project. I would particularly like to thank Lei Jhang, Majed Jehani and Song Han for their kindness in helping me with various experiments.

Finally I would like to thank my parents, brothers and Amanda for their continued support over the course of my studies.

Abbreviations

APRT	Adenine phosphoribosyltransferase
ARX	Aristaless-related homeobox gene
β-Gal	β-galactosidase
BMR	Basal metabolic rate
BMZ	Basement membrane zone
bp	Base pair
BPES	Blepharophimosis–ptosis–epicanthus inversus syndrome
Ca^{2+}	Calcium
$CaCl_2$	Calcium chloride
cAMP	Cyclic adenosine monophosphate
cDNA	Complementary DNA
CH	Congenital hypothyroidism
CO_2	Carbon dioxide
COL	Collagen
Ct	Threshold cycle
DIT	Diiodotyrosine
DMEM	Dulbecco's Modified Eagle's Minimal Essential Medium
DMSO	Dimethyl sulfoxide
DNA	Deoxyribose nucelic acid
DNase	Deoxyribonuclease
dNTP	Deoxynucleotide Triphosphate
DREAM	Downstream regulatory element antagonist modulator
dsDNA	Double stranded DNA
dsRNA	Double stranded RNA
DTT	Dithiothreitol
E.coli	Escherichia coli
EDTA	Ethylenediamine tetraacetic acid
EGF	Epidermal growth factor
ELISA	Enzyme-Linked ImmunoSorbent Assay
ER	Oestrogen receptor
ERDS	Endoplasmic reticulum storage disease
EtBr	Ethidium Bromide
FCS	Fetal calf serum
FGF	Fetal Growth Factor
FKH	Forkhead
FKHL	Forkhead homolog-like
FOX	Forkhead box
FREAC	Forkhead related activator
gDNA	Genomic DNA
GLI	Glioma associated oncogene homolog
HAT	Histone acetyltransferase
HDAC	Histone deacetylase

HEK	Human Embryonic Kidney
Hhex	Hematopoietically expressed homeobox
HNF	Hepatocyte nuclear factor
HOX	Homeobox
HSP40	Heat shock protein 40
IgG HRP	Immunoglobulin G horseradish peroxidase
IRS	Inner root sheath
K	Keratin
kDa	Kilo dalton
KGM	Keratinocyte growth medium
ml	Milliliter
min	Minute
mRNA	Messenger RNA
Mg^{2+}	Magnesium
$MgCl_2$	Magnesium chloride
miRNA	Micro ribonucleic acid
MIT	Monoiodotyrosine
MMP	Matrix Metalloproteinase
µg	Micrograms
Na	Sodium
NaAcetate	Sodium acetate
NADPH	Nicotinamide adenine dinucleotide phosphate
NIS	Sodium-iodide symporter
NLS	Nuclear localisation signals
nM	Nano moles
ORS	Outer root sheath
pAb	Polyclonal antibody
PABPN1	Poly(A) binding protein, nuclear 1
PAX	Paired box
PBS	Phosphate buffered saline
PCR	Polymerisation Chain Reaction
PEG	Polyethylene glycol
PDS	Pendrin
PHOX	Paired mesoderm homeobox
PKA	Protein kinase A
POF	Premature ovarian failure
polyAla	Polyalanine
pri-miRNA	Primary micro RNA
PSM	Position scoring matrices
PWM	Position weight matrices
QPCR	Quantitative polymerase chain reaction
RISC	RNA-induced silencing complexe
RNA	Ribonucleic acid
RNasin	Ribonuclease inhibitor
RNaseIII	Riboendonucleases III
RNAi	RNA interference
RT	Room temperature
RT-QPCR	Real time quantitative polymerase chain

	reaction
RUNX2	Runt-related transcription factor 2
S.D	Standard deviation
SDS PAGE	Sodium dodecyl sulphate polyacrilamide ge electrophoresis
shRNA	Small hairpin RNA
SHH	Sonic Hedgehog
siRNA	Small interfering ribonucleic acid
SKIP	Ski-interacting protein
SNP	Single Nucleotide Polymorphisms
T3	Triiodothyronine
T4	Thyroxine
taq	Derived from *Thermus aquaticus* bacterium
TD	Thyroid dysgenesis
TFC	Thyroid follicular cells
TG	Thyroglobulin
THOX	Thyroid oxidase
TIMP	Tissue Inhibitor of Metalloproteinase
TIP	Tat-interactive protein
TITF	Thyroid transcription factor
Tm	Melting temperature
TPO	Thyroid peroxidase
Tris-HCl	Tris (hydroxymethyl) aminomethane Hydrochloride
TRH	Thyrotropin releasing hormone
TSHR	Thyroid stimulating hormone receptor
TTF	Thyroid transcription factor

List of Publications and Abstracts Arising from this Work

Publications:

Bullock, M., Zhang, L., Locantore, P., Grave, R., Bowden, P., Ludgate, M. (2007). FOXE1 Polalanine Tract Variants: Evidence for a Role in Thyroid Function. (Submitted to Journal of Human Mutation)

Baker, G., Morton, M., Rajapaska, R., Bullock, M., Gullu, S., Mazzi, B., Ludgate, M. (2006). Altered Tear Composition in Smokers and Patients with Graves' Opthalmopathy. *Arch Ophthalmol.* **124(10):** 1451-1456.

Abstracts:

International Meetings:

2006 European Thyroid Association (ETA), Naples, Italy
The Role of FoxE1 in Thyrocytes and Keratinocytes (Poster)

2006 Society for Investigative Dermatology (SID), Philadelphia, USA
Calcium Regulation of FOXE1 in Human Keratinocytes (Poster)

2005 European Conference of Endocrinology (ECE), Glasgow, Scotland
Similarities in the Role of FoxE1 in Thyrocytes and Keratinocytes? (Poster)

Cardiff University Meetings

2007 Interdisciplinary Research Group (IRG) Annual Meeting
Functional Comparison of FOXE1 Polyalanine Tract Variants (Oral)
(Winner of Best Oral Presentation)

2005 Postgraduate Research Day

Keratinocyte Differentiation *In Vitro* is Accompanied by Up-regulation of FOXE1 Transcripts and Transcriptional Activity (Poster)

2004 Postgraduate Research Day

Investigation of TTF2 Expression in the Hair Follicle (Poster)

Table of Contents

Contents

Chapter 2. Localisation of FOXE1 Expression in Human Skin

Chapter 3. Bioinformatics: Search for Potential Downstream Targets of FOXE1

Chapter 4. Gene Expression Profiling and siRNA Knockdown Experiments

Chapter 5. Functional Analysis of FOXE1 Polyalanine Tract Variants

List of Tables

Chapter 3:

Chapter 4:

Chapter 5:

List of Figures

Chapter 1:

Chapter 2:

Chapter 3:

Chapter 4:

Chapter 5:

Chapter 1.

General Introduction

1.1. Transcription Factors

The numerous cell-types that make up a multicellular organism differ widely in both their structure and function. These differences occur despite the fact that each cell-type has an identical genetic make-up. Thus, there must be some mechanism that controls which genes are expressed. Actually, gene expression can be regulated at several different levels: transcription, RNA processing, RNA transport, translation and RNA stability/degradation. Transcriptional regulation is mediated in part by transcription factors, nuclear proteins that are able to recognise and bind to specific DNA sequences. By binding to sequences within the regulatory regions (promoter, enhancer or repressor sites) of target genes they are able to modulate transcriptional activity. Examples of transcription factor families include:

HOX (Homeobox) family: Members are characterised by a DNA-binding domain known as the homeobox. The homeobox comprises a helix-turn-helix domain that is able to recognise and bind to sites with a consensus core sequence [TAAT] (Daftary *et al.*, 2006).

PAX (Paired box) family: Members are characterised by a DNA-binding domain known as the paired box. There are nine mammalian PAX proteins, classified into subgroups, according to the presence/absence of additional structural domains (homeobox and octapeptides). The consensus sequence for the PAX binding-site is (G/T)T(T/C)(C/A)(C/T)(G/C)(G/C), although some PAX proteins have more specific requirements e.g. PAX8 binds to GTCAC(G/C) (Lang *et al.*, 2006).

1.2. Forkhead Transcription Factors

1.2.1. Discovery

The *Drosophila melanogaster* forkhead gene (fkh) is essential for the proper formation of the terminal structures of the embryo. Mutations of the gene were found to cause a homeotic transformation of the gut structures, resulting in replacement of fore- and hind-gut with ectopic 'fork-like' head structures, hence the name forkhead

(Weigel *et al.*, 1989). Shortly after the discovery of fkh, a family of hepatocyte-enriched transcription factors, the HNF-3 (hepatocyte nuclear factor-3) protein family, were isolated from rodents (Lai *et al.*, 1990). A comparison of the amino acid sequences of fkh and HNF-3α revealed a strikingly high degree of sequence conservation within their DNA-binding domains (Weigel & Jäckle, 1990; Lai *et al.*, 1991). Thus, the two proteins were identified as belonging to a novel transcription factor family that was conserved between *D. melanogaster* and vertebrates. As fkh was the first member to be isolated, the authors proposed that the DNA-binding domain, and hence the transcription factor family, be named after this gene.

Since the discovery of the forkhead family, around 200 forkhead genes have been identified in species ranging from yeast to human, but interestingly none in plants. Also, the number of forkhead genes in different species is found to rise with their increasing anatomical complexity, from four known family members in *Saccharomyces cerevisiae* (Wijchers *et al.*, 2006) to at least 43 in man (Katoh & Katoh, 2004). Forkhead genes have been implicated in a huge range of biological processes such as proliferation, differentiation, DNA-repair, apoptosis, metabolism and immunoregulation (Lam *et al.*, 2006; Zeigler, 2006; Wijchers *et al.*, 2006; Laoukili *et al.*, 2007).

1.2.2. Nomenclature

The repeated discovery of the same forkhead gene by different laboratories has led to the use of multiple names and classification systems [e.g. FREAC (forkhead related activator), HFH (HNF-3/forkhead homolog) and FKHL (forkhead homolog-like)], making it very difficult to follow the literature. In 2000, a standardized nomenclature was devised that suggested Fox (Forkhead box) be adopted as the unified symbol for all chordate forkhead genes (Kaestner *et al.*, 2000). Furthermore, Fox genes were grouped into subclasses on the basis of structural similarity and sequence conservation within the forkhead domain, with each subclass being assigned a different letter (currently ranging from A to S). Genes belonging to the same subclass were then assigned individual numbers. In addition, the nomenclature also allowed forkhead genes from different species to be distinguished: All uppercase letters for

human (e.g. FOXE1); only the first letter capitalized for mouse (e.g. Foxe1); and the first and subclass letters capitalized for all other chordates (e.g. FoxE1).

1.2.3. Forkhead DNA-Binding Domain

1.2.3.1. Three-Dimensional Structure

Members of the forkhead transcription factor family are characterised by a highly conserved DNA-binding domain, consisting of approximately 100 amino acids. The three-dimensional structure of the DNA-bound forkhead domain has been determined for six mammalian forkhead proteins: FoxA3 (Clark *et al.*, 1993), Foxd3 (Jin *et al.*, 1999), FOXC2 (Van Dongen *et al.*, 2000), FOXO4 (Weigelt *et al.*, 2001), FOXK1 (Tsai *et al.*, 2006) and FOXP2 (Stroud *et al.*, 2006), using either X-ray crystallography or nuclear magnetic resonance (NMR) imaging.

The first structure to be determined was that of a FoxA3 fragment, encompassing the forkhead domain, bound to a 13bp-duplex oligonucleotide, containing the transthyretin promoter-binding site (Clark *et al.*, 1993). The DNA-bound forkhead domain was found to consist of three α-helices, three β-sheets, and two wing-like loops arranged in a α1-β1-α2-α3-β2-W1-β3-W2 order. The authors likened the shape of the structure to that of a butterfly, and suggested that 'winged-helix' be an appropriate name to describe this DNA-binding motif. The structure was also found to be remarkably similar to the central globular domain of the avian erythrocyte linker histone H5, and its homologue H1 (Clark *et al.*, 1993). Thus, forkhead and histone proteins can be classified as belonging to the same superfamily of winged-helix DNA-binding proteins (Gajiwala *et al.*, 2000).

The overall structures of the other forkhead domains were very similar to that of FoxA3, however there were some important differences observed. For instance, W1 of FOXP2 was truncated and FOXO4 had a fourth α-helix situated between α2 and α3 (Stroud *et al.*, 2006; Weigelt *et al.*, 2001). Also, in Foxd3, FOXK1 and FOXP2, the region corresponding to W2 was replaced by a fourth α-helix (Jin *et al.*, 1999;

Tsai *et al.*, 2006; Stroud *et al.*, 2006). These structural differences are likely to contribute towards regulation and/or specificity of DNA-binding.

1.2.3.2. Sequence Conservation

Conservation of the structure of the forkhead domain is mirrored at the amino acid level. Alignment of the DNA-binding domains of the 43 known human forkhead proteins revealed that the highest degree of sequence similarity is found in the α-helices and β-sheets, particularly in α3 (Figure 1.1). The same is true of forkhead proteins from other mammalian species (Wijchers *et al.*, 2006).

1.2.3.3. Protein-DNA Interactions

FoxA3 was found to bind DNA as a monomer and interact with the double helix over a linear distance of 40Å. A total of 14 protein-DNA contacts were distributed throughout the whole forkhead domain. The main interactions were contributed by α3, dubbed the recognition helix, which made several contacts with the major groove of DNA. Other regions of the forkhead domain that also made important interactions with DNA were α1 and W2 (Figure 1.2).

1.2.3.4. Consensus Sequence

A comparison of the binding-site consensus sequences of four human FOX proteins: FOXC1, FOXD1, FOXF2 and FOXL1, revealed that they all shared a requirement for the core sequence (A/G)TAAA(T/C)A. The nucleotides flanking this core sequence were less well defined, and together with the variable nucleotides within the core sequence, were found to be important for determining DNA-binding specificity (Pierrou *et al.*, 1994). The core sequence was also present in the binding-site consensus sequences of rat FoxA2: (A/G)(T/C)(A/C)AA(T/C)A, FoxQ1: (A/C)TAAACA and FoxD3: (A/T)GAAACA, AA(T/C)AACA, and (A/G)CAAA(T/C)A, with minor variations occurring in the first three nucleotides (Overdier *et al.*, 1994). Again, the authors demonstrated that the variable nucleotides had an important role to play in determining DNA-binding specificity. The occurrence

of the AA(T/C)A motif in all of these consensus sequences suggests that it is an essential requirement for the DNA-binding of all forkhead proteins.

Figure 1.1. Amino Acid Alignment of the 43 Known Human Forkhead Domains. The structural features of the FoxA3 DNA-binding domain are aligned with the corresponding amino acid sequences. The level of sequence conservation at each of the aligned positions is also represented: (*) means all the amino acid residues are identical, (:) means conserved substitutions have been observed and (.) means semi-conserved substitutions have been observed.

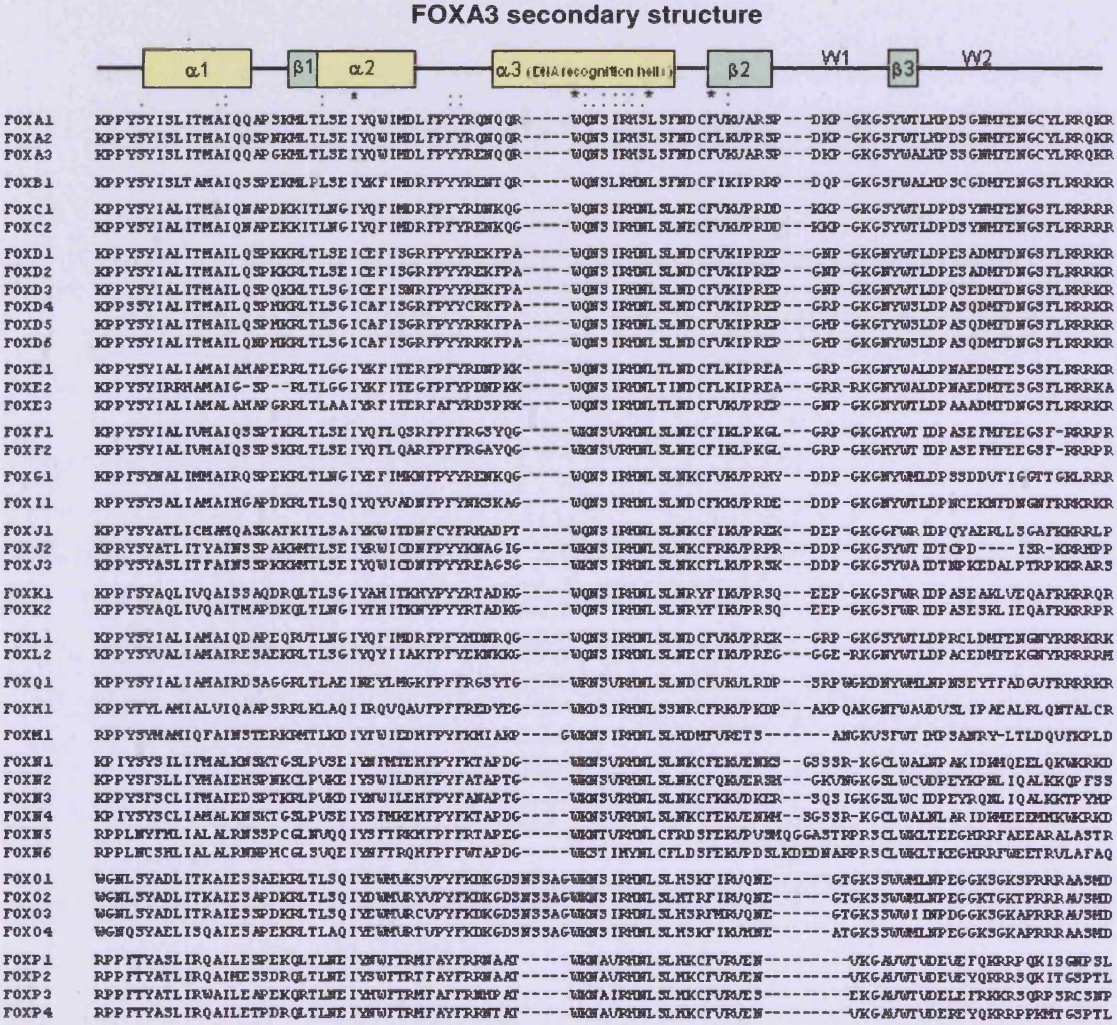

Figure 1.2. Major Interactions between the FoxA3 Forkhead Domain and DNA. **A)** Sequence of the FoxA3 DNA-binding site present in the transthyretin promoter. The core sequence is highlighted in red. **B)** Schematic representation of DNA-bound FoxA3 showing the major protein-DNA interactions. Hydrogen bonds and Van der Waals contacts are represented by arrowed thin lines and dashed lines respectively. The core sequence of the DNA-binding site is highlighted in red. The two GC base pairs separated by a dashed line were not part of the transthyretin promoter and were introduced to increase stability of the DNA duplex for purposes of the experiment.

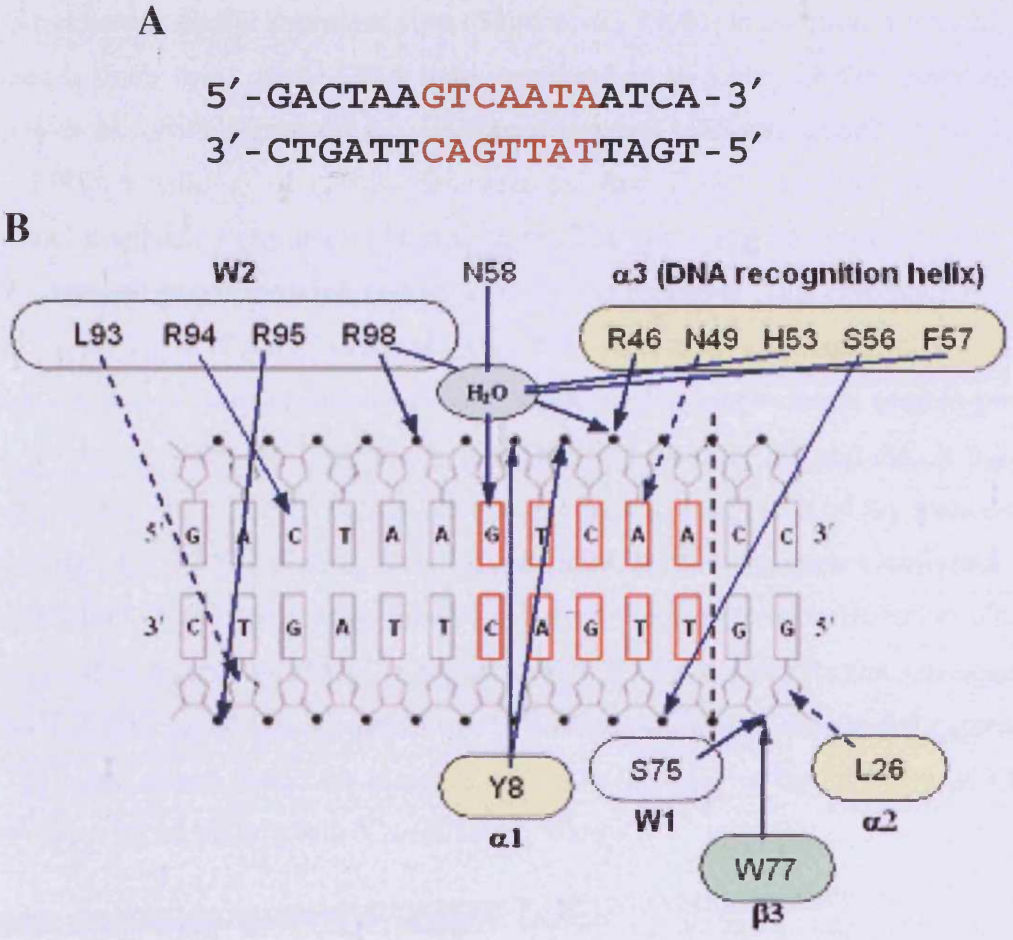

1.2.4. Mechanism of Transcriptional Regulation

The DNA-binding domains of forkhead and histone proteins are remarkably similar, and the two are classified as belonging to the same superfamily of winged-helix class DNA-binding proteins (Gajiwala *et al.*, 2000). Members of the forkhead family have

clearly been shown to function as tissue-specific transcriptional regulators with sequence-specific DNA-binding properties (Lam *et al.*, 2006; Zeigler, 2006; Wijchers *et al.*, 2006; Laoukili *et al.*, 2007). In contrast to this, linker histones are ubiquitously expressed and do not have sequence-specific DNA targets to which they bind. Despite their distinct roles, the similarity in structure suggested that there are overlapping mechanisms as to how the two types of protein interact with DNA.

This has been most extensively studied in the case of the FoxA subclass of forkhead proteins. FoxA factors have been shown to be able to bind nucleosomal core histones, thereby replacing linker histones and relieving chromatin compaction at target enhancer and/or promoter sites (Shim *et al.*, 1998). In addition, FoxA binding causes a sharp bend of the DNA helix, resulting in widening of the minor groove (Clark *et al.*, 1993; Pierrou *et al.*, 1994) and increased DNaseI sensitivity (Cirillo *et al.*, 1998). Cirillo *et al* (2002) demonstrated that FOXA proteins were able to 'invade' compacted chromatin, bind to their sites, and open the chromatin in a way that allows other transcription factors access to the promoter. This chromatin opening was shown not to require the recruitment of the 'classical' chromatin modifiers and remodelers, but instead required only DNA-binding and direct protein-protein interactions between the C-terminus of FOXA and histones H3 and H4. It was not clear whether these critical FOXA-histone interactions take place on the nucleosome underlying the FOXA binding sites or with flanking nucleosomes. Consistent with this, a study on the long-range gene regulation by ER (oestrogen receptor) binding revealed the presence of FoxA1 in the proximity of sites where ERs can subsequently bind. The binding of FoxA1 appeared to be an essential requirement for expression of ER target genes, since the removal of FoxA1 resulted in the inability of ER to associate with its binding site (Carroll *et al.*, 2005).

Whilst the activity of FOXA proteins appears to be independent of 'classical' chromatin remodellers, other forkhead proteins have been shown to interact with such proteins. The transcriptional repressor Foxk1 interacts with the scaffolding protein Sin3b, (Yang *et al.*, 2000) which forms part of a co-repressor complex that also includes HDACs (histone deacetylases) and/or nucleosomal remodelling factors. Since this complex lacks DNA-binding activity, recruitment by Foxk1 could direct a reversal of open chromatin conformation, and specific repression of downstream

target genes. Similarly, the transcriptional repressor Foxn3 associates with SKIP (Ski-interacting protein) (Scott *et al.*, 2005), a transcriptional adaptor protein known to interact with repressor complexes that involve Sin3a and HDACs. Also, the transcriptional repression by FOXP3 involves its interaction with a HAT-HDAC (histone acetyltransferase-histone deacetylase) complex that includes HAT TIP60 (Tat-interactive protein, 60 kDa) and two HDACs, HDAC7 and HDAC9 (Li *et al.*, 2006).

Other mechanisms of transcriptional regulation may involve direct interactions with the basal transcriptional machinery, as has been described for FOXF2 (Hellqvist *et al.*, 1998).

1.3. FOXE1

FOXE1, formerly called TTF2 (thyroid transcription factor 2) and FKHL15 (forkhead homolog-like 15) is a forkhead transcription factor. The human (FOXE1), mouse (Foxe1) and rat (FoxE1) gene loci are located on chromosomes 9q22, 4qB1, and 5q22 respectively. Each gene consists of a single exon and encodes a 42 kDa protein of approximately 370 amino acids. The main features of the FOXE1 protein include a 97 amino acid forkhead DNA-binding domain and a polyalanine (polyAla) tract domain of variable length.

The rat FoxE1 protein is phosphorylated *in vivo* (Dathan *et al.*, 2002), but the effect on the protein has not been explored. FOXE1 protein contains two identical NLSs (nuclear localisation signals) that flank the forkhead DNA-binding domain. The translocation of FOXE1 to the nucleus occurs via an importin α-dependent pathway (Jäkel *et al.*, 1998) that requires at least one of these NLSs to be present. In addition, amino acid residues within the forkhead domain were also shown to have a possible influence on FOXE1 localisation (Romanelli *et al.*, 2003).

FOXE1 has been shown to be expressed in the developing and mature thyroid gland, and to play an essential role in both.

Ortiz *et al* (1997) showed that Thyroid Stimulating Hormone (TSH), via the cAMP pathway, and insulin via the IGF-1 pathway, stimulated FoxE1 gene expression in a

dose- and time-dependent manner. The TSH-induced effect was the greatest and could be mimicked using forskolin (activates the enzyme adenylyl cyclase, increasing cAMP levels). More recently, FoxE1 expression was shown to be regulated by calcium signalling mediated by the transcriptional repressor DREAM (downstream regulatory element antagonistic modulator) (D'Andrea *et al.*, 2005). This will be discussed in more detail in Chapter 4.

1.4. Thyroid Gland

1.4.1. Location and Structure

The thyroid gland is the largest of the human endocrine glands, and the first gland to become recognisable during development. It is located anterior to the larynx cartilage and consists of two lobes connected by a thin band of connective tissue called the isthmus. The mature thyroid gland is made up of two main cell-types: thyroid follicular cells (TFCs) and parafollicular cells (C-cells) that synthesize and secrete thyroid hormones and calcitonin respectively (Braverman & Utiger, 2005).

TFCs are the most numerous cell-type within the thyroid gland and are arranged into spherical structures called follicles. Each follicle consists of a single layer of polarised TFCs surrounding a central colloid-filled lumen. The TFCs are orientated with their bases near the capillary blood supply and the apices adjacent to the colloid. The C-cells comprise only about 10% of the total thyroid mass and are located within the interfollicular spaces (Braverman & Utiger, 2005).

1.4.2. Morphogenesis

The two main cell-types, TFCs and C-cells, each originate from different embryological structures. The ultimobranchial bodies (transient embryonic structures), located in the fourth pharyngeal pouch, are of neural crest origin and differentiate into C-cells. The TFCs originate from the thyroid anlage (De Felice & Di Lauro, 2004).

1. Specification: Formation of the Thyroid Anlage

Morphogenesis of many endoderm-derived organs typically begins with an event, termed specification, where a group of endoderm cells are recruited and instructed to follow a specific developmental program. In the case of the thyroid, the cells are instructed to follow all the developmental steps necessary to achieve the TFC phenotype. The first visible change is a thickening of the endoderm in the floor of the primitive pharynx. This thickening, known as the thyroid anlage, is located between the first and the second branchial arches, and first becomes visible around embryonic day (E) 18-20 in humans and E8–8.5 in mice (De Felice & Di Lauro, 2004).

2. Migration

At around E24 in humans and E9.5 in mice the thyroid anlage descends forming a thyroid bud. The bud then expands ventrally as a diverticulum, with rapid cellular proliferation at its distal end, but remains attached to the pharyngeal floor by a tubular stalk called the thyroglossal duct. TFC precursors continue to proliferate laterally, which leads to the formation of the thyroid gland's characteristic bilobed structure. The thyroid primordium then begins to migrate towards the base of the neck. This is accompanied by rapid elongation of the thyroglossal duct, which eventually fragments and degenerates at E30-40 in humans and E11.5 in mice, forming the foramen caecum (a remnant of the embryonic thyroid) (De Felice & Di Lauro, 2004).

3. Completion of Organogenesis

Once the thyroid primordium reaches its final position along the trachea, the two lobes expand and the gland exhibits its definitive shape, two lobes connected by an isthmus. At around E60 in humans and E15–16 in mice, the first evidence of follicular organization can be seen. Also, at around the same time, cells from the ultimobranchial bodies migrate, resulting in the incorporation of C-cells into the thyroid. After fusion of the two cell populations, TFCs undergo further differentiation marked by the onset of thyroid-specific gene expression, synthesising TSHR (thyroid stimulating hormone receptor), NIS (Na^+-I^- symporter), TPO (thyroid peroxidase) and TG (thyroglobulin) (De Felice & Di Lauro, 2004).

1.4.3. Genes Involved in Morphogenesis

Morphological and functional differentiation along the gut tube is likely to be due to the establishment of overlapping expression domains of transcription factors that, through the activation of target genes, result in the formation of organ or area-specific domains (Grapin-Botton *et al.*, 2000).

Both precursor and mature TFCs are uniquely characterised by the co-expression of four transcription factors: Titf1, Pax8, Hhex and Foxe1. Gene-targeting experiments have revealed that each of these genes plays an essential role in thyroid gland organogenesis. These experiments also show that the onset of expression of each gene is independent of the others, but maintenance requires a cross-regulatory network between them (Parlato *et al.*, 2000).

1.4.3.1. Titf1

Titf1/Nkx2.1, formerly called TTF1 (thyroid transcription factor 1) is a homeodomain-containing transcription factor (Civitareale *et al.*, 1989; Guazzi *et al.*, 1990). In the primitive pharynx, Titf1/Nkx2.1 is found exclusively in the thyroid anlage (Figure 1.3), and its appearance coincides with anlage specification. Its expression is maintained in the TFCs throughout all stages of development and into adulthood.

In Titf1$^{-/-}$ mice at E9, both morphology of the mutant thyroid anlage and levels of Pax8, Foxe1, and Hhex are comparable to those of the wild-type bud (Kimura *et al.*, 1996; Parlato *et al.*, 2004). However by E10, the developing thyroid of the mutant is smaller than that of the wild-type, Pax8 shows a slightly reduced expression, while Foxe1 and Hhex are strongly down-regulated. Furthermore, the TFCs appear to undergo apoptosis and disappear at E10.5–11.5 (Kimura *et al.*, 1996).

1.4.3.2. Pax8

Pax8 is a member of the paired box family of transcription factors (Plachov *et al.*, 1990). Within the endoderm, Pax8 mRNA is localised specifically to the thyroid anlage (Figure 1.3).

In Pax8$^{-/-}$ mice at E9, the thyroid anlage is present and its morphology cannot be distinguished from that of wild-type (Mansouri *et al.*, 1998; Parlato *et al.*, 2004). Correspondingly, the levels of Titf1 protein and Hhex mRNA remain unaltered. In contrast, the levels of Foxe1 protein in the thyroid anlage are dramatically reduced. At E10, the thyroid primordium migrates into the underlying mesenchyme. At this stage, no relevant changes occur in the expression pattern of Titf1 (Mansouri *et al.*, 1998; Parlato *et al.*, 2004). However, the downregulation of Foxe1 expression becomes even more pronounced and Hhex mRNA levels are almost undetectable (Parlato *et al.*, 2004).

Figure 1.3. Schematic Representation of the Primitive Pharynx Showing the Expression Domains of Genes Relevant to Early Thyroid Morphogenesis. The expression domains of each gene at E9 of mouse development are shown in red. Pp = Pharyngeal pouch; Pa = pharyngeal arch (Adapted from De Felice & Di Lauro, 2004).

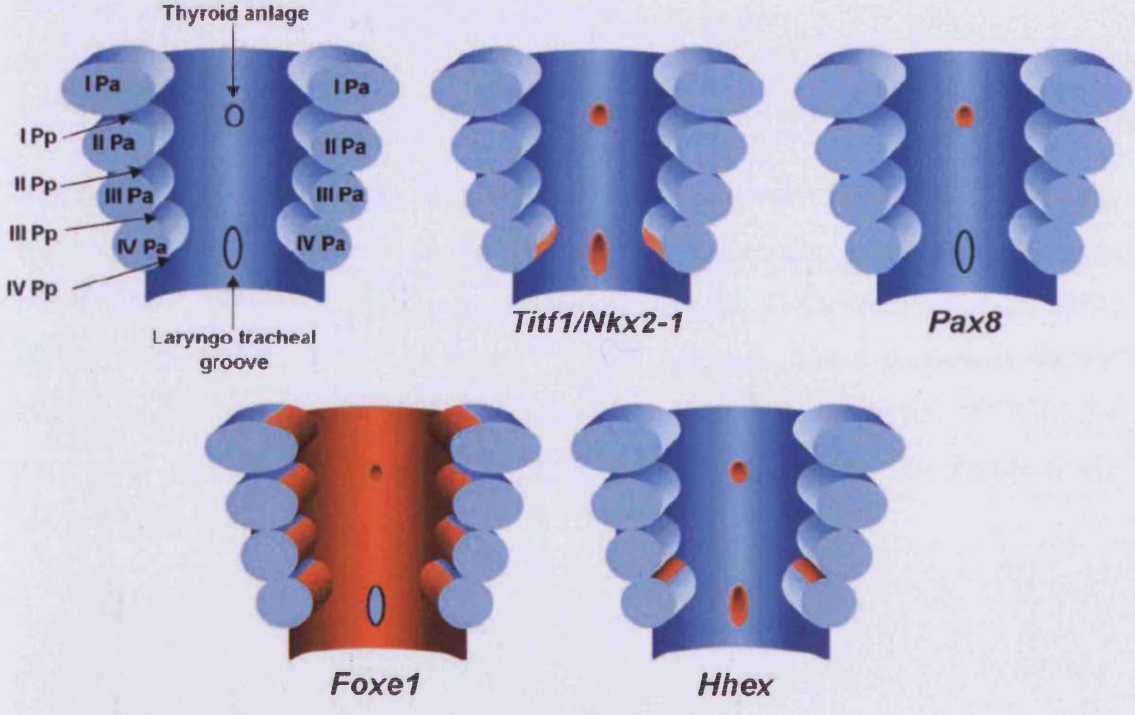

1.4.3.3. Hhex

Hhex (haematopoietically expressed homeobox) is a homeodomain-containing transcription factor (Crompton *et al.*, 1992; Bedford *et al.*, 1993). During mouse development, Hhex mRNA is expressed in the primitive endoderm, and then in the presumptive definitive endoderm cells (Thomas *et al.*, 1998). At later stages, the endodermal expression of Hhex is localized in the ventral gut and, from E8.5 onwards, is localised to the primordium of several foregut-derived organs, such as thyroid, liver, thymus, pancreas, and lungs (Thomas *et al.*, 1998; Bogue *et al.*, 2000).

In $Hhex^{-/-}$ mice at E9, the thyroid anlage was present and morphologically comparable to the wild-type bud (Martinez Barbera *et al.*, 2000; Parlato *et al.*, 2004). Also, the expression of Titf1, Pax8 and Foxe1 was not affected. However, by E10 the thyroid primordium was either absent or hypoplastic. Concurring with the morphological alteration was the strong reduction in Pax8 and Foxe1 proteins in mutant embryos. Martinez Barbera *et al* (2000) found the levels of Titf1 mRNA to be significantly reduced. However, Parlato *et al* (2000) analysed Titf1 expression at the protein level and found it not to be affected. This discrepancy could be explained assuming that the Titf1 protein was more stable than the corresponding mRNA. However, given the fact that phenotypes of varying severity have been described in Hhex mutants, it is possible that the three mutant embryos examined by Parlato *et al* exhibited a phenotype milder than that previously reported.

1.4.3.4. Foxe1

At E8.5 Foxe1 mRNA can be detected in all the endodermal cells of the floor of the foregut, including the thyroid anlage (Figure 1.3). Expression of Foxe1 in TFCs is maintained throughout development and persists in adult TFCs (Zannini *et al.*, 1997; 2001; Parlato *et al.*, 2000). In $Foxe1^{-/-}$ mouse embryos, TFCs precursors do not migrate and disappear at around E11.5 in about 50% of the embryos. At E10, the expression of Titf1, Pax8 and Hhex was found to be unchanged (De Felice *et al.*, 1998; Parlato *et al.*, 2004).

1.4.4. Thyroid Hormone Synthesis and Secretion

The production and secretion of thyroid hormones involves four main steps (summarised in Figure 1.4):

1. Active Uptake of Iodide

The first step in thyroid hormone synthesis is the active transport of iodide (I^-) into the TFCs. This is facilitated by NIS (Na^+-I^- symporter), an integral plasma membrane glycoprotein, situated within the basolateral membrane of TFCs. The symporter couples the inward translocation of sodium (Na^+) 'along' its electrochemical gradient to the inward translocation of I^- 'against' its electrochemical gradient. The Na^+/K^+ ATPase maintains the electrochemical Na^+ gradient across the basolateral membrane (Dohán & Carrasco, 2003). It has also been hypothesized that Pendrin, an 86 kDa chloride-iodide transporter protein localized to the apical membrane, transports intracellular I^- into the lumen space (Royaux *et al.*, 2000).

2. Organification of Iodide

The precursor of thyroid hormones is TG (thyroglobulin), a homodimer consisting of two 330 kDa subunits. TPO (thyroid peroxidase) is an apical membrane-bound enzyme that catalyses the oxidation of I^-, and its subsequent addition to the tyrosine residues of TG. This results in the formation of monoiodotyrosine (MIT) and diiodotyrosine (DIT) residues within the TG molecule. The H_2O_2 required for the oxidation reaction is generated by two NADPH oxidases, THOX1 and THOX2 (thyroid oxidase 1 & 2), also located at the apical membrane (Caillou *et al.*, 2001).

Figure. 1.4 Schematic Representation of a TFC Illustrating the Main Steps in Thyroid Hormone Synthesis (Park & Chatterjee, 2005)

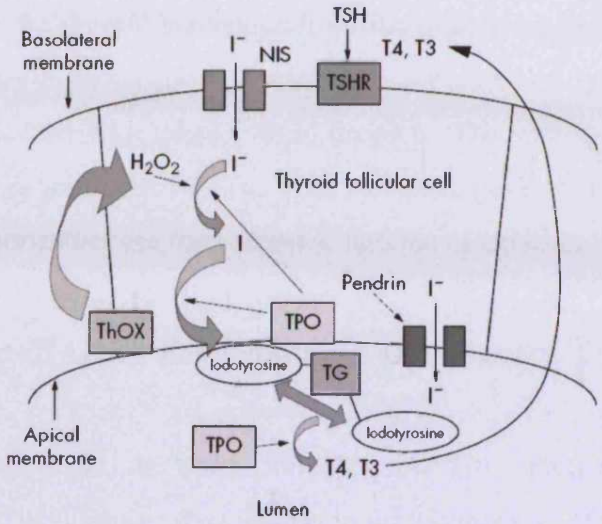

3. Coupling of Iodotyrosines

The TPO enzyme also catalyses the coupling of the iodotyrosines to form hormonally active iodothyronines. This coupling can either occur between two DITs to form thyroxine (T4), or an MIT and DIT to form triiodothyronine (T3) (Figure 1.5). These structures continue to remain an integral part of the TG molecule. Mature TG containing MIT, DIT, T4 and T3 is stored in the lumen as colloid, whilst poorly iodinated TG (immature TG) is internalized from the lumen and sent to the Golgi apparatus for recycling.

Figure 1.5. Chemical Stucture of Thyroxine (T4) and Triiodothryronine (T3)

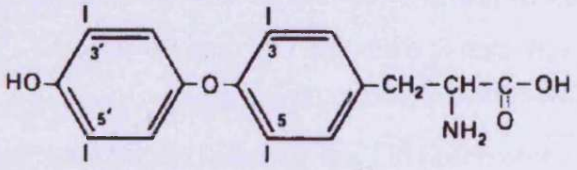

3,5,3′,5′-Tetraiodothyronine (thyroxine, T_4)

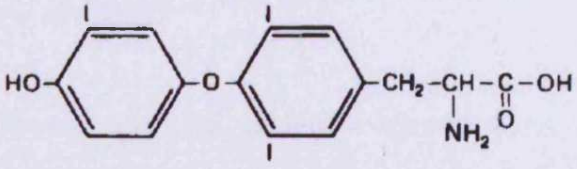

3,5,3′-Triiodothyronine (T_3)

4. Proteolysis of Thyroglobulin

When required, the stored TG is internalised by TFCs and then digested by proteolytic enzymes to liberate the thyroid hormones from the protein backbone. TG is enclosed in colloid droplets by pinocytosis at the apical membrane, and lysosomes containing proteolytic enzymes fuse with these colloid droplets. The subsequent degradation of TG by these enzymes produces T3, T4, MIT and DIT, peptide fragments and amino acids. The thyroid hormones are then secreted into the circulation.

1.4.5. Regulation of Gene Expression in the Mature Thyroid

In the mature thyroid gland, the transcription factors Titf1, Pax8 and FoxE1 play an additional role in regulating thyroid hormone synthesis. Together, the three transcription factors bind to sites within the proximal promoter of rat TPO and TG (Figure 1.6) to modulate transcriptional activity (Sinclair *et al.*, 1990; Francis-Lang *et al.*, 1992).

Pax8 and Titf1 have been shown to functionally cooperate in the activation of TPO (Miccadei *et al.*, 2002) and TG (Di Palma *et al.*, 2003) gene expression. The C-region of the TG promoter was sufficient to mediate Pax8/Titf1 synergy, however synergistic activation of TPO required promoter/enhancer interplay. The Pax8/Titf1 synergy at the TG promoter was shown to arise from a direct physical interaction between the two proteins. Titf1 contains two distinct activation domains, one at the N-terminus and the other at the C-terminus, which are functionally equivalent (De Felice *et al.*, 1995). However, the synergism was shown to be mediated specifically by physical interactions of the N-terminal domain of Titf1 and a C-terminal portion of Pax8.

Pax8-mediated transcriptional activation of the TPO promoter is also enhanced by the direct interaction of Pax8 with two co-activator proteins, p300 (De Leo *et al.*, 2000) and pRb (Miccadei *et al.*, 2005).

FoxE1 is able to repress the Titf1 mediated transcriptional activation of the TG promoter. This repressor activity was shown to require the C-terminal region of both

proteins, although a direct physical interaction between the two could not be detected. Similarly, FoxE1 was also found to repress Pax8 induced transcriptional activation at the TPO promoter (Zannini *et al.*, 1997; Perrone *et al.*, 2000). Interestingly, the transcriptional repressor activity of FoxE1 was found to be DNA-independent (Zannini *et al.*, 1997).

Figure 1.6. Schematic Representation of the Rat TG and TPO Proximal Promoters Illustrating Protein-DNA Interactions. Those regions that are protected from DNase I digestion by the binding of nuclear proteins are highlighted in bold (Sinclair *et al.*, 1990; Francis-Lang *et al.*, 1992). The nucleotides that make direct contact with the FoxE1 protein, as determined by methylation interference analysis (Francis-Lang *et al.*, 1992), are highlighted in red. The arrows represent the transcriptional start site.

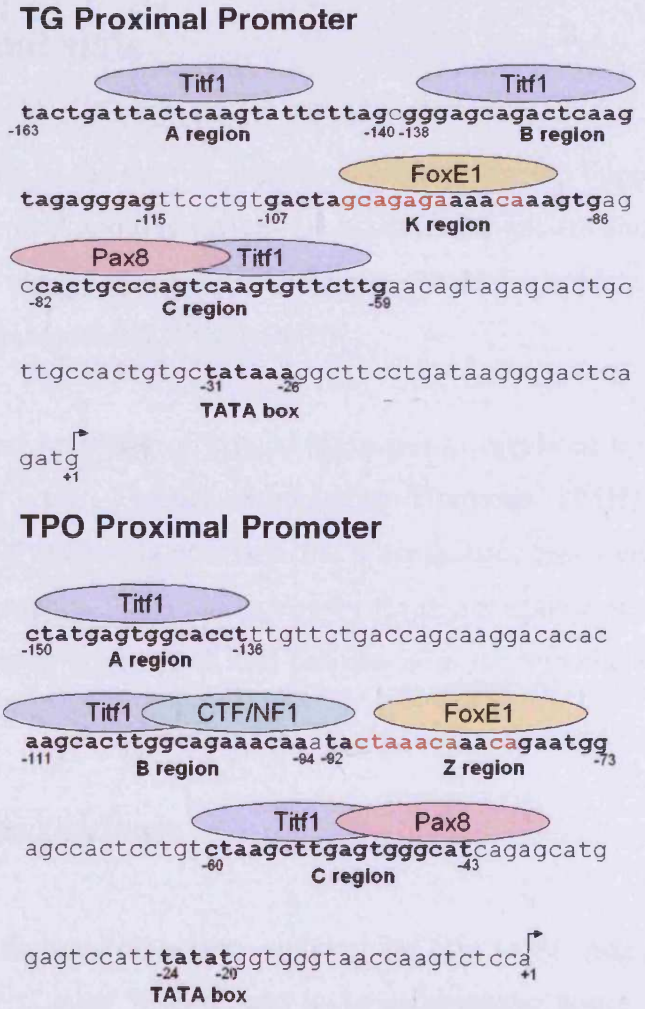

A direct interaction between FoxE1 and Pax8 and/or Titf1 has not been demonstrated. However in humans, another forkhead protein, FOXA1 has been shown to form a complex with TITF1 *in vivo*. The two proteins were shown to physically interact via their DNA-binding domains in a DNA-independent manner (Minoo *et al.*, 2006). Interestingly, FOXA1 was shown to repress TITF1-mediated transcriptional activation at the Spc (surfactant protein C) gene promoter (contains TITF1 binding-sites only), whilst it was unable to do so at the Ccsp (clara cell secretory protein) gene promoter (contains TITF1 and FOXA binding sites). The authors proposed that in the latter case, the FOXA1 protein was preferentially bound by its DNA-binding site and was unable to interact with TITF1. As the forkhead domain is highly conserved among family members, interactions between TITF1 and other FOX proteins is not inconceivable, and this may represent a novel mechanism of gene regulation in tissues where TITF1 and FOX genes are co-expressed.

1.5. Euthyroid state

The main function of the thyroid gland is to produce thyroid hormones to control the rate of metabolism. Thyroid hormones are essential for growth and differentiation, for the regulation of energy metabolism, and for the physiological function of virtually all human tissues (Braverman & Utiger, 2005).

The synthesis and secretion of thyroid hormones is regulated by the hypothalamic-pituitary-thyroid axis. Thyroid Stimulating Hormone (TSH), also known as thyrotropin, is a glycoprotein hormone that is synthesised and secreted by thyrotrophs in the anterior pituitary. TSH production by the thyrotrophs is stimulated directly by thyrotropin releasing hormone (TRH) derived from the hypothalamus. In a negative feedback loop, T3 suppresses TSH secretion.

1.6. Hyperthyroidism

Two intrinsic thyroid disorders account for the vast majority of cases of hyperthyroidism: Graves' disease, and toxic multinodular goitre. Graves' disease is the most common cause of hyperthyroidism and is the result of IgG antibodies

binding to the TSHR and stimulating thyroid hormone production (Paschke & Ludgate, 1997).

1.7. Hypothyroidism

Hypothyroidism is the result of insufficient thyroid hormone production, causing a general slowing of the BMR (basal metabolic rate), which manifests itself clinically as weight gain, cold intolerance, fatigue, lethargy, depression, hoarseness, dry skin, decreased appetite and menstrual disturbances.

Hypothyroidism can be classified as: primary, due to thyroid gland failure which is the most common form; secondary, due to lack of pituitary TSH; tertiary, due to lack of hypothalamic TRH or a peripheral resistance to thyroid hormones (Lania *et al.*, 2001). The most common cause of primary hypothyroidism is thyroiditis due to anti-thyroid antibodies, a condition called Hashimoto's thyroiditis. Another common cause is prior treatment for Graves' disease with surgery or radioiodine. There are also congenital forms of hypothyroidism, which are detected by neonatal screening and require immediate treatment in order to avoid irreversible developmental defects.

1.8. Congenital Hypothyroidism

Congenital hypothyroidism (CH) is the most common neonatal endocrine disorder, occurring at a rate of 1 in 3000-4000 live births (Toublanc, 1992). It also represents a common preventable cause of mental retardation. Very rarely, CH can be due to pituitary or hypothalamic defects (secondary or tertiary CH respectively), however the majority of cases are the result of defects at the level of the thyroid gland (primary CH). In 15% of primary CH cases, the disease is caused by defects in thyroid hormone synthesis (dyshormonogenesis). However, 85% of the cases are due to defects in thyroid gland development leading to thyroid dysgenesis (TD). Whilst dyshormonogenetic causes of primary CH are associated either with an enlarged (goitre) or a normal thyroid gland, the spectrum of dysgenetic disorders includes complete thyroid agenesis (35–40%), ectopy (55–60%), or hypoplastic gland development (5%) (Park & Chatterjee, 2005).

The majority of cases of CH occur sporadically. However, cases of thyroid dyshormonogenesis often show classical Mendelian inheritance, and 2% of TD patients present with a family history of the disorder (Castanet *et al.*, 2000). Also, non-thyroidal congenital anomalies and chromosomal defects occur in infants with CH at a higher frequency than they do in the general population (Castanet *et al.*, 2001).

The candidate genes associated with primary CH can be divided into two main groups: those causing TD and those associated with defects in thyroid hormone synthesis. The genes that have been linked to dyshormonogenesis include TPO, TG, NIS, PDS (Pendrin syndrome gene) and THOX2. The genes associated with TD include those causing non-syndromic CH (TSHR) and those causing syndromic CH (TITF1, PAX8, and FOXE1).

1.9. Genetic Causes of Congenital Hypothyroidism (CH)

1.9.1. Genes Associated with Dyshormonogenesis

1.9.1.1. Thyroid Peroxidase (TPO)

Defects in the TPO gene have been reported to cause CH by a total iodide organification defect (Bikker *et al.*, 1995). Increasing numbers of mutations have been reported, occurring throughout the 17 exons of the TPO gene, each resulting in an inactive TPO protein (Bikker *et al.*, 1995; Abramowicz *et al.*, 1992; Bikker *et al.*, 1994; Bikker *et al.*, 1996; Medeiros-Neto *et al.*, 1998; Kotani *et al.*, 1999; Pannain *et al.*, 1999; Santos *et al.*, 1999; Bakker *et al.*, 2000; Kotani *et al.*, 2001; Ambrugger *et al.*, 2001).

1.9.1.2. Thyroglobulin (TG)

TG mutations are associated with moderate to severe CH, due to its ineffective formation of T4 and T3 resulting from a coupling defect. TG is normally exported

through the secretory pathway into the lumen of thyroid follicles to undergo iodination. However, mutations in the TG coding sequence can result in defective trafficking of TG from the endoplasmic reticulum to the Golgi apparatus, leading to an endoplasmic reticulum storage disease (ERSD; Hishinuma *et al.*, 1999). A particular feature of some TG mutations involving cysteine residues in the protein is disruption of the three dimensional structure of the molecule, causing it to form aggregates in the endoplasmic reticulum.

1.9.1.3. Sodium-Iodide Symporter (NIS)

Several different heterozygous mutations have been described in the NIS gene (Fugiwara *et al.*, 1998). The loss of function associated with some of these mutations (Q267E and S515X) was found to be due to a failure to localize NIS to the basolateral membrane (Pohlenz *et al.*, 2000). The associated hypothyroidism is of variable severity and goitre is not always present. Individuals with a higher dietary iodine intake are less likely to develop severe hypothyroidism than those with diets deficient in iodine.

1.9.1.4. Thyroid Oxidase 2 (THOX2)

To date, eleven individuals from nine unrelated families have been identified with THOX2 mutations. They can be divided into two groups: (1) Individuals with homozygous or compound heterozygous mutations associated with severe CH (Moreno *et al.*, 2002; Vigone *et al.*, 2005; Varela *et al.*, 2006) or (2) Individuals with monoallelic heterozygous mutations associated with transient CH, which is believed to persist only during neonatal life when the body's requirement for thyroid hormones is much greater (Moreno *et al.*, 2002).

1.9.1.5. Pendred Syndrome (PDS gene)

Mutations in the PDS gene are associated with Pendred syndrome (OMIM: 274600), an autosomal recessive disorder characterised by deafness and goitre. The PDS gene encodes a chloride-iodide transporter, known as pendrin, which is expressed in the

inner ear and thyroid. Thyroid disease usually presents as a multinodular or diffuse goitre of varying size, and is usually not evident until the second decade of life. Despite the goitre, individuals are likely to be euthyroid and only rarely present with CH. However, TSH levels often reach the upper end of the normal range, and hypothyroidism may eventually develop (Reardon & Trembath, 1996).

1.9.2. Genes Associated with Thyroid Dysgenesis (TD)

1.9.2.1. PAX8

Heterozygous PAX8 mutations have been described in patients with CH of varying severity in six families: four familial cases where CH appears to be inherited in an autosomal dominant manner and two sporadic cases (Macchia *et al.*, 1998; Vilain *et al.*, 2001; Congdon *et al.*, 2001; Meeus *et al.*, 2004). The thyroid glands in most of these individuals were hypoplastic and sometimes ectopic in location. However, in one family, the thyroid gland was of normal size at birth but failed to develop normally postnatally, becoming hypoplastic (Meeus *et al.*, 2004). These individuals also showed decreased iodide trapping, suggestive of dyshormonogenesis, as a basis for their CH.

1.9.2.2. TSH Receptor (TSHR)

Homozygous or compound heterozygous mutations in the TSHR gene resulting in TSH resistance were first described in 1995 (Sunthornthepvarakul *et al.*, 1995). Since then, additional loss of function TSHR mutations have been identified in other families showing variable TSH resistance due to reduced thyroid sensitivity to TSH. In some of these families, compensated TSH resistance was associated with euthyroid hyperthyrotropinaemia and either a normal or a hypoplastic thyroid gland (Russo *et al.*, 2000; Tonacchera *et al.*, 2001). Also, subclinical hypothyroidism associated with TSHR mutations has been identified (Alberti *et al.*, 2002).

1.9.2.3. Bamforth-Lazarus Syndrome

Bamforth-Lazarus syndrome (OMIM: 241850) is a recessively inherited syndromic form of CH that was first identified in 1989 (Bamforth *et al.*, 1989). To date, eight individuals in five different families have been reported with the disorder. The features that consistently present in all of these patients are CH, cleft palate and abnormal hair growth (Bamforth *et al.*, 1989; Buntincx *et al.*, 1993; Castanet *et al.*, 2002; Huebner *at al.*, 2004; Barış *et al.*, 2006).

Bamforth-Lazarus syndrome has been linked to homozygous missense mutations in the FOXE1 gene (A65V, S57N, W97R and R102C). All four mutations affect highly conserved residues within the FOXE1 DNA-binding domain (Clifton-Bligh *et al.*, 1998; Castenet *et al.*, 2002; Huebner *et al.*, 2004; Barış *et al.*, 2006). An *in vitro* comparison of the A65V, S57N and R102C mutants with wild-type FOXE1 protein revealed that the mutations were highly deleterious to the transcriptional activity of FOXE1 (the W97R mutant has not been analyzed). The A65V and R102C mutants showed a complete lack of transcriptional activity, while the activity of the S57N was only partially lost.

One of the striking features of FOXE1 loss-of-function mutations is the heterogeneity displayed by the associated phenotype. The A65V mutation was identified in a non-consanguineous Welsh family with two male siblings presenting with CH, cleft palate, choanal atresia, bifid epiglottis and spiky hair. The second reported mutation, S57N, was in a consanguineous Tunisian family with two male siblings exhibiting a milder clinical phenotype consisting of CH, cleft palate and spiky hair. With these cases, ^{123}I scanning and ultrasonography showed the CH to be caused by complete thyroid agenesis. The R102C mutation was identified in a female child of consanguineous parents of Turkish origin presenting with CH, cleft palate, spiky hair and bilateral choanal atresia. Unlike the first two cases, the thyroid was present in its normal location, however its function was severely compromised.

The partial preservation of activity demonstrated by the S57N mutant could explain the incomplete nature of the associated phenotype. It may be the case that this

"residual" activity is above a threshold level required for the normal regulation of some developmental processes (formation of the nasal airways) and not others (thyroid gland development). The A65V and R102C mutations have a similar effect on transcriptional activity, so an explanation of the differences between their associated phenotypes probably lies elsewhere. It may be the case that other, as yet unidentified mutations or polymorphic variations also have a modulating effect on the severity of the phenotype.

Foxe1$^{-/-}$ mice also exhibit cleft palate and thyroid dysgenesis, mirroring the phenotype seen in humans. The Foxe1$^{-/-}$ mice were born at the expected ratio, but died within 48 hrs due to respiratory distress caused by the severe cleft palate. Unfortunately, this was before completion of hair follicle development, so a corresponding hair phenotype could not be observed directly (De Felice *et al.*, 1998). More recently though, Foxe1$^{-/-}$ mouse skin grafted onto immunodeficient mice were shown to produce a sparse hair coat, composed of thin and kinky pelage hair, which closely resembles the spiky hair phenotype seen in Bamforth-Lazarus syndrome. Histological analysis revealed that their hair follicles were misaligned and variably angled, compared with the orderly array of follicles found in wild-type skin (Brancaccio *et al.*, 2004).

The range of physical and physiological abnormalities associated with Bamforth-Lazarus syndrome suggested that FOXE1 plays an important role in tissues other than the thyroid gland. Our group were the first to demonstrate that detectable expression of FOXE1 protein occurs in human extrathyroidal tissues, prepubertal testes and skin (Sequeira *et al.*, 2003). The expression of FOXE1 in prepubertal testes was specifically localised to the exocrine cells of the seminiferous tubules. While, the expression in the skin was found to localise specifically to the keratinocytes of the basal layer of the epidermis and the hair follicle outer root sheath (ORS). Subsequently, another group also detected FOXE1 expression, at the transcript level, in the basal and suprabasal layers of the epidermis and hair follicle ORS (Eichberger *et al.*, 2004).

In addition, FOXE1 transcripts and protein have been observed in the hair follicle ORS, but not epidermis, of normal mouse skin (Brancaccio *et al.*, 2004).

1.10. Skin

The skin is the largest organ in the human body, making up approximately 15% of the total bodyweight and covering a surface area of about two square meters. Structurally, the skin is made up of two layers, the outer epidermis and the inner dermis. Beneath the dermis, but not part of the skin, is the hypodermis or subcutaneous layer made up of adipose tissue and muscle.

Skin has several important functions, including protecting the body against the external environment, thermoregulation, excretion via sweating, the synthesis of melanin pigment (melanocytes) to protect against harmful UV irradiation, the synthesis of vitamin D important for bone and teeth maintenance, synthesis of vitamin B, a major role in sensory perception (Merkel Cells, Pacian Corpuscles, Meissner's Corpuscle), a major role in antimicrobial activity (defensins) and an essential role in the immune system (Langerhans Cells and T-cells).

Anatomically, skin consists of six structures:

- Subcutaneous Muscle
- Subcutaneous Adipose Fat
- Dermis
- Basement Membrane Zone
- Epidermis
- Appendages (hair follicles, nails/claws, sebaceous glands, apocrine and eccrine sweat glands)

1.10.1. Epidermis

The surface layer of the skin is a keratinising stratified epithelium, the epidermis, which is composed of several cell layers or strata. The majority of cells forming the epidermis are keratinocytes but melanocytes, Langerhans cells and Merkel cells are also present in small numbers. The main function of the melanocyte is the production of pigment secreted in melanosomes and transferred to keratinocytes, forming a supranuclear cap to protect nuclear DNA from UV irradiation. Langerhans cells are

important for immune surveillance and Merkel cells are transducers of fine touch stimuli.

Keratinocytes are epithelial cells that undergo terminal differentiation to produce corneocytes, dead cells that form the outer layers of the skin surface. During terminal differentiation, the epidermal cells pass through different morphological stages that can be identified as distinct cell layers. Based on histology, there are five types of structure: stratum basale (basal layer), stratum spinosum (spinous layer), stratum granulosum (granular layer), stratum lucidum (transition layer), and the superficial stratum corneum (horny layer). As cells transit from the basal layer to the stratum corneum, they change morphologically and biochemically (Bowden *et al.*, 1984; Eckert, 1989; Watt, 1989; Fuchs, 1990).

The keratinocyte has three major cytoskeletal networks of which two are ubiquitous in all mammalian cell types: the microtubule filament network (tubulin) and the microfilament network (actin). The other cytoskeletal structure, the intermediate filament (IF) network, is highly variable in different cell types and is composed of six different classes of structural protein (types I-VI). The majority of these are cytoplasmic but one class (type V) are the nuclear lamins (Goldman *et al.*, 2002).

The other five classes are cell type specific and types I and II comprise the keratin (K) multigene family which are specific to epithelial cells (Moll *et al.*, 1982; Bowden *et al.*, 1987; Irvine & McLean, 1999). However, while all these proteins form 10 nm intermediate filaments, also called tonofilaments in the epidermis, they are a very diverse group of structural proteins. Each of the 54 known keratins is encoded by its own keratin gene (KRT) and these genes are localised in two large multigene clusters on chromosomes 12 and 17 (Popescu *et al.*, 1989; Bowden, 1993). The type II gene cluster at 12q11-13 contains 27 functional genes and 5 pseudogenes while the type 1 cluster at 17q11.2 contains 27 functional genes and 4 pseudogenes (Hesse *et al.*, 2004). The type II genes encode basic-neutral keratin proteins and the type I genes encode acidic keratins (Moll *et al.*, 1982; Bowden, 1993). The nomenclature of keratins has evolved over the last 25 years and a new unifying labelling system has been developed recently (Schweizer *et al.*, 2006).

Keratins are obligate heteropolymers and one type I keratin must bind with one type II keratin to allow polymerisation into the higher order structures required to form an intermediate filament network (Steinert & Parry, 1993). There is also a deal of complexity with regard to keratin (K) expression. In terms of the epidermis, there are five major keratins at most anatomical sites (K1, K2e, K5, K10 and K14). However, in palmar-plantar epidermis, which is structurally distinct, five other keratins (K6a, K6b, K9, K16 and K17) are constitutively expressed. Four of these (K6a, K6b, K16 and K17) are also expressed in the outer root sheath of the hair follicle and expression can be induced in the epidermis under specific conditions (UV exposure, wounding, etc). In addition to keratin gene expression varying in different anatomical regions and different epithelia, differential gene expression also occurs in these tissues as differentiation proceeds. Thus, K5 and K14 are mainly expressed in the basal layer of the epidermis and their synthesis does not occur once cells have committed to differentiation. The daughter suprabasal cells on the other hand are committed to terminal differentiation and express what are termed differentiation-specific keratins, K1, K2e and K10. The palmar-plantar epidermal keratin (K9) is also a differentiation specific keratin. Thus, by examining the expression of different epidermal keratins, an accurate evaluation of the level of tissue differentiation can be obtained and this is very useful when using tissue culture and animal models.

The keratin intermediate filaments bind to two junctional structures within keratinocytes, the desmosomes that bind adjacent keratinocytes together and the hemidesmosomes that bind the basal cells to the basement membrane zone (BMZ) and the underlying dermis. This confers integrity and resilience to the living epidermis and is also very important for the formation of the corneocyte, the final stage in terminal differentiation.

Keratinocytes of the granular layer have this appearance due to the presence of keratohyalin granules which contain two other structural proteins that are essential for the formation of a functional environmental barrier. These are loricrin, a major structural protein component of the cell envelope and filaggrin, an intermediate filament associated protein that is required for the dense packing of keratin IF in the corneocyte (Ishida-Yamamoto *et al.*, 1997; 2002; Candi *et al.*, 1999; 2001). Another important protein in terms of epidermal differentiation is involucrin, which is

expressed by the spinous cells and forms the initial scaffold adjacent to the inner leaflet of the plasma membrane for cell envelope formation (Watt, 1983; Eckert *et al.*, 1993. The granular cells also contain another organelle, the membrane coating granule (MCG) that contains specialised lipid for deposition between the corneocytes (O'Guin *et al.*, 1989; López *et al.*, 2007; Kuechle *et al.*, 1999; Irvine & McLean, 2006; Smith *et al.*, 2006; Barker *et al.*, 2007)

The outermost layer of the epidermis is the horny layer (statum corneum). It is made up of dead and flattened cells (corneocytes) that are filled with keratin filaments embedded in a matrix derived from the keratohyalin granules. The cells in the lower horny layer are bound together tightly by desmosomes but nearer the skin surface these are degraded and corneocytes at the surface are lost (desquamation). This degradation required specific stratum cornenum proteases (Caubet *et al.*, 2004). The thickness of the epidermis can vary from less than 0.1 mm on the eyelids to over 1 mm on the palms and soles. The thickness of the horny layer is a major determinant of epidermal thickness, especially in palmar-plantar skin.

1.10.2. Basement Membrane Zone (BMZ)

The basement membrane zone (BMZ) forms the junction between the lower dermis and upper epidermis. The major structural component in this region of the skin is the hemidesmosome which ensures a firm connection between the dermis and epidermis. The BMZ has other specialised collagens such as type VII (anchoring fibrils), type IV (anchoring filaments) (Ball *et* al., 2003), and type XVII (transmembrane component of hemidesmosome) (Van den Bergh & Giudice, 2003), some of which are synthesised by the epidermal keratinocytes. The hemidesmosome forms a link between the anchoring fibril complex of the dermis which itself is tightly bound to the collagen matrix and the cytoskeletal proteins of epidermal keratinocytes (keratin intermediate filaments) which are connected to the attachment plaque, a structure made from plectin and IFAP300, on the internal surface of the keratinocyte plasma membrane (Wiche, 1998; Steinböck & Wiche, 1999, Clubb *et al.*, 2000). These structural proteins thus form a continuous molecular link between these two structures, which is essential to maintain skin integrity.

1.10.3. Dermis

The dermis is a mesenchymal structure consisting of a collagen and elastin matrix in which the major cell type, the fibroblasts, are embedded. This structure supports the epidermis above, the appendages within and sits on a cushion of subcutaneous adipose and muscle. The dermis has an extensive vascular system necessary for thermoregulation and the supply of nutrients to the epidermis which has no blood supply. The upper papillary dermis undulates and forms rete ridges, which increases the surface area in contact with the epidermis providing better adhesion and allowing a greater exchange of nutrients by diffusion. The lower regions of the dermis are reticular and form the major portion. The interlacing (reticular) structure of collagen and elastin fibres provides resilience and elasticity to the skin. The bulk of the dermis is composed of type I and type III collagen synthesised by the fibroblast.

1.10.4. Hair Follicles

The hair follicle develops from an ectodermal bud that grows down into the underlying mesenchyme during embryogenesis (Stark *et al.*, 1987). The major structural components of the hair follicle include the connective tissue sheath, the dermal papilla (DP), the germinative epithelium (GE), the epithelial hair matrix (HM), the hair cortex or shaft (HC), the hair medulla (HM), the hair cuticle (HC), the inner root sheath (IRS) which comprises of a further three layers, the Henle's and Huxley's layer and the IRS cuticle and the outer root sheath (ORS).

Hair production originates from proliferating germinative epithelial cells located in the hair follicle bulb, which is under the control of the dermal papilla (Philpott *et al.*, 1990). Complex cell signalling within the germinative cells of the hair follicle bulb instructs lineage restricted differentiation to produce concentric rings of cells which form the cortex and cuticle of the hair fibre as well as the cuticle, Henle's and Huxley's layer of the inner root sheath (IRS).

1.10.4.1. Outer Root Sheath

The outer root sheath (ORS) is continuous with the epidermis and the upper part, termed the infundibulum, is identical in structure to the epidermis. The outermost layer of the ORS consists of germinative cells and differentiation occurs in an inward direction towards the IRS and hair fibre. The ORS is several cells thick in the upper hair follicle but narrows to 1-2 cells thick in the lower hair follicle. Keratin expression is similar to the epidermis in that K5 and K14 are expressed in basal cells but differs in terms of differentiation-specific keratin expression. As in the palmar-plantar epidermis, constitutive expression of K6a, K6b, K16 and K17 occurs and another specialised keratin (K6hf) is also expressed (Winter *et al.*, 1998).

1.10.4.2. Inner Root Sheath

The inner root sheath (IRS) forms a slippage zone between the outer root sheath (ORS), a continuation of the epidermis, and the growing hair fibre. It has three different layers: Henle's layer, Huxley's later and the IRS cuticle. All three layers are formed from hair bulb epithelial cells under the influence of matrix cells in the dermal papilla. Differentiation occurs in a specific direction from Henle's layer through Huxley's layer to the cuticle. The IRS moulds the hair fibre and allows this to move through the hair follicle. IRS cells also express specific keratins and to date 8 have been identified (Porter *et al.*, 2001; Rogers *et al.*, 2004), 4 type I (K25irs1, K25irs2, K25irs3 and K25irs4) and 4 type II (K6irs1, K6irs2, K6irs3 and K6irs4).

1.10.4.3. Hair Fibre

The bulk of the hair fibre is formed by the cortical cells or trichocytes and there is an outer cuticle and an inner medulla. The fibre itself is almost entirely composed of keratins and matrix proteins. Initially, only four keratin intermediate filament proteins were isolated from the hair (H1, H2, H3 and H4; Bowden *et al.*, 1987) but more recent molecular approaches (Bowden *et al.*, 1998; Rogers *et al.*, 2000; 2004; 2005; Schweizer *et al.*, 2006; Langbein *et al.*, 2007) have elucidated that there are eleven

type 1 proteins (Ha1, Ha2, Ha3a, Ha3b, Ha4, Ha5, Ha6, Ha7, Ha8 [K31-K38} plus K39 and K40) and six type II keratins (Hb1, Hb2, Hb3, Hb4, Hb5 and Hb6 [K81-K86]). Some of these are cortex specific (Ha1, Hb1, Hb3, Hb6), some are cuticle specific (Ha2, Ha5, Hb2, Hb5) and other are expressed in both regions. Thus, these can be used as molecular markers for specific cell lineages that are undergoing different programmes of epithelial cell differentiation.

1.10.5. Hair Growth Cycle

The most unique feature of hair growth is cycling. The growth cycle consists of four different phases: anagen, catagen, telogen and exogen. All body hair goes through this cycling process but the duration of each individual phase and the length of the resulting hair fibre varies depending on the type of follicle and its location. In man, each hair follicle has its own pace and rhythm and cycling is termed asynchronous. However, in some animals such as the mouse, a large group of hair follicles cycle synchronously. Moreover, waves of the synchronous hair growth sweep over the body posteriorly and dorsally. Hair growth in animals also has a circannual rhythm, as exemplified by seasonal moulting. This phenomenon is not so obvious in humans and hair growth is largely independent of the sun and seasons (Peus & Pittelkow, 1996)

The exact reasons why the hair follicle needs to cycle remains unclear. A commonly used explanation is that this cyclic growth provides a mechanism by which a mammal's fur can adapt to a changing environment (e.g. seasonal moulting) or as a result of procreational activities (e.g. mating season). However, there are many mammalian species that possess a mosaic hair cycle where each hair follicle has its own pace and rhythm that is largely independent of the seasons. Even in those mammals that do possess fairly well-synchronised hair follicles (e.g. the mouse), cycling becomes increasingly heterogeneous with age and does not seem to be at all influenced by the environment.

Another explanation is that cyclic growth of the hair follicles provides a mechanism by which mammals can control the length of their body hair from site to site. For instance, over-long eyelashes, eyebrows and nose, ear and facial hair would severely

compromise an animal's ability to see, smell and hear. Their movement would similarly be compromised if their body hair grew too long. The cyclical growth may also allow animals to shed fur periodically to clean the body surface of debris and parasites that accumulate in the follicular canal.

Another possible function of the hair growth cycle is to prevent accumulation of abnormal cells. As there are a lot of rapidly dividing cells in the hair follicle, the cycling process may prevent somatic malignant changes from persisting. For the majority of mammalian species the continual possession of hair (fur) that is appropriate to their specific habitat is a necessity for survival. Given how important this is, the hair growth cycle may serve to keep the hair follicle in a continuous state of optimal regeneration.

1.10.6. FOXE1 Expression in Skin

The Sonic Hedgehog (SHH)/GLI signalling pathway modulates FOXE1 expression in the skin. The transcription factor GLI2 is the major transcriptional effector of SHH signaling during epidermal development (Mill *et al.*, 2003). In humans, FOXE1 has been shown to be a direct target gene of GLI2 (Eichberger *et al.*, 2004 and 2006). Interestingly, although FOXE1 and GLI2 expression both localize to the hair follicle and epidermis, upstream components of the SHH pathway are mainly restricted to the follicular regions of the skin. Therefore, epidermal expression of GLI2 may be controlled by signals other than SHH. Such a situation has been described for the formation of the ventroposterior mesoderm of Xenopus, where FGF induces GLI2 expression (Brewster *et al.*, 2000).

The situation in the mouse seems to be even less clear, although strong evidence indicates Foxe1 is a downstream target of Shh/Gli signalling, no Gli binding sites could be identified in the Foxe1 promoter (Brancaccio *et al.*, 2004). Possible explanations include that Foxe1 is either an indirect downstream target or that the GLI proteins are able to bind to a non-canonical site. A comparison of Foxe1 expression with that of upstream components of the Shh pathway has shown that it has a much narrower expression range. This suggests that other factors play a role in refining

Foxe1 expression. Inactivation of epidermal growth factor (EGF) signalling has been shown to produce a hair phenotype (Sibilia *et al.*, 1995; Miettinen *et al.*, 1995; Hansen *et al.*, 1997) very similar to that of Foxe1$^{-/-}$ mice. Recently, it has been shown that EGF signalling, via RAF/MEK/ERK, modulates the expression of GLI target genes in human keratinocytes (Kasper *et al.*, 2006). Interestingly, GLI and EGF signalling were shown to synergistically induce expression of the forkhead protein FOXA2 (HNF-3β). In the thyroid, FoxA2 and FoxE1 have been shown to have a redundant role in the modulation of TPO expression (Sato & Di Lauro, 1996), so it may be possible that FOXE1 expression is regulated in a similar fashion.

1.11. Thesis Aims

The spiky hair phenotype of Bamforth-Lazarus patients suggested that FOXE1 had an important role to play in hair follicle morphogenesis. Although the skin of these patients was not been examined in detail, the morphology of Foxe1$^{-/-}$ mouse skin suggested that a defect in keratinocyte migration was the most likely cause. Previous studies had shown that FOXE1 expression was localised to the basal layer of the epidermis and hair follicle ORS.

The first three chapters of this thesis are concerned with deducing the biological role of FOXE1 in human skin. The aim of chapter 2 was to determine the precise location of FOXE1 expression in the human hair follicle, by colocalisation of an anti-FOXE1 pAb with known hair differentiation markers. Chapter 3 was concerned with identifying potential FOXE1 downstream target genes using a bioinformatics approach. In chapter 4, the expression profile of FOXE1 and several candidate target genes was determined throughout keratinocyte differentiation, using real-time quantitative PCR (RT-QPCR). A link between FOXE1 and the target genes was also investigated using siRNAs to knockdown FOXE1 expression.

In the mature thyroid gland, FOXE1 plays an essential role in mediating the control of thyroid hormone synthesis. Chapter 5 was concerned with determining the role polymorphic variations in FOXE1 (in particular its polyalanine tract) may have on thyroid gland function. The allele frequency was determined in a small cohort of

subclinical hypothyroid subjects and the transcriptional activity of the allelic variants compared using a luciferase reporter assay.

Chapter 2.

Localisation of FOXE1 Expression in Human Skin

2.1. Introduction

2.1.1. Defective FOXE1 Causes Abnormal Hair Growth

As described in chapter 1, non-functional FOXE1 causes Bamforth-Lazarus syndrome characterised by CH, cleft palate and abnormal spiky hair growth. Scanning electron microscopy of hair fibres from Bamforth-Lazarus patients revealed a reduced hair shaft diameter, a loss of scale patterning and pili torti, a combination of features that produced a spiky hair phenotype (Bamforth *et al.*, 1989). The possibility that spiky hair was a systemic manifestation of the CH seemed unlikely as it persisted despite adequate thyroid hormone replacement therapy (Bamforth *et al.*, 1989).

An immunohistochemical approach was undertaken to detect and localise the expression of FOXE1 protein in human skin. Initial experiments using a rabbit pAb raised to a synthetic FOXE1 peptide produced disappointing results. This was not unexpected, as it is often the case that such antibodies are unable to recognise the epiptope in the folded native protein. More appropriate for immunohistochemical analysis are antibodies raised against full-length native proteins. This is commonly achieved by immunising rabbits with the purified recombinant protein of interest.

The recombinant protein can be synthesised in a variety of organisms, including bacteria (such as *Escherichia coli*), baculovirus and eukaryotic cells. The protein is then extracted from these organisms, purified and used to immunise an animal (typically rabbit) for antibody production.

The coding sequence for FOXE1 was cloned into pTrcHis-C vector, a pBR322-derived expression vector designed to allow enhanced initiation of translation, and high-level expression of eukaryotic genes in *E. coli*. Main features of the vector include:

Promoter. The *trc* promoter is a synthetic hybrid promoter derived from the fusion of the *E. coli trp* and *lac* operones. It is regulated by the *lacO* promoter and the product of the *lacZ* gene. In addition, the vector also contains a minicistron element upstream of the start codon. This element contains a ribosome binding sites and a translation termination codon enabling efficient translation of eukaryotic proteins in *E. coli* (Figure 2.1).

PolyHistidine Tag. The vector also included a nucleotide sequence that encoded six consecutive histidine residues expressed as an N-terminal fusion to the protein of interest, allowing for the rapid purification of the protein with nickel-chelating resin (Figure 2.1).

Figure 2.1. Schematic Representation of pTrcHis Vectors. A) Structural features such as promoter, histidine-tag and multiple cloning site are shown, **B)** Nucleotide sequence of multiple cloning site (Invitrogen, 2002).

A

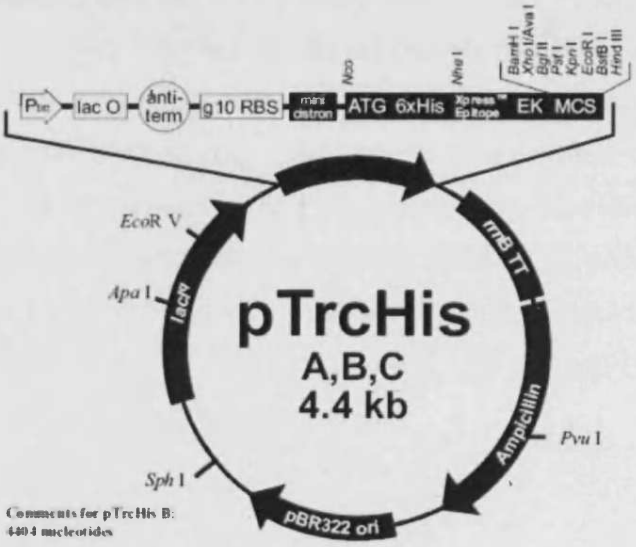

B

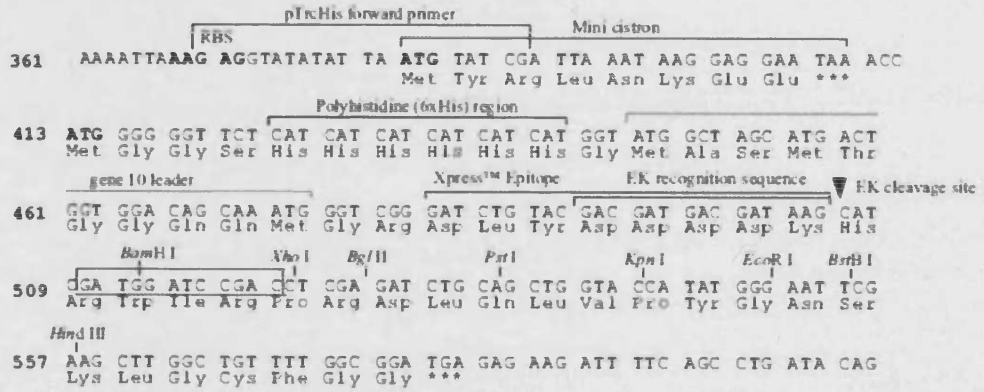

Using the anti-FOXE1 pAb, our group were the first to demonstrate that detectable expression of human FOXE1 protein occurs in normal human skin. This expression was found predominantly in the keratinocytes of the ORS of the hair follicle, and also in the basal cell layer of interfollicular epidermis (Sequeira *et al.*, 2003). Subsequently, another group also detected FOXE1 expression, at the transcript level, in the basal and suprabasal layers of the interfollicular epidermis and hair follicle ORS (Eichberger *et al.*, 2004).

2.1.2. Aims

The aim of this chapter was to use the same polyclonal antibody (pAb) used by Sequeira *et al* (2003) to investigate the precise location of FOXE1 expression within the human hair follicle. Colocalisation of the anti-FOXE1 pAb with known hair differentiation markers (e.g. Keratins [K] K16 and K17, markers of the outer root sheath, $K6_{IRS}$, an inner root sheath marker and Hb1 and Ha2, which are hair shaft specific keratins) was to be used to assess whether FOXE1 expression was specific to certain cell lineages. The preferred method for visualizing dual-labelled antibodies in tissue was immunofluorescence and confocal laser scanning microscopy. Therefore, prior to the start of the project, attempts had been made to detect the anti-FOXE1 pAb with a fluorescein isothiocyanate (FITC) labelled secondary antibody. This produced very poor results (data not shown), possibly due to a lack of specificity of the anti-FOXE1 pAb. Thus, affinity purification of the antibody was attempted.

2.2. Material and Methods

2.2.1. Immunohistochemistry

Formalin-fixed paraffin-embedded biopsy specimens of human thyroid and beard skin were obtained from two Cardiff University Departments, Pathology and Dermatology, respectively. The specimens were sectioned at 5 μm and mounted on superfrost slides [Menzel-Glaser, Germany]. Mounting was performed in a preheated water bath containing distilled water free from contaminants in order to prevent wrinkling of the specimen. The slides were then left to dry overnight in an oven at 40°C.

Sections were heated at 60°C for 20 mins to melt the wax, and then dewaxed with three aliquots of xylene and reducing grades of alcohol (100%, 90%, 70%) for 5 mins per step. Sections were rehydrated in tap water for 5 mins at room temperature (RT), followed by three washes in phosphate buffered saline (PBS) for 5 mins at RT.

In brief, dewaxed sections were incubated in 0.3% hydrogen peroxide [Fisher Scientific UK Ltd, Leicestershire, UK], and then 5% milk. The sections were thoroughly washed in PBS between these steps and prior to the addition of the rabbit anti-FOXE1 pAb (Sequeira *et al.*, 2003). Optimisation of anti-FOXE1 pAb staining was obtained using a range of doubling dilutions from 1:10 to 1:20,000 combined with overnight incubation at 4°C. Subsequent stages were performed using a Dako Envision Detection Kit following the supplied protocol. All sections were counterstained with Harris' haematoxylin.

2.2.2. pTrcHisC-FOXE1 Construct

The construct consisted of a 1.3 kb BamHI-XbaI fragment, encompassing the entire FOXE1 coding region (accession number 51294, National Center for Biotechnology Information [NCBI]), subcloned in-frame into the polylinker of pTrcHisC prokaryotic expression vector from Invitrogen (Sequeira *et al.*, 2003). This vector was designed to allow enhanced initiation of translation and high-level expression of eukaryotic genes in

E. coli. The vector also included a nucleotide sequence that encoded six consecutive histidine residues expressed as an N-terminal fusion to the FOXE1 protein, allowing for the rapid purification of the protein with nickel-chelating resin.

Sequeira *et al* (2003) used a pTrcHisC-FOXE1 construct to transform the *E. coli* (TOP10 strain), and frozen stocks were prepared and kept at -80°C.

2.2.3. Confirming the Integrity of the pTrcHisC-FOXE1 Construct

2.2.3.1. Small-Scale Plasmid DNA Preparation (Minipreps)

All reagents from Fisher Scientific UK Ltd (Leicestershire, UK) unless otherwise stated.

Minipreps of pTrcHisC-FOXE1 DNA were prepared using a standard alkali lysis protocol. A single *E. coli* colony was inoculated into 5 ml Luria Bertani (LB) broth containing 100 μg/ml ampicillin [Sigma-Aldrich Company Ltd, Dorset, UK] and incubated overnight at 37°C in an orbital incubator shaking at 250 rpm. The following day, 1.5 ml of the overnight culture was transferred to a 1.5 ml microtube, pelleted (13,000 rpm for 1 min at RT), washed once in 1 ml SET solution (20% sucrose, 50 mM EDTA, 50 mM Tris-HCl, pH 7.5), and finally resuspended in 150 μl SET solution. Then, 5 μl DNase-free RNase A (4 mg/ml) [Promega UK Ltd, Hampshire, UK] was added followed by 350 μl of freshly prepared lysis reagent (0.2N NaOH, 1% SDS). The whole solution was vortexed and incubated on ice for 10 mins. Then, 250 μl 3M NaAcetate (pH 4.8) was added to stop the lysis reaction. The solutions were mixed by inverting the tube several times, followed by incubation on ice for 30 mins and centrifugation at 13,000 rpm for 5 mins at 4°C. The supernatant was transferred to a new tube, mixed with an equal volume of isopropanol and the plasmid DNA pelleted (8000 rpm for 30 mins at RT). After two washes with 70% ethanol, the plasmid DNA was air-dried and then redissolved in 20 μl $T_{10}E_1$ buffer (10 mM Tris-HCl, 1 mM EDTA, pH 8.0).

2.2.3.2. Restriction Enzyme Analysis

To confirm the identity of the pTrcHisC-FOXE1 construct, a double restriction digestion with BamHI and XbaI enzymes was performed. For a single reaction, the following components were added to a sterile 100 µl microtube: 2 µl 10× reaction buffer E, 0.5 µl 10 U/µl BamHI, 0.5 µl 12 U/µl XbaI, 1 µg plasmid DNA and the final volume made up to 20 µl with nuclease-free water [all reagents from Promega UK Ltd]. The reaction was mixed gently by pipetting, briefly spun in a microcentrifuge before being transferred to a 37°C waterbath for 1 hr. The digestion products were separated on a 1% agarose gel and DNA visualised by ethidium bromide (EtBr) staining.

Linearisation of the plasmid prior to sequence analysis was performed with a single digest using BamHI or XbaI. The reaction was set-up exactly as described above except that only one enzyme was added to the reaction.

2.2.3.3. Purification of Restriction Digest Products

For optimal sequencing results, purification of the linearised plasmid was performed either by ethanol precipitation or using a gel extraction method.

Ethanol precipitation: 2 µl 3 M NaAcetate (pH 4.8) and 50 µl ice-cold 100% ethanol were added to the reaction mixture, which was then incubated on dry ice for 30 mins. The tube was then centrifuged (13,000 rpm for 20 mins at 4°C), the supernatant removed and the pellet washed in 200 µl ice-cold 70% ethanol. The pellet was allowed to air-dry and then resuspended in 20 µl nuclease-free water. The solution was incubated on ice for 20 mins, vortexed and briefly spun down before being transferred to a clean tube.

Gel extraction: This was performed using the QIAquick Gel Extraction Kit (Qiagen, Heidelberg, Germany) according the manufacturer's protocol. The restriction digest products were separated on a 1% agarose gel [Sigma-Aldrich Company Ltd] and the band

corresponding to the linearised plasmid excised using a clean sharp scalpel. The gel slice was weighed and resuspended in buffer QG (100 µl buffer/100 mg gel). Heating the sample to 50°C and frequent vortexing was performed to dissolve the gel. Isopropanol (100 µl/100 mg gel) was added and the mixture applied to a QIAquick column that was then centrifuged (13,000 rpm for 1 min at RT). This was followed by sequential addition of 500 µl buffer QG and 750 µl buffer PE, each followed by centrifugation (13,000 rpm for 1 min at RT). Finally, 30 µl buffer EB (10 mM Tris-HCl, pH 8.5) was applied to the column, left for 1 min, and then centrifuged (13,000 rpm for 1 min at RT).

The concentration of the purified plasmid DNA was determined by spectrophotometry [GeneQuant, GE Healthcare].

2.2.3.4. Direct Sequencing

The nucleotide sequence of the insert and flanking vector of the pTrcHisC-FOXE1 was obtained using the Dideoxy Sanger method (Sanger *et al.*, 1977) with Applied Biosystems' BigDye Terminator v3.1 Cycle Kit. The forward primers used were FOXE1-F2 (5′-TGG CTA CCG TGA AGG AAG AGC-3′), FOXE1-P (5′-ATC TTC CCA GGC GCG GTG CCC-3′) and FOXE1-F7 (5′-CCG GCA GTG CGA TCT TTG-3′). The reverse primers used were FOXE1-R1 (5′-AGC TGT AGG GCG GCT TCC-3′) and FOXE1-B (5′-GGC CTG CTC GGT CTT TTC C-3′).

The following components were added to a nuclease-free 500 µl microtube: 2 µl 5× sequencing buffer, 2 µl BigDye v3.1 reaction mix, 1 µl 5 µM primer, 300 ng plasmid DNA and the volume made up to 10 µl with nuclease-free water [Promega UK Ltd]. The reaction mixture was gently vortexed, briefly spun in a microcentrifuge before being transferred to the PE Applied Biosystems 9700 thermocycler.

Thermocycler protocol:

- Initial denaturation: 1 min at 96°C

- 25 cycles of Denaturation: 10 secs at 94°C
  Annealing: 5 secs at 50°C
  Extension: 4 mins at 60°C

DNA samples were precipitated by the addition of 1 µl 3 M NaAcetate and 25 µl ice-cold 95% ethanol, then left at -20°C for 15 mins. Samples were centrifuged (15,000 rpm at 4°C for 30 mins), and DNA pellets washed twice with 180 µl ice-cold 70% ethanol. Finally, the pellets were resuspended in 10 µl ice-cold 70% ethanol for subsequent analysis on an ABI PRISM DNA sequencer.

2.2.4. Production of the Polyhistidine-Tagged FOXE1 Fusion Protein

Having confirmed the identity of the pTrcHisC-FOXE1 construct, large-scale production of the polyhistidine-tagged FOXE1 fusion protein (referred to as FOXE1-HIS) was undertaken using the methods described by Sequeira *et al* (2003). Briefly, 1 ml of the miniprep culture was used to inoculate 1 L LB broth containing 100 µg/ml ampicillin [Sigma-Aldrich Company Ltd]. This was then incubated overnight at 30°C in an orbital incubator shaking at 250 rpm until the optical density $(OD)_{600}$ of the culture reached 0.3 (which took approximately 2 hrs). Expression of the FOXE1-HIS was induced by the addition of isopropylthiogalactopyranoside (IPTG) [Sigma-Aldrich Company Ltd] to a final concentration of 0.1 mM. The culture was then returned to the orbital incubator for a further 4 hr incubation.

The bacterial cells were harvested by centrifugation at 3000×g for 30 mins at 4°C. The pellet was then resuspended in native binding buffer (20 mM phosphate, 500 mM NaCl, pH 7.8) [Invitrogen, Paisly, UK] at a ratio of 5 ml buffer per 100 ml culture, and the resulting cell suspension stored in 5 ml aliquots at -20°C until required.

The 5 ml aliquots were thawed on ice, and the serine/cysteine protease inhibitor phenylmethanesulfonyl (PMSF) [Sigma-Aldrich Company Ltd] added to a final

concentration of 1 mM. The aliquots were then subjected to three cycles of freeze thawing, followed by the addition of lysozyme [Sigma-Aldrich Company Ltd] to a final concentration of 100 μg/ml and incubated on ice for 15 mins. The suspension was kept on ice, and sonicated at medium intensity with five 5 sec bursts. Finally, insoluble debris was removed by passing the lysate through a 0.45 μm filter.

2.2.5. Nickel Column Purification of FOXE1-HIS

The 5 ml cellular lysate was applied to a column containing 4 ml Probond nickel resin [Invitrogen, Paisly, UK] equilibrated with native binding buffer. The resin was resuspended and the column placed on a mechanical shaker, for 1 hr at 4°C. The lysate was allowed to flow out of the column, which was then repeatedly washed with 10 ml native wash buffer (20 mM sodium phosphate, 500 mM sodium chloride, pH 6.0) until the OD_{280} of the flow-through fell below 0.01. Finally, the bound protein was eluted by addition of 6 ml of native imidizole elution buffer (20 mM sodium phosphate, 500 mM sodium chloride, 10-300 mM imidizole, pH 6.0). The eluate was collected in 1 ml fractions and 25 μl samples taken from each for analysis by sodium dodecyl sulphate-polyacrylamide gel electrophoresis (SDS-PAGE).

2.2.6. Gel Analysis of Eluted Fractions

Twenty-five microlitre samples were mixed with an equal volume of SDS-PAGE loading buffer (4% SDS; 100 mM Tris-HCl, pH 6.8; 20% glycerol; 2% β-mercaptoethanol; 1 mM PMSF [Sigma-Aldrich Company Ltd]; 2 mM EDTA, pH 8.0, 0.004% pyronin Y [Sigma-Aldrich Company Ltd]), boiled for 5 mins, and centrifuged at 13,000 rpm for 5 mins at RT.

The estimated molecular size of FOXE1 was 42 kDa, and so the proteins were separated on 10% polyacrylamide gel (resolves proteins in the size range: 21-100 kDa). Separation was performed using a mini-protean II apparatus [Bio-Rad Laboratories] at a constant voltage of 200V for 40 mins.

Coomassie blue (0.5%) staining of gels was performed using standard laboratory methods, while silver staining of gels was performed using the PlusOne silver staining kit [GE Healthcare], following the manufacturers protocol.

The protein was transferred to a Hybond™-P polyvinylidene fluoride (PVDF) membrane [GE Healthcare] using a mini-protean II apparatus [Bio-Rad Laboratories]. Transfer took place over 1 hr at 350 mA in a blotting buffer (25 mM Tris-HCl, 182 mM glycine, 20% methanol) with cooling. Following transfer the membranes were blocked for 1 hr at RT, using TBS-Tween (0.1%), 5% non-fat dried milk [Marvel].

Western blots were incubated with a rabbit pAb raised against a synthetic FOXE1 peptide (GVPGEATGRGAGGRRRJRPLQ-COOH) at a 1:1,000 dilution in TBS-Tween containing 5% non-fat dried milk for 1 hr at RT. The membrane was washed with TBS-Tween and then incubated with an anti-rabbit IgG-HRP conjugate at a 1:5,000 dilution in 5% milk for 60 mins at RT. Proteins were visualised using ECL Plus (GE Healthcare) following the manufacturers instructions.

2.3. Results

2.3.1. Optimisation of Immunohistochemistry

Initial experiments involved incubating tissue sections from Graves' thyroid (positive control: known to express FOXE1) with the anti-FOXE1 pAb at different dilutions. As was found by Sequeira *et al* (2003), a 1:500 dilution produced optimum antibody staining. This was characterised by staining of the nuclei/cytoplasm of thyroid TFCs, little or no staining of the surrounding interstitium, connective tissue, smooth muscle and endothelium. The majority of thyrocytes showed nuclear and cytoplasmic staining, while others showed only cytoplasmic staining (Figure 2.2A). The preimmune serum (PI), at the same dilution produced no specific staining (Figure 2.2B).

Use of the anti-FOXE1 pAb on tissue sections from human beard revealed positive staining in the epidermis, sebaceous gland and the ORS of the hair follicle. High levels of background staining, a problem often encountered when using a rabbit pAb, was not observed. Beard tissue sections incubated with a 1:1,000 dilution of the anti-FOXE1 pAb were overstained (Figure 2.3A), while a 1:5,000 dilution achieved the optimum level of staining (Figure 2.4A). All PI controls were negative for any specific staining (Figure 2.3B, 2.4B).

Despite the specificity of the antibody using immunohistochemical revelation, attempts to use immunofluoresence-based detection techniques produced high levels of background staining.

Figure 2.2. Paraffin Sections of Tissue from Graves' Thyroid Showing Immunohistochemical Staining. A) Incubation with anti-FOXE1 pAb at 1:500 dilution. (1) Thyrocyte with nuclear and cytoplasmic staining. (2) Thyrocyte with cytoplasmic staining alone **B)** Incubation with PI at 1:500 dilution. (20× magnification)

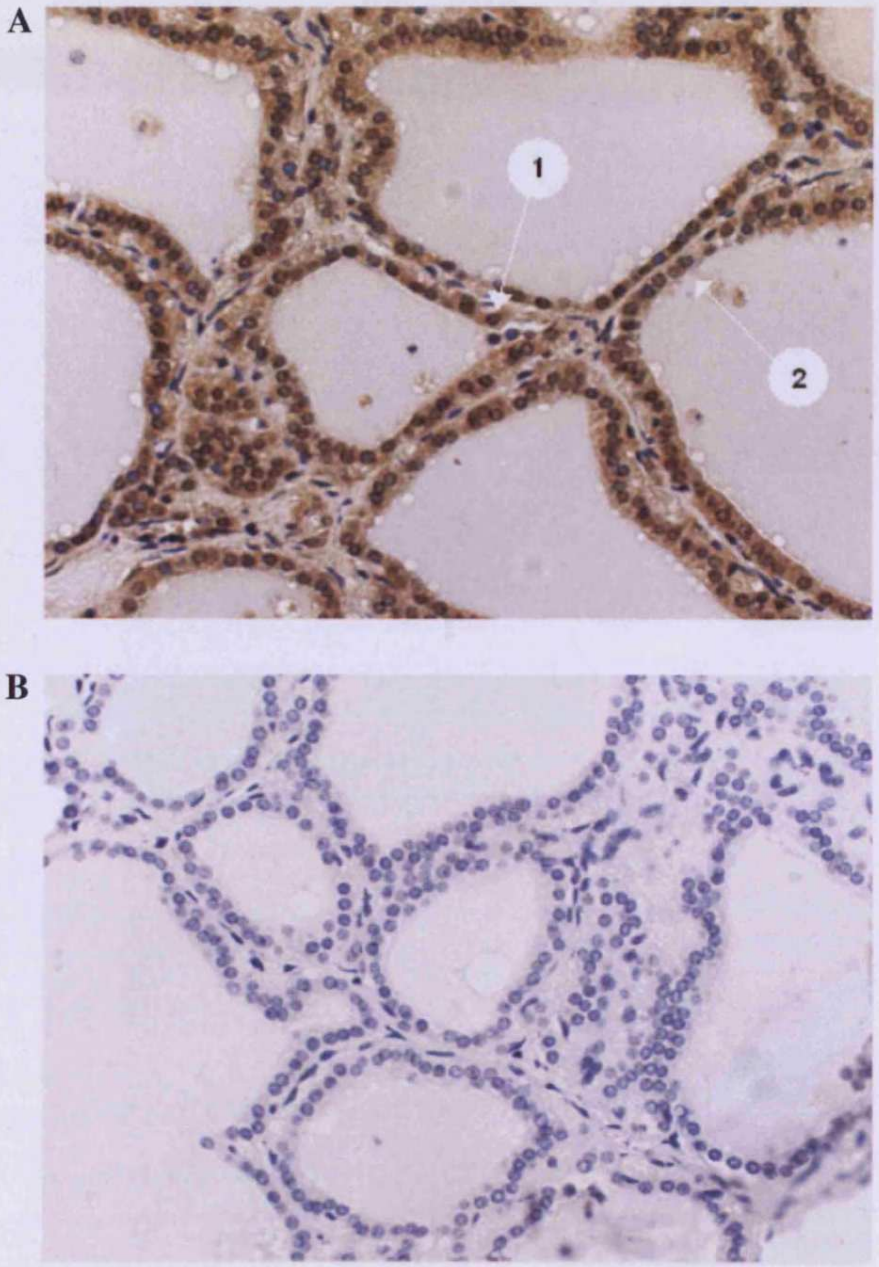

Figure 2.3. Paraffin Sections of Tissue from Beard Skin Showing Immunohistochemical Staining. A) Incubation with anti-FOXE1 pAb at 1:1,000 dilution, **B)** Incubation with PI at 1:1,000 dilution. (10× magnification).

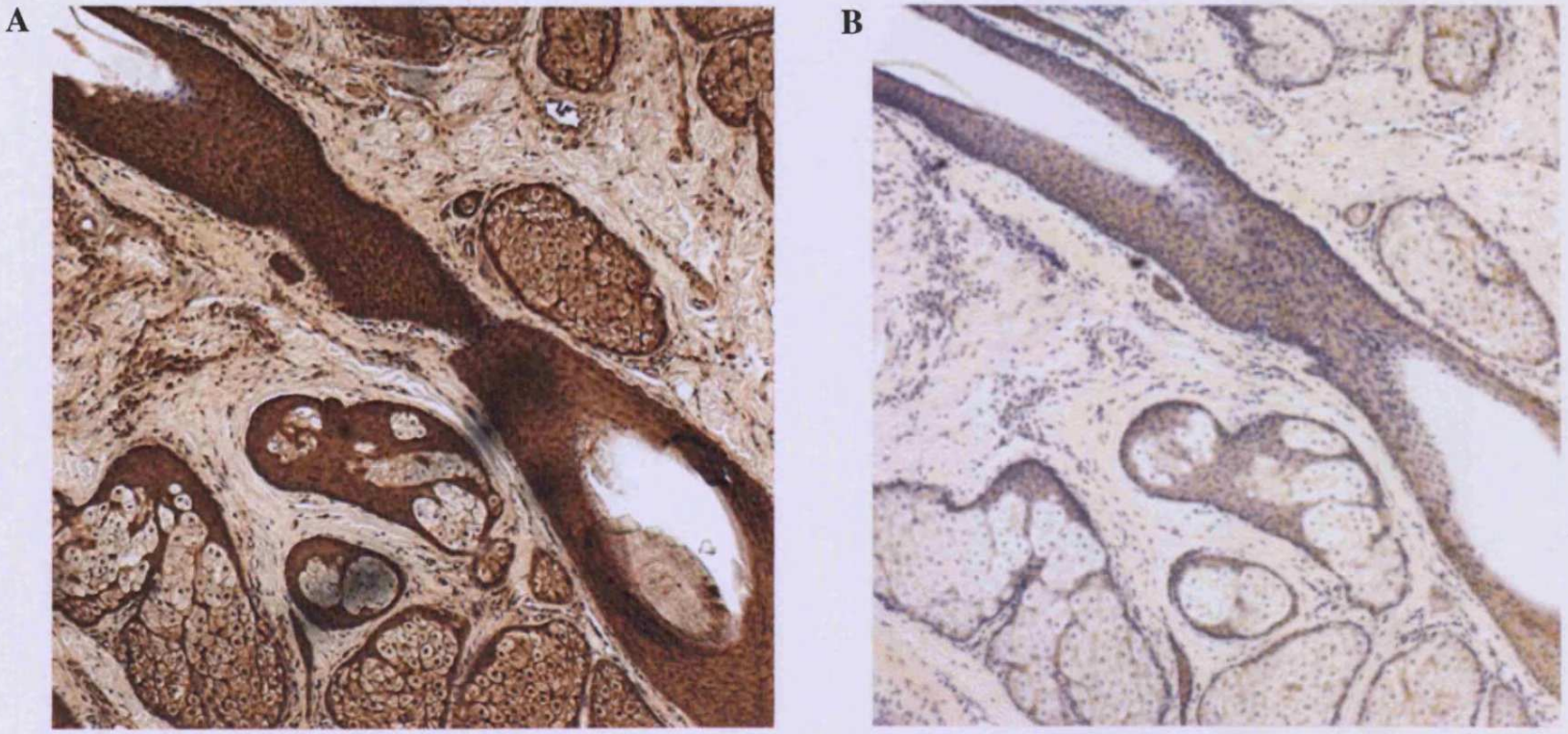

Figure 2.4. Paraffin Sections of Tissue from Beard Skin Showing Immunohistochemical Staining. A) Incubation with anti-FOXE1 pAb at 1:5,000 dilution. **B)** Incubation with PI at 1:5,000 dilution. (10× magnification).

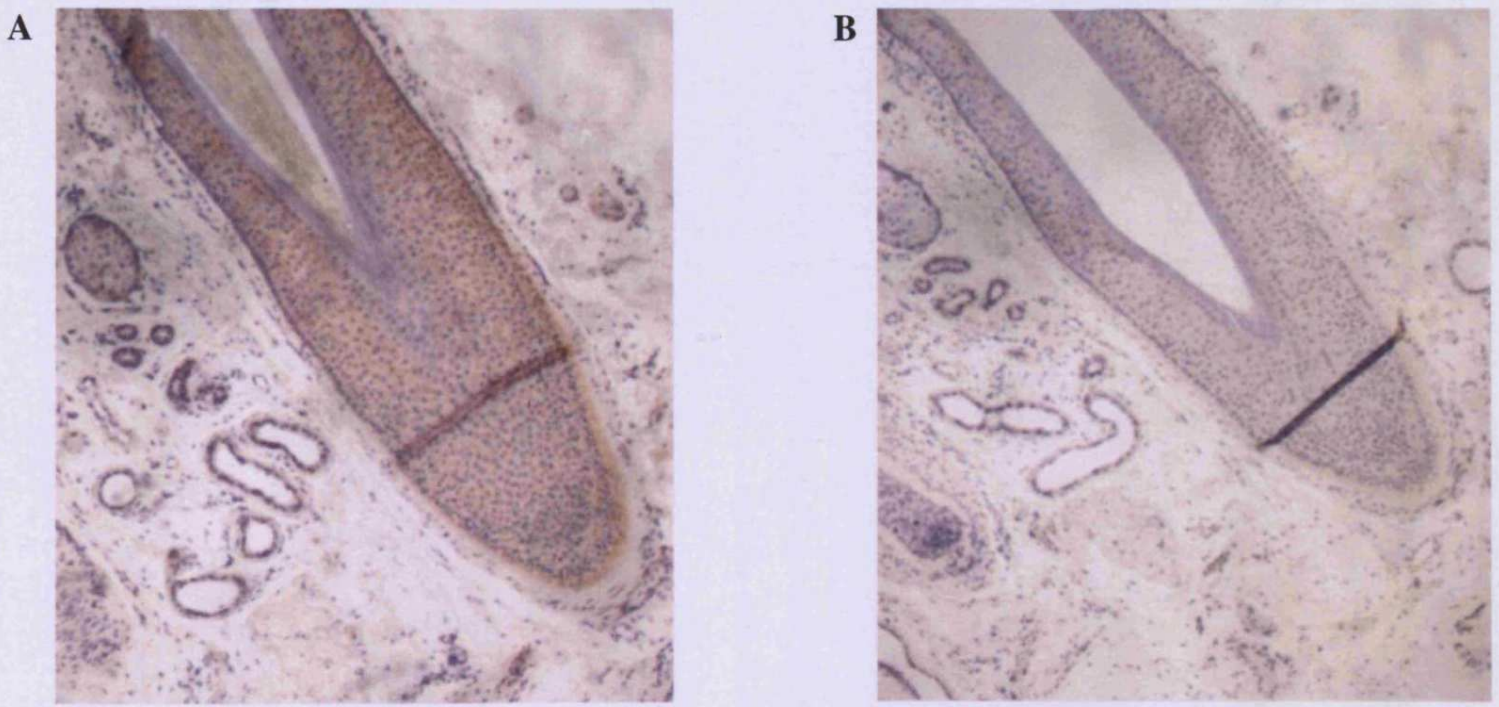

2.3.2. Affinity Purification of Anti-FOXE1 pAb

The same FOXE1-HIS fusion protein that was used to raise the anti-FOXE1 pAb was also to be used for the affinity purification of the antibody. This was to be achieved by coupling the FOXE1-HIS fusion protein to a CNBr sepharose column.

2.3.2.1. Bacterial Expression of FOXE1-HIS Protein

Bacterial expression of the FOXE1-HIS protein was performed using conditions recommended by Sequeira *et al* (2003). According to the authors, optimum expression of the FOXE1-HIS fusion protein by *E.coli* TOP10 was achieved after 4 hrs induction with 0.1 mM IPTG at 30°C. Aliquots were taken from the culture immediately before addition of IPTG and at 1 and 4 hrs after induction.

Coomassie blue staining confirmed that the total protein concentration of each sample was approximately the same. A major protein band could be seen at approximately 60 kDa (Figure 2.5A). A western blot of a similar gel probed with the anti-FOXE1 peptide pAb showed immunoreactivity with multiple proteins, however the highest immunoreactivity was shown with a protein at 60 kDa (Figure 2.5B). The higher sensitivity of the western blot also revealed there was an increase in the intensity of these protein bands, indicating that at least a small increase in FOXE1-HIS expression had occurred. An explanation for the immunoreactive proteins <42 kDa was that premature transcription termination resulted in the expression of truncated forms of FOXE1. The presence of the histidine tag might cause protein aggregation, providing a possible explanation for proteins >42 kDa. Later experiments found that increasing the incubation time to 6 hr produced more significant quantities of FOXE1 (data not shown).

Figure 2.5. Addition of IPTG to *E.coli* Topp 10 to Induce Expression of FOXE1. A) Coomassie blue stain of the bacterial lysate, prepared from 1 ml aliquots taken before and during induction, separated on a 10% polyacrylamide gel. **B)** A similar gel was western blotted and probed with a rabbit antibody raised against a synthetic peptide of FOXE1.

2.3.2.2. Nickel Column Purification of FOXE1-HIS

After nickel purification, western analysis using the anti-FOXE1 peptide pAb revealed that a 60 kDa protein (believed to be an aggregated form of FOXE1-HIS) to be a major component of the purified lysate eluted at 300 mM imidizole (Figure 2.6). As suggested earlier, immunoreactivity demonstrated at additional molecular weights could be explained due to the presence of truncated forms of FOXE1. However, immunoreactivity to the band at 25 kDa was also present in the preimmune serum from the rabbit used to raise the FOXE1 peptide antibody (Sequeira *et al.*, 2003). This indicated that the purified lysate was still contaminated with other proteins.

The amount of FOXE1-HIS protein present in the eluate from a single column was very small (µg quantities). Furthermore, repeated experiments showed that maximal FOXE1 protein did not always elute in the same fraction.

Figure 2.6. Analysis of Eluate. A 25 µl sample was taken from each of the elution fractions. These were separated by 10% SDS-PAGE, western blotted and probed with a rabbit antibody raised to a synthetic peptide of FOXE1. **1-6)** Successive 1ml fractions eluted with 300mM imidazole.

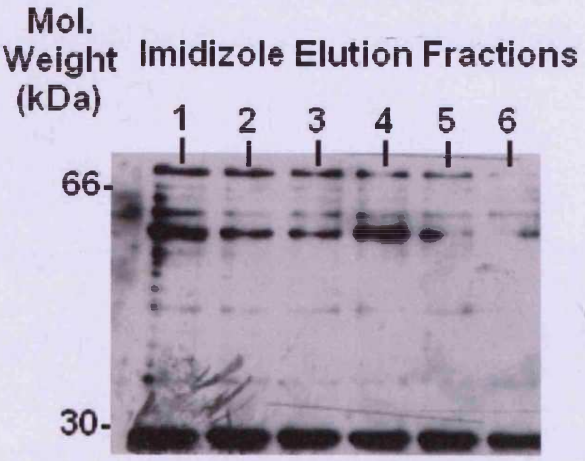

The results of the above experiments showed that despite repeated washing of the nickel column with native wash buffer, the purified lysate was still contaminated with other proteins that had a similar high affinity for the nickel-chelating resin as the FOXE1-HIS protein. If the minimum concentration of imidizole required to elute FOXE1 could be identified, assuming some proteins had a slightly lower affinity for the resin, then further purification could be achieved. Figure 2.7 shows the results of such an optimization experiment. After washing with native wash buffer, the column was washed further with progressively higher concentrations of imidizole. The first wash at 10 mM imidizole was able to remove some of the contaminating proteins without eluting FOXE1. The second wash with 25 mM imidizole resulted in removal of most of the remaining proteins but did elute some FOXE1. However, subsequent washes at higher imidizole concentrations showed that while 25 mM imidizole had completely removed most contaminating proteins, some FOXE1 still remained bound to the resin. Thus, a higher degree of FOXE1 purity was achieved, but this did not solve the problem of the low yield of FOXE1 produced by subsequent elution of the column with 300 mM imidizole.

Figure 2.7. Protein Composition of the Eluate Produced by each Concentration of Imidizole Elution Buffer. The elution fractions for each imidizole concentration were pooled and a 25 µl sample removed from each for SDS-PAGE analysis. The proteins were visualized by silver staining. **1)** Molecular weight marker, **2)** 10 mM Imidizole, **3)** 25 mM Imidizole, **4)** 50 mM Imidizole and **5)** 300 mM Imidizole elution buffer.

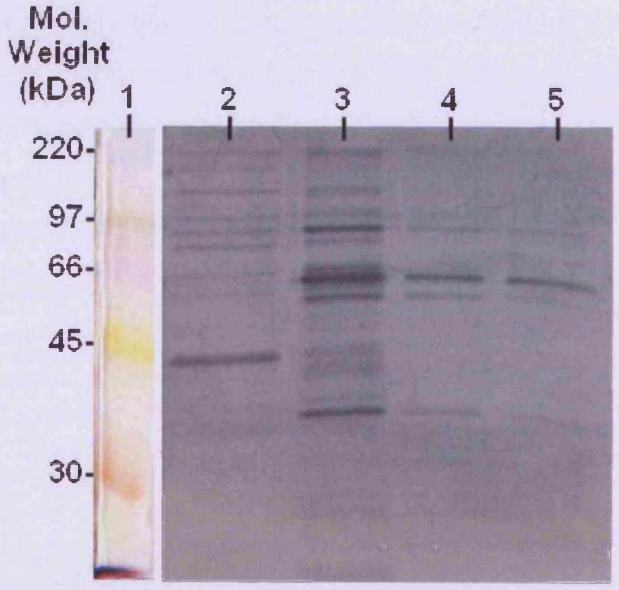

2.3.2.3. Purification of the FOXE1 pAb

As insufficient quantities of FOXE1 protein were produced for coupling to a CNBr sepharose column, an alternative approach to antibody purification was undertaken. In this technique developed by Gu *et al* (1994), the purified FOXE1 protein was maintained bound to the nickel resin. The nickel column itself was then used for the antigen-affinity purification of the FOXE1 pAb. Briefly, the standard purification protocol was performed as described early; but instead of elution of FOXE1-HIS with imidazole the column was equilibrated in a salt buffer that provided the optimum conditions for antibody binding (150 mM NaCl, 50 mM Tris-HCl, pH 7.4). Then the immune serum was added to the column and the antibody allowed to bind. The column was then washed with 5 column volumes of 150 mM NaCl buffer, followed by 5 column volumes of 2 M NaCl 50 mM Tris-HCl, pH 7.4. Finally, the antibody was eluted with one column volume of 4 M $MgCl_2$. To remove the $MgCl_2$ several elution fractions were collected and dialysed exhaustively against PBS.

Western analysis of the eluate from this purification (Figure 2.8), with an anti-rabbit IgG-HRP conjugate, revealed bands at 50 kDa and 25 kDa, equal to the molecular weights of the IgG heavy and light chains. A band at 42 kDa, equal to the predicted molecular weight of FOXE1, was also visible but appears to react less with the IgG-HRP conjugate.

Figure 2.8. Analysis of the Protein Content of Purified pAb. A 25 µl sample was taken from the 2 ml of pooled eluate and the proteins separated by 10% SDS-PAGE. The gel was blotted onto a PVDF membrane and probed with anti-rabbit IgG-HRP conjugate (1:5,000 dilution) and developed with ECL (2 mins exposure).

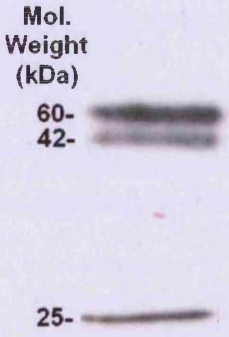

The purified anti-FOXE1 pAb was tested to determine its staining characteristics (e.g. optimum dilution for specific staining). The protocol that produced optimum results for the unpurified anti-FOXE1 pAb was used. As the characteristics of the serum were unknown a broad range of dilutions from neat to 1:10,000 were tested. Figure 2.9 shows that the FOXE1 pAb when used neat resulted in the tissue being over-stained (A) but at 1:10 dilution, there was no visible staining (B).

Figure 2.9. Determining the Staining Characteristics of the Purified Anti-FOXE1 pAb. Paraffin sections of tissue from beard skin were incubated with purified anti-FOXE1 pAb at a range of dilutions from neat to 1:10,000. The protocol optimised for the unpurified anti-FOXE1 pAb was used. **A)** Incubation with serum applied neat. **B)** Incubation with serum at 1:10 dilution.

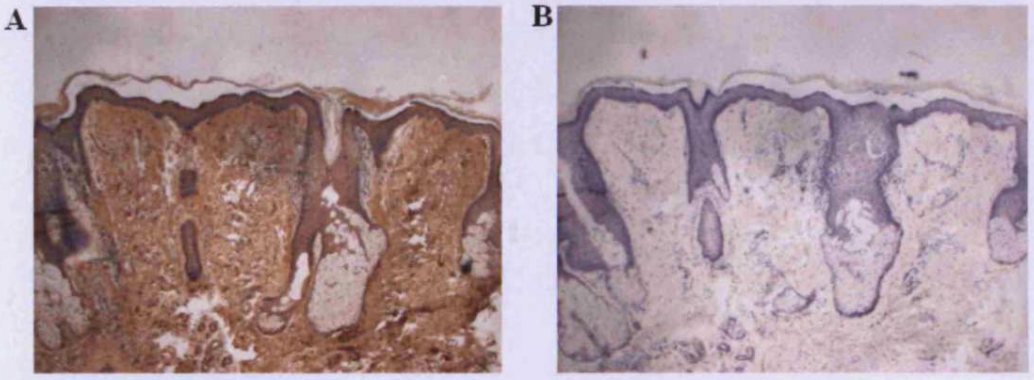

2.3.3. Alternative Methods of Dual Labelling

However, further characterisation of the anti-FOXE1 pAb, exploring the extent to which it could be diluted whilst maintaining definite positive staining, showed that the dilution could be raised to an unexpectedly high level (up to 1:20,000 dilution), reducing the non-specific background staining (data not shown). This demonstrated that specificity of the antibody was not the problem. Further attempts at immunofluoresence, experimenting with alternative methods of fixation (methanol, formaldehyde, etc) concluded that the anti-FOXE1 pAb was unsuitable for detection by this method.

Initial attempts at an enzymatic method of dual labelling, combining horseradish-peroxidase and alkaline phosphatase showed that the system was not as good as immunofluorscence for examining colocalisation of antigens (Figure 2.10). Ideally, in areas of overlap, the two chromophores should mix to produce a clearly distinguishable third colour, a task easily achieved with the use of primary colour fluorochromes. However, areas of overlap between the brown and red coloured end products of the DAB and the New Fuchin reactions could not be easily identified, as the colours were not sufficiently contrasting. Nickel chloride could be added to the DAB reaction mixture, producing an alternative blue coloured end product. Thus, when combined with the red alkaline phosphatase staining a clearly distinguishable purple colour could be produced. Although a possibility, optimisation proved to be difficult in order to obtain meaningful data.

Figure 2.10. Hair Follicle Sections Stained with FOXE1 and K17. **A)** K17 mAb at 1:100 visualised with alkaline phosphatase. **B)** Anti-FOXE1 pAb at 1:5,000 visualised with peroxidase (Dako Envision System), **C)** Dual labelling. All magnification: 20×

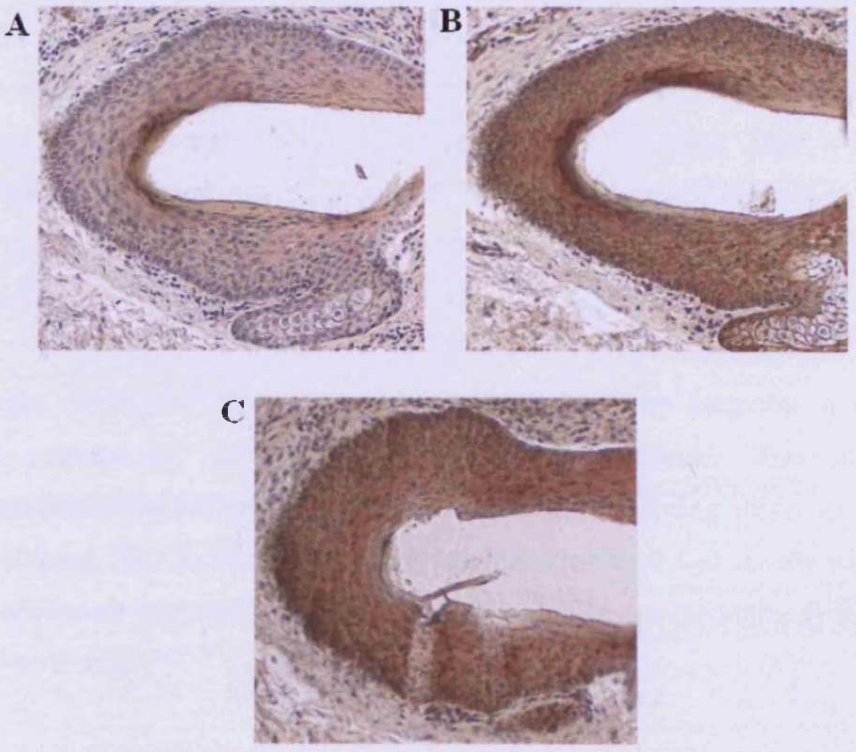

2.4. Discussion

Sequeira *et al* (2003) were the first to demonstrate that FOXE1 protein is expressed in human adult hair follicles. One of the initial goals of this project was to confirm this result. Immunohistochemical studies using the same anti-FOXE1 pAb, demonstrated immunoreactivity in the epidermis and the ORS of the hair follicle. An unexpected observation was to find that the levels of FOXE1 protein in skin were much higher than anticipated, being approximately ten times greater than those observed in Grave's thyroid tissue (diseased tissue in which FOXE1 is over-expressed). In addition, we also observed positive staining in the sebaceous glands, which had not previously been described.

These findings differ to the observations of Branaccio *et al* (2004), who found Foxe1 expression in mouse skin to be to be restricted entirely to the hair follicle. This difference between species was confirmed in a recent correspondence with the senior author of the paper who revealed that they too had observed FOXE1 protein in human epidermis (they did not mention if they had seen staining of the sebaceous glands). Interestingly, patients with Bamforth-Lazarus syndrome in addition to having abnormal hair growth also have flaky skin, suggesting a possible defect in epidermal differentiation (Bamforth *et al.*, 1988). In contrast, histological analysis of Foxe1$^{-/-}$ skin grafted onto nude mice showed the epidermis to be normal in appearance (Branaccio *et al.*, 2004). Thus, it appears that FOXE1 has an important role to play in the human epidermis, but not in that of the mouse. This obviously raises questions of the suitability of the mouse model in understanding the role of FOXE1 in human skin.

Interestingly, in contrast to the nuclear staining reported by Sequeira *et al*, we only observed cytoplasmic staining of the ORS keratinocytes. This was despite experimentation with several different IHC protocols, including different methods of antigen retrieval. The ability of the pAb to produce the expected results when staining sections of Graves' thyroid tissue ruled out the possibility that the antibody had degraded in long-term storage.

One possibility that could explain our different results, and if true may lead to new insights into FOXE1 biology, is that the expression pattern of FOXE1 varies between hair follicles obtained from different body sites. Due to a lack of patient material our study was restricted to the analysis of biopsies from beard skin, whereas Sequeira *et al* had access to skin biopsies from variety of different body locations. If nuclear staining was observed in the hair follicles of non-beard skin (unfortunately the authors did not state what type of skin they used) then this would be in support of such an idea. If a variety of skin biopsies from different body sites could be obtained, then a single experiment would be sufficient to prove this hypothesis.

Having confirmed FOXE1 expression, the next aim of the project was to perform colocalisation experiments with known hair follicle proliferation and differentiation markers, to determine whether FOXE1 expression was specific to certain cell-lineages or regions of the hair follicle. The preferred method of choice for observing dual-labelled antibodies in tissue is by immunofluorescence. However, despite good results when using the anti-FOXE1 pAb antibody in IHC, preliminary fluorescein isothiocyanate (FITC) studies by Sequeira *et al* (2003) showed that the antibody produced high background levels of staining. It was decided that the pAb did not possess the necessary specificity and that purification of the immune serum was required. The initial approach was to obtain a sufficient quantity of pure FOXE1 to couple to a CNBr sepharose column, to affinity purify the FOXE1 pAb. However, the method we used to purifying histidine tagged FOXE1 produced poor yields. Despite Sequeira being able to obtain obtaining yields of 9mg/L of bacterial culture using the same system, be were unable to generate µg quantities.

Sequencing of the pTrcHis construct confirmed its identity and the absence of any mutations that would compromise protein expression. Solubility of fusion proteins is a common problem, but it is not clear why this should have arisen. A possible reason, and a common problem with histidine tagged proteins, is that they have a high affinity for one another and form aggregates that are then unable to bind the nickel resin.

One of the major problems we faced was our inability to confidently detect the recombinant FOXE1 protein. Detection of the FOXE1 protein in the eluate was performed by western blot analysis using an anti-FOXE1 peptide pAb. Confusingly, the Ab did not detect a protein at the predicted molecular weight of FOXE1 (42 kDa), but instead had high affinity for a protein at 60 kDa. Subsequent experiments (see Chapter 4) taught us that this higher molecular weight protein is actually an aggregated form of FOXE1 protein, an artefact of the method used for sample preparation. However, at the time we were not sure if this higher molecular weight protein was due to non-specific binding or protein aggregation. We hypothesised that if aggregation was the cause; it may be due to the presence of the histidine tags as described above.

The pTRcHis construct was designed to express an N-terminal His Tag. As a result truncated forms of FOXE1 that result from premature termination of translation or protein degradation would have been co-purified along with full-length FOXE1. We believe this to be the source of the low molecular weight proteins detected by western blot analysis of the eluate. Future attempts to purify FOXE1 could use an expression vector that attaches C and N-terminal tags to the protein, which would have a higher affinity for the nickel column, thus allowing the full-length FOXE1 to be isolated.

Having failed to produce sufficient quantities of FOXE1 to couple to a CNBr sepharose column we decided to try an alternative approach to affinity purifying immune serum. Combining the optimised FOXE1 purification protocol with a method by Gu *et al* (1994), this used the purified FOXE1 bound to the nickel resin to affinity purify the anti-FOXE1 pAb. Western blot analysis of the final eluate revealed two bands at 50 and 25 kDa, equal to the molecular weight of the heavy and light chains of an Ab, indicating that antibody was present in the eluted fractions. Also present was a protein with a molecular weight equal to that estimated for FOXE1. This indicated that the elution of the column with 4 M $MgCl_2$ was sufficient to elute the entire antigen-FOXE1 complex from the nickel resin. This may be undesirable as the presence of FOXE1 in the pAb may block binding of the FOXE1 specific antibodies to FOXE1 present in tissue. Results of the immunohistochemistry with the purified pAb indicated that this might be the case, as it

possessed some unusual staining characteristics (high background when applied neat, but negative staining at 1:10 dilution). If so, the use of milder elution conditions could be investigated to prevent elution of FOXE1.

In summary, although technical difficulties prevented us from performing the intended series of colocalisation experiments, we have still been able to make some novel findings and have generated results, which will prove useful in the design of future experiments.

It is well documented that there are major disadvantages associated with using mouse models to understand human hair skin function, owing to the many subtle differences there are between the species. We and others have made observations that suggest that FOXE1 may play an important role in the human epidermis, but not in mouse.

The purely cytoplasmic staining we observed in the ORS keratinocytes would suggest that the activation of FOXE1 is not required in these cells. Maybe FOXE1 activity is only required in certain types of hair follicle. We have observed for the first time the expression of FOXE1 in the sebaceous gland, and have shown that the overall level of expression of FOXE1 is at a much higher level than in the thyroid gland. The high level of FOXE1 protein throughout the skin and its appendages suggests that it plays an important role in skin biology.

Chapter 3.

Bioinformatics: Search for Potential Downstream Targets of FOXE1

3.1. Introduction

The work of Branaccio *et al* (2004) led us to look for likely candidate genes that would be involved in hair follicle remodelling. A review of the literature generated a number of likely genes for further investigation:

Matrix metalloproteinases (MMPs)

GLI2 and GLI1 are known regulators of FOXE1 expression in human keratinocytes (Eichberger *et al.*, 2004). Over-expression of activated GLI2 or GLI1 resulted in repression of MMP1, MMP10 and MMP13 expression after 24 hrs, and, reversal of this repression after 72 hrs (Eichberger *et al.*, 2006). The authors suggested that this regulation was likely mediated by FOXE1, which strongly induces expression of these genes when overexpressed in HaCaT (Eichberger *et al*, unpublished observations).

Tissue Inhibitor of MMPs 3 (TIMP3)

Zeng *et al* (1998) found high levels of human TIMP3 promoter activity in those tissues of the foetal mouse that undergo extensive tissue remodelling: bones, joints, hair follicles, sweat glands and teeth. In adult human skin, TIMP3 mRNA was detectable in the hair follicles but absent from the epidermis, sebaceous and sweat glands. This expression was restricted to the basal cell layer of the outer root sheath surrounding the lower portion of the hair follicle (Airloa *et al.*, 1998). This was very similar to the spatial pattern of Foxe1 expression found in the hair follicles of normal mice (Branaccio *et al.*, 2004). The temporal pattern of TIMP3 and Foxe1 expression was also very similar with both being upregulated during anagen, lost during catagen and absent during telogen (Airloa *et al*, 1998; Branaccio *et al.*, 2004).

More recently, TIMP3 expression has been shown to be regulated by another forkhead transcription factor FOXO1A (Grinius *et al*, 2006; Buzzio *et al*, 2006).

3.1.2. Bioinformatics

3.1.2.1. Representing Transcription Factor Binding Sites

Many of the approaches to computational prediction of functional transcription factor binding sites are based upon pattern matching. Pattern matching utilizes previous knowledge of verified binding sites for a given protein. Finding these patterns within the human genome may thus represent uncharacterised regulatory elements (Van Helden, 2003). The simplest representation is a consensus sequence, created by alignment of experimentally verified binding sites, and recording the possible nucleotides that can occur at each position. To represent different bases that can occur at the same position, the degenerate code defined by the International union of Pure and Applied Chemistry (IUPAC) commission is used. This consists of a 15-letter alphabet, where a single letter can represent one or several nucleotides (Table 3.1).

Although consensus sequences are able to represent the fact that more than one base can be found at a given position, binding bias towards one of the possible nucleotides is not reflected in the model. However, this additional information can be included with position weight matrices (PWMs) or position scoring matrices (PSSMs). These incorporate pattern variability by recording the frequencies of nucleotides at each site, or by assigning penalties to nucleotides that should not appear. Such matrices can be generated by specific programs (e.g. consensus, gibbs), or imported from databases on transcriptional regulation, such as TRANSFAC (Heinemeyer *et al.*, 1998). Although matrix models represent an improvement over consensus sequences in sensitivity (i.e. they have a lower false negative rate), when used as the sole means of identifying binding sites they still suffer from the limited amount of experimental data available (Roulet *et al.*, 1998) and often result in a high rate of false-positive predictions (Tompa *et al.*, 2005; Jolly *et al.*, 2005).

Table. 3.1. IUPAC Nucleotide Ambiguity Symbols

Symbol	Nucleotides	
A	Adenine	A
C	Cytosine	C
G	Guanine	G
T	Thymine	T
R	puRines	A or G
Y	pYrimidines	C or T
W	Weak bonding (2 Hydrogen bonds)	A or T
S	Strong bonding (3 Hydrogen bonds)	G or C
M	aMino group at common position	A or C
K	Keto group at common position	G or T
H	not G	A, C or T
B	not A	G, C or T
V	not T	G, A, C
D	not C	G, A or T
N	aNy	G, A, C or T

3.1.2.2 Pattern detection

A number of algorithms have been developed for the *de nova* pattern detection. Examples include Hidden Markov Models (Pedersen & Moult, 1996), Gibbs sampling (Lawrence *et al.* 1993) and greedy alignment algorithms (e.g., CONSENSUS, Hertz & Stormo, 1999).

The web resource Regulatory Sequence Analysis Tools (RSAT) (http://rsat.ulb.ac.be/rsat) provides a collection of software tools dedicated to the prediction of regulatory sites in non-coding DNA sequences. The main tools featured include sequence retrieval, pattern discovery, pattern matching, genome-scale pattern matching, feature-map drawing, and random sequence generation. Alternative formats are supported for the representation of regulatory motifs (strings or position-specific scoring matrices) and several algorithms are proposed for pattern discovery. RSAT currently holds >100 fully sequenced genomes and these data are regularly updated from GenBank.

3.1.2.3. Chapter Aims

The aim of this chapter was to apply a bioinformatics approach to identify potential direct downstream target genes of FOXE1. This was to be achieved through the generation of a consensus sequence based on the two known FOXE1 binding sites. The Genome-Scale Patter program from RSAT was used to search the upstream regulatory regions of known and predicted genes within the human genome for sequences matching this consensus sequence. The sequences generated by our search were filtered to provide a list consisting entirely of TIMP and MMP genes.

3.2. Materials and Methods

This figure (3.1) demonstrated the settings used to search for the consensus sequence.

Figure 3.1. User-Interface of the (strings) program

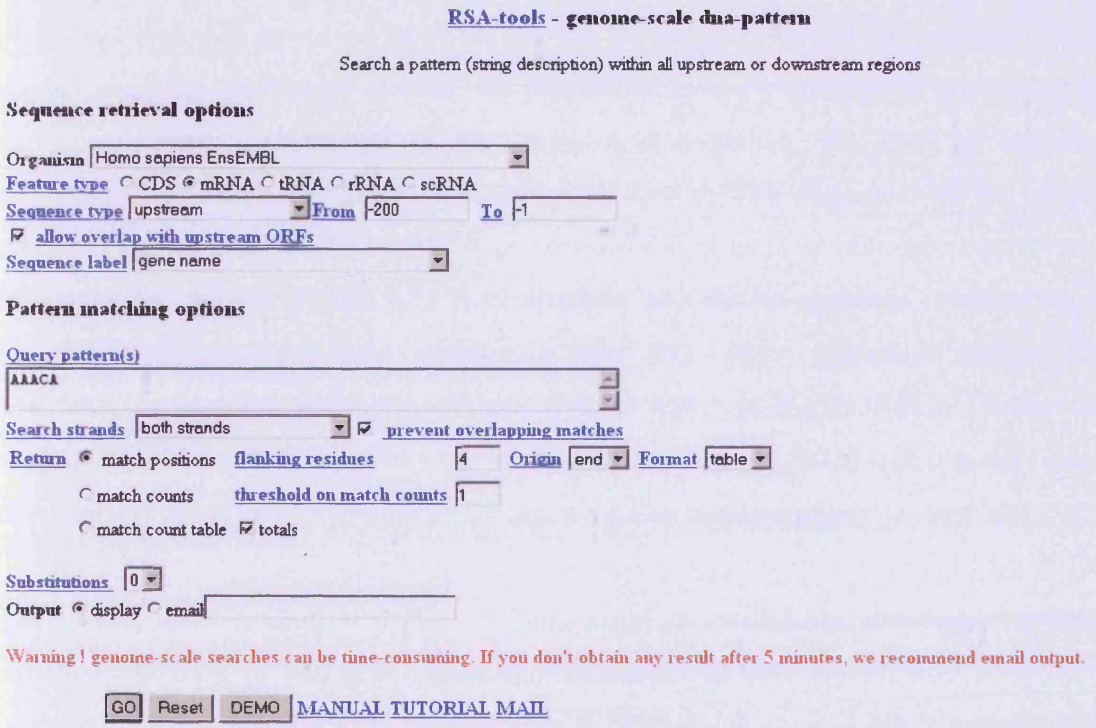

3.3. Results

3.3.1. Generation of a DNA-Binding Consensus Sequence Compatible with Known FOXE1 Binding Sites

3.3.1.1. Phylogenetic Analysis of FOXE1 Proteins

A transcription factor consensus sequence is derived from all experimentally verified binding sites. At the time of this study the only two experimentally verified binding sites for FOXE1 were the Z and K regions, located within the proximal promoters of rat TPO and TG genes respectively. As only two binding sites were available, a position weight matrix could not be generated, and the consensus sequence would have to be composed of the less informative IUPAC code.

Differences in the DNA-binding specificity of human and rat FOXE1 could mean that the consensus sequence generated from the two rat binding-sites would be inappropriate for use in searching the human genome. As the DNA-binding properties of a transcription factor are largely determined by its amino acid sequence, the level of sequence conservation between rat and human was investigated. The alignment of rat, mouse, macaque and human FOXE1 revealed an extremely high level of sequence conservation between these species (Figure 3.2). A comparison with the rat sequence revealed 98, 85 and 87% conservation of the mouse, macaque and human sequences respectively. Sequence conservation within the forkhead domain was even higher with all four species sharing ≥ 98% conservation. The high sequence similarity suggested that it is very likely that their structural and functional properties were also highly similar.

The similar DNA-binding properties of human and rat species has also been confirmed experimentally, by the ability of human FOXE1 to activate transcription from an artificial promoter consisting of rat TPO binding sites (Clifton-Bligh *et al.*, 1998; Castanet *et al.*, 2002).

Figure 3.2. Alignment of FOXE1 Amino Acid Sequences from Four Mammalian Species. The forkhead DNA-binding domain is boxed. Amino acids are coloured on the basis of the physiochemical properties considered important for determining protein structure: red for hydrophobic residues, blue for acidic, purple for basic and green for polar residues. The level of sequence conservation at each of the aligned positions is also represented: (*) means all the amino acid residues are identical, (:) means conserved substitutions have been observed and (.) means semi-conserved substitutions have been observed.

3.3.1.2. Phylogenetic Analysis of TPO and TG Proximal Promoters

Alignment of the rat TPO and TG promoters with those of four other mammalian species revealed a high level of sequence conservation in these regions. Of particular interest, were those aligned positions corresponding to the FOXE1 binding sites (designated K and Z-regions). In the case of thyroglobulin K-region, comparison with the rat sequence

revealed the mouse to have 95% sequence conservation, while the other three species all shared 76% conservation. However, those nucleotides that have been shown to make direct contacts with the FOXE1 protein (Francis-Lang *et al.*, 1992) were 100% conserved among all five species (Figure 3.3.)

The Z-region of the TPO promoter was less well conserved among the five species. Interestingly, the Z region of the primate species contained additional nucleotides not present in two rodent species. As a result the region no longer contains the sequence AAYA that appears to be a requirement of all forkhead-binding sites. However, this sequence is present at several other sites within the human promoter (Figure 3.3.)

Figure 3.4 demonstrates how the FOXE1 consensus sequence was generated from the alignment of the K and Z regions.

Figure 3.3. Sequence Alignment of the TPO and TG Proximal Promoters from Five Mammalian Species. Aligned regions that correspond with known transcription factor binding sites in the rat TPO and TG promoter are boxed. Those nucleotides that are conserved among all five species are designated by an (*), and the forkhead core sequence (AAYA) is highlighted in red.

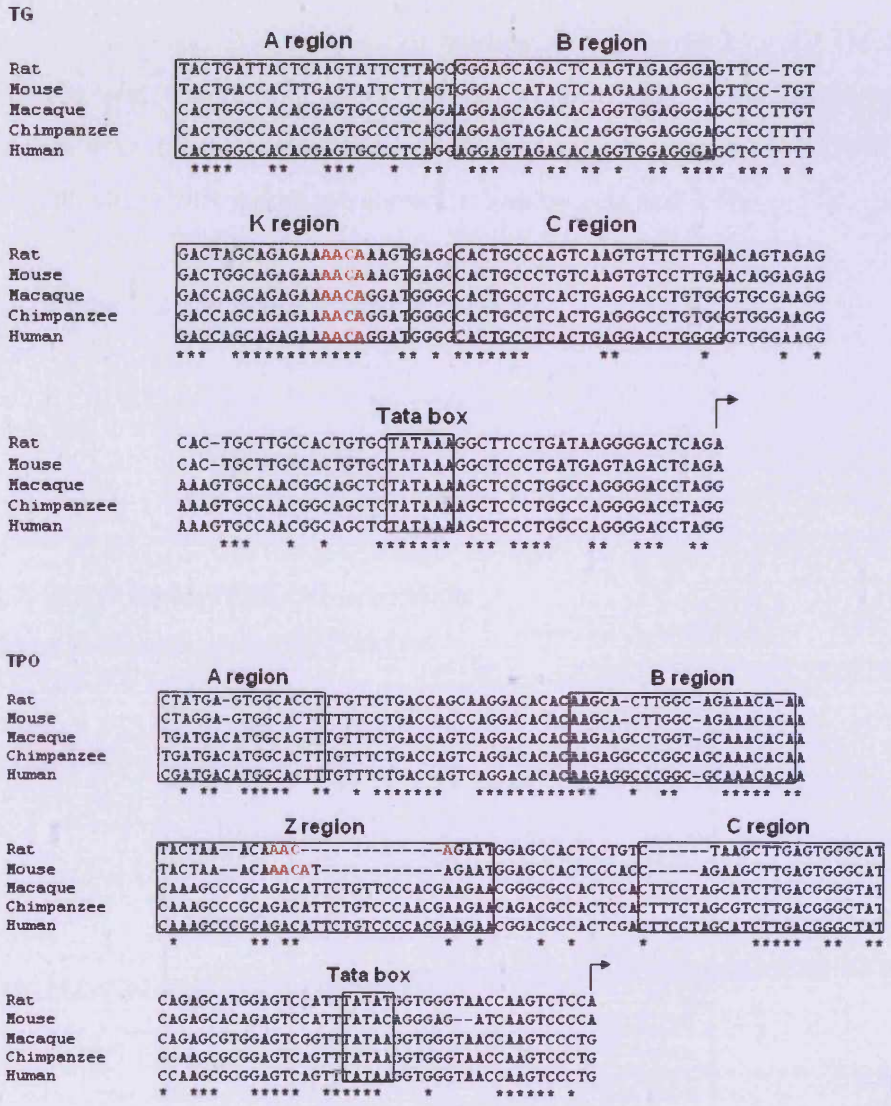

Figure 3.4. Generation of the FOXE1 Consensus Sequence. The forkhead core sequence is shown in red.

```
Core                AAYA
K-region   GCAGAGAAAACA
Z-region   ACTAAACAAACA
Consensus          AAACA
```

We looked for TPO and TG in the list of binding sites generated by the Genome-Scale-Pattern search and found both to be present (Table 3.2.) This confirmed that the programme was working successfully. Next, the list was searched for TIMP and MMP genes. The results of this search are shown in Tables 3.3a and 3.3b.

Table 3.2. Known target genes (positive control)

Gene	Position		Sequence
TPO	-124	-120	gcgcAAACAcaac
TPO	-162	-158	tcagAAACAaagt
TG	-99	-95	gagaAAACAggat

Table 3.3. Genes involved in cell-migration

a. Matrix metalloproteases (MMPs)

Gene	Position		Sequence
MMP1	-191	-187	cttcAAACAagat
MMP3	-46	-42	atccAAACAaaca
MMP7	-78	-74	aagaAAACActca
MMP8	-72	-68	tcttAAACAattg
MMP10	-197	-193	tacAAACAcaga
	-78	-74	taaaAAACAcatg
	-102	-98	tcacAAACAttta
MMP13	-183	-179	gctgAAACAagag
	-96	-92	aggtAAACAtgct
MMP20	-123	-119	tctcAAACAgtaa
	-82	-78	agtcAAACAggtc
MMP26	-196	-192	ttaaAAACAcctt
	-107	-103	tatgAAACAcaaa
MMP27	-175	-171	tactAAACAattg
	-183	-179	tagtAAACAcagt

b. Tissue inhibitors of MMPs (TIMPs)

Gene	Position		Sequence
TIMP3	-53	-49	tttcAAACAtgcc
TIMP4	-97	-93	cagcAAACAgtaa

3.4 Discussion

The aim of this chapter was to identify genes involved in ECM remodelling (specifically the ECM that surrounds hair follicles) that could be potential downstream targets of FOXE1, as judged by the presence of forkhead consensus binding sites within their proximal promoters. The most promising candidate genes were then chosen for further investigation in Chapter 4.

A comparison of hair follicle and thyroid gland development revealed that the early developmental stages of these organs are actually quite similar. The first stage of thyroid gland morphogenesis involves a thickening of a region of endodermal epithelium, located in the floor of the primitive pharynx. These endodermal cells then proliferate and invade the surrounding mesenchyme. Similarly, hair follicles form as thickenings in the ectodermal epithelium, which then subsequently grow downward into the mesenchyme beneath. FOXE1 has been shown to play an essential role in the migration of these epithelial cells. De Felice *et al* (1998) found that in the case of the developing thyroid, the absence of FOXE1 resulted in failure of the epithelial cells to migrate, and they remained attached to the wall of the primitive pharynx. Branaccio *et al* (2004) demonstrated that although the developing hair follicles were able to descend into the mesenchyme, the mechanism that controlled the direction of this migration was disrupted.

How the epithelium of the primitive hair follicle invades the mesenchyme still remains unclear. Fortunately, the mature hair follicle (which as been studied in much more detail) undergoes constant cycles of remodelling throughout adult life, and the anagen (growth phase) closely resembles follicle morphogenesis. The downward movement of the growing follicle is driven by growth pressure as a consequence of cell proliferation rather than active migration of the keratinocytes. However, in order for the cells to penetrate the dermis, they have to loosen the collagen and elastin matrix that lies in their migratory path. Unsurprisingly then, the anagen follicle has been found to be associated with the production of ECM remodelling enzymes e.g. MMPs

Recently, Eichberger *et al* (2004) observed that overexpression of GLI1 and GLI2 (known activators of FOXE1 expression) in epidermal keratinocytes resulted in the modulation of MMP1, MMP10 and MMP13 expression, and this was likely to be mediated by FOXE1 (based upon their unpublished observations). This, together with the observations described above, led to the hypothesis that FOXE1 controls cell-migration by modulating the expression of genes that encode proteins involved in ECM remodelling.

Using a bioinformatics approach, we obtained a list of MMPs and TIMPs (the natural inhibitors of MMPs), which contain forkhead binding sites in their proximal promoters. The list included MMP1, MMP10 and MMP13 and so it was decided that these would be a good candidate genes for investigation. However, due to time constraints, we decided that we would only examine MMP13 in this study. The others will be studied in future experiments.

Also of particular interest was TIMP3, which is expressed by the ORS keratinocytes of the anagen follicle. In fact, the spatio-temporal pattern of TIMP3 as described by Airloa *et al* (1998) showed some striking similarities with that of FOXE1. Both are expressed by the basal ORS keratinocytes surrounding the lower portion of the hair follicle and both are upregulated during anagen and downregulated during catagen. TIMP3 has been shown to be regulated by another forkhead transcription factor FOXO1A (Grinius *et al*, 2006; Buzzio *et al*, 2006.) Therefore, it was also chosen as one of our candidate genes.

Hishinuma *et al* (2001) observed that overexpression of FOXE1 in a thyroid cell-line resulted in upregulation of the COL1A1 (a major constituent of dermis). We decided that it would be worthwhile to investigate if a similar relationship occurs in keratinocytes. Although, we did not detect a forkhead-binding site in the proximal promoter of COL1A1 it is possible that such a regulatory site was present further upstream/downstream of the transcriptional start site. Alternatively, the FOXE1 overexpression may have enhanced COL1A1 by an indirect mechanism e.g. by inducing expression of another transcription factor which modulates COL1A1 expression.

Chapter 4.
Gene Expression Profiling and siRNA Knockdown Experiments

4.1. Introduction

4.1.1. Identification of Potential Direct Target Genes of FOXE1 in Skin

Before this study, only two genes were known to be direct downstream targets of FOXE1. These were the thyroid-specific TG (Civitareale *et al.*, 1989) and TPO (Francis-Lang *et al.*, 1992) genes. In Chapter 3, we used a bioinformatics approach to identify human genes which possess forkhead binding sites within their proximal promoter. On the basis of the findings by Branaccio *et al* (2004), we hypothesised that FOXE1 controls the orientation of the growing hair follicle, by modulating the expression of genes that encode for proteins involved in ECM remodelling. Therefore we searched our list of potential forkhead target genes for those known to involved in such processes e.g. MMPs and TIMPs. As discussed in Chapter 3, a literature search provided further evidence in support of three of these genes (TIMP3, MMP13 and COL1A1) being regulated by FOXE1. In this chapter we used a combination of QPCR-based expression profiling and siRNA-based gene knockdown to determine whether these genes were indeed targets of FOXE1.

4.1.2. Identification of a Role for Calcium Signalling in Controlling FOXE1 Expression in Skin

Recently, it has been shown that in addition to the cAMP-dependent protein kinase A (PKA) and IGF-I signalling pathways, FOXE1 expression in the mature thyroid gland is also regulated by calcium signalling. D'Andrea *et al* (2005) were able to demonstrate that this control was mediated by the transcriptional repressor DREAM (downstream regulatory element antagonistic modulator).

DREAM, also known as Calsenilin (Buxbaum *et al.*, 1998), was first identified in neuroblastoma cells as a transcriptional repressor of the human Prodynorphin gene (encodes for a neuropeptide precursor), which contains a consensus sequence called DRE

(downstream regulatory element) in its 5'-UTR, to which DREAM binds (Carrion *et al.*, 1999).

It possesses significant homology with members of the neuronal calcium sensor (NCS) protein superfamily, and possesses four Ca^{2+} chelating EF-hand motifs (Carrion *et al.*, 1999). It is among the first transcription factors to be regulated directly by the binding of Ca^{2+}. In the absence of stimulated levels of nuclear calcium, DREAM binds with high affinity to DRE sites as a tetramer. However, upon stimulation and increase of nuclear calcium, Ca^{2+} ions bind to DREAM and induce a conformational change that causes the complex to dissociate into dimers, which are then unable to bind to DNA (Osawa *et al.*, 2001).

As the majority of functional DRE sites have been found localised downstream of the TATA box, it has been hypothesized that the DREAM complex represses transcription by physically impeding the movement of the transcriptional machinery along the gene (Ledo *et al.*, 2000). Interestingly, in addition to calcium, DREAM mediated derepression of the prodynorphyn gene was shown to occur via activation of the PKA signalling pathway, a surprising finding since DREAM did not possess any PKA phosphorylation motifs (Carrion *et al.*, 1998 & 1999). However, the mechanism of this regulation was solved when DREAM was found to physically interact and form a complex with αCREM, an interaction that was strengthened by PKA-mediated phosphorylation of αCREM (Ledo *et al.*, 2000). The binding of αCREM to DREAM was found to cause the DREAM complex to dissociate from the DRE site, thus enabling prodynorphyn gene to be transcribed (Ledo *et al.*, 2000). Therefore, neuroblastoma cells DREAM activity can be regulated through two distinct and parallel signalling pathways, calcium and PKA activation.

In this chapter we able to detect DREAM expression in cultured keratinocytes, and using an siRNA based approach produced evidence that DREAM is able to modulate FOXE1 expression, mirroring the role that it plays in the thyroid gland.

4.1.3. Epidermal Differentiation Model

The technical difficulties faced with creating *in vitro* models of the human hair follicle (Randall *et al.*, 2003) led us to focus our attention on the role of FOXE1 in the human epidermis. An *in vitro* model for epidermal differentiation was created, based on the commonly used calcium-switch method. With limited availability of human tissue, sufficient quantities of primary keratinocytes were not available. Thus, we used HaCaT cells, a widely used and well-characterised human epidermal keratinocyte cell-line.

HaCaT (calcium- and temperature-dependent) is a spontaneously immortalised human epidermal keratinocyte cell-line. Despite the presence of extensive chromosomal abnormalities, HaCaT has a highly preserved differentiation capacity (Boukamp *et al.*, 1988). It is also capable of forming epidermal-like organization in organtotypic cultures (Schoop *et al.*, 1999; Mass-Szabowski *et al.*, 2003) and of forming an epidermis when transplanted onto nude mice (Breitkreutz *et al.*, 1998).

Proliferation and differentiation of keratinocytes is regulated by changes in the extracellular Ca^{2+} concentration. An increase in Ca^{2+} concentration in the culture media (a calcium-switch) results in a several-fold increase in the intracellular Ca^{2+} concentration (Jones *et al.*, 1994; Bikle *et al.*, 1996). This is followed by G1/G0 cell-cycle arrest via the activity of the cyclin-dependent kinase inhibitors $p21^{Cip1/WAF1}$, $p27^{KIP1}$ (Missero *et al.*, 1996) and $p16^{INK4a}$ (Paramio *et al.*, 2001). Differentiation occurs in parallel and the cells flatten, assemble adherens and desmosome type intracellular junctions and synthesize differentiation markers such as involucrin and keratins (K1 and K10).

To date, only one group has reported FOXE1 expression in cultured human keratinocytes. Eichberger *et al* (2004; 2006) reported that FOXE1 mRNA levels were increased in HaCaT cells and primary human keratinocytes, over-expressing either GLI1 or an activated form of GLI2. Unfortunately, analysis of FOXE1 expression was confined to the mRNA level, and the effect on the level of FOXE1 protein in these cells was

undetermined. Importantly, the authors also failed to describe if detectable levels of FOXE1 were present in the non-transfected keratinocytes.

4.1.4. Gene Expression Profiling

Our aim was to monitor the expression profile of FOXE1 and each candidate downstream genes throughout keratinocyte differentiation using real-time quantitative PCR (real-time QPCR). The expressions profiles would then been compared, looking for any similarities that could be indicative of a common mechanism of regulation.

4.1.4.1. Limitations of Endpoint QPCR

In endpoint QPCR, reaction products are run on an agarose gel and stained with ethidium bromide (EtBr). The level of EtBr fluorescence is then used to back-calculate the amount of DNA template that was present prior to amplification. This method of quantification assumes that reaction efficiency remains constant throughout the amplification. However, as the amplification proceeds, reagents are consumed and reaction inhibitors accumulate, causing the reaction efficiency to decrease. These effects can vary from sample to sample, which will result in differences in the final fluorescence values that are not related to the starting amount of DNA template (Figure 4.1). Therefore, this method is not suitable for the precise measurements required for gene expression analysis.

Figure 4.1. Amplification Plots for 96 Identical PCR Reactions. Despite identical samples and reaction conditions being used for each reaction, the fluoresence readings taken at the reaction endpoint show great variability (Stratagene, 2005).

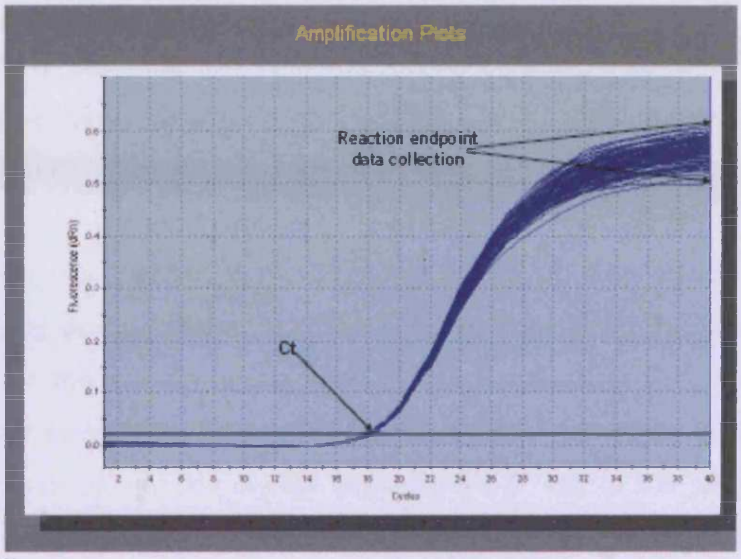

4.1.4.2. Real-Time QPCR

This relatively modern technique is widely used for gene expression profiling. The chemistry of real-time QPCR is identical to conventional PCR, except that the reaction includes a fluorescent reporter molecule that allows the user to monitor progress of the amplification in real-time. There are two types of reporter molecule: 1) dsDNA-binding dyes (e.g. SYBR Green I). 2) Dye-labelled probes (e.g. Taqman® probes, Molecular Beacons and Scorpions).

The most commonly used dsDNA-binding molecule is SYBR Green I. When free in solution SYBR displays a relatively low level of fluorescence. However, the SYBR molecule has a strong affinity for, and binds to dsDNA. Upon binding, the level of fluorescence emitted by the molecule is increased approximately 1,000-fold, and so reaches a detectable level. Compared to probe-based methods, SYBR based assays are relatively easy to design and optimize. However, a distinct disadvantage of SYBR chemistry is its inherent non-specificity. SYBR molecules will bind to all dsDNA

molecules, and so care has to be taken that the fluorescent signal is not contaminated due to non-specific amplification (e.g. primer dimers or amplification of contaminating gDNA).

There are several probe based detection chemistries currently available, of which Taqman® probes are the most widely used (Figure 4.2). In addition to the PCR primers, a third oligonucleotide known as the probe is included in the reaction. The probe is designed to bind to a target sequence downstream of one of the PCR primers. A fluorescent reporter is attached to the 5′ end of the probe. Also attached is a quencher molecule. As long as the reporter and quencher are maintained in close proximity, the fluorescence from the reporter is quenched and no fluorescence is detected. As the *Taq* DNA polymerase extends the primer, it encounters the 5′ end of the probe. Then, via its 5′–3′ nuclease activity, the polymerase degrades the 5′ end of the probe, releasing the reporter molecule into solution. Following the separation of reporter dye and quencher, fluorescence can be detected from the reporter dye. One advantage of probe-based chemistry over SYBR is that multiple probes can be labeled with different reporter dyes, and combined to allow detection of more than one target in a single reaction (multiplex QPCR). However, probe based chemistry is much more expensive and optimization can prove difficult.

As the PCR proceeds, the increase in fluorescence, and therefore accumulation of PCR product is measured at every cycle. This allows initial template quantity to be calculated from fluorescent readings taken during the exponential phase of amplification. Fluorescent readings at these earlier cycles will measure the amplified template quantity when the reaction is more efficient, and more reproducible than at the reaction endpoint (as performed for endpoint QPCR). The first cycle at which the instrument is capable of distinguishing the amplification-generated fluorescence from the ambient background fluoresence is called the "Ct" or threshold cycle. This Ct value can be directly correlated to the starting amount of DNA template.

Figure 4.2. Main Features of the Taqman® Probe Based QPCR chemistry. This method relies on the 5′–3′ nuclease activity of the *Taq* DNA polymerase to degrade the 5′ end of the probe. This activity results in the release of the reporter dye into solution where it is no longer quenched (Stratagene, 2005).

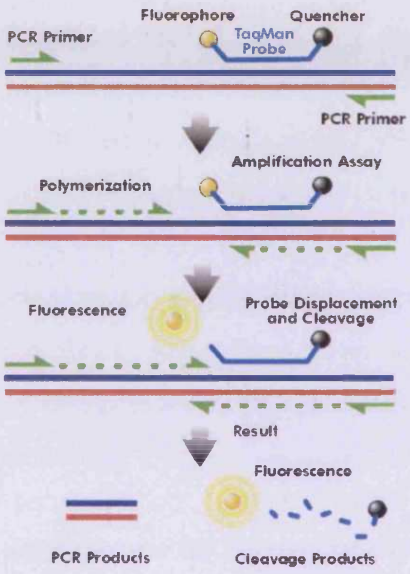

4.1.4.3. Methods of Quantification

There are two basic methods for quantification:

1) Absolute Quantification

The assay includes a standard curve prepared from a dilution series of control template of known concentration e.g. gDNA, cDNA or a plasmid containing the cloned gene of interest. Following amplification of the standard dilution series, a standard curve can be generated by plotting the log of initial template copy number against the corresponding Ct value generated for each dilution. If the aliquoting was accurate and the efficiency of

the amplification does not change over the concentration range, then the plot should generate a straight line. The comparison of the Ct values of an unknown sample to this standard curve allows the calculation of initial copy number.

2) Relative Quantification

Here, one of the samples is designated the calibrator (e.g. the zero time point in a time-course experiment, or an untreated sample) which provides the baseline that all other samples are compared to. The differences in the Ct values between unknown samples and the calibrator are expressed as fold-changes (i.e. up or down-regulated) relative to the calibrator.
It is common practice to normalize the results with a normalizing target, typically a housekeeping gene whose expression is constant in all samples. This normalization controls for differences in RNA isolation and in the efficiency of the reverse transcription reaction arising from sample to sample.

Although a standard curve is not necessary for the purposes of relative quantification, it is still required during the design stage of the assay to determine reaction efficiency. It is common practice not to run a standard curve on every plate. However, it is also not accurate to assume that the amplification efficiency between individual runs remains constant.

4.1.5. Confirming a Link Between the Expression of Two Genes Using an RNAi Based Approach

RNAi is a relatively new technique that has replaced the older generation of RNA targeting reagents such as ribozymes and antisense, as the most widely used way of achieving sequence-specific gene knockdown. Thus, by knocking down the expression of FOXE1 and analysing the effect on the other genes, a link between them can be confirmed.

In cultured mammalian cells, RNAi is commonly induced by one of two techniques:

1. The Transfection of Cultured Cells with Synthetic siRNAs

Cells are transfected with a 19-bp synthetic dsRNA, with a sequence complemenary to the target mRNA and bearing 2-nt 3′ overhangs at each end (Elabshir *et al.*, 2001). These siRNAs mimic the structure of the ~22-nt RNA intermediates formed during the RNaseIII processing of endogenous miRNA transcripts (Cullen *et al.*, 2004).

RNase III and/or other components of the RNAi machinery are able to specifically recognize an siRNA duplex and selectively incorporate one of the siRNA strands into different RNA-induced silencing complexes (RISCs), including the catalytic endonuclease-containing complex, which is responsible for the strong siRNA gene-knockdown effect (Sontheimer, 2005; Tomari & Zamore, 2005). The strand with sequence complementary to the targeted mRNA (the guide strand) is incorporated into the RISC, where it then acts to direct the RISC to the target mRNA. Meanwhile the other strand (the passenger strand) is degraded (Rand *et al.*, 2005; Leuschner *et al.*, 2006). The catalytic RISC recognizes mRNAs containing perfect or near-perfect complementary sequence to the guide strand and cleaves the mRNAs at a site precisely 10 nt upstream of the nucleotide opposite the most 5′-nucleotide of the guide strand. The mRNA fragments are subsequently degraded by cellular nucleases, resulting in knockdown of the expression of the corresponding gene.

One of the main disadvantages of transfecting the cells with synthetic siRNAs as a method to knockdown gene expression is that the siRNA concentration is not maintained (due to siRNA degradation and dilution as a result of cell proliferation). Therefore, their effect is only temporary (typically 2-3 days) and is of no use in studying the effects on biological processes that take longer periods of time.

2. The Stable Induction of RNAi Using Expression Plasmids

These approaches generally rely on the expression of RNAs that mimic other, earlier intermediates in the processing of endogenous miRNAs (Cullen, 2004). The most common approach involves the transcription by RNA polymerase III of short hairpin RNAs (shRNAs), ~50 nt long RNA hairpins consisting of a stem of 19–26 bp linked to a small, ~6-nt terminal loop and bearing a 2-nt 3′ overhang. shRNAs mimic the pre-miRNA hairpins that result from the processing of endogenous primary miRNA (pri-miRNA) transcripts by the RNase III enzyme Drosha (Lee *et al.*, 2003; Cullen, 2004). In the case of both endogenous pre-miRNAs and artificial shRNAs, processing by a second RNase III enzyme called Dicer, then produces the siRNA/miRNA duplex intermediate (Lee *et al.*, 2003; Cullen, 2004).

The introduction of siRNAs into mammalian cells can lead to activation of the antiviral/interferon signalling pathway, resulting in the global shutdown of protein synthesis. The higher the siRNA concentration the more likely this is to occur, however the exact amount required is siRNA and cell-type dependent. Semizarov *et al* (2003) demonstrated that transfection of cells with siRNA concentrations of >100 nM frequently produces non-specific off-target effects, and a concentration of 20–100 nM only occasionally produces such effects. However, others groups have noted non-specific off-target effects with siRNA concentrations as low as 10 nM (Sledz *et al.*, 2003). For a given siRNA, the concentration required to produce non-specific effects, varies significantly with the cell-type being analysed (Reynolds *et al.*, 2006). This may result from the fact that some cells are more readily transfectable and hence take up higher levels of siRNA even at low siRNA concentrations.

4.1.6. Chapter Aims

The overall aim of the chapter was to identify upstream and downstream targets of FOXE1 in skin. This would be achieved by addressing a number of specific goals:

1. Quantification of FOXE1 transcripts through HaCaT differentiation to establish

expression profile.

2. Quantification of transcripts of candidate downstream targets implicated in ECM remodelling, through HaCaT differentiation. This would identify genes whose expression profile mirrored that of FOXE1.

3. Use siRNA to determine whether any observed co-expression was of functional significance.

4. Investigate DREAM expression in HaCaT, if present perform similar experiments to those described in 2 and 3.

4.2. Materials and Methods

4.2.1. HaCaT cells

HaCaT cells were kindly provided by Prof. N. E. Fusenig (Deutches Krebsforschungszentrum Heidelberg, Germany). Cell passage numbers 42-46 were used for this research.

4.2.2. Maintaining and Storing HaCaT Cells

4.2.2.1. Culture Conditions

HaCaT cells were grown in 80 cm^2 Nunclon™ delta surface flasks [Nunc, UK] containing 10 ml culture medium. The medium consisted of Dulbecco's modified Eagle medium (DMEM) (with 4.5 g/L glucose, L-glutamine and without sodium pyruvate) supplemented with 10% heat-inactivated fetal calf serum (FCS) (EU approved), 50 U/ml penicillin, 50 µg/ml streptomycin and 2.5 µg/ml fungizone (amphotericin B) [all reagents from Cambrex, Berkshire, UK]. The cells were kept in a humidified 5% CO_2 atmosphere at 37°C, and the culture medium was routinely replaced every 2 days.

4.2.2.2. Trypsinisation

The cells were passaged when they reached 80% confluency. The culture medium was removed and the cells washed three times with 10 ml sterile PBS. Then, 2 ml of trypsin-EDTA [Cambrex, Berkshire, UK] was added and the flask incubated at 37°C until the majority of the cells were in suspension (~5-10 min). To aid the release of the cells the flask was lightly tapped every couple of mins. Once in suspension, 20 ml DMEM with 10% FCS was added to inactivate the trypsin. The cells were then reseeded in a fresh flask (if split 1:5 they were ready to passage again within 7 days).

4.2.2.3. Cryo-Preservation of Cells

The cells were trypsinised as described above and the resulting suspension of cells centrifuged at 1000 rpm for 5 mins at RT. The cell pellet was then resuspended in 0.5 ml culture medium and 0.5 ml freezing mixture (FCS with 20% dimethyl sulfoxide (DMSO) [Sigma-Aldrich Company Ltd, Dorset, UK] and transferred to a 2 ml sterile cryotube. The cryotube was placed in an insulating polystyrene freezing box containing isopropanol [Fisher Scientific UK Ltd, Leicestershire, UK] (ensuring a cooling rate of 1°C/min) and placed in an -80°C freezer overnight. The next day the cryotube was transferred to liquid nitrogen (-190°C) for long-term storage.

4.2.3. Populations of HaCaT Cells to be Studied

In addition to the non-modified HaCaT cells, a population stably expressing a FOXE1 responsive luciferase reporter (Z16TKLUC) were also studied. This HaCaT subclone was created with the initial aim of investigating possible upstream signalling pathways implicated in the modulation of FOXE1 expression in keratinocytes. The experimental design included stable transfection of HaCaT with Z16TKLUC reporter (as described in Chapter 5) and addition of known regulators of major signalling cascades. These experiments were not successful (as discussed in Chapter 6) but the cells provided a useful additional population for study.

4.2.4. Calcium-Shift Induced Differentiation

4.2.4.1. Culture Conditions

The day that the cells were plated was designated day 0. Following trypsinisation of an 80% confluent T75 flask, the resulting cell suspension was centrifuged at 1000 rpm for 5 mins at RT. The cell pellet was resuspended in 20 ml KGM® (keratinocyte growth medium) supplemented with KGM® SingleQuots® (bovine pituitary extract, human

epidermal growth factor, insulin and hydrocortisone) [Cambrex, Berkshire, UK]] and 0.06 mM $CaCl_2$ [Sigma-Aldrich Company Ltd, Dorset, UK]. This was repeated to ensure all traces of the DMEM and serum were removed. The volume of medium was then adjusted to give a cell density of 5×10^4 cells/ml. The cells were plated in 35 mm wells at a cell density of 1×10^5 cells/well (2 ml/well). The cultures were maintained in a humidified 5% CO_2 atmosphere at 37°C and the culture medium replaced every two days.

When the cells reached 80% confluency (day 6) the medium used was switched to KGM® supplemented with KGM® SingleQuots® and 1.8 mM $CaCl_2$, and the cells were maintained for a further 6 days in this high calcium medium.

4.2.4.2. Isolation of Total RNA from HaCaT Cells

RNA samples were collected on day 3 (30% confluency), 6 (80% confluency), 7 (1 day post-shift), 9 (3 days post-shift) and 12 (6 days post-shift). Additional samples were also collected from some experiments at 1, 3, 6, 9, 14, 15, 18, 21 and 24 hrs post-calcium shift.

In each case, the culture medium was removed and the cells washed three times with 1 ml PBS. Total RNA was isolated using Invitrogen's TRIzol reagent according to the manufacturer's instructions. The cells were lysed by the addition of 1 ml TRIzol reagent and passing the cell lysate several times through a pipette. Visual inspection was performed using light microscopy to ensure complete cell lysis. To allow the dissociation of nucleoprotein complexes the cell lysate was transferred to a nuclease-free 1.5 ml microtube, and left for 5 mins at RT. The RNA was separated from DNA and protein by adding 200 µl chloroform [Fisher] and mixing the solutions vigorously. This was followed by incubation for 3 mins at RT and then centrifugation at 12,000×g for 15 mins at 4°C. The upper aqueous phase (~500µl), containing the RNA, was transferred to a fresh nuclease-free 1.5 ml microtube and the RNA precipitated by adding 500 µl isopropanol [Fisher]. The sample was vortexed briefly, incubated for 10 mins at RT, and

then centrifuged at 12,000×g for 10 mins at 4°C. The supernatant was removed and the RNA pellet washed with 1 ml 75% ethanol [Fisher]. The sample was vortexed and then centrifuged at 7,500×g for 5 mins at 4°C. The supernatant was removed, the RNA pellet air-dried and resuspended in 20 µl nuclease-free water [Promega].

Total RNA quantity and integrity were assessed by spectrophotometer [GeneQuant, GE Healthcare] and 1% agarose gel analysis. RNA samples were stored at -80°C until required.

4.2.4.3. DNase Treatment of RNA

Traces of gDNA were removed from the RNA samples using Promega's RNase-Free DNase according to the manufacturer's instructions. The following components were added to a nuclease-free 200 µl microtube: 1 µg RNA, 1 µl DNase 10× buffer, 1 µl DNase and the reaction made up to 10 µl with nuclease-free water [Promega]. The reaction mixture was mixed gently by pipetting, briefly spun in a microcentrifuge, and then transferred to a 37°C waterbath for 30 mins. Adding 1 µl Stop Solution and transferring to a 65°C waterbath for 10 mins terminated the reaction.

4.2.4.4. Reverse Transcription

Reverse transcription was performed using Invitrogen's [Paisly, UK] Superscript™ III Reverse Transcriptase according to the manufacturer's instructions. The following components were added to a nuclease-free 500 µl microtube: 1 µl 500 ng/µl oligo$(dT)_{15}$ [Promega], 1 µl 10 mM dNTPs mix [Sigma-Aldrich Company Ltd, Dorset, UK] and 11 µl DNase-treated RNA. These components were heated at 65°C for 5 mins before being incubated on ice for 2 mins. The following were then added: 1 µl 40U/µl RNasin [Promega], 4 µl 5× First-Strand buffer, 1 µl 0.1 M DTT and 1 µl 200U/µl SuperScript III RT. The reaction mixture was mixed gently by pipetting, briefly spun in a

microcentrifuge before being transferred to the PE Applied Biosystems 9700 thermocycler.

PCR cycling protocol:

- 1 cycle of 2 hrs at 50°C
- Inactivation 15 mins at 70°C

cDNA samples from primary keratinocytes were a kindly provided by Dr. S. Han (Cardiff).

cDNA samples were stored at -20°C until required.

4.2.5. Conventional PCR

Conventional PCR was performed using two different methods. For the majority of PCRs method 1 was used. However for templates difficult to amplify such as GC-rich sequences method 2 was used.

Method 1: PCR was performed using Applied Biosystems [Chershire, UK] polymerase according to the manufacturer's instructions. The following components were added to a nuclease-free 500 µl microtube: 2.5 µl 10× PCR buffer, 1.0 µl 10 mM dNTP mix, 1.0 µl 5 µM forward primer, 1.0 µl 5 µM reverse primer, 0.125 µl DNA polymerase, 0.1-1.0 µg DNA template and the reaction made up to 25 µl with nuclease-free water [Promega]. The reaction was mixed gently by vortexing, briefly spun in a microcentrifuge before being transferred to the PE Applied Biosystems 9700 thermocycler.

PCR cycling protocol:

- 35 cycles of Denaturation: 1 min at 94°C
  Annealing: 1 min at 60°C
  Extension: 1 min at 72°C

Method 2: PCR was performed using Qiagen's HotStarTaq® *Plus* DNA polymerase according to the manufacturer's instructions. The following components were added to a nuclease-free 500 µl microtube: 2.5 µl 10× PCR buffer, 5 µl Q-solution, 0.5 µl 10 mM dNTP mix, 5 µM forward primer, 5 µM reverse primer, 0.5 µl DNA polymerase, 0.1-1.0 µg DNA template and the reaction made up to 25 µl with nuclease-free water [Promega]. The reaction mixture was vortexed and then briefly spun in a microcentrifuge before being transferred to the PE Applied Biosystems 9700 thermocycler.

PCR cycling protocol:

- Activation: 1 min at 95°C
- 35 cycles of Denaturation: 1 min at 94°C
  Annealing: 1 min at 60°C
  Extension: 1 min at 72°C
- Final extension: 10 mins at 72°C

Depending on their size, PCR products were analysed on a 1.5-2% agarose gel and DNA visualised with 0.5µg/ml EtBr [Sigma].

4.2.6. Purification of PCR Products

For optimal results of downstream applications (e.g. direct sequencing), removal of unused dNTPs and primers was performed. If the PCR produced single specific products then these were purified by PEG precipitation. In the case of multiple PCR products, specific amplicons were isolated using Qiagen's QIAquick Gel Extraction Kit.

PEG precipitation method: 16 µl of PCR product was mixed with 20 µl PEG mix (26% PEG 8000, 6.6 mM $MgCl_2$, 0.6 M NaAcetate, pH 5.2), and the DNA allowed to precipitate at RT for 10 mins. The mixture was then centrifuged (13,000 rpm for 25 mins at RT), the supernatant aspirated and the DNA pellet resuspended in 200 µl ice-cold 70% ethanol. This was mixed gently by inversion and centrifuged (15,000 rpm for 2 mins at

4°C). The supernatant was removed and the DNA pellet left to dry in a 37°C oven for 5 mins. Finally, the sample was resuspended in 16 µl of nuclease-free water [Promega].

Gel extraction method: This was performed as described previously (Section 2.2.3.3), except that the PCR products were separated on a 2% agarose gel.

The DNA yield was determined by spectrophotometer [GeneQuant, GE Healthcare].

4.2.7. Direct Sequencing of PCR Products

Sequencing was performed as described previously (Section 2.2.3.4), except 20 ng DNA template was added to the reaction.

4.2.8. Protein Extraction from HaCaT cells

The culture medium was removed, the cells washed three times with 1 ml chilled PBS, and 300 µl chilled SDS-PAGE loading buffer (Section 2.2.6) added. The surface of the well was rubbed vigorously with the plunger from a plastic syringe to aid cell lysis. The cell lysate was then transferred to sterile 200 µl microtube (25 µl/tube) and these were stored at -80°C until required.

4.2.9. Isolation of HaCaT Nuclear and Cytosolic Fractions

To prepare nuclear and cytosolic fractions cells were harvested in ice-cold PBS, centrifuged and resuspended in HEPES buffer (400 mM HEPES, pH 7.9; 60 mM $MgCl_2$; 400 mM KCl; 20 mM DTT) containing protease inhibitors (leupeptin, PMSF, aprotinin, pepstatin). The supernatant produced by centrifugation at 12,000 × g provided the cytosolic and high salt extraction (100 mM HEPES, pH 7.9; 2.5 ml glycerol; 4M NaCl; 15 mM $MgCl_2$; 2 mM EDTA; 5 mM DTT; 5 mM PMSF) of the pellet, the nuclear fractions respectively.

4.2.10. Western Blot Analysis

Western blot analysis was performed as described in Section 2.2.6. Except, in some experiments the method for sample preparation was varied (the sample was heated at 37°C for 1 hr, 70°C for 5 mins, 70°C for 10 mins, 100°C for 5 mins or 100°C for 5 mins).

Additionally, an affinity purified goat anti-FOXE1 peptide (Abcam, Cambridge, UK) was used. This was visualised using an anti-goat IgG-HRP conjugate (Santa Cruz, California, US).

4.2.11. Plasmid Standards for QPCR

4.2.11.1. APRT Standard

The APRT standard (a gift from Dr. A. Janezic, Cardiff) consisted of a 247 bp APRT PCR product ligated into pGEM®-T Easy vector [Promega].

4.2.11.2. FOXE1 Standard

The FOXE1 construct consisted of a 1.3 kb BamHI-XbaI fragment, encompassing the entire FOXE1 coding region, cloned into the pcDNA3 vector [Invitrogen] (Clifton-Bligh *et al.*, 1998).

4.2.11.3. TIMP3, MMP13 and COL1A1 Standards

4.2.11.3.1. Generation of cDNA

PCR amplicons were generated from HaCaT cDNA using conventional PCR (Section 4.2.5) and the primers shown in Table 4.3. The identity of each PCR amplicon was confirmed by analysis on a 2% agarose gel and by direct sequencing (Section 4.2.7).

4.2.11.3.2. Ligations

The PCR products were ligated into pGEM®-T Easy Vector System [Promega], following the manufacture's instructions. Briefly, the following components were added to a nuclease-free 200 µl microtube: 5 µl 2× rapid ligation buffer, 1 µl 50ng/µl pGEM®-T vector, 1 µl 3U/µl T4 DNA ligase, PCR product and the reaction made up to 10 µl with nuclease-free water [Promega]. The reaction was then incubated at 4°C overnight.

In order to optimise the ligation reaction different insert:vector ratios (1:3, 1:1, 3:1) were tried. The concentration of the PCR product was estimated by comparison with DNA molecular weight markers. The quantity of PCR product required for each insert:vector molar ratio was calculated using the following equation:

$$\frac{\text{mass of vector (ng)} \times \text{length of insert (kb)}}{\text{length of vector (kb)}} \times \text{insert:vector molar ratio} = \text{ng insert}$$

4.2.11.3.3. Transformation of Plasmid Constructs

All the plasmid constructs were transformed into One Shot® TOP10 Competent Cells [Invitrogen], following the chemical transformation procedure provided by the manufacturer. A vial of One Shot® cells was taken from -80°C, thawed on ice and the transformation started immediately. Then, 3 µl of the ligation product was pipetted into the vial and the cells mixed by gently tapping. The cells were then incubated on ice for 30 mins followed by a heat-shock at 42°C for 30 secs and then transferred back to ice. Then, 250 µl S.O.C medium [Invitrogen] prewarmed to RT was added to the cells. The vial was placed on its side in a microtube rack, secured with tape, and shaken at 37°C for 1 hr at 225 rpm in an orbital incubator. One hundred microlitres of the transformation culture was spread onto a LB agar/ampicillin/X-Gal plate and incubated overnight at 37°C.

Small-scale mini-prep isolation of plasmid constructs was performed as described previously (Section 2.2.3.1) on single selected colonies.

Restriction enzyme analysis (Section 4.2.11.3.5) and direct sequencing (Section 2.2.3.4) was performed to identify the correct plasmid constructs.

4.2.11.3.5. Restriction Enzyme Analysis of Minipreps

Table 4.1. gives the Promega enzymes and optimal reaction buffer used for each digestion. For a single reaction, the following components were added to a sterile 100 µl microtube: 2 µl 10× reaction buffer, 0.5 µl restriction enzyme, 1 µg plasmid DNA and the final volume made up to 20 µl with nuclease-free water. Each reaction was incubated in a waterbath at 37°C for 1 hr. The digestion products were separated and visualised on a 0.8% agarose gel.

Table 4.1. Restriction Digests Performed on each Construct

Construct	Enzymes used	Buffer used	Purpose
pcDNA3-FOXE1	10 U/ml *BamH I*	E	Linearise
	10 U/ml *BamH I* + 12 U/ml *Xba I*	E	Excise insert
pGEMT-constructs	10 U/ml *Sal I*	D	Linearise
	12 U/ml *EcoR I*	H	Excise insert

4.2.11.3.6. Direct Sequencing of Minipreps

Direct sequencing was performed as described previously (Section 2.2.3.4).

4.2.11.3.7. Large-Scale Plasmid DNA Preparation (Maxipreps)

Having confirmed the identity of each plasmid construct, large-scale production was undertaken. Plasmid isolation was performed using a Qiagen's QIAfilter™ Plasmid Maxi Kit, according to the manufacturer's instructions. Briefly, 200 µl of the miniprep culture

was used to inoculate 100 ml LB broth containing ampicillin (100 μg/ml). This was then incubated overnight at 37°C in an orbital incubator shaking at 250 rpm. The bacterial cells were harvested by centrifugation at 3000×g for 30 mins at 4°C. The pellet was then resuspended in 10 ml buffer P1 (resuspension buffer), before addition and gentle mixing with 10 ml buffer P2 (lysis buffer). The precipitation of bacterial gDNA, proteins and other cell debris was enhanced by the addition of 10 ml chilled buffer P3 (neutralization buffer), before transferring the lysate to a QIAfilter cartridge. The cell lysate was filtered into an equilibrated QIAGEN-tip 500, allowing the plasmid DNA to bind to the Qiagen anion-exchange resin. Bound DNA was washed twice with 20 ml buffer QC (medium-salt buffer) in order to remove RNA, proteins and other low molecular weight impurities. The plasmid DNA was then eluted from the column with 15 ml buffer QF (high-salt buffer) before subsequent desalting with 10.5 ml isopropanol. A DNA pellet was formed by centrifugation at 15,000×g for 30 mins at 4°C. This was washed with 5 ml 70% ethanol, before being air dried and redissolved in nuclease-free water [Promega].

The DNA concentration of each maxiprep was determined by spectrophotometer analysis [GeneQuant, Amersham]. The number of cDNA copies per μl of plasmid DNA was calculated with the aid of a formula obtained from http://www.promega.com/biomath/. The calculation of the number of copies of FOXE1 cDNA per μl is shown below (Table 4.2). The maxipreps were then diluted to a concentration of 10^7copies per μl, divided into single use aliquots and stored at -80°C until required.

Table 4.2. Spectrophotometer Analysis of the pcDNA3-FOXE1 Maxiprep

	Abs260	Abs280	Concentration (ng/μl)	260:280 ratio
pcDNA3-FOXE1 (neat)	2.899	1.603	2899	1.808
pcDNA3-FOXE1 (1:10 dilution)	0.304	0.152	304	1.758

Calculation of the number of copies of FOXE1 present in the pcDNA3-FOXE1 maxiprep:

1. Values required for the calculation:

   DNA concentration of maxiprep = 0.304 µg/µl

   Size of pcDNA3-FOXE1 construct = size of pcDNA3 + size of FOXE1 insert

   = 5,446bp + 1,300bp

   = 6,746bp

2. Calculation of the DNA concentration (pmole/ml) of the maxiprep:

$$\text{pmoles/µl} = \text{DNA concentration (µg/µl)} \times \frac{\text{pmole}}{660\text{pg}} \times \frac{10^6\text{pg}}{1\text{µg}} \times \frac{1}{N}$$

Where, N = the size of the construct (bp)
660pg/pmole = the average weight of a nucleotide pair

$$= 0.304 \times \frac{\text{pmole}}{660\text{pg}} \times \frac{10^6\text{pg}}{1\text{µg}} \times \frac{1}{6{,}746\text{bp}}$$

$$= 6.83\times10^{-2} \text{ pmoles/µl}$$

3. Calculation of the number of copies of FOXE1 present in the maxiprep:

$$\text{moles/µl} = \text{pmoles/µl} \times (1\times10^{-12})$$
$$= (6.83\times10^{-2}) \times (1\times10^{-12})$$
$$= 6.83\times10^{-14}$$

$$\text{copies/µl} = \text{moles/µl} \times \text{Avogadro's constant}$$
$$= (6.83\times10^{-14}) \times (6.02\times10^{23})$$

$= 4.11\times10^{10}$copies of pcDNA3-FOXE1/µl of maxiprep

4.2.12. Real-time QPCR

Real-time QPCR was performed using Stratagene's Brilliant® SYBR® Green QPCR master mix according to the manufacturer's instructions. Reactions were set up in a Stratagene 96-well PCR plate. Each 25 µl reaction consisted of 12.5 µl Master Mix,

forward primer, reverse primer and nuclease-free water [Promega]. The reaction mixture was briefly spun in a microcentrifuge before being transferred to the Stratagene MX3000P® thermocycler.

Thermocycling protocol:

- Enzyme activation: 10 mins at 95°C
- 40 cycles of Denaturation: 30 sec at 94°C
  Annealing: 60 sec at 60°C
  Extension: 30 sec at 72°C

Profile for dissociation Program:

- Melt DNA: 60 sec at 95°C
  30 sec at 55°C
  30 sec at 95°C

4.2.13. Real-time QPCR Optimisation

4.2.13.1. Primer Design

Nucleotide sequences for each gene were obtained from GENEATLAS (http://www.dsi.univ-paris5.fr/genatlas/). To avoid amplification from contaminating gDNA all PCR primer pairs were designed to span exon-intron boundaries (the exception to this was the FOXE1 gene which consists of a single exon). The exons were chosen on the basis that they were present in all known splice variants of the gene. The primer design program Primer3 (http://frodo.wi.mit.edu/cgi-bin/primer3/primer3_www.cgi) using default settings was used to generate a list of potential primer sequences. In order to maximise the efficiency of the PCR reaction, primers that span a region <300 bp in length were chosen. Finally, a BLAST search (http://www.ncbi.nlm.nih.gov/) was performed on all primer sequences to ensure there was no significant homology with non-specific targets. The chosen primers are shown in the Table 4.3.

Table 4.3. A List of All the Primers Used in QPCR Experiments. Details include the exons where the primers are located, the nucleotide sequence and Tm (melting temperature) of each primer and the expected size of the PCR amplicons

Gene	Exons	Forward primer		Reverse primer		Size (bp)	
		Sequence (5'→3')	Tm	Sequence (5'→3')	Tm	gDNA	cDNA
APRT	3+5	GCT GCG TGC TCA TCC GAA AG	65.1	CCT TAA GCG AGG TCA GCT CC	59.9	749	247
FOXE1	/	GCG GAG GAC ATG TTC GAG A	56.5	GTA AGC CGG GTA GGT GGA GA	59.9	84	84
TIMP3	3+4	GTA CCG AGG CTT CAC CAA GA	60.3	TGC AGT TAC AAC CCA GGT GA	60.2	886	230
MMP13	6+7	AAC ATC CAA AAA CGC CAG AC	60	GGA AGT TCT GGC CAA AAT GA	60.1	1,117	166
COL1A1	6+7	ACT TTG CTC CCC AGC TGT C	60.4	CCA GGG AGA CCA CGA GGA	62.3	327	117
DREAM	3+4	AGT GAG CTG GAG CTG TCC AC	60.6	CTG CGC GTA AAT GAG TTT GA	60	589	168

4.2.13.2. Primer Optimisation

An important contributory factor to suboptimal amplification efficiency is the difference in Tm between forward and reverse primers. Even in cases where theoretical Tm values are identical, "real life" differences can exist. Common methods of PCR optimisation such as changing the annealing temperature or Mg^{2+} concentration of the reaction will affect both primers at the same time. However, the Tm of a primer in a given reaction will be determined by its own concentration. Thus, this allows the Tm for each primer to be altered independently simply by changing its concentration. To determine the optimum combination of forward and reverse primer concentrations a primer matrix test was performed (Figure 4.3). The optimal primer combination (producing the lowest Ct value) was determined for both high (10^6) and low copy numbers (10^2) of the target gene. The results of the matrix test performed for the APRT primer pair are shown in Table 4.4. Ct values for each primer combination are given, each being the mean average of 3 replicates. The optimal primer combination for all primer pairs is shown in Table 4.5.

Figure 4.3. Primer Matrix Test

10^6 cDNA Copies

Forward primer concentration (nM) \ Reverse primer concentration (nM)	100	300	500
100	16.52	15.05	14.74
300	16.80	15.02	**14.39**
500	16.29	14.56	14.40

10^2 cDNA Copies

Forward primer concentration (nM) \ Reverse primer concentration (nM)	100	300	500
100	30.19	27.88	27.39
300	30.15	27.14	**26.90**
500	29.42	27.20	27.00

Table 4.4. Primer Matrix Test for APRT. Ct values for each primer combination are shown, and the lowest is highlighted in bold

Reverse primer concentration (nM) \ Reverse primer concentration (nM)	100	300	500
100	100/100	100/300	100/500
300	300/100	300/300	300/500
500	500/100	500/100	500/500

Table 4.5. Optimal Primer Combinations for Each Gene

Gene	Primer concentration (nM)	
	Forward	Reverse
APRT	300	500
FOXE1	500	100
TIMP3	500	500
MMP13	300	500
COL1A1	500	500

4.2.14. Design of FOXE1 and DREAM Specific siRNAs

The first step was to perform a literature search to see if other groups had already designed and validated siRNAs that effectively knockdown FOXE1 and DREAM expression. A number of online databases are available that archive this information (Truss M *et al.*, 2005 and Ren Y *et al.*, 2006). In addition, validated siRNAs for a number of human genes are now commercially available (e.g. Ambion *Silencer*® Validated siRNAs that have been verified for their ability to achieve ≥70% knockdown of the target gene of interest). Unfortunately, for FOXE1 and DREAM no existing siRNAs were available.

Several online siRNA design tools are in the public domain. These design tools vary in their approach to target selection, but the majority use a series of rules based on the current literature and empirical observations made by company researchers. Two of these algorithms were used: Ambion siRNA target finder (http://www.ambion.com/techlib/misc/siRNA_finder.html) and Clontech siRNA Selector (http://bioinfo2.clontech.com/rnaidesigner/sirnaSequenceDesign.do), each using default settings.

Nucleotide sequences for the coding region of FOXE1 and DREAM were obtained from GENEATLAS (http://www.dsi.univ-paris5.fr/genatlas/). DREAM exons were chosen on

the basis that they were present in all known splice variants. Using the online design tools, two lists of potential target sequences were generated for each gene. These lists were then cross-matched for overlapping sequences, and these selected for further analysis.

Ambion researchers have found that siRNAs with 30-50% GC content are more active than those with a higher G/C content, so only these sequences were selected. To reduce the chances of off-target effects, a BLAST search (http://www.ncbi.nlm.nih.gov/) was performed on all sequences to ensure there was no significant homology with non-specific targets. Finally, two sequences were selected for siRNA synthesis and these are shown in the Table 4.6.

To ensure efficient synthesis, T7 RNA polymerase requires that the first two nucleotides of the RNA transcript be GG or GA (Milligan *et al.*, 1987). Ordinarily, this would significantly reduce the number of potential target sequences that may be used. However, Ambion's *Silencer*® siRNA Construction Kit overcomes this problem by using siRNA oligonucleotides containing a "leader" sequence that is complementary to the T7 promoter primer used in the kit. The oligonucleotide sequences are shown in Table 4.6.

As a negative control a scrambled siRNA was generated for each gene. This was achieved by scrambling the nucleotide sequence of the gene-specific siRNA. A BLAST search (http://www.ncbi.nlm.nih.gov/) was performed to ensure there was no significant homology with any human gene.

Table 4.6. Selected Target Sequences with Corresponding Sense and Anti-sense Oligo Sequences

siRNA	Target sequence (5'→3')	Sense oligo sequence (5'→3')	Anti-sense siRNA sequence (5'→3')	GC content
FOXE1-SCRAM	UAG CUA CAA GCU CGG UCA UCC	(AA)G GAT GAC CGA GCT TGT AGC (CCT GTC TC)	TAG CTA CAA GCT CGG TCA TCC (CCT GTC TC)	52.4%
FOXE1-241	AAG UUC AUC ACC GAG CGC UUC	(AA)G AAG CGC TCG GTG ATG AAC (CCT GTC TC)	AAG TTC ATC ACC GAG CGC TTC (CCT GTC TC)	52.4%
FOXE1-283	AAA AAG UGG CAG AAC AGC AUC	(AA)G ATG CTG TTC TGC CAC TTT (CCT GTC TC)	AAA AAG TGG CAG AAC AGC ATC (CCT GTC TC)	42.9%
DREAM-SCRAM	AAC GAU AGC AGG UGU AGA CAC	(AA)G TGT CTA CAC CTG CTA TCG (CCT GTC TC)	AAC GAT AGC AGG TGT AGA CAC (CCT GTC TC)	47.6%
DREAM-76	AAG AAG GAG GGU AUC AAG UGG	(AA)C CAC TTG ATA CCC TCC TTC (CC TGT CTC)	AAG AAG GAG GGT ATC AAG TGG (CCT GTC TC)	47.6%
DREAM-259	AAG UUC ACC AAG AAG GAG CUG	(AA)C AGC TCC TTC TTG GTG AAC (CCT GTC TC)	AAG TTC ACC AAG AAG GAG CTG (CCT GTC TC)	47.6%

4.2.15. siRNA Synthesis by *in vitro* Transcription

The *in vitro* synthesis of siRNAs by T7 RNA polymerase was performed using Ambion's *Silencer*® siRNA Construction Kit, following the manufacturer's instructions. The protocol was carried out over 2 days and is briefly described below.

1. The generation of double-stranded siRNA templates. In order to hybridize a template oligonucleotide to the T7 primer the following components were mixed in a nuclease-free microtube: 2 µl T7 primer, 6 µl DNA hybridization buffer and 2 µl oligonucleotide. The mixture was then heated to 70°C for 15 mins and then left at RT for 5 mins. Then, the 3' ends of the hybridised oligonucleotides were extended to create double-stranded siRNA transcription templates. This was achieved by the addition of 2 µl 10× Klenow reaction buffer, 2 µl 10× dNTP mix, 4 µl nuclease-free water and 2 µl Exo-Klenow and incubating the tube in a waterbath at 37°C for 30 mins.

2. dsRNA synthesis. Sense and antisense templates were transcribed separately to eliminate the potential for unequal competition between the templates for reagents. For each transcription the following reagents were mixed in a nuclease-free microtube: 2 µl oligo, 4 µl nuclease-free water, 10 µl 2× NTP mix, 2 µl 10× T7 reaction buffer and 2 µl T7 enzyme mix. The reaction was incubated in a water bath at 37°C for 2 hrs. The sense and anti-sense transcription reactions were combined and the reaction allowed to continue at 37°C overnight.

5' overhanging leader sequences were removed by mixing the dsRNA components with the following components: 6 µl digestion buffer, 48.5 µl nuclease-free water, 3 µl RNase and 2.5 µl DNase. This was then incubated at 37°C for 2 hrs.

Purification. The siRNA were recovered from the mixture of nucleotides, enzymes and salts etc. by column purification. 400 µl of siRNA binding buffer was added to the nuclease digestion reaction and left at RT for 5 mins. This was then added to a filter

cartridge, pre-wet with siRNA wash buffer, and centrifuged at 10,000 rpm for 1 min. Then, the column was washed twice with 500 µl siRNA wash buffer. Finally, to elute the siRNA, 100 µl preheated nuclease free water was added to the column and centrifuged at 12,000 rpm for 2 mins.

Purified siRNA concentration and integrity were assessed by spectrophotometer and 2% agarose gel analysis. Then, each was divided into single-use aliquotes and stored at -80°C.

4.2.16. Transfection of HaCaT with siRNAs

The day before transfection HaCaT cells were plated in 35 mm wells at a cell density of 5×10^5 cells/well in DMEM (with 4.5 g/L Glucose, with L-Glutamine and without Na Pyruvate) supplemented with 10% heat-inactivated FCS (EU approved).

To prepare the transfection mixture, the following components were mixed in a sterile 500 µl microtube: 200 µl DMEM, 6 µl Metafectamine Pro [Biotex] and the appropriate volume of siRNA. The siRNA-lipid complex was allowed to form by incubation at RT for 20 mins. The culture medium was removed and the cells washed three times with 2 ml sterile PBS. The transfection mix was added dropwise to the cells, which were then transferred to a 37°C incubator for 1 hr. Then, 2 ml DMEM + 10% FCS was added and the cells returned to the incubator for 48 hrs.

RNA was extracted from the HaCaT, reverse transcribed and gene expression analysed by real-time QPCR (as described previously).

4.2.17. Statistical Analyses

Pairwise comparisons were made using Student's T test (one-tailed).

4.3. Results

4.3.1. Detection of FOXE1 and Candidate Target Gene mRNA in Cultured Human Keratinocytes

To determine if the HaCaT and HaCaT-LUC cell-lines were suitable for gene expression profiling, the expression levels of FOXE1, TIMP3, MMP13 and COL1A1 in these cells was determined by RT-PCR analysis. Since the results for the HaCaT cell-lines may not have reflected the situation in primary keratinocytes, gene expression was also analysed in primary cells.

The results of the RT-PCR analysis are shown in Figure 4.4. Amplification of the APRT housekeeper gene (positive control) confirmed the integrity of the cDNA samples. Both FOXE1 and TIMP3 expression were detected in all three cell-types at similar levels. COL1A1 was also detected in all three samples, but at variable levels, being highest in the HaCaT cells but only just detectable in primary keratinocytes. In contrast, MMP13 mRNA was only detected in HaCaT cells.

4.3.2. Detection of FOXE1 Protein in HaCaT cells

The expression of FOXE1 in HaCaT cells was also confirmed at the protein levels (Figure 4.5). Western blot analysis of HaCaT nuclear extracts was performed using three different antibodies: 1) Rabbit anti-whole FOXE1 pAb. 2) Rabbit anti-FOXE1 peptide pAb. 3) Affinity purified goat anti-FOXE1 pAb. All three antibodies showed immunoreactivity with a multitude of different molecular weight proteins, however they possessed the strongest affinity for protein(s) that were approximately 70 kDa.

Further studies investigate the apparent Mr were undertaken with the affinity purified goat anti-FOXE1 pAb. Samples were mixed with loading buffer and subjected to a range of temperature treatments. As shown in Figure 4.6 a band of the expected Mr (42 kDa)

was present in the gentlest treated sample with the high Mr protein increasing with temperature.

Figure 4.4. RT-PCR Analysis: Detection of FOXE1, TIMP3, MMP13, and COLA1 mRNA in Cultured Human Keratinocytes, 1) 100bp DNA ladder, **2)** HaCaT cDNA, **3)** HaCaT-LUC cDNA, **4)** Primary keratinocyte cDNA, **5)** No template control.

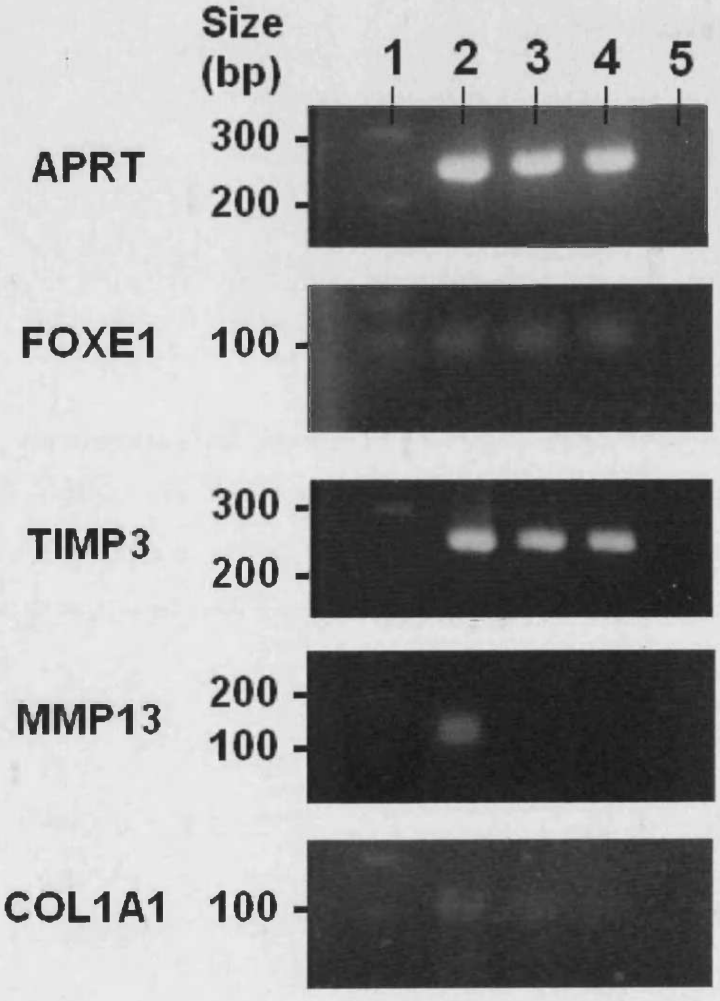

Figure 4.5. HaCaT Nuclear Proteins Separated by 10% SDS-PAGE. 1) Silver stain showing total protein, **2)** Western blot: Rabbit anti-FOXE1 peptide pAb, **3)** Western blot: Rabbit anti-whole FOXE1 pAb, **4)** Western blot: Commercial (Abcam) affinity purified goat anti-FOXE1 peptide pAb.

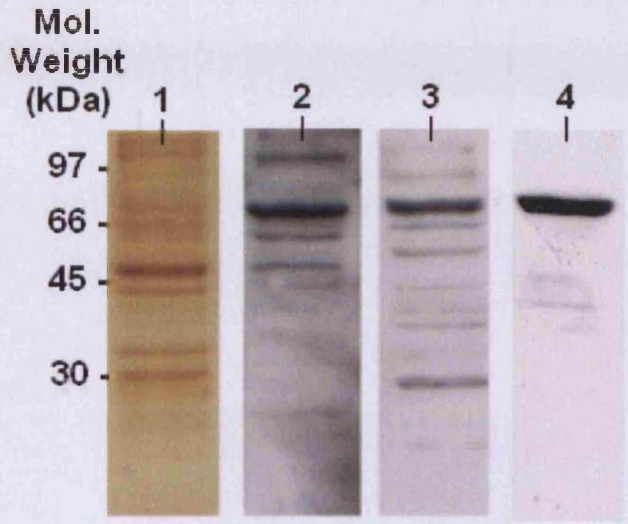

Figure 4.6. Optimisation of Sample Preparation. HaCaT nuclear extracts **1)** Kept at R.T for 1 hr, **2)** Heated to 37°C for 1hr, **3)** Heated to 70°C for 5 mins **4)**, Heated to 70°C for 10 mins, **5)** Heated to 100°C for 5 mins and **6)** Heated to 100°C for 10 mins. The western blot was probed with a commercial (Abcam) affinity purified goat anti-FOXE1 peptide pAb.

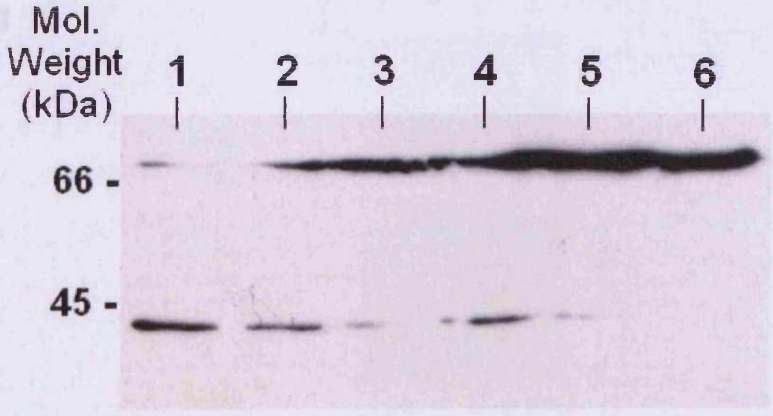

4.3.3. Real-time QPCR: Generation of Plasmid Standards

The identity of each plasmid-cDNA standard was confirmed by restriction enzyme analysis. For example, the digests of pcDNA3-FOXE1 that consisted of a 1.3 kb BamHI-XbaI fragment cloned into pcDNA3 (5.4 kb) are shown in Figure 4.7. Similarly, Figure 4.8 shows the digests of pGEM-T-APRT that consisted of 0.2 kb APRT cDNA fragment cloned into pGEM-T (3.0 kb). Additionally, direct automated sequencing of the constructs was performed, with T7 and SP6 primers.

Figure 4.7. Restriction Enzyme Analysis of pcDNA3-FOXE1. 1) 1 kb DNA ladder, **2)** BamHI restriction digestion to linearise plasmid, **3)** BamHI and XbaI restriction digestion to excise insert.

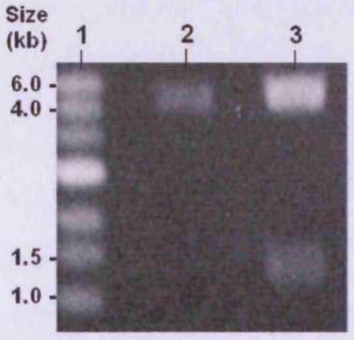

Figure 4.8. Restriction Enzyme Analysis of pGEMT-APRT. 1) 2-Log DNA ladder, **2)** Uncut plasmid **3)** SalI restriction digestion to linearise plasmid, **4)** EcoRI restriction digestion to drop out insert.

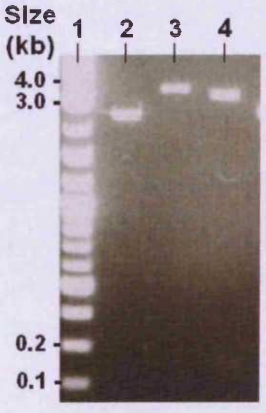

4.3.4. Real-time QPCR: Validation of Standard Curves

Each standard curve consisted of a 10× dilution series from 10^6 to 10^2 cDNA copies. To allow accurate quantification, each standard curve had to remain linear over this entire concentration range. The linearity was donated by the Pearson correlation coefficient (R^2), a value between 0 and 1, which becomes greater with increasing linearity (an $R^2 \geq$ 0.985 is considered acceptable). In addition, the reaction efficiency also had to be close to 100% (when the amount of amplicon doubles every cycle), with acceptable values for reaction efficiency being between 90% and 110%. The slope of the curve was directly related to the average reaction efficiency. The equation that relates the slope to amplification efficiency was: Efficiency = $10^{(-1/\text{slope})} - 1$. Thus, a reaction with 100% efficiency would result in a slope of –3.322. As an example, validation of the APRT and FOXE1 standard curves is shown in Figure 4.9. The validation of the TIMP3, MMP13 and COL1A1 standards produced similar results.

Figure 4.9. Validation of APRT and FOXE1 Standards Curves

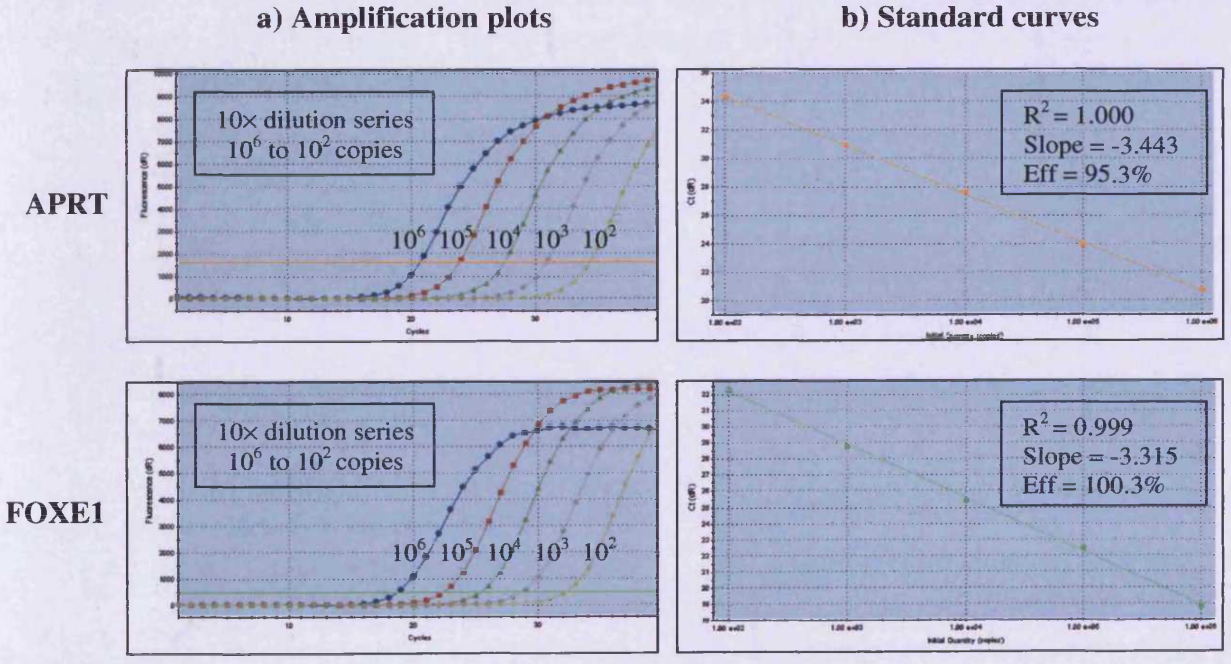

4.3.5. HaCaT Differentiation

The process of epidermal growth and differentiation can be subdivided into at least 4 functional compartments in epidermis. As cells move through the distinct epidermal layers, they are converted from proliferative, undifferentiated keratinocytes into highly differentiated post-mitotic cells. K14 is down-regulated as cells migrate upwards away from the dividing basal cells and K10 become the predominant keratin expressed.

Immunocytochemical analysis of proliferation (ki67 and K14) and differentiation markers (K10) was performed on HaCaT cells grown in parallel under identical conditions.

At culture day 6 (70-80% confluence) all the HaCaT cells were positive for K14 and Ki67 (Figure 4.10 & Figure 4.11) staining, but were negative for K10 staining (Figure 4.10). Therefore, they were judged to have a proliferative undifferentiated phenotype as possessed by the basal cells of the epidermis. In contrast, by culture day 12 (6 days post-calcium shift), the cell population was found to be rather heterogeneous. The most densely populated areas where the cell start to stratify are K10 positive indicating that they contain differentiating cells (Figure 4.12). The presence of differentiating HaCaT cell correlated well with a reduction in the number of cells positive for Ki67 staining (Figure 4.14).

Figure 4.10. Expression of Keratin 14 (K14) and Keratin 10 (K10) in HaCaT Cells at Culture Day 6. 1) Cell nuclei were counterstained with DAPI (blue channel), **2)** K14 was visualised by immunofluorescence with Texas Red (red channel), **3)** K10 was visualised by immunofluorescence with FITC (green channel), **4)** Composite image of red and green channels showing K14 and K10 proteins. Magnification: × 200. (Data kindly provided by Miss. T. Easter and Dr. P. Bowden, Cardiff).

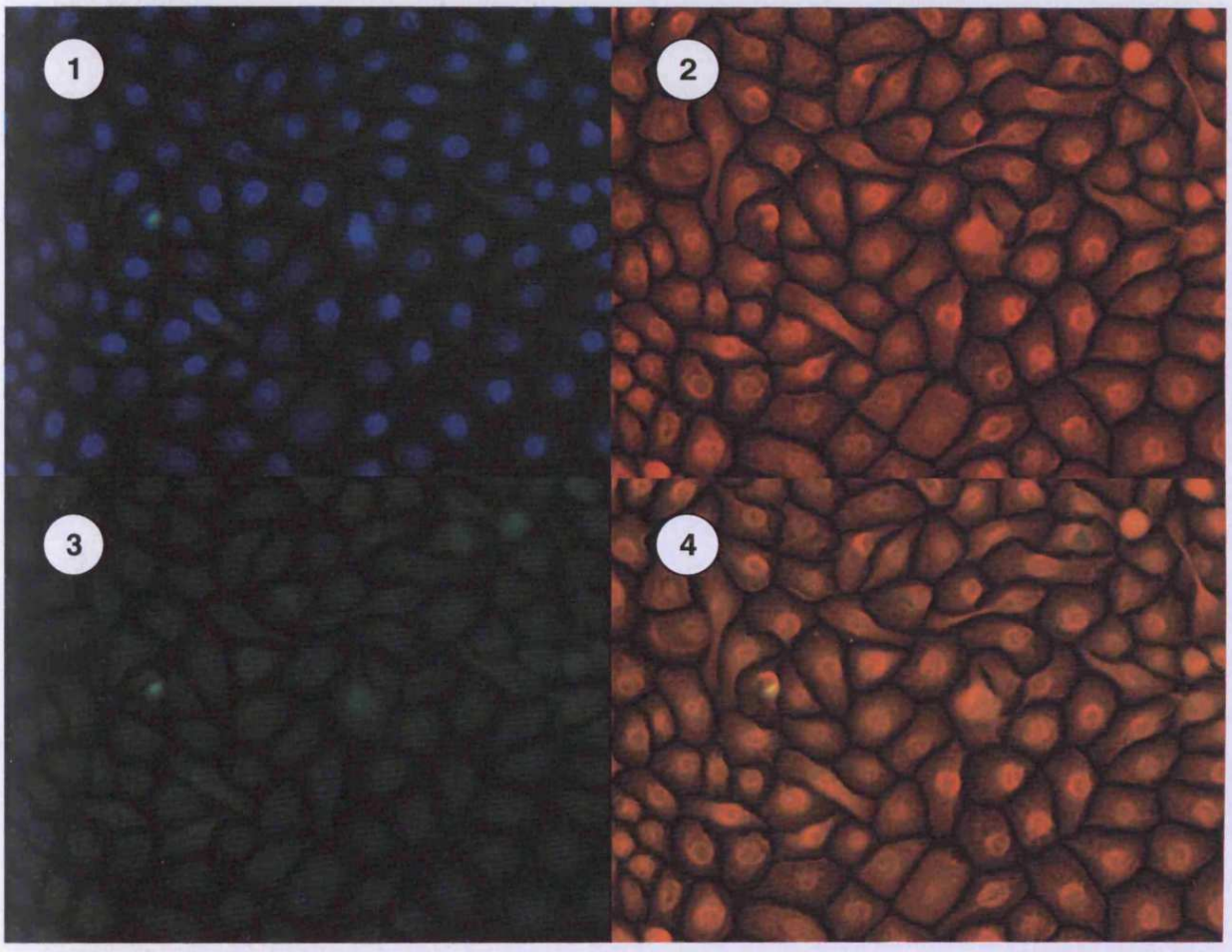

Figure 4.11. Expression of Keratin 14 (K14) and Ki67 in HaCaT Cells at Culture Day 6. 1) Cell nuclei were counterstained with DAPI (blue channel), **2)** K14 was visualised by immunofluorescence with Texas Red (red channel), **3)** Ki67 was visualised by immunofluorescence with FITC (green channel), **4)** Composite image of red and green channels showing K14 and Ki67 proteins. Magnification: × 200. (Data kindly provided by Miss. T. Easter and Dr. P. Bowden, Cardiff).

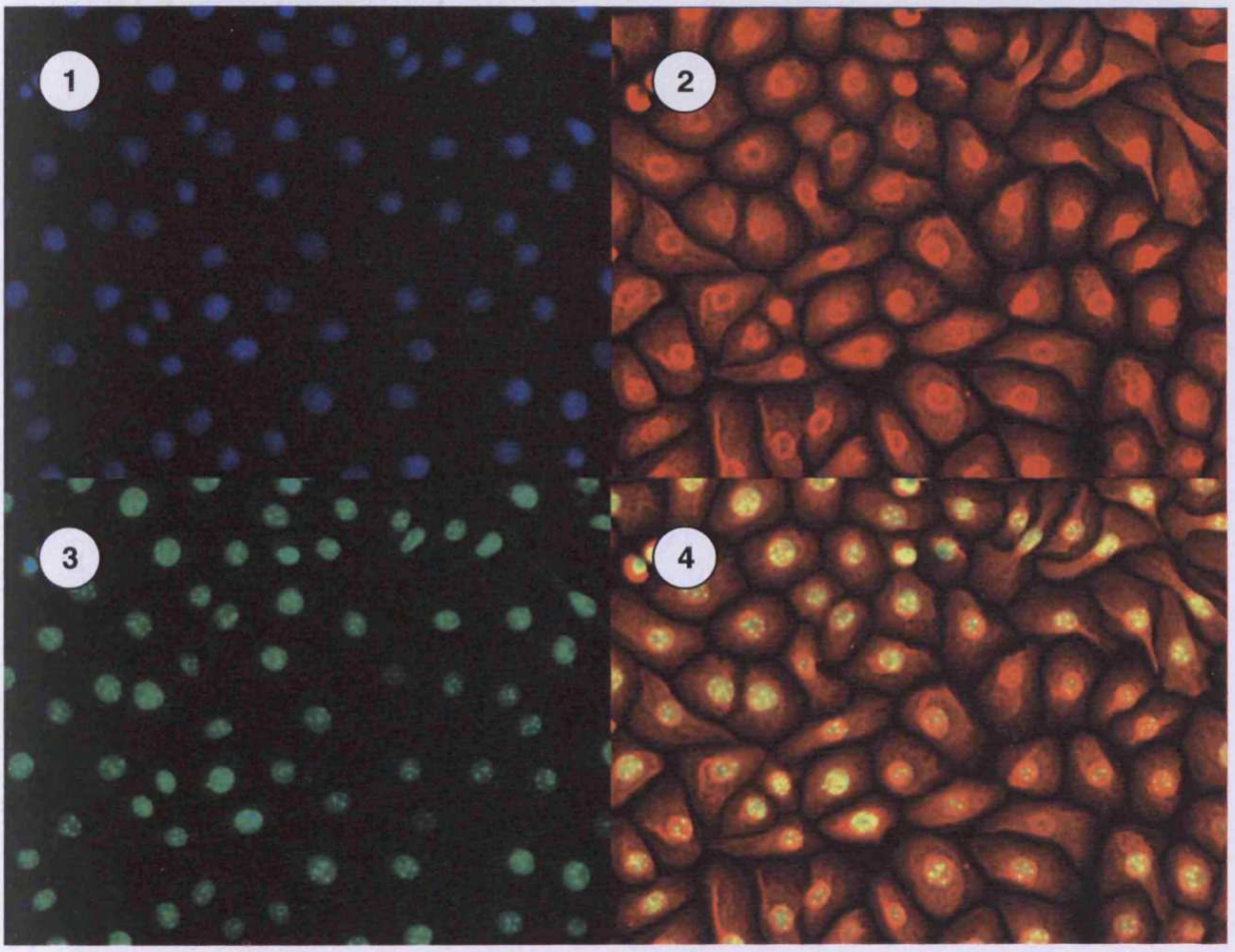

Figure 4.12. Expression of Keratin 14 (K14) and Keratin 10 (K10) in HaCaT Cells at Culture Day 12 (6 Days Post Calcium-Shift). **1)** Cell nuclei were counterstained with DAPI (blue channel), **2)** K14 was visualised by immunofluorescence with Texas Red (red channel), **3)** K10 was visualised by immunofluorescence with FITC (green channel), **4)** Composite image of red and green channels showing K14 and K10 proteins. Magnification: × 200. (Data kindly provided by Miss. T. Easter and Dr. P. Bowden, Cardiff).

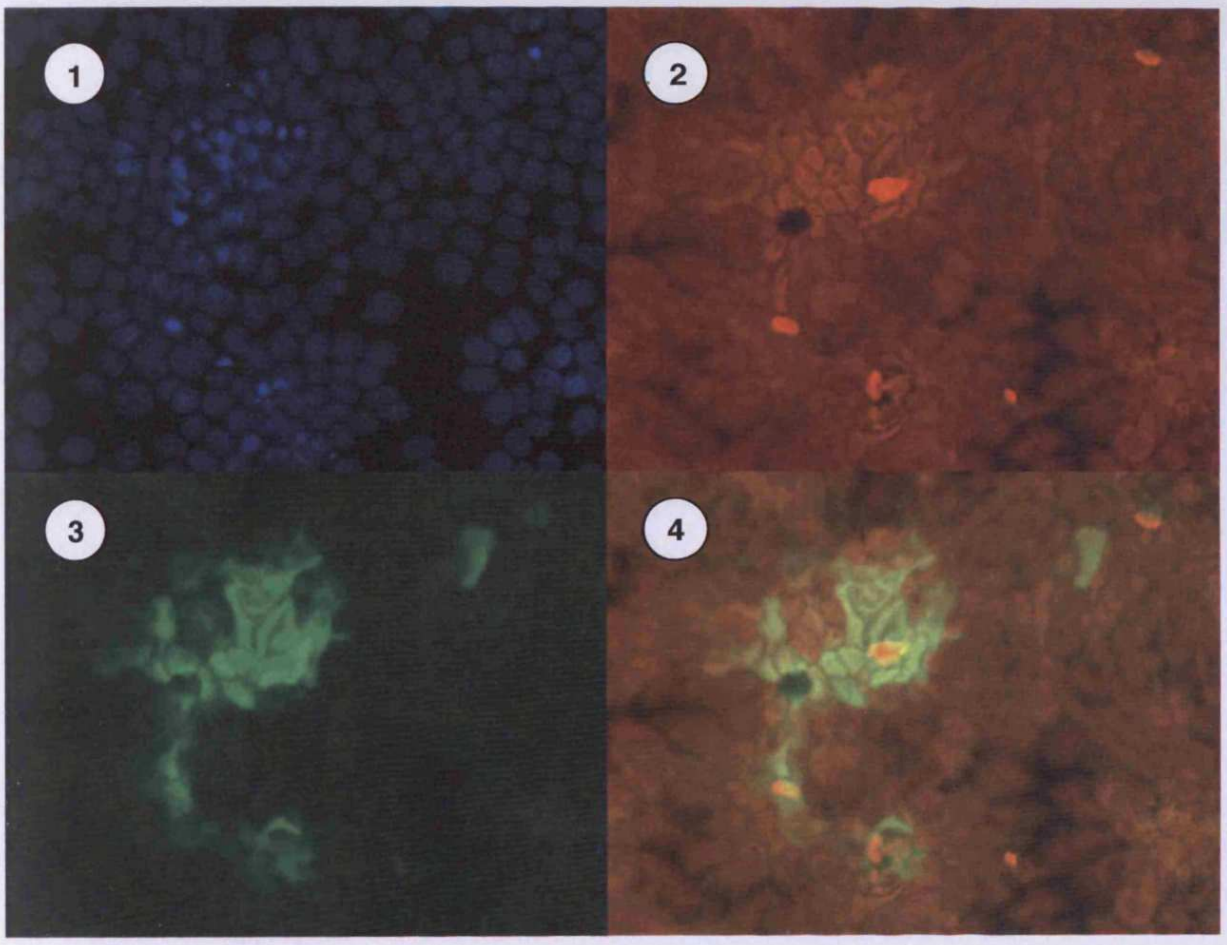

Figure 4.13. Expression of Keratin 14 (K14) and Ki67 in HaCaT Cells at Culture Day 12 (6 Days Post Calcium-Shift). **1)** Cell nuclei were counterstained with DAPI (blue channel), **2)** K14 was visualised by immunofluorescence with Texas Red (red channel), **3)** Ki67 was visualised by immunofluorescence with FITC (green channel), **4)** Composite image of red and green channels showing K14 and Ki67 proteins. Magnification: × 200. (Data kindly provided by Miss. T. Easter and Dr. P. Bowden, Cardiff).

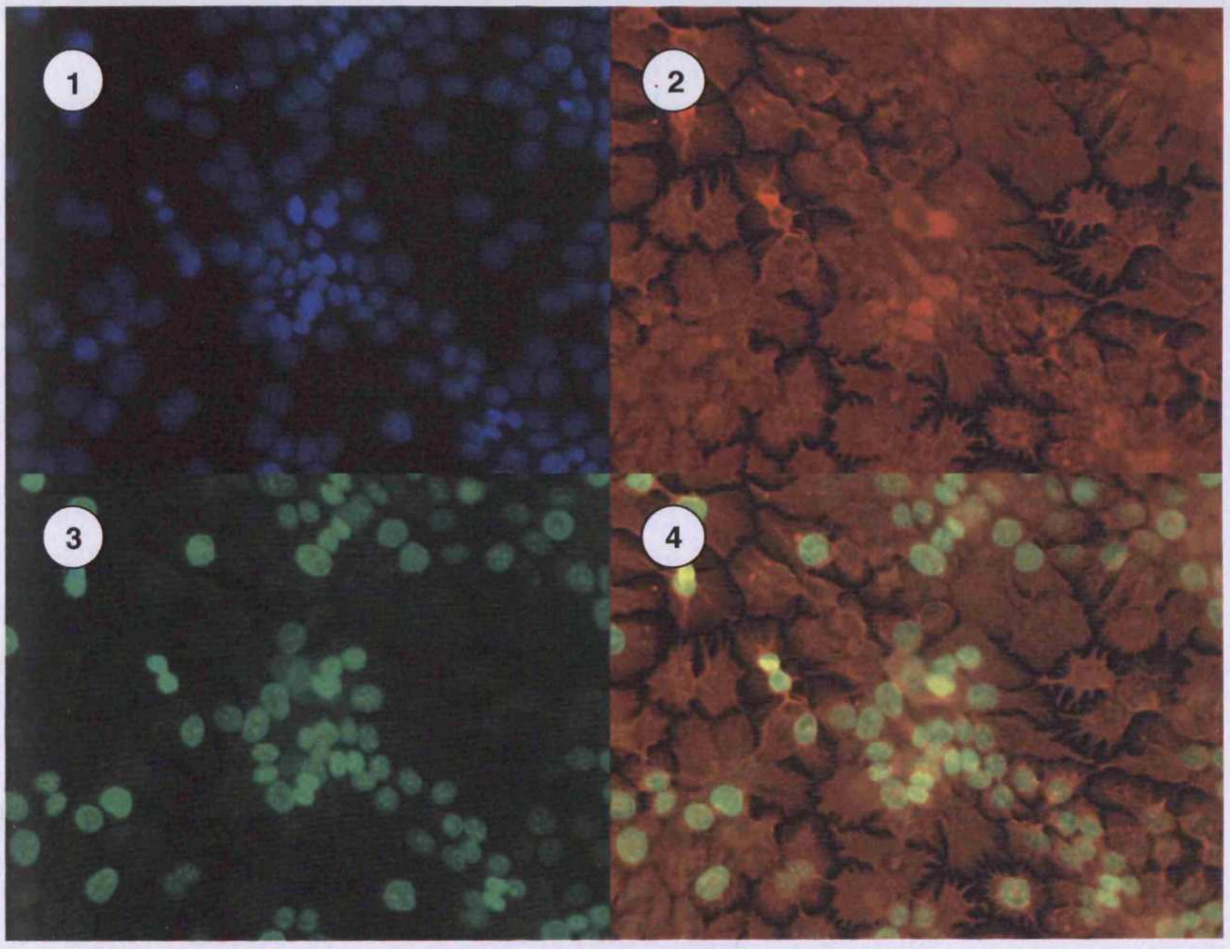

4.3.6. Spectrophotometer and Agarose Gel Analysis of Total RNA Samples

The concentration and purity of the RNA samples was determined by spec analysis and the readings are shown in Table 4.7. Integrity of the RNA was assessed by analysis on a 0.8% agarose gel (Figure 4.14).

Table 4.7. Spectrophotometer Analysis of HaCaT RNA

Sample	Abs_{260}	Abs_{280}	RNA concentration (ng/µl)	Ratio
Day 3 - 30-40% confluent	0.210	0.114	168.0	1.842
Day 6 - 70-80% confluent	0.495	0.237	396.0	2.089
Day 7 - 1 day post-shift	0.615	0.302	492.0	2.036
Day 9 - 3 days post-shift	0.886	0.451	708.8	1.965
Day 12 - 6 days post-shift	0.893	0.453	714.4	1.971
Day 12 - 6 days control	0.626	0.316	500.8	1.981

Figure 4.14. Agarose Gel Analysis of HaCaT RNA. 1) Day 3 - 30-40% confluent, **2)** Day 6 - 70-80% confluent, **3)** Day 7 - 1 day post-shift, **4)** Day 9 - 3 days post-shift, **5)** Day 12 - 6 days post-shift, **6)** Day 12 - 6 days control. Bands corresponding to the 28S, 18S rRNA can clearly be seen.

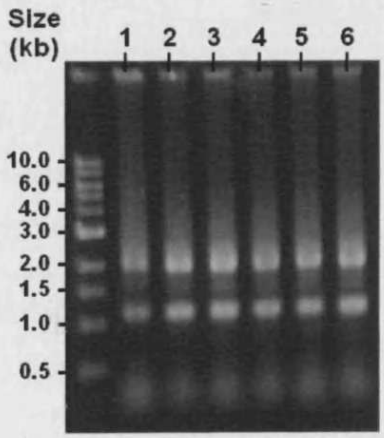

4.3.7. Absolute Quantification of FOXE1 Transcripts From a Typical Experiment

To allow the absolute quantification of FOXE1 transcripts two dilution series of standards were included in the assay, one for the APRT (the normaliser gene) and one for FOXE1. Due to run-to-run variations in reaction efficiency a fresh dilution series was prepared and included in every assay. Each standard curve was generated from a dilution series of plasmid-cDNA ranging 10^6 to 10^2 copies per reaction. Each plasmid-cDNA was amplified in triplicate and the mean average Ct value calculated. Table 4.8 shows the mean average Ct values generated from APRT and FOXE1 standards for a typical experiment. These were used to generate the standard curves shown in Figure 4.15. The equation of the line was then used to calculate the absolute transcript copy number of APRT and FOXE1. Finally the FOXE1 was normalised against APRT and expressed as number of FOXE1 copies per 10,000 APRT shown in Table 4.9. The same process was repeated for the TIMP3, MMP13 and COL1A1 genes (Table 4.10, Table 4.11 & Table 4.12).

Table 4.8. Ct Values for the APRT and FOXE1 Standards. Values are the mean average of a single experiment performed in triplicate.

APRT standards		FOXE1 standards	
No. of copies	Ct value	No. of copies	Ct value
1,000,000	17.77	1,000,000	18.71
100,000	20.79	100,000	22.31
10,000	24.37	10,000	25.34
1,000	27.89	1,000	28.67
100	31.34	100	32.18

Figure 4.15. APRT and FOXE1 Standard Curves. The linearity (represented by R^2) and equation of the line, as well as reaction efficiency are shown.

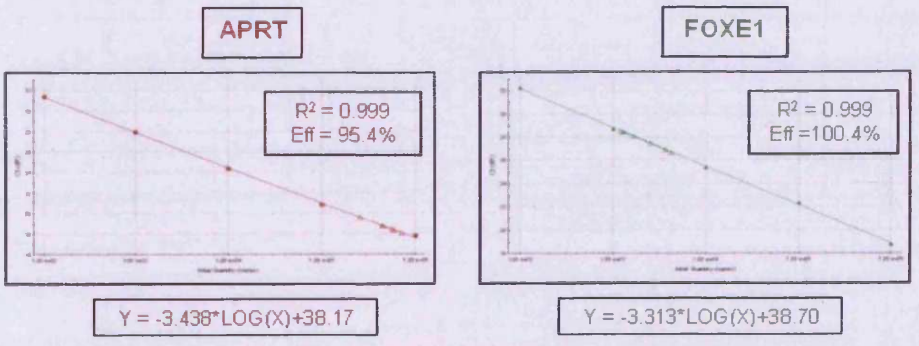

Table 4.9. Absolute Copy Numbers for APRT and FOXE1 Transcripts Throughout Cell Differentiation. For each sample, values were obtained from three independent experiments each performed in triplicate. The APRT values were used to normalise the FOXE1 values, to control for differences in RNA integrity and efficiency of reverse transcription. Statistical analysis used Students T test.

a. HaCaT

Sample	FOXE1	APRT	Normalised	Mean	S.D	P-Value
Day 3 (30% Confluence)	1,108	547,800	20	20	12.79	/
	1,459	782,200	19			
	1,847	444,600	42			
Day 6 (80% Confluenece)	3,048	430,800	71	63	9.22	0.0510
	3,240	497,600	65			
	3,347	634,800	53			
Day 7 (1 Day Post-Shift)	1,487	590,900	25	31	5.51	0.0313
	2,069	678,600	30			
	1,630	450,400	36			
Day 9 (3 Days Post-Shift)	2,152	608,400	35	53	11.37	0.0492
	4,384	852,000	51			
	2,500	343,400	73			
Day 12 (6 Days Post-Shift)	3,143	505,900	62	65	19.52	0.1640
	3,391	723,900	47			
	2,940	343,500	86			

b. HaCaT-LUC

Sample	FOXE1	APRT	Normalised	Mean	S.D	P-Value
Day 3 (30% Confluence)	924	292,000	32	27	5.00	/
	881	400,300	22			
	1,287	476,600	27			
Day 6 (80% Confluenece)	4,594	918,800	50	42	7.21	0.0051
	3,335	926,300	36			
	3,427	856,700	40			
Day 7 (1 Day Post-Shift)	3,842	937,100	41	36	4.58	0.0296
	2,959	924,600	32			
	2,834	809,700	35			
Day 9 (3 Days Post-Shift)	3,346	408,000	82	72	9.07	0.0025
	2,540	396,900	64			
	2,676	376,900	71			
Day 12 (6 Days Post-Shift)	4,374	433,100	101	86	13.45	0.0180
	3,437	458,200	75			
	4,672	569,700	82			

Table 4.10. Absolute Copy Numbers for APRT and TIMP3 Transcripts Throughout HaCaT Differentiation. For each sample, values were obtained from three independent experiments each performed in triplicate. The APRT values were used to normalise the TIMP3 values, to control for differences in RNA integrity and efficiency of reverse transcription. Statistical analysis used Students T test.

a. HaCaT

Sample	TIMP3	APRT	Normalised	Mean	S.D	P-Value
Day 3 (30% Confluence)	11,550	559,400	206	213	23.43	/
	12,580	650,100	194			
	12,733	532,788	239			
Day 6 (80% Confluenece)	26,360	838,500	314	360	55.39	0.0345
	27,890	661,800	421			
	26,310	766,600	343			
Day 7 (1 Day Post-Shift)	14,280	778,300	183	189	23.67	0.0080
	17,960	834,200	215			
	13,820	817,600	169			
Day 9 (3 Days Post-Shift)	19,360	917,100	211	252	43.70	0.0343
	10,380	418,600	248			
	28,320	949,800	298			
Day 12 (6 Days Post-Shift)	38,500	710,800	542	573	161.46	0.0269
	40,480	942,500	429			
	62,780	839,500	748			

b. HaCaT-LUC

Sample	TIMP3	APRT	Normalised	Mean	S.D	P-Value
Day 3 (30% Confluence)	10,550	639,600	165	136	26.85	/
	7,398	660,500	112			
	8,843	675,000	131			
Day 6 (80% Confluenece)	31,710	623,000	509	498	10.60	0.0003
	12,000	246,000	488			
	37,500	756,000	496			
Day 7 (1 Day Post-Shift)	15,620	694,000	225	217	7.64	0.0000
	10,710	510,000	210			
	19,140	890,000	215			
Day 9 (3 Days Post-Shift)	26,260	750,400	350	324	24.64	0.0041
	21,240	705,600	301			
	23,550	733,600	321			
Day 12 (6 Days Post-Shift)	57,100	818,100	698	665	31.19	0.0001
	50,080	787,500	636			
	51,030	772,000	661			

Table 4.11. Absolute Copy Numbers for APRT and MMP13 Transcripts Throughout HaCaT Differentiation. For each sample, values were obtained from three independent experiments each performed in triplicate. The APRT values were used to normalise the MMP13 values, to control for differences in RNA integrity and efficiency of reverse transcription. Statistical analysis used Students T test.

a. HaCaT

Sample	MMP13	APRT	Normalised	Mean	S.D	P-Value
Day 3 (30% Confluence)	5,701	439,790	130	137	39.06	/
	6,652	648,200	103			
	7,809	434,790	180			
Day 6 (80% Confluenece)	6,022	400,660	150	138	11.68	0.4944
	7,231	533,290	136			
	5,367	421,810	127			
Day 7 (1 Day Post-Shift)	10,280	291,070	353	438	75.73	0.0130
	17,030	341,780	498			
	15,440	333,210	463			
Day 9 (3 Days Post-Shift)	40,750	256,490	1,589	1,701	137.15	0.0014
	58,290	351,090	1,660			
	53,910	290,800	1,854			
Day 12 (6 Days Post-Shift)	40,200	230,580	1,743	1,475	287.60	0.2264
	48,450	320,930	1,510			
	47,900	408,910	1,171			

b. HaCaT-LUC

Sample	MMP13	APRT	Normalised	Mean	S.D	P-Value
Day 3 (30% Confluence)	678	521,900	13	10	4.16	/
	247	493,900	5			
	540	490,800	11			
Day 6 (80% Confluenece)	2,153	430,500	50	39	10.54	0.0087
	1,162	400,600	29			
	2,026	533,200	38			
Day 7 (1 Day Post-Shift)	3,857	428,600	90	59	27.23	0.0878
	3,609	949,800	38			
	3,554	710,800	50			
Day 9 (3 Days Post-Shift)	9,426	698,200	135	92	37.86	0.0345
	3,560	474,700	75			
	2,610	401,600	65			
Day 12 (6 Days Post-Shift)	12,950	501,900	258	243	13.23	0.0047
	13,950	598,900	233			
	12,350	518,900	238			

Table 4.12. Absolute Copy Numbers for APRT and COL1A1 Transcripts Throughout HaCaT Differentiation. For each sample, values were obtained from three independent experiments each performed in triplicate. The APRT values were used to normalise the COL1A1 values, to control for differences in RNA integrity and efficiency of reverse transcription. Statistical analysis used Students T test.

a. HaCaT

Sample	COL1A1	APRT	Normalised	Mean	S.D	P-Value
Day 3 (30% Confluence)	23	505,680	5	5	0.79	/
	25	535,840	5			
	30	501,980	6			
Day 6 (80% Confluenece)	25	498,940	5	8	3.91	0.1406
	30	508,930	6			
	49	402,190	12			
Day 7 (1 Day Post-Shift)	49	389,230	13	13	2.01	0.1075
	78	502,910	16			
	50	429,080	12			
Day 9 (3 Days Post-Shift)	97	389,230	25	29	10.30	0.0415
	121	298,970	40			
	101	480,910	21			
Day 12 (6 Days Post-Shift)	115	261,970	44	45	6.69	0.0096
	109	209,090	52			
	152	390,890	39			

b. HaCaT-LUC

Sample	COL1A1	APRT	Normalised	Mean	S.D	P-Value
Day 3 (30% Confluence)	213	531,400	4	3	1.00	/
	97	483,100	2			
	148	492,300	3			
Day 6 (80% Confluenece)	587	533,200	11	10	1.53	0.0012
	343	428,900	8			
	563	563,000	10			
Day 7 (1 Day Post-Shift)	620	442,600	14	10	3.21	0.3174
	443	553,800	8			
	542	601,900	9			
Day 9 (3 Days Post-Shift)	933	777,100	12	11	1.00	0.3333
	438	438,100	10			
	596	541,400	11			
Day 12 (6 Days Post-Shift)	1,097	421,900	26	23	3.51	0.0076
	949	499,700	19			
	1,150	500,200	23			

4.3.8. FOXE1 Transcript Levels Vary During Differentiation of HaCaT and HaCaT-LUC Cells

In both HaCaT and HaCaT-LUC cells, FOXE1 transcript levels were lowest at culture day 3, when the cells are at a low density (30-40% confluent). In keeping with recent findings that the differentiation of human keratinocytes can be induced by cell-contact, even in the presence of a low extracellular Ca^{2+} concentration, we observed a reduction in the percentage of proliferating cells by culture day 6 (as indicated by K10 and Ki67 staining). The level of FOXE1 transcripts was found to increase during this time ($P<0.01$ for HaCaT-LUC). At culture day 6, the Ca^{2+} concentration of the medium was increased and this was found to initiate a transient dip in the level of FOXE1. Levels then continue to rise in both cell populations, as shown in Figure 4.16.

Our attempts to use the HaCat-LUC cells in reporter-style assays to investigate the signalling cascades implicated in regulating FOXE1 expression in HaCaT were not successful. However, in keeping with the increase in FOXE1 transcripts as differentiation proceeds, there was an elevation in luciferase reporter transcripts, after the calcium-shift, as shown in Figure 4.20. This suggests that the method is suitable for the investigation of FOXE1 target genes.

4.3.9. Transcript Levels of TIMP3, MMP13 and COL1A1 Vary During Keratinocyte Differentiation of HaCaT and HaCaT-LUC Cells

The system was then applied to the investigation of genes identified as being potential down-stream targets for FOXE1 in Chapter 3. The expression profile of TIMP3 most closely resembled that of FOXE1, in both cell populations (Figure 4.17). In contrast MMP13 and COL1A1, although both increased by keratinocyte differentiation, did not mirror exactly the expression of FOXE1 (Figures 4.18 & 4.19). The fold-changes in all four transcription factors are in Figures 4.20 & 4.21.

4.3.10. Transcript Levels of TIMP3 and FOXE1 Demonstrate a Transient Decrease Following the Calcium-Shift in HaCaT and HaCaT-LUC Cells.

In all experiments a transient dip in FOXE1 transcript copy number was noticed post calcium-shift. To investigate in more detail, samples were taken at 2 hour intervals and demonstrate that transcript levels of both FOXE1 (Figure 4.22) and TIMP3 (Figure 4.23) decrease for the first 8 hours, when they reach a plateau, and then begin to increase, although not reaching pre-shift levels until more than 24 hours later. Transcripts for MMP13 and COL1A1 did not follow this pattern (data not shown). The fold-changes in both transcription factors is shown in Figure 4.24.

4.3.11. FOXE1 and DREAM Transcripts can be 'Knocked Down' using Specific siRNAs

In an attempt to confirm that TIMP3 transcription is regulated by FOXE1, siRNA experiments were undertaken. The same approach was applied to investigate whether FOXE1 expression is regulated by the calcium-binding transcription factor DREAM, as has been to be the case in the thyroid gland (D'Andrea *et al.*, 2005). Titration curves were performed using two specific siRNAs, and a scrambled control sequence, for FOXE1 and DREAM, transfected into HaCaT cells at 80% confluence. As shown in Figure 4.25, a dose dependent decrease in FOXE1 transcript copy number, plateauing at 3 nM transfected siRNA for one, but not both of the selected sequences for this transcription factor. In contrast, dose dependent knock-down, again with a plateau at 3 nM, was obtained with both specific DREAM sequences, as demonstrated in Figure 4.26.

4.3.12. FOXE1 and DREAM 'knock-down' Influences Other Gene Transcripts

Experiments were then performed using the optimal concentration (3 nM) and sequence for knockdown of FOXE1 (283) and DREAM (76). An approximately 30% reduction in FOXE1 transcripts, accompanied by 40% and 10% reductions in TIMP3 and DREAM respectively, when

applying FOXE1-283, as shown in Figure 4.27. The results of the DREAM knockdown were more puzzling, resulting in the expected 60% and 50% reduction in DREAM and TIMP3 respectively, but FOXE1 transcripts were increased (Figure 4.28). Time limits precluded further investigation

Figure. 4.16. FOXE1 Expression Profile Throughout HaCaT and HaCaT-LUC Differentiation. The values are the mean (± S.D) of three independent experiments each performed in triplicate, normalised to APRT i.e. each value is expressed as the number of FOXE1 copies / 10,000 APRT copies. Statistical analysis used Student's T test (* represents P<0.05, ** represents P<0.01).

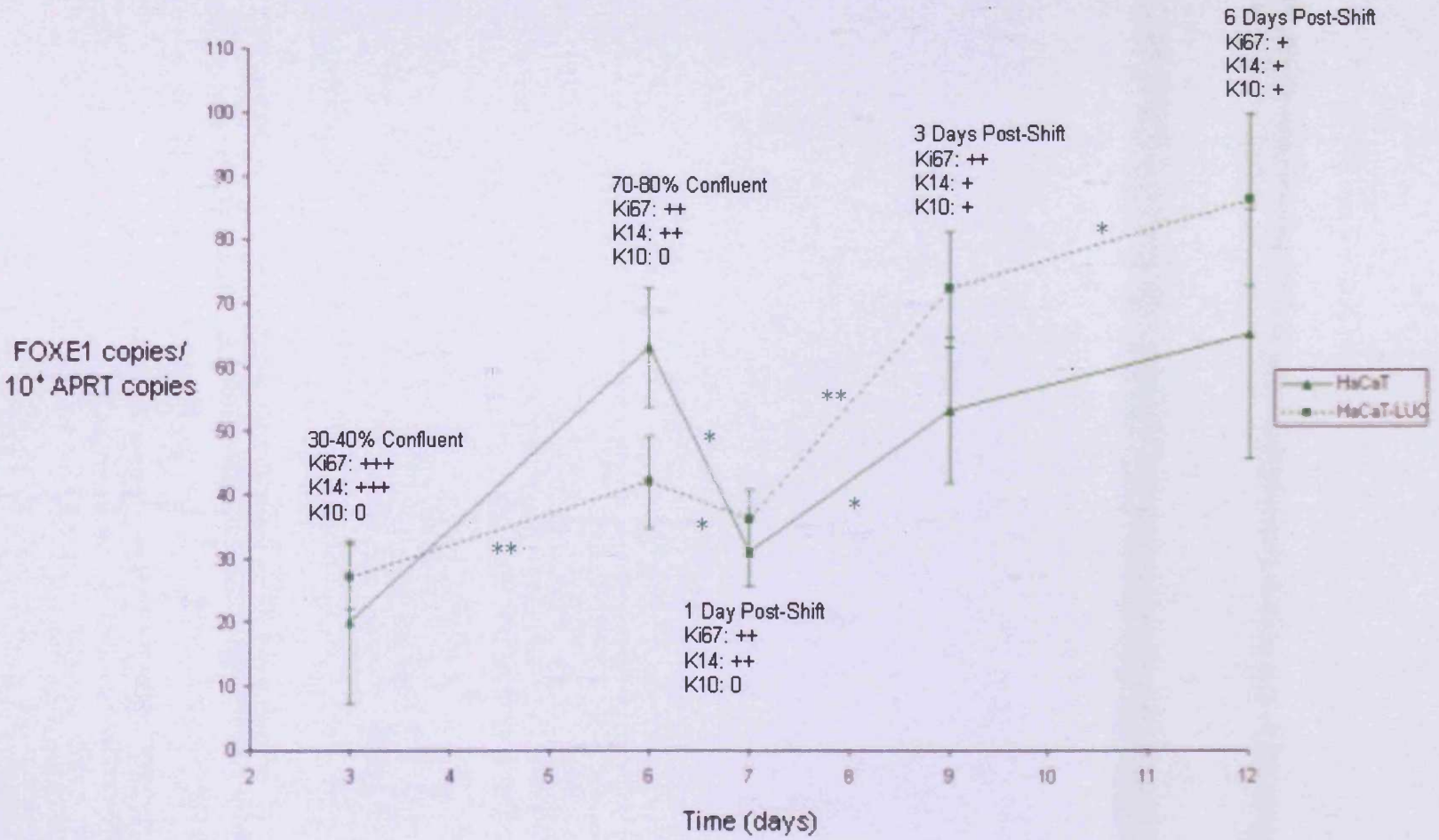

Figure. 4.17. TIMP3 Expression Profile Throughout HaCaT and HaCaT-LUC Differentiation. The values are the mean (± S.D) of three independent experiments each performed in triplicate, normalised to APRT i.e. each value is expressed as the number of TIMP3 copies / 10,000 APRT copies. Statistical analysis used Student's T test (* represents P<0.05, ** represents P<0.01).

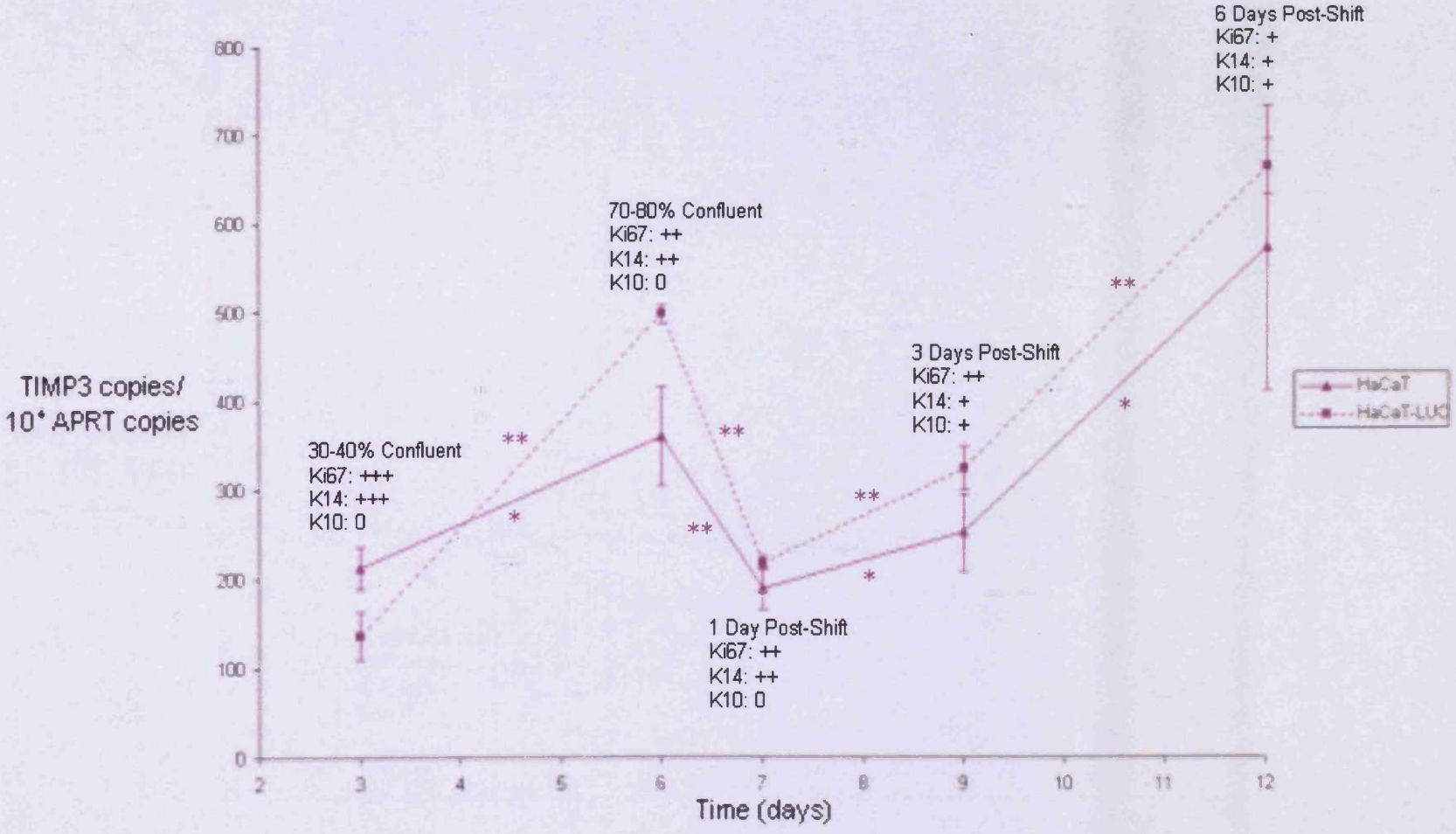

Figure. 4.18. MMP13 Expression Profile Throughout HaCaT and HaCaT-LUC Differentiation. The values are the mean (± S.D) of three independent experiments each performed in triplicate, normalised to APRT i.e. each value is expressed as the number of MMP13 copies / 10,000 APRT copies. Statistical analysis used Students T test (* represents $p<0.05$, ** represents $p<0.01$) .

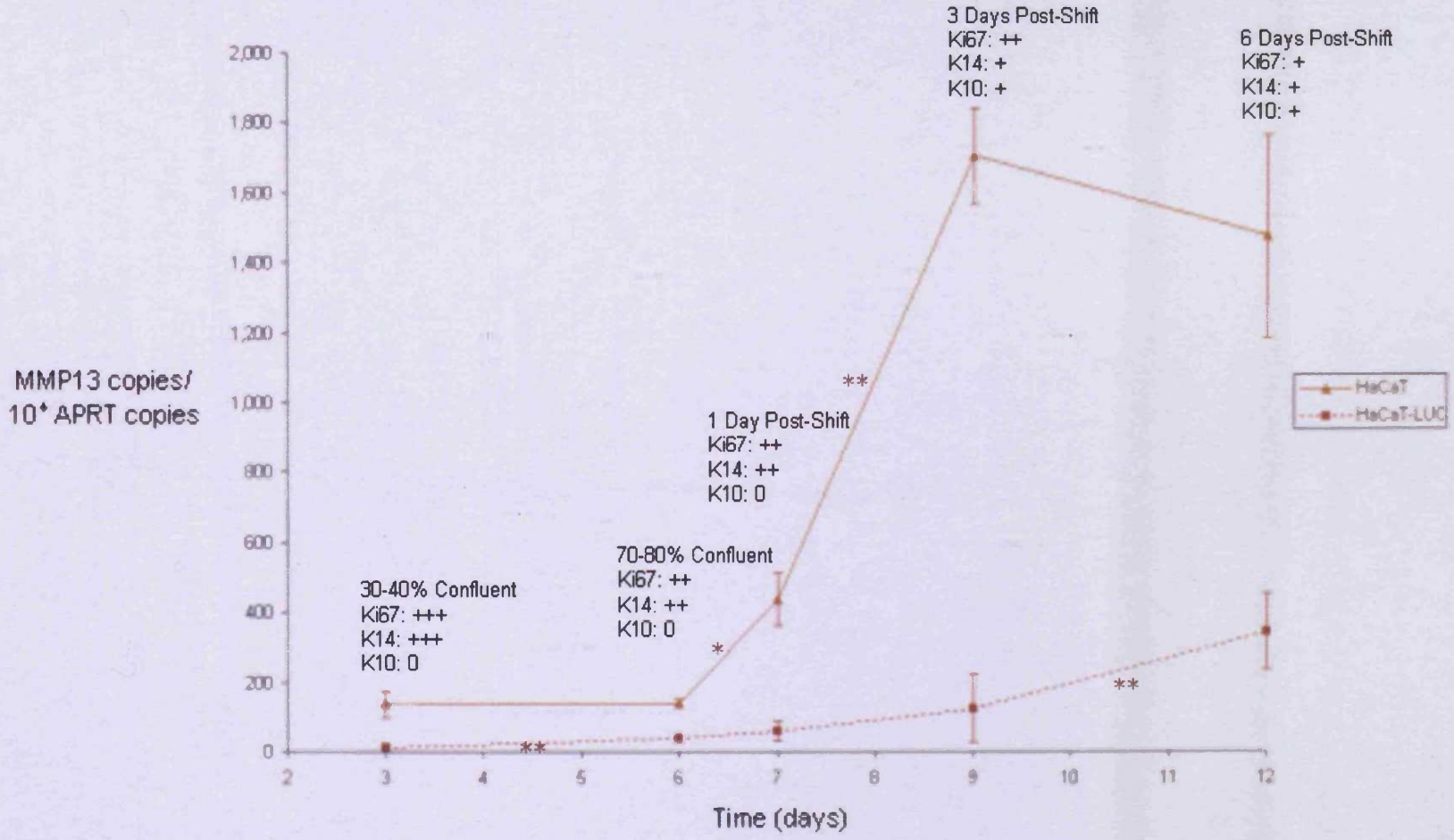

Figure. 4.19. COL1A1 Expression Profile Throughout HaCaT and HaCaT-LUC Differentiation. The values are the mean (± S.D) of three independent experiments each performed in triplicate, normalised to APRT i.e. each value is expressed as the number of COL1A1 copies / 100,000 APRT copies. Statistical analysis used Students T test (* represents $p<0.05$, ** represents $p<0.01$).

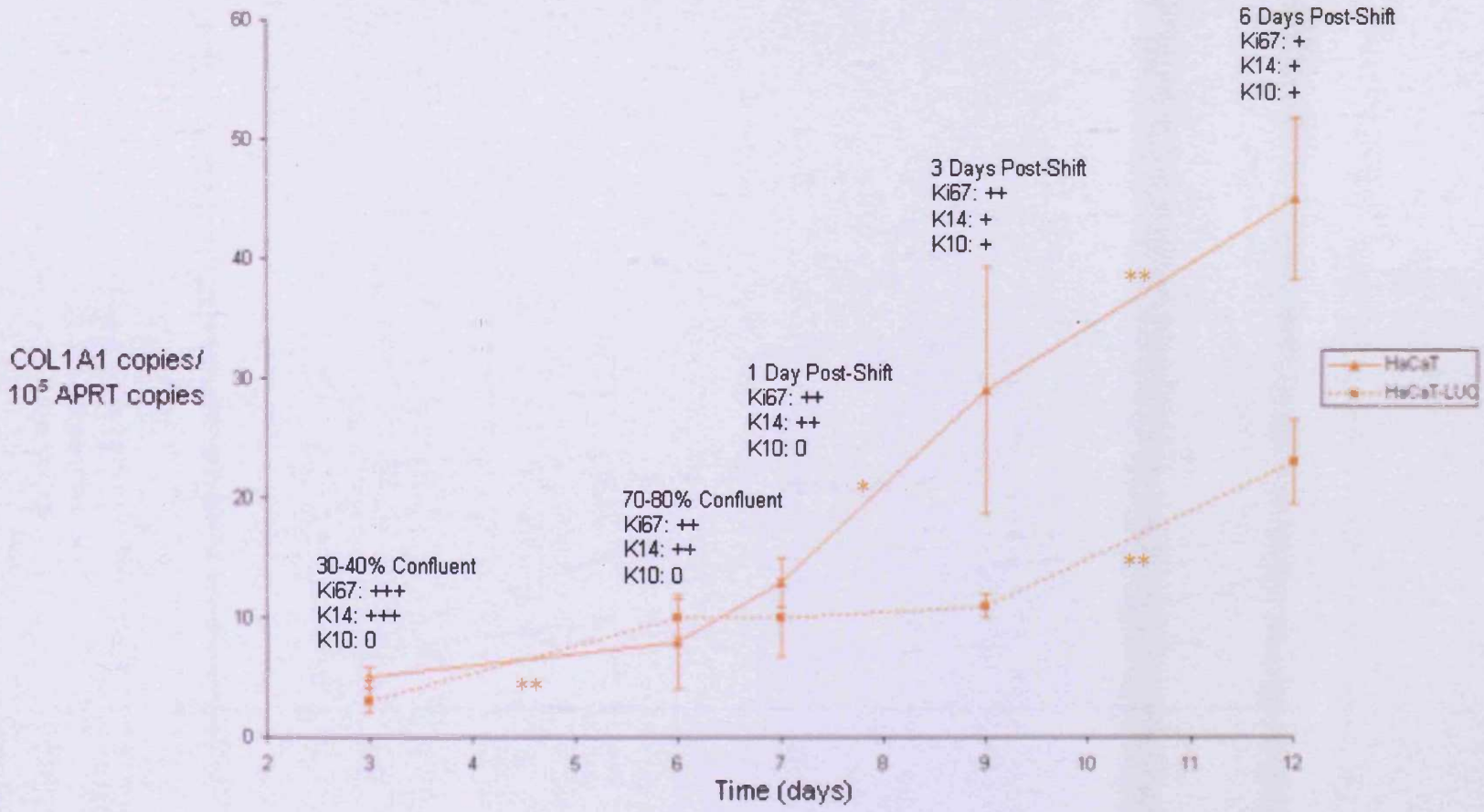

Figure. 4.20. Fold Change in Transcript Levels Relative to Day 3. The values are the mean (± S.D) of three independent experiments each performed in triplicate, normalised to APRT.

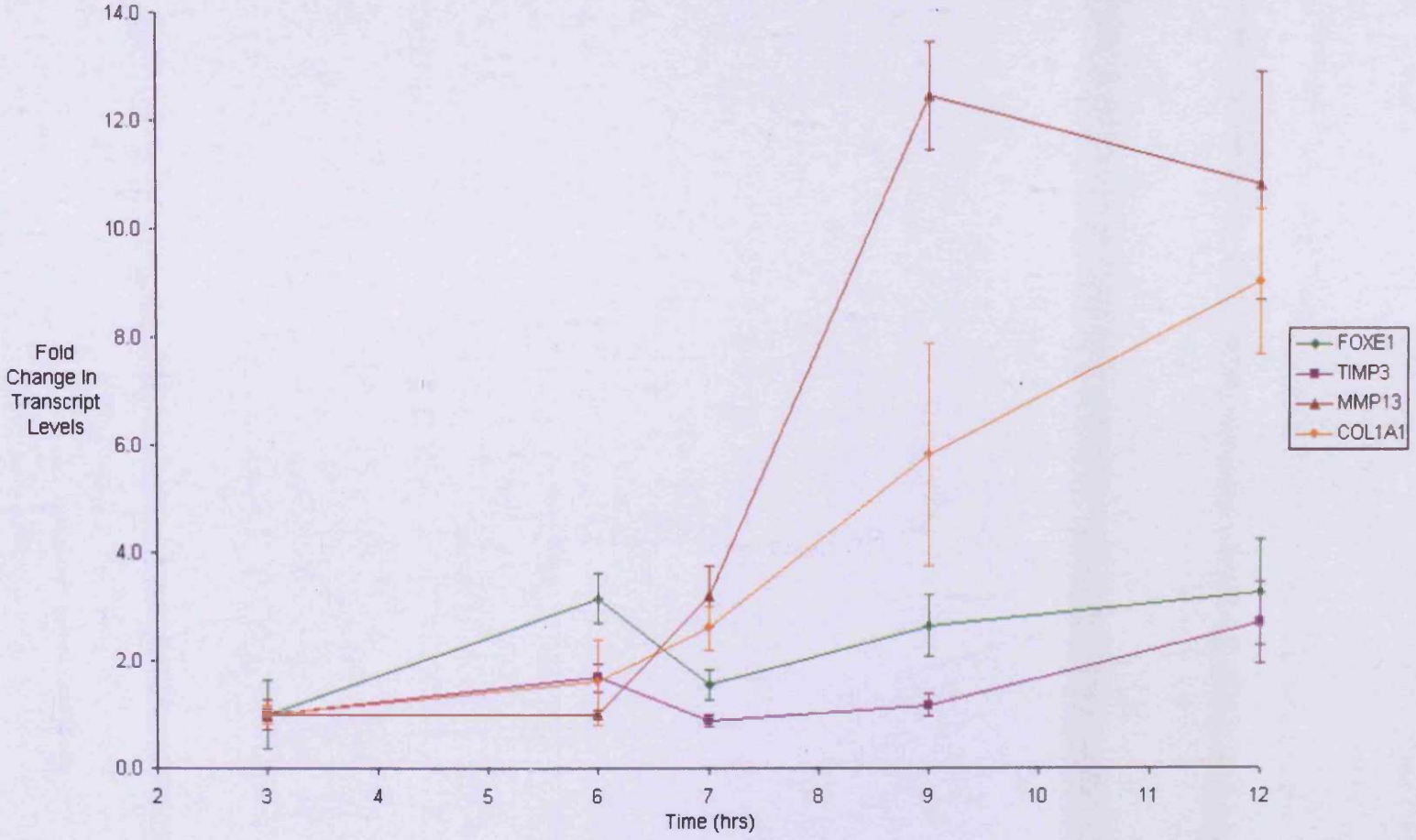

Figure. 4.21. Fold Change in Transcript Levels Relative to Day 3. The values are the mean (± S.D) of three independent experiments each performed in triplicate, normalised to APRT.

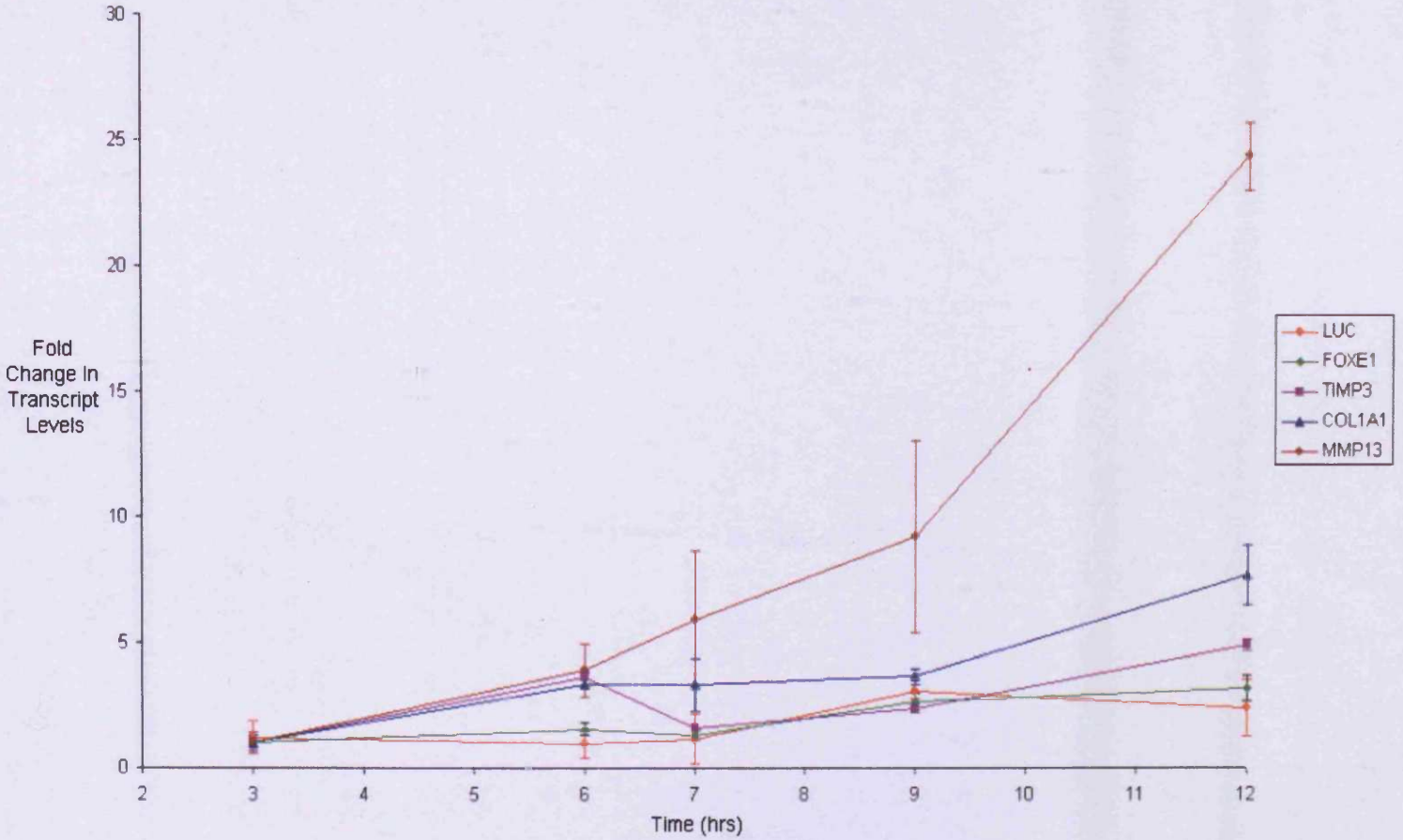

Figure. 4.22. FOXE1 Transcript Profile 0-24hrs Post-Calcium Shift. Values are the mean (± S.D) of triplicates normalised to APRT i.e. each value is expressed as number of FOXE1 copies / 10,000 APRT copies.

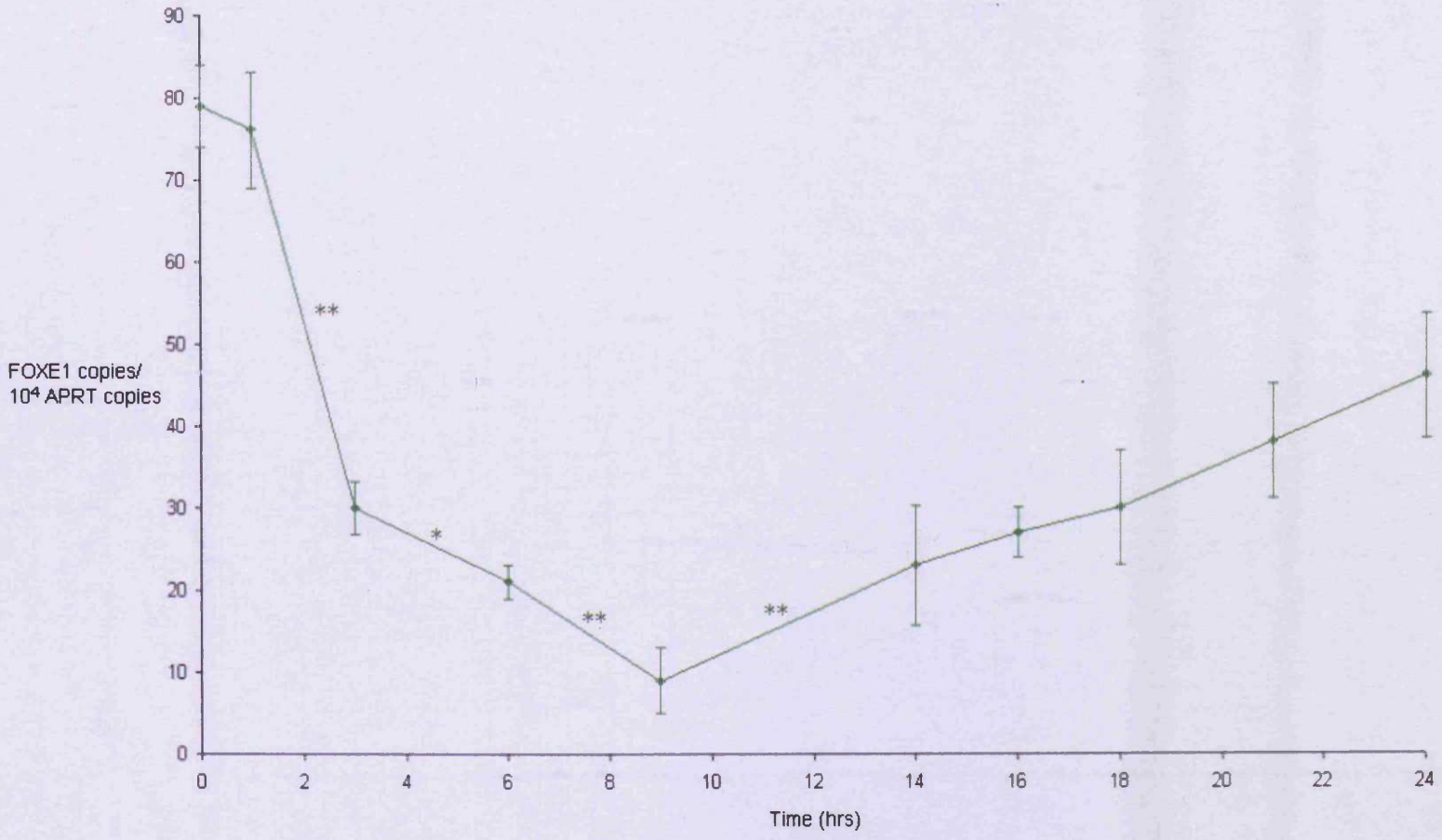

Figure. 4.23. TIMP3 Transcript Profile 0-24hrs Post-Calcium Shift. Values are the mean (± S.D) of triplicates normalised to APRT i.e. each value is expressed as number of TIMP3 copies / 10,000 APRT copies.

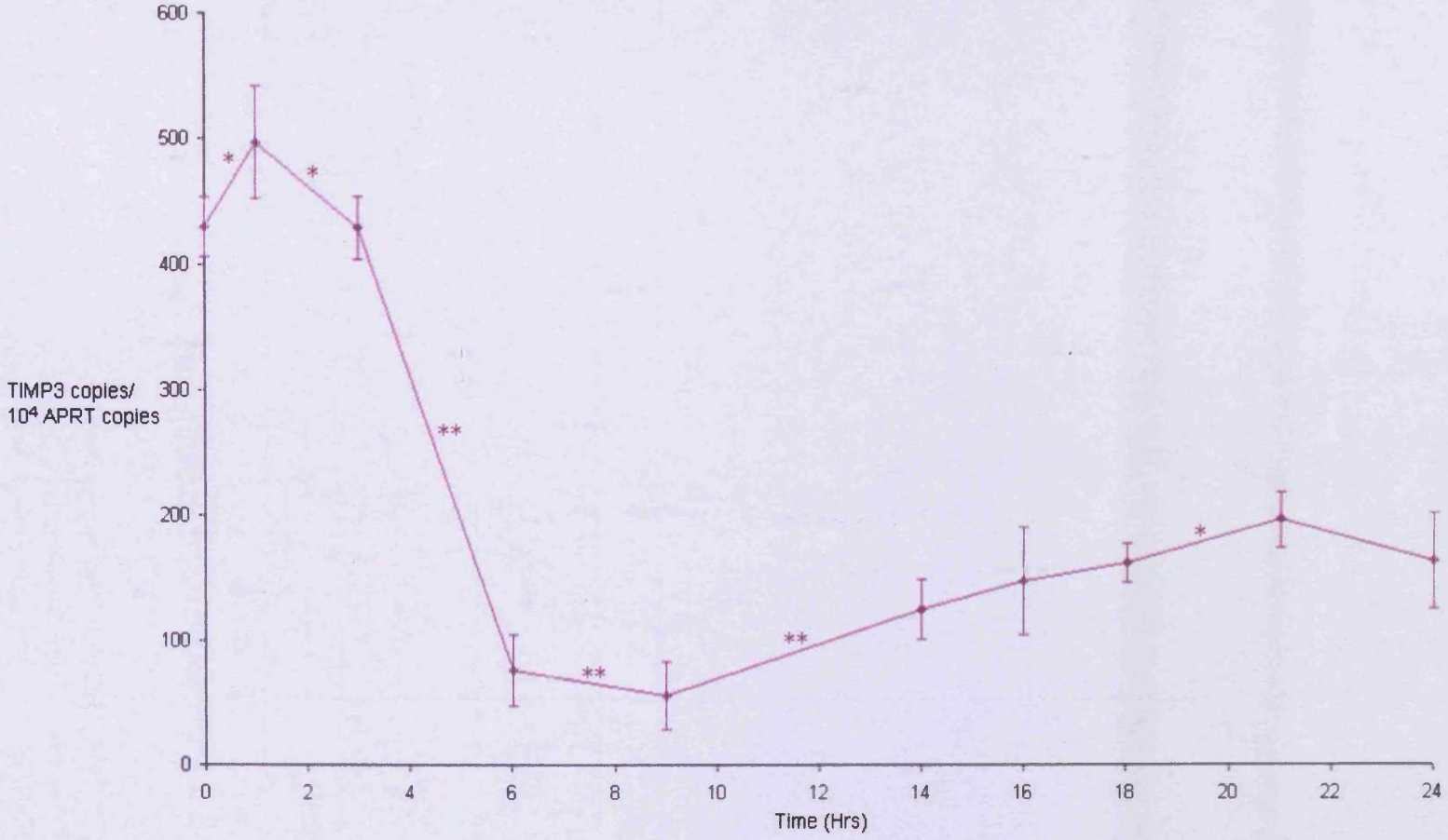

Figure. 4.24. Fold Change in FOXE1 and TIMP3 Transcript Levels Relative to 0hrs (Time of Calcium-Shift). The values are the mean (± S.D) of three independent experiments each performed in triplicate, normalised to APRT.

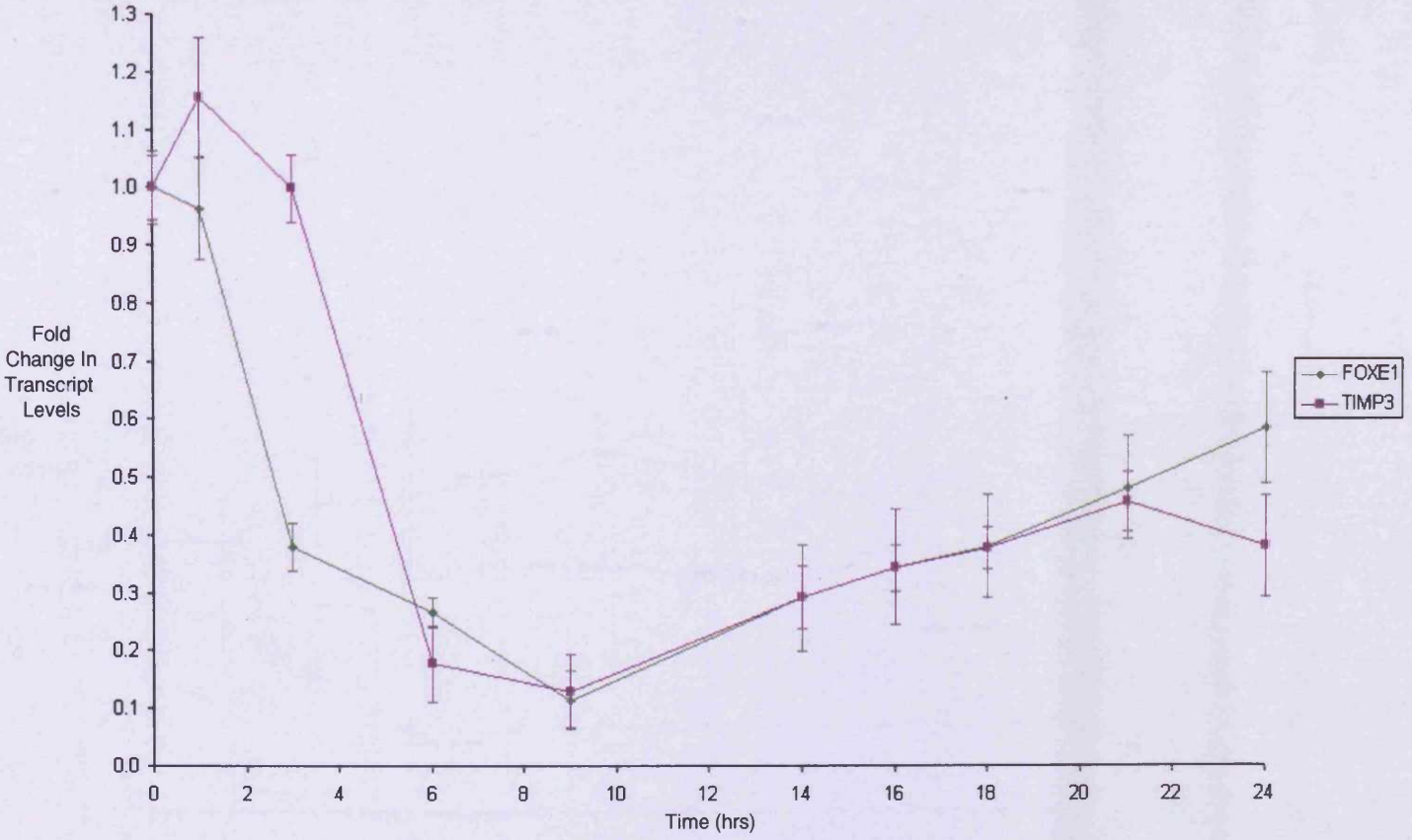

Figure 4.25. FOXE1 siRNA Titrations. Values are the mean (± S.D) of a single experiment performed in triplicate normalised to APRT i.e. each value is expressed as number of FOXE1 copies / 10,000 APRT copies.

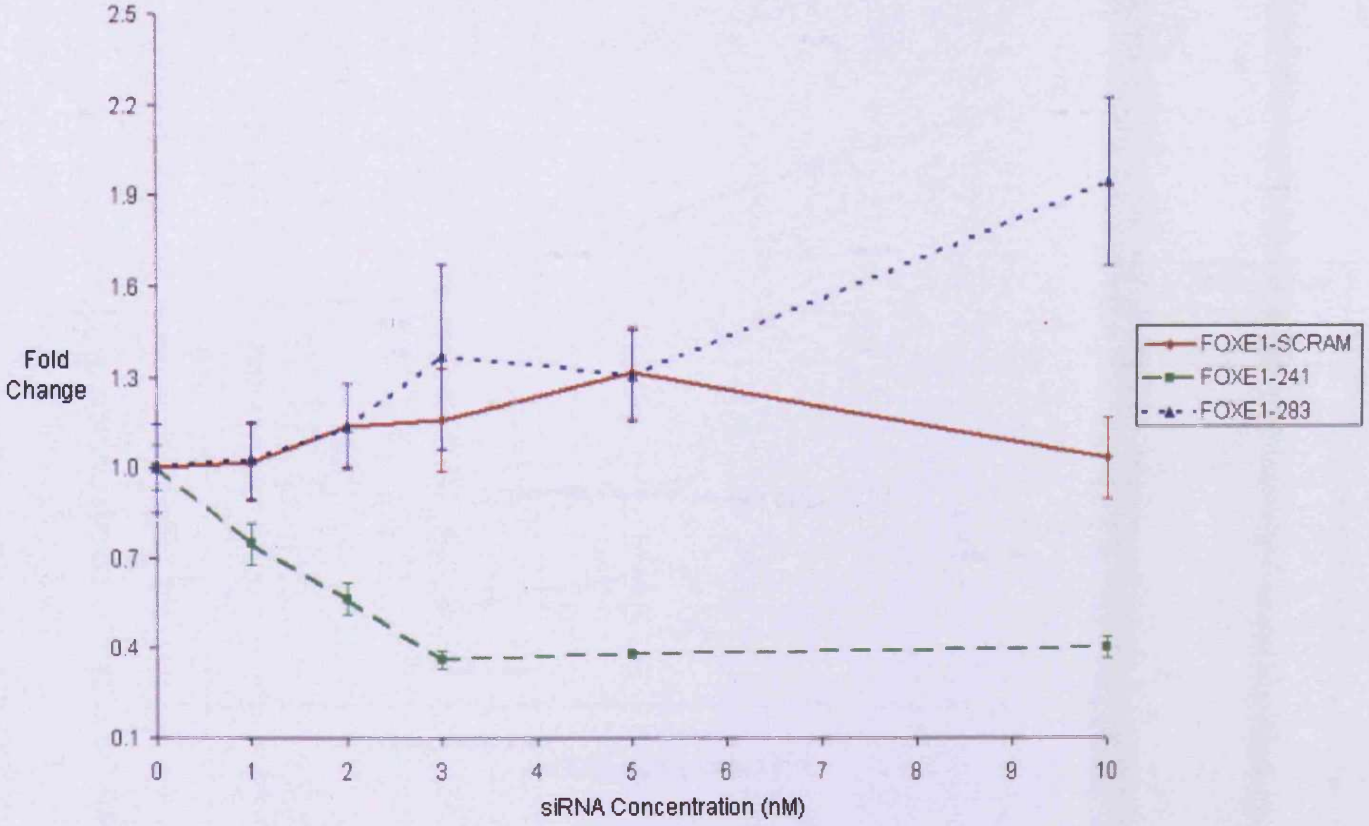

Figure 4.26. DREAM siRNA Titrations. Values are the mean (± S.D) of a single experiment performed in triplicate normalised to APRT i.e. each value is expressed as number of DREAM copies / 10,000 APRT copies.

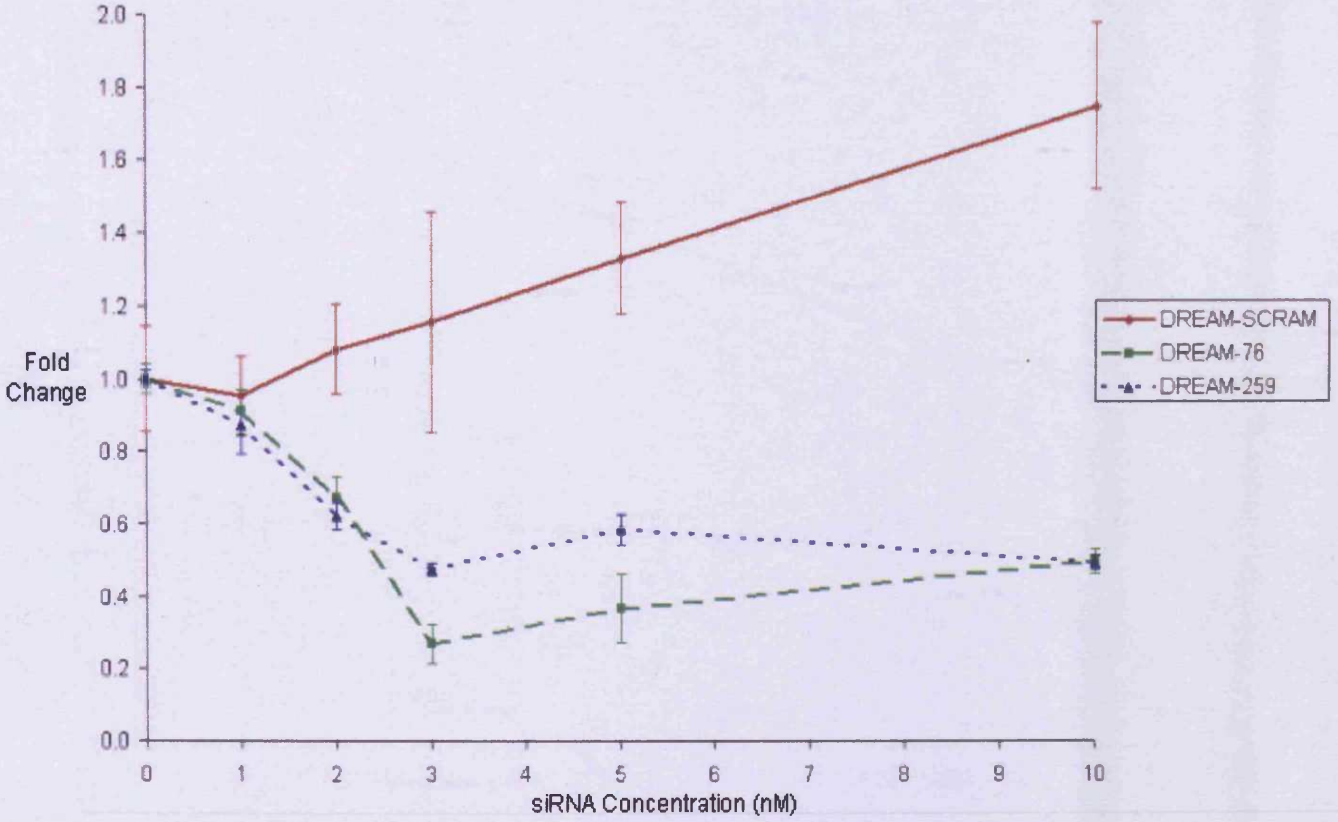

Figure 4.27. FOXE1 Knockdown. Values are the mean (± S.D) of three independent experiment, each performed in triplicate normalised to APRT i.e. each value is expressed as number of DREAM copies / 10,000 APRT copies. Statistical analysis used Students T test (all values < 0.01)

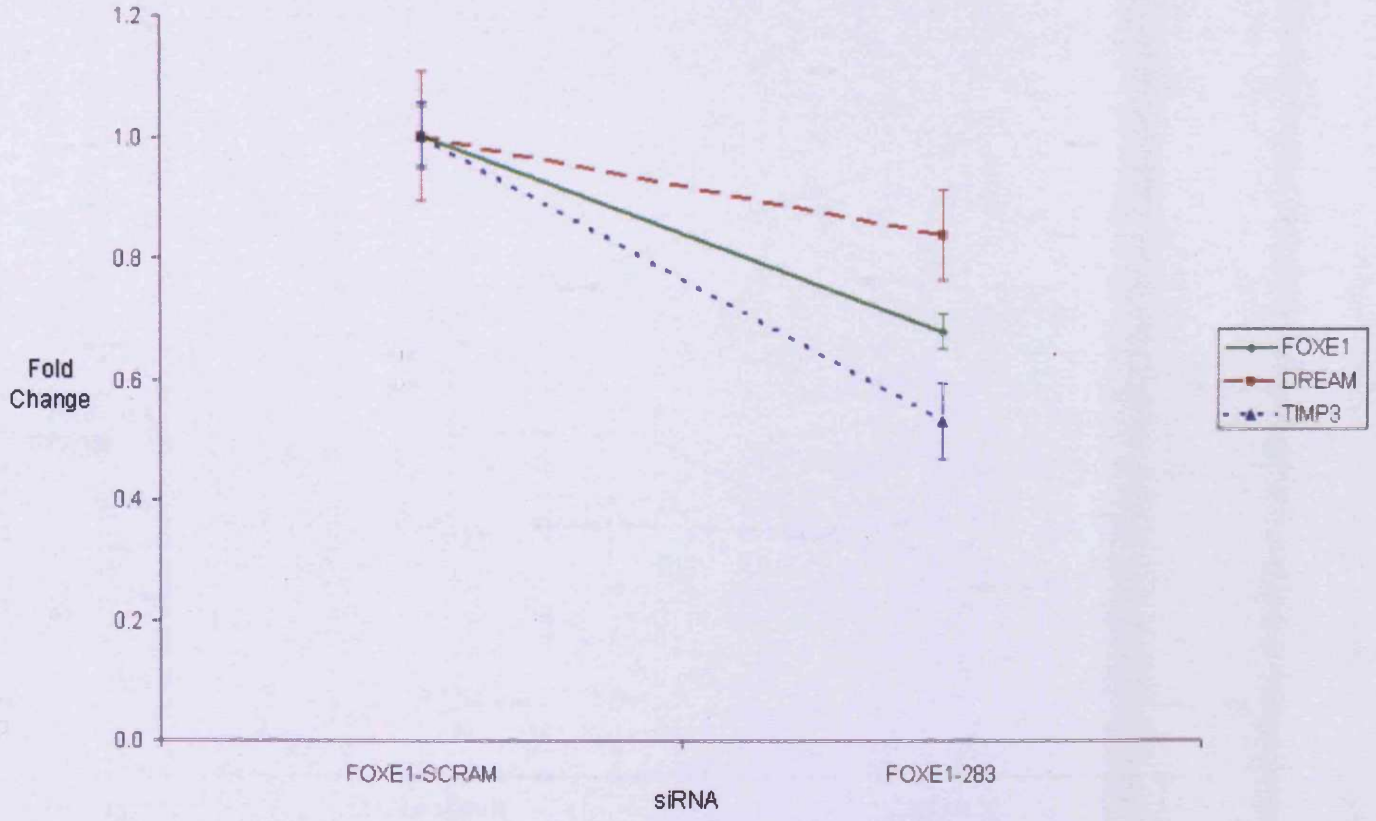

Figure 4.28. DREAM Knockdown. Values are the mean (± S.D) of three independent experiments, each performed in triplicate normalised to APRT i.e. each value is expressed as number of DREAM copies / 10,000 APRT copies. Statistical analysis used Students T test (all values < 0.01).

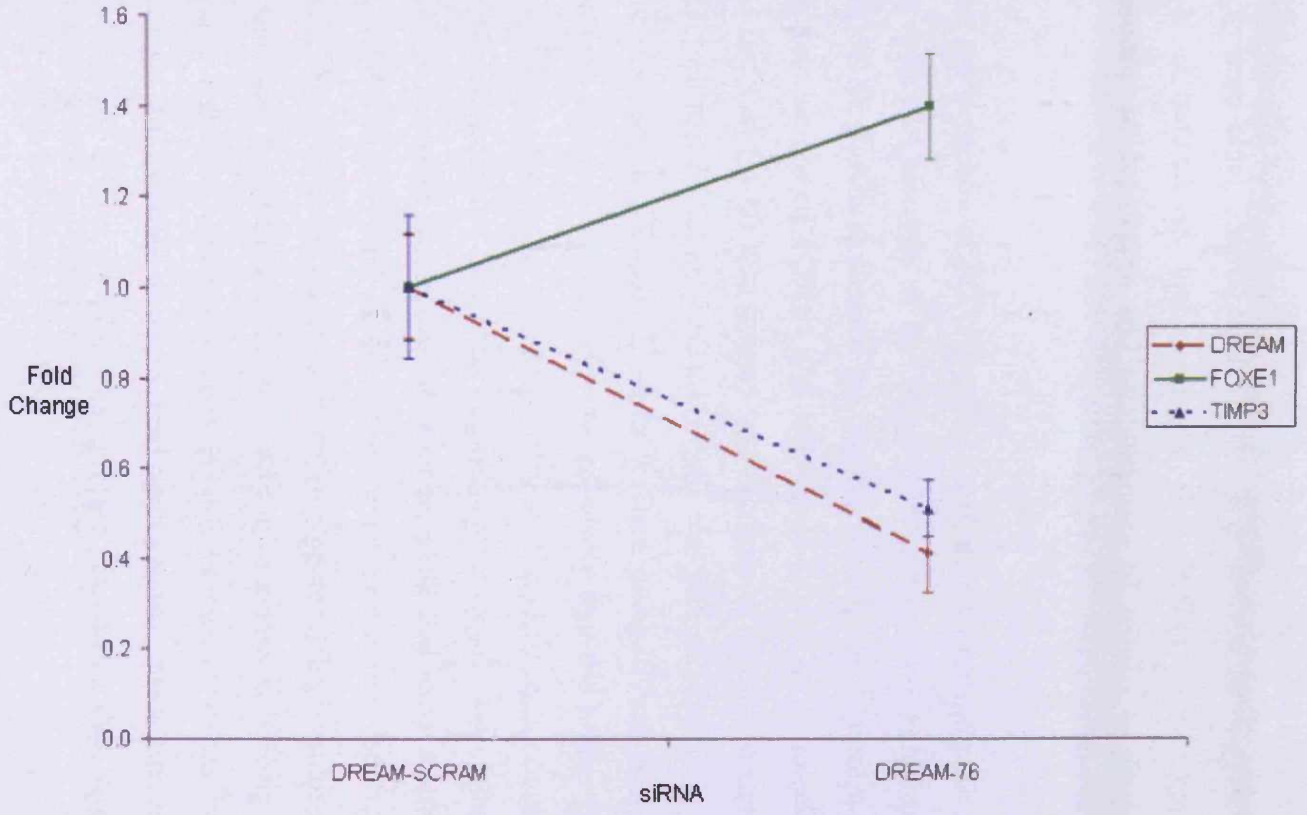

4.4. Discussion

The main achievements of this chapter were the production a series of plasmid-cDNA standards and optimization of conditions for real-time QPCR measurement of transcripts for FOXE1, TIMP3, MMP13 and COL1A1; confirmation that FOXE1 transcripts are translated into protein; explanation of the aberrant apparent molecular weight of FOXE1 in western blots; participation in the establishment of the HaCaT model of keratinocyte differentiation, demonstration that HaCaT cells express DREAM and some success in the design and establishment of siRNA to produce specific gene knock down.

In order to confirm that the detection of FOXE1 mRNA correlated with the presence of FOXE1 protein, western blot analysis of HaCaT protein extracts was performed. However, all three anti-FOXE1 pAbs possessed the highest affinity for a protein not at the predicted molecular weight of FOXE1 (42 kDa), but at a higher molecular weight of 60 kDa. The fact that the 60 kDa protein was recognised by three different anti-FOXE1 pAbs suggested that the identity of this protein was indeed FOXE1. Also, as similar results were obtained in Chapter 2, when western analysis was used to detect recombinant FOXE1 expressed in *E. coli.*, the possibilty that the higher than expected molecular weight was the result of post-translational modification could be ruled out, as such modifications cannot take place in prokaryotic expression systems. This led to a search of the literature for reports of other proteins that show aberrant migration when analysed by SDS-PAGE. Interestingly, we found a few reports of instances where transmembrane proteins migrated at an unexpectedly high molecular weight. Furthermore, this was found to occur specifically in response to boiling the cell lysate. Although the cause of this phenomena is still unknown, it has been hypothesised that heating the protein exposes the hydrophobic transmembrane domains that usually remained coiled up inside the protein, and these then clump together to form aggregates which migrate aberrantly.

Although this has only ever been reported to occur in the case of proteins with transmembrane domains, the hydrophobic nature of the FOXE1 protein (its polyalanine tract is particularly hydrophobic, analogous to a transmembrane domain)

made this explanation worth investigating further. Indeed, variation in the preparation of the sample, prior to SDS-PAGE, revealed that at low temperatures the FOXE1 protein migrates at the expected molecular weight of 42 kDa. However, exposure to higher temperatures increased the 60 kDa molecular weight form with longer incubations eventually resulting in complete loss of the predicted molecular weight protein. This is the first reported case of a transcription factor migrating aberrantly during SDS-PAGE as a direct result of a commonly used method of sample preparation (boiling the sample for 5 mins). This knowledge may prove useful in future studies where polyalanine tract containing proteins are analysed by SDS-PAGE.

Having confirmed that FOXE1 was expressed in HaCaT cells, the next task was to examine if this expression varied as the cells exited the cell-cycle and embarked on their differentiation protocol. This was achieved with the use of a commonly used *in vitro* model of epidermal differentiation – known as the 'calcium-switch' method. This model is based on the observations that mouse epidermal keratinocytes grown in low Ca^{2+} environment (<0.07 mM) proliferate rapidly and are unable to differentiate (i.e. they have a basal cell phenotype). However, simply raising the Ca^{2+} concentration above 1.0 mM (the calcium-switch) is sufficient to trigger cell-cycle arrest and to start epidermal differentiation.

In contrast, our results show that some keratinocytes had stopped proliferating before the calcium-switch was performed (as indicated by a reduction in the percentage of ki67 and K10 positive cells). This was found to occur specifically in areas where cell-density was sufficient to allow cell-contacts to be made by neighbouring cells. Although the calcium-shift was not required to initiate cell-cycle withdrawal of human keratinocytes, a comparison of the morphology of shifted with non-shifted cells at later time points showed that the presence of high calcium concentration resulted in better epidermal organisation (i.e. the cell organisation more closely resembled that of *in vivo*). The calcium-shift was also found to increase the rate of differentiation by approximately 2-3 days (as indicated by K14 staining).

The calcium-shift produced a transient dip in FOXE1 transcripts, which then continued to rise achieving levels 3 to 5 fold higher than at the outset. This was accompanied by temporal expression of differentiation markers, keratins 10 & 14 and filaggrin, evaluated by immunocytochemistry. Similar results were obtained with the HaCaT-LUC subclone. Furthermore a 3-fold increase in luciferase transcripts was observed in these cells, indicating production of functional FOXE1 protein. It is not clear why this up-regulation in luciferase transcripts was not measurable in a luminescent bioassay, however possible explanations are discussed in Chapter 5.

Although FOXE1 expression is increased during keratinocyte differentiation, the expression profiles of markers of this process did not correlate with that of the transcription factor. This suggests that FOXE1 is a consequence, rather then a cause, of differentiation and is in agreement with the findings of Brancaccio *et al* (2004), who found that in FOXE1$^{-/-}$ mice, the hair follicle structures are preserved, as is the expression of markers of hair follicle proliferation (K14) and differentiation (K17, an ORS marker).

Subsequent studies revealed that TIMP3 (a gene whose promoter contains the FOXE1 consensus) transcripts were upregulated 4 to 5 fold overall and also displayed a temporal reduction after adding Ca^{2+}, i.e. mirrored very closely the expression profile of FOXE1. Furthermore, siRNA knockdown with FOXE1, resulting in 70% reduction in this target gene also produced a 30% fall in TIMP3 transcript copy numbers. Transcription of other genes implicated in modification of the ECM, MMP13 and COL1A1, although increased during keratinocyte differentiation did not demonstrate the transient dip but remained fairly constant until the Ca^{2+} shift, when they started to increase.

The effect of Ca^{2+} is interesting in the context of DREAM, a calcium regulated transcriptional repressor. DREAM is expressed in differentiated (but not undifferentiated FRT) thyroid cells. Its effects are somewhat conflicting with evidence that it represses transcription of PAX8 and FOXE1 (but not TITF1) in a calcium dependent manner, by binding to DRE sites in the promoters of each gene (D'Andrea *et al.*, 2005); in contrast Rivas *et al* (2004) report an action of DREAM on thyroglobulin expression - via modulation of TTF1.

We demonstrated DREAM transcript expression in 80% confluent HaCaT cells using RT-PCR. Subsequent experiments transfecting siRNA were also performed in 80% confluent cells and showed that FOXE1 and DREAM siRNAs at 3 nM, achieved 70% and 60% knockdown of the relevant gene respectively (unaltered APRT transcript levels confirmed their specificity). The observations that a 30% knockdown in FOXE1 expression was accompanied by a 40% TIMP3 expression supports our hypothesis that TIMP3 is a direct target of FOXE1. However, the 30% reduction in DREAM expression was unexpected and suggests that FOXE1 may also modulate the transcription of DREAM. The increase in the level of FOXE1 transcripts in response to a reduction in DREAM expression supports a role for DREAM in the modulation of FOXE1 expression in keratinocytes. However, we did not expect to see a fall in TIMP3 levels with increasing FOXE1 levels. This suggests that the mechanisms that control TIMP3 expression may be more complex than originally thought.

In summary, we provided substantial evidence that TIMP3 is indeed a direct downstream target of FOXE1. This enables us to propose a model to explain how FOXE1 is able to control the orientation of the growing hair follicle. We propose that the FOXE1 expressing ORS keratinocytes, which are located specifically around the hair follicle bulb are able synthesise and secrete TIMP3 into the surrounding ECM. The inhibition of MMP activity by TIMP3 maintains the structural integrity of the ECM surrounding the sides of the hair follicle, and in doing so prevents the follicle from migrating side-ways through the dermis (as observed in Foxe1$^{-/-}$ mouse skin)

As well as providing a model for hair follicle, this may also have implications for understanding the biology of infiltrative skin tumours. The similarity of the basal carcinomas invading surrounding tissues has with the anagen hair follicle invading into the dermis suggests the two use a common mechanism. However, unlike the orderly migration of hair follicles, the infiltration of the tumours are highly disorganised. Recently, Eichberger *et al* (2004) showed that FOXE1 is highly upregulated in BCCs. Could FOXE1 be involved in this process? If so, FOXE1 may also be have a role in other more serious skin malignancies e.g. squamous cell carcinoma and malignant melanoma.

In conclusion FOXE1 transcript levels and transcriptional activity increase as keratinocytes commit to differentiation *in vitro* and target at least one gene (TIMP3) implicated in modification of the extra-cellular matrix, a situation of potential relevance to hair-follicle migration. Further experiments are required to clarify the role of DREAM in controlling FOXE1 expression and whether this occurs at a non-transcriptional level but is dependent on concentrations of intracellular Ca^{2+}.

Chapter 5.

Functional Analysis of FOXE1 Polyalanine Tract Variants

5.1. Introduction

5.1.1. FOXE1 has a Polyalanine Tract

The FOXE1 gene consists of a single exon and encodes for a 42 kDa protein of 372 amino acids. The main structural features of the FOXE1 protein include a 97 amino acid forkhead DNA-binding domain, and a polyalanine (polyAla) tract domain of variable length. The polyAla tract is coded for by an imperfect trinucleotide repeat (GCN), among which the GCC codon is significantly over-represented (Figure 5.1). PolyAla tracts are frequently observed in forkhead family members e.g. our own analysis revealed that 13 of the 43 human forkhead proteins contain at least one polyAla tract greater than 4 residues in length: FOXC1, FOXD1, FOXD2, FOXD3, FOXE1, FOXE2, FOXE3, FOXF2, FOXK1, FOXK2, FOXL2, FOXO1 and FOXQ1.

5.1.2. The FOXE1 Polyalanine Tract is Highly Polymorphic

Five separate studies, screening apparently normal individuals from Italy (Macchia *et al.*, 1999; Tonacchera *et al.*, 2004; Santarpia *et al.*, 2007), Japan (Hishinuma *et al.*, 2001), New Zealand and Slovenia (Watkins *et al.*, 2006) have shown that the FOXE1 polyAla tract length is highly polymorphic. Together, the five studies have detected several alleles, encoding for polyAla tracts consisting of 12, 14, 16, 17 and 19-Ala residues (Figure 5.2).

In all five studies only one nucleotide sequence for the 14, 16 and 17-Ala alleles was detected. However, Watkins *et al* (2006) were able to detect two different nucleotide sequences that make up the 12 (designated 12_a and 12_b) and 19-Ala (designated 19_a and 19_b) alleles. The 12_a, 14, 16 and 17-Ala alleles all exist as: GCG GCG GCT GCC GCA $(GCC)_n$, where the number of GCC repeats determines the length of the polyAla tract. However, the 12_b, 19_a and 19_b-Ala alleles exist as GCG GCG GCT $(GCC)_9$, GCG GCG (GCT GCC GCA GCC GCC$)_2$(GCC$)_7$ and GCG GCG GCT GCC (GCA GCC GCC$)_2$(GCC$)_9$ respectively (Figure 5.2). The existence of these alleles suggests that simple expansion/contraction in the GCC repeat region is not the only mechanism that has resulted in variation in the FOXE1 polyAla tract length.

Figure 5.1. Nucleotide and Amino Acid Sequence of Human FOXE1. The nucleotide sequence for human FOXE1 was obtained from GENEATLAS (http://www.dsi.univ-paris5.fr/genatlas/). Nucleotide and amino acid residues are numbered on the left.

```
   1 ATG ACT GCC GAG AGC GGG CCG CCG CCG CCG CAG CCG GAG GTG CTG GCT ACC
   1 Met Thr Ala Glu Ser Gly Pro Pro Pro Pro Gln Pro Glu Val Leu Ala Thr
  52 GTG AAG GAA GAG CGC GGC GAG ACG GCA GCA GGG GCC GGG GTC CCA GGG GAG
  18 Val Lys Glu Glu Arg Gly Glu Thr Ala Ala Gly Ala Gly Val Pro Gly Glu
 103 GCC ACG GGC CGC GGG GCG GGC GGG CGG CGC CGC AAG CGC CCC CTG CAG CGC
  35 Ala Thr Gly Arg Gly Ala Gly Gly Arg Arg Arg Lys Arg Pro Leu Gln Arg
 154 GGG AAG CCG CCC TAC AAC TAC ATC GCG CTC ATC GCC ATG GCC ATC GCG CAC
  52 Gly Lys Pro Pro Tyr Ser Tyr Ile Ala Leu Ile Ala Met Ala Ile Ala His
 205 GCG CCC GAG CGC CGC CTC ACG CTG GGC GGC ATC TAC AAG TTC ATC ACC GAG
  69 Ala Pro Glu Arg Arg Leu Thr Leu Gly Gly Ile Tyr Lys Phe Ile Thr Glu
 256 CGC TTC CCC TTC TAC CGC GAC AAC CCC AAA AAG TGG CAG AAC AGC ATC CGC
  86 Arg Phe Pro Phe Tyr Arg Asp Asn Pro Lys Lys Trp Gln Asn Ser Ile Arg
 307 CAC AAC CTC ACA CTC AAC GAC TGC TTC CTC AAG ATC CCG CGC GAG GCC GGC
 103 His Asn Leu Thr Leu Asn Asp Cys Phe Leu Lys Ile Pro Arg Glu Ala Gly
 358 CGC CCG GGT AAG GGC AAC TAC TGG GCG CTT GAC CCC AAC GCG GAG GAC ATG
 120 Arg Pro Gly Lys Gly Asn Tyr Trp Ala Leu Asp Pro Asn Ala Glu Asp Met
 409 TTC GAG AGC GGC AGC TTC CTG CGC CGC CGC AAG CGC TTC AAG CGC TCG GAC
 137 Phe Glu Ser Gly Ser Phe Leu Arg Arg Arg Lys Arg Phe Lys Arg Ser Asp
 460 CTC TCC ACC TAC CCG GCT TAC ATG CAC GAC GCG GCG GCT GCC GCA GCC GCC
 154 Leu Ser Thr Tyr Pro Ala Tyr Met His Asp Ala Ala Ala Ala Ala Ala Ala
 511 GCC GCC GCC GCC GCC GCC GCC GCC GCC ATC TTC CCA GGC GCG GTG CCC GCC
 171 Ala Ala Ala Ala Ala Ala Ala Ala Ala Ile Phe Pro Gly Ala Val Pro Ala
 562 GCG CGC CCC CCC TAC CCG GGC GCC GTC TAT GCA GGC TAC GCG CCG CCG TCG
 188 Ala Arg Pro Pro Tyr Pro Gly Ala Val Tyr Ala Gly Tyr Ala Pro Pro Ser
 613 CTG GCC GCG CCG CCT CCA GTC TAC TAC CCC GCG GCG TCG CCC GGC CCT TGC
 205 Leu Ala Ala Pro Pro Pro Val Tyr Tyr Pro Ala Ala Ser Pro Gly Pro Cys
 664 CGC GTC TTC GGC CTG GTT CCT GAG CGG CCG CTC AGC CCA GAG CTG GGG CCC
 222 Arg Val Phe Gly Leu Val Pro Glu Arg Pro Leu Ser Pro Glu Leu Gly Pro
 715 GCA CCG TCG GGG CCC GGC GGC TCT TGC GCC TTT GCC TCC GCC GGC GCC CCC
 239 Ala Pro Ser Gly Pro Gly Gly Ser Cys Ala Phe Ala Ser Ala Gly Ala Pro
 766 GCT ACC ACC ACC GGC TAC CAG CCC GCA GGC TGC ACC GGG GCC CGG CCG GCC
 255 Ala Thr Thr Thr Gly Tyr Gln Pro Ala Gly Cys Thr Gly Ala Arg Pro Ala
 817 AAC CCC TCC GCC TAT GCG GCT GCC TAC GCG GGC CCC GAC GGC GCG TAC CCG
 272 Asn Pro Ser Ala Tyr Ala Ala Ala Tyr Ala Gly Pro Asp Gly Ala Tyr Pro
 868 CAG GGC GCC GGC AGT GCG ATC TTT GCC GCT GCT GGC CGC CTG GCG GGA CCC
 289 Gln Gly Ala Gly Ser Ala Ile Phe Ala Ala Ala Gly Arg Leu Ala Gly Pro
 919 GCT TCG CCC CCA GCG GGC GGC AGC AGT GGC GGC GTG GAG ACC ACG GTG GAC
 306 Ala Ser Pro Pro Ala Gly Gly Ser Ser Gly Gly Val Glu Thr Thr Val Asp
 970 TTC TAC GGG CGC ACG TCG CCC GGC CAG TTC GGA GCG CTG GGA GCC TGC TAC
 323 Phe Tyr Gly Arg Thr Ser Pro Gly Gln Phe Gly Ala Leu Gly Ala Cys Tyr
1021 AAC CCT GGC GGG CAG CTC GGA GGG GCC AGT GCA GGC GCC TAC CAT GCT CGC
 340 Asn Pro Gly Gly Gln Leu Gly Gly Ala Ser Ala Gly Ala Tyr His Ala Arg
1072 CAT GCT GCC GCT TAT CCC GGT GGG ATA GAT CGG TTC GTG TCC GCC ATG TGA
 357 His Ala Ala Ala Tyr Pro Gly Gly Ile Asp Arg Phe Val Ser Ala Met Stop
```

Forkhead domain PolyAla tract

Figure 5.2. Nucleotide Sequence Alignment of All Known FOXE1 Polyalanine Alleles

	Codon																		
Allele	1	2	3	4	5	6	7	8	9	10	11	12	13	14	15	16	17	18	19
12_a*§	GCG	GCG	GCT	GCC	GCA	GCC	GCC	GCC	GCC	GCC	GCC	GCC							
12_b§	GCG	GCG	GCT	GCC	GCC	GCC	GCC	GCC	GCC	GCC	GCC	GCC							
14*†‡§	GCG	GCG	GCT	GCC	GCA	GCC	GCC	GCC	GCC	GCC	GCC	GCC	GCC	GCC					
16*†‡§	GCG	GCG	GCT	GCC	GCA	GCC	GCC	GCC	GCC	GCC	GCC	GCC	GCC	GCC	GCC	GCC	GCC		
17*§	GCG	GCG	GCT	GCC	GCA	GCC	GCC	GCC	GCC	GCC	GCC	GCC	GCC	GCC	GCC	GCC	GCC	GCC	GCC
19_a§	GCG	GCG	GCT	GCC	GCA	GCC	GCC	GCT	GCC	GCA	GCC	GCC	GCC	GCC	GCC	GCC	GCC	GCC	GCC
19_b§	GCG	GCG	GCT	GCC	GCA	GCC	GCC	GCA	GCC	GCC	GCC	GCC	GCC	GCC	GCC	GCC	GCC	GCC	GCC

* Macchia *et al.*, 1999
† Hishinuma *et al.*, 2001
‡ Tonacchera *et al.*, 2004
§ Watkins *et al.*, 2006

The percentage frequency of each allele within the five populations is shown in Table 5.1. Although there appears to be population-specific differences in the frequency of each FOXE1 polyAla allele, there are also some notable similarities. For instance, the most common allele in all five populations was the 14-Ala allele. In the New Zealand, Slovenian and Italian populations, the 14-Ala allele was present at frequencies of 67.5%, 66.2% and 54% respectively. The Japanese and Sicilian populations appeared to be more homogeneous, with the 14-Ala allele being over-represented at 97% and 90% respectively. The second most common allele in all five populations was the 16-Ala allele. This was present in the Italian, New Zealand and Slovenian populations at frequencies of 40%, 30% and 23% respectively. In all populations, the 12, 17 and 19-Ala alleles were either not detected, or were observed at significantly lower frequencies (< 10%).

Table 5.1. Frequency of FOXE1 Polyalanine Alleles in Five Normal Populations

	Frequency [n (%)]				
Allele	Italian*	Japanese†	Sicilian#	New Zealand§	Slovenian§
12	4 (2)	/	/	1 (0.4)	1 (1.4)
14	106 (54)	196 (97)	63 (90)	162 (67.5)	49 (66.2)
16	78 (40)	6 (3)	7 (10)	72 (30)	17 (23)
17	9 (4)	/	/	/	/
19	/	/	/	5 (2.1)	7 (9.5)
Total number of alleles	196	202	70	240	74

* Macchia *et al.*, 1999
† Hishinuma *et al.*, 2001
# Santarpia *et al.*, 2004
§ Watkins *et al.*, 2006

Theoretically, different combinations of the FOXE1 polyAla alleles could yield 12 possible genotypes. However, within the Japanese, New Zealand and Slovenian populations (genotype data for the Italian and Slovenian groups was not available), only six different genotypes were observed: 12/14, 14/14, 14/16, 14/19, 16/16 and 16/19 (Table 5.2). Interestingly, all six genotypes possessed at least one copy of either the 14 or the 16-Ala allele, suggesting there may be a requirement for at least one of these alleles to be present. Also, in all three populations, 14/14 and 14/16 were found to be the first and second most common genotypes respectively. For the other four genotypes, there were population specific differences in the order of their frequency.

Table 5.2. Frequency of FOXE1 Polyalanine Genotypes in Three Normal Populations

	Frequency [n (%)]				
Genotype	**Italian***	**Japanese†**	**Sicilian#**	**New Zealand§**	**Slovenian§**
12/12		/		/	/
12/14		/		1 (0.8)	1 (2.7)
12/16		/		/	/
12/17		/		/	/
12/19	Data	/	Data	/	/
14/14	not	96 (95)	not	57 (47.5)	16 (43.2)
14/16	available	4 (4)	available	45 (37.5)	11 (29.8)
14/17		/		/	/
14/19		/		2 (1.7)	5 (13.5)
16/16		1 (1)		12 (10)	2 (5.4)
16/17		/		/	/
16/19		/		3 (2.5)	2 (5.4)
Total number of subjects		101		120	37

* Macchia *et al.*, 1999
† Hishinuma *et al.*, 2001
# Santarpia *et al.*, 2004
§ Watkins *et al.*, 2006

5.1.3. Polyalanine Tracts are Common in the Human Proteome

The human proteome contains 494 known or predicted proteins that have at least one polyAla tract greater than four alanines in length (Lavoie *et al.*, 2003). The polyAla tracts were found to be five times more abundant in transcriptional regulators than in other proteins. In total, there were 21 protein families represented by three or more members, of which 13 were transcription factor families. Analysis of 98 of these polyAla tracts revealed that 32% exist as at least two alleles (Lavoie *et al.*, 2003).

5.1.4. Mechanisms of Polyalanine Tract Expansion/Contraction

There are two mechanisms that have been proposed to explain the polymorphic variations (expansions and/or deletions) seen in repeat regions of DNA: replication slippage and unequal crossing-over (Brown & Brown, 2004; Chen *et al.*, 2005; Robinson *et al.*, 2005).

Replication slippage is thought to account for the expansion of perfect trinucleotide repeats. In this model, secondary structures (e.g. hairpins) that form in the repeat region cause the DNA polymerase to pause during replication. This in turn causes a transient dissociation of the new and template DNA strands, which subsequently reassociate in a misaligned configuration ('slippage') (Figure 5.3). If slipping forward occurs, this will lead to a deletion, and if slipping backwards occurs, this will lead to an insertion in subsequent rounds of replication (Nag, 2003; Chen *et al.*, 2005).

Figure 5.3. Replicative Slippage Model for Perfect Trinucleotide Repeat Expansion/Contractions

(http://www.stanford.edu/group/hopes/causes/mutation/q5.html)

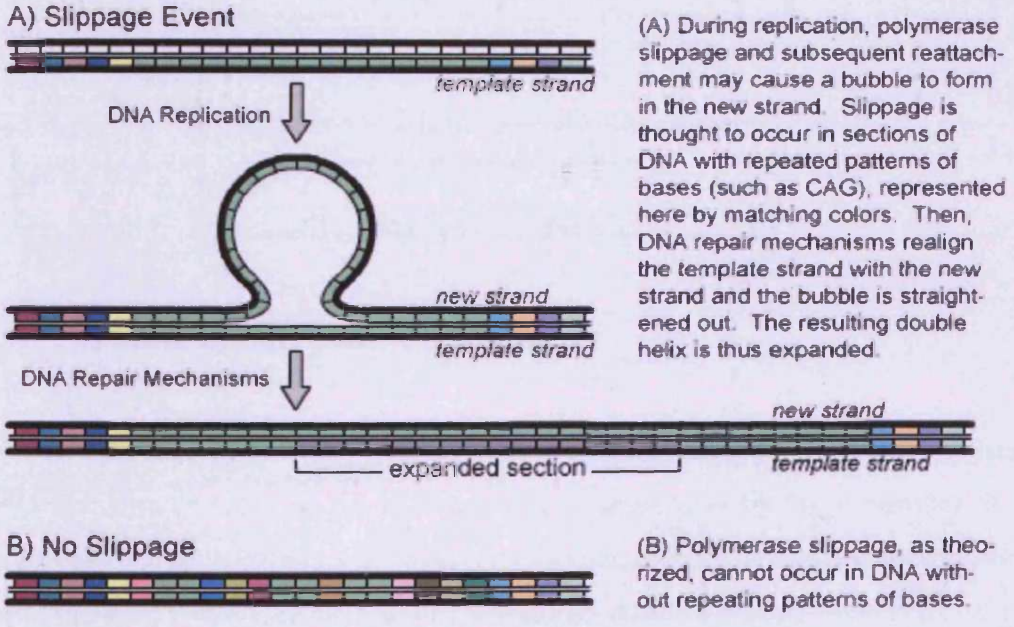

It has been suggested that unequal crossing-over, a form of allelic homologous recombination, is the most likely mechanism for polyAla expansions (Figure 5.4). The evidence supporting this hypothesis includes: (1) Almost all polyAla allelic variants appear as in-frame duplications. (2) PolyAla allelic variants are stable, both mitotically and meiotically over several generations. (3) Contractions (the mirror image of expansions during the recombination event) are observed as polymorphisms in several genes, for which expansions lead to human diseases (PHOX2B, ARX, RUNX2).

Figure 5.4. Unequal Crossing-Over Model for Trinucleotide Repeat Expansions/ Contractions

(Adapted from http://www.informatics.jax.org/silver/figures/figure5-5.shtml)

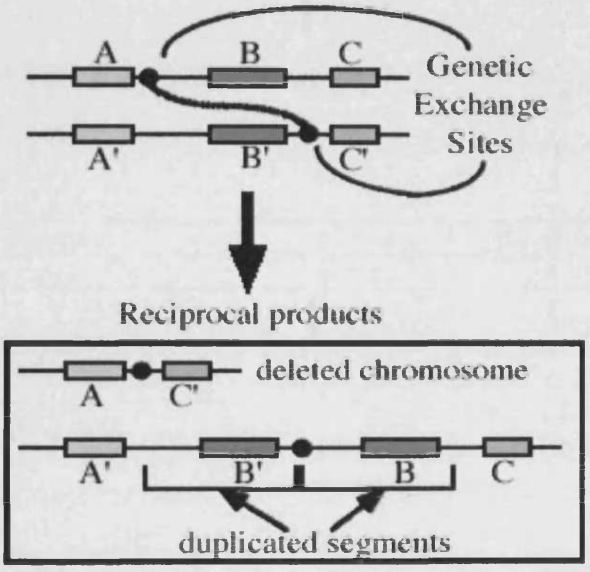

5.1.5. Purpose of Polyalanine Tracts

The exact purpose of polyAla tracts, if any, remains unclear. However, it has been shown that slowly evolving proteins contain an unexpectedly large number of amino acid repeats. As such proteins only rarely incorporate new structures, their amino acid repeats are likely to be relatively old structures that have been preserved by natural selection (Mularoni *et al.*, 2006).

It has been proposed that polyAla tracts act as flexible spacer elements between functional domains of the protein, and are therefore essential to protein conformation, protein-protein interactions and/or DNA-binding (Goodman *et al.*, 1997; Karlin *et al.*, 2002). Studies have also shown that polyAla tracts are often associated with transcriptional repressor domains (Licht *et al.*, 1990; 1993; Han *et al.*, 1993; Kim *et al.*, 1996).

5.1.6. Polyalanine Tracts and Human Disease

Expansions of polyAla tracts are responsible for nine autosomal dominant or X-linked human diseases. All occur in genes that code for nuclear proteins: eight transcription factors and a protein involved in mRNA polyadenylation (PABPN1). A list of these diseases, the affected genes and the size of the expansions are shown in Table 5.3.

Table 5.3. A List of the Nine Human Diseases Caused by Polyalanine Expansions

Disease	Gene	Size of known expansions
Synpolydactily	HOXD13	15 to 22–29
Cleidocranial Dysplasia	RUNX2	17 to 27
Oculopharyngeal Muscular Dystrophy	PABPN1	10 to 11–17
Familial Holoprosencephaly	ZIC2	15 to 25
Hand–Foot–Genital Syndrome	HOXA13	18 to 26
X-linked Mental Retardation and Epilepsy	ARX	12–16 to 20–23
X-linked Mental Retardation with Growth Hormone Deficiency	SOX3	15 to 26
Congenital Central Hypoventilation Syndrome	PHOX2B	25 to 29
Blepharophimosis/Ptosis/Epicanthus Inversus Syndrome Type II	FOXL2	14 to 24

5.1.7. Polyalanine Containing Forkhead Proteins and Human Disease

5.1.7.1. FOXL2 Polyalanine Tract and Human Disease

Variations in the length of the FOXL2 polyAla tract have been shown to be associated with human disease. The FOXL2 gene consists of a single exon and encodes for a 45 kDa protein of 376 amino acids. It contains a forkhead DNA-binding domain and a polyAla tract domain of 14-Ala residues, which is highly conserved in mammals (Cocquet *et al.*, 2002). FOXL2 is expressed in the peri-ocular tissues as well as in fetal and adult ovaries (Cocquet *et al.*, 2002; 2003).

Blepharophimosis–ptosis–epicanthus inversus syndrome (BPES, OMIM 110100) mostly occurs as a dominantly inherited genetic disorder characterised by eyelid and craniofacial abnormalities, associated with (Type I) or without (Type II) premature ovarian failure (POF). Mutations in the FOXL2 gene have been shown to cause both types. To date, a large spectrum of different mutations have been described in the coding sequence of the FOXL2 gene (details in the human FOXL2 database at http://medgen.ugent.be/foxl2). Mutations expected to lead to a truncated protein are essentially responsible for BPES Type I. In contrast, mutations leading to elongated proteins often lead to BPES Type II. Approximately 30% of these mutations result in an expansion of the polyAla, from 14 to 24 residues, and this is mainly responsible for BPES Type II.

Caburet *et al* (2004) showed the FOXL2-14Ala (wild-type) protein to be localized almost entirely to the nucleus of COS-7 cells. However, the FOXL2-24Ala allele was shown to localize to both the nucleus and the cytoplasm forming intranuclear and cytoplasmic aggregates. They also showed that FOXL2-24Ala aggregates were able to sequester and retain a fraction of the normal FOXL2-14Ala protein, suggesting that the expanded protein may have a dominant negative effect.

Deletions of the FOXL2 appear to be associated with some cases of isolated POF. Partial deletions of the FOXL2 polyAla tract (-1 and –10 Ala residues) were identified in individuals with POF in the absence of BPES (Harris *et al.*, 2002; Gersak *et al.*,

2004; Watkins *et al.*, 2006). Moumne *et al* (2005) showed that deletion of the FOXL2 polyAla tract induced significant intranuclear aggregation. Over-expression of the protein chaperone HSP40 (heat shock protein 40) significantly reduced the proportion of cells with nuclear aggregates, indicating that the aggregates were likely to consist of mis-folded protein (Moumne *et al.*, 2005).

Most recently, an apparently recessive form of BPES was identified (Nallathambi *et al.*, 2006). The phenotype of affected individuals was indistinguishable from those with the dominant form of BPES. Genotyping revealed them to be homozygous for FOXL2-19Ala allele (+5 Ala residues). Aggregation analysis showed the level of cytoplasmic retention to be intermediate between wild-type protein and the FOXL2-24Ala mutant (Nallathambi *et al.*, 2007).

5.1.7.2. FOXE1 Polyalanine Tract and Human Disease

Three separate studies have shown that the FOXE1-14Ala allele is underrepresented in patients with CH. In contrast, the FOXE1-16Ala allele was found to be significantly more common in these individuals (Hishinuma *et al.*, 2001; Tonacchera *et al.*, 2004; Santarpia *et al.*, 2007). Hishinuma *et al* (2001) detected polyAla contractions (FOXE1-11Ala and FOXE1-12Ala) that were not present in their control group. However, subsequent *in-vitro* analysis revealed these alleles to have the same transcriptional activity as the FOXE1-14Ala allele.

As 10-20% POF patients also have an autoimmune disease, most commonly hypothyroidism (Conway, 1997), Watkins *et al* (2006) compared the frequency of FOXE1 polyAla alleles in POF patients with normal controls. Similarly to the CH patients, the FOXE1-14Ala allele was significantly less common in the POF patient while FOXE1-16Ala allele was significantly more common. This suggested that FOXE1 may have play a biological role in the ovary, and that alteration from the FOXE1-14Ala allele to the 16Ala allele may increases the risk of developing POF. Alternatively, this result may also reflect an increased incidence of the mechanisms postulated to account for polyAla tract expansions (replicative slippage and unequal

crossing-over). However, this seems unlikely as Watkins *et al* (2006) found there to be no correlation between the size of FOXE1 and FOXL2 expansions or deletions.

Expansions of the polyAla tract in FOXL2 are associated with reduced (but not abolished) transcriptional potency. If FOXE1 is similarly affected, a mild phenotype might be expected, such as subclinical hypothyroidism.

5.1.8. Subclinical Hypothyroidism

Subclinical hypothyroidism (SH) defines a condition that is characterized by elevated serum TSH associated with normal serum levels of T3 and T4, and the individual has few or no symptoms of thyroid dysfunction (Surks *et al.*, 2004). It represents the most frequent alteration of thyroid function, occurring in 5–15% of the general population. Also, a particularly high prevalence is observed in women over 60 years of age (Owen & Lazarus, 2003). SH patients can be divided into two groups: (1) Patients who have never received thyroid medication, the so-called endogenous SH group, and (2) Those on medication or with SH as the result of other iatrogenic procedures, the exogenous SH group. The most common cause of endogenous SH is autoimmune (Hashimoto's) thyroiditis (Rapoport, 1991), which is usually associated with raised levels of anti-TPO antibodies. Also, germline mutations in the TSHR have been found to be associated with some cases of non-autoimmune SH (Alberti *et al.*, 2002; Locantore *et al.*, 2007). However, in a many patients the origins of elevated TSH level remains obscure, in particular those where the condition does not evolve into overt disease.

A comparison of serum thyroid hormone levels in healthy individuals, revealed there to be substantial inter-individual variability, whereas the intra-individual variability remained within a narrow range (Andersen *et al.*, 2002). This suggests that genetic variation, in addition to environmental factors such as iodine intake, play an important role in the regulation of thyroid hormone production. This also means that the thyroid hormone levels are different for each individual. This is supported by a classical twin study that showed heritability accounted for ~65% of the variation in serum TSH and free T3 and T4 levels (Hansen *et al.*, 2004). In a Mexican–American population, total

heritability in serum thyroid parameters ranged from 26 to 64% of the total inter-individual variation observed (Samollow *et al.*, 2004).

These observations could be explained by polymorphisms that have subtle effects on the functional activity of proteins involved in thyroid hormone metabolism. Presently, only the TSHR and iodothyronine deiodinases have been analysed for an association between polymorphisms (specifically SNPs) and serum thyroid hormone levels (Peeters *et al.*, 2006).

Mutations in both of these genes have been found in CH, with less severe mutation, e.g. affecting only one allele, being associated with SH. It is possible that polymorphic variation could produce a similar phenotype, and since FOXE1 is a transcription factor, luciferase reporter assays provide a method of investigation.

5.1.9. Luciferase Reporter Assays

The transcriptional activity of FOXE1 polymorphic variants was analysed using the same *in-vitro* reporter assay used to analyse the A65V and S57N mutants (Clifton-Bligh *et al.*, 1998; Castanet *et al.*, 2002). This assay uses ZI6TKLUC, a FOXE1 responsive luiferase reporter that contains sixteen concatamerised FOXE1 binding sites from the rat TPO promoter (able to bind human FOXE1) linked to a thymidine kinase (TK) promoter within pA3TKLUC (Clifton-Bligh *et al.*, 1998).

The pA3TKLUC construct itself is derived from the pGEM7zf(+) vector into which firefly luciferase coding sequence has been inserted. Also inserted, between the plasmid and luciferase coding sequence, is a trimerized SV40 polyadenylation termination signal. This functions as an inhibitor of spurious reporter gene transcription caused by "pseudo-promoters" which are prokaryotic DNA sequences contained in bacterial plasmids (Maxwell *et al.*, 1989). Blocking of non-specific luciferase activity allows the activity of relatively weak promoters to be analysed.

As with previous studies, the human embryonic kidney-293 (HEK293) cell-line was used to measure FOXE1 transcriptional activity (Clifton-Bligh *et al.*, 1998; Castanet *et al.*, 2002; Barış *et al.*, 2006). Interestingly, the luciferase assay did not work in two

other cell lines – HaCaT and COS. Possible explanations are discussed at the end of the chapter.

5.1.10. Chapter Aims

The aim was to investigate the possible role of FOXE1 polyAla polymorphisms in SH or other thyroid dysfunction. This was achieved by the genotyping of individuals with SH or CH and comparing them with normal controls. The transcriptional activity of different FOXE1 PolyAla variants was compared using an *in vitro* reporter assay.

5.2. Materials and Methods

5.2.1. Patients

5.2.1.1. Syndromic Congenital Hypothyroidism: Patient VL

Patient VL was a boy born to non-consanguineous parents of Spanish ethnicity. This was their second child, their first child having died shortly after birth due to bilateral choanal atresia and pulmonary hypertension. VL presented with a range of physical and physiological abnormalities including CH, hypoparathyroidism, bilateral choanal atresia and facial defects. Patient VL's gDNA was kindly provided by Dr. A. Aytès, (Valencia, Spain)

The features shared with Bamforth-Lazarus syndrome made FOXE1 a prime candidate gene for investigation. However, direct sequencing of the FOXE1 gene revealed there to be no mutations in the forkhead domain (as occurs in cases of Bamforth-Lazarus syndrome) or in any other part of the coding sequence.

5.2.1.2. Non-familial Subclinical Hypothyroidism: Patients HN, HC, VN, TA, RR and JR

Genomic DNA (Section 5.2.2.1) was extracted from the blood (kindly provided by Dr. P. Owen, Cardiff, Wales) of six female patients with sporadic SH.

Patients HN, HC, VN, TA, RR and JR were six unrelated women who presented with non-familial SH. The level of anti-TPO antibodies in the serum of these individuals had previously been measured using an electrochemiluminescence immunoassay method [Roche Diagnostics, Indianapolis, USA]. Patients HN, VN and HC had anti-TPO antibody serum levels that were elevated above the normal range (>32 kU/L), and so were diagnosed with autoimmune SH. Patients TA, RR and JR were diagnosed with non-autoimmune SH, as they had anti-TPO antibody titres that were within the normal range (<32 kU/L) (Table 5.4).

Table 5.4. Anti-TPO Antibody Titres in Six Female Subjects with Sporadic SH. The normal range for anti-TPO antibody < 32 kU/L.

Subject	Anti-TPO antibody titre (kU/L)	
HN	600.0	
HC	129.0	Autoimmune
VN	600.0	
TA	25.9	
RR	7.7	Non-autoimmune
JR	9.2	

5.2.1.3. Familial Subclinical Hypothyroidism: Patients A, B and IS

Genomic DNA was obtained from three unrelated patients each with a family history of SH, defined as persistently elevated serum TSH associated with thyroid hormones in the normal range (kindly provided by clinical colleagues in Newport and Manchester).

5.2.1.4. Normal controls: NI, MA

Genomic DNA was obtained from two unrelated subjects with no apparent thyroid abnormalities.

5.2.2. FOXE1 Genotyping

5.2.2.1. Extraction of Patient's gDNA

Genomic DNA was extracted from peripheral blood leukocytes using Qiagen's QIAamp® Blood Mini Kit according to the manufacturer's instructions. Briefly, 20 µl Qiagen protease was transferred to a nuclease-free 1.5 ml microtube, followed by 200 µl of fresh EDTA blood and 200 µl buffer AL. The solutions were mixed by vortexing and incubated in a water bath at 56°C for 10 mins. Subsequently, 200 µl of absolute ethanol was added, the solutions vortexed again, and the whole sample transferred to a QIAamp spin column placed in a Qiagen 2 ml collection tube. This was then centrifuged at 6000×g for 1 min at RT. The filtrate was discarded and the

column washed once with 500 µl buffer AW1 followed by 500 µl buffer AW2. DNA was eluted from the column by adding 200 µl nuclease-free water and centrifuging the column, placed in a nuclease-free 1.5 ml microtube, for 6000×g for 1 min at RT.

Concentration and purity of the extracted gDNA was assessed by spectrophotometric measurement of the absorbance at 260 nm and 280 nm.

5.2.2.2. Amplification of the FOXE1 Polyalanine Tract

A portion of the FOXE1 coding sequence encompassing the FOXE1 polyAla tract was amplified using FOXE1-F8 (5'-CTCGGACCTCTCCACCTACC-3') and FOXE1-R8 (5'-GCGCGTAGCCTGCATAGAC-3') primers. Due to the high GC-content of the amplicon, the PCR was performed using Qiagen's HotStarTaq® *Plus* DNA polymerase in combination with the PCR additive Q-solution (Section 4.2.5).

5.2.2.3. Agarose Gel Analysis of PCR Products

The previously reported FOXE1 polyAla variants range in length between 12 and 19-Ala residues (7 codons = 21 nucleotides). In order to be able to resolve PCR amplicons that may vary in length ≤ 21 nucleotides they were separated on a 4% (3% Nusieve [Cambrex], 1% Agarose) gel.

5.2.2.4. Direct Sequencing

Homozygous individuals could be genotyped directly by sequencing of their gDNA (Section 4.2.7). However, in the case of some heterozygous individuals, the presence of two sequences that were out of alignment made it difficult to determine their genotype. In these cases it was necessary to physically separate the two alleles by subcloning and then sequence each individually. As described above, the FOXE1 F8R8 fragment was amplified by conventional PCR, and the amplicons separated on a 4% agarose gel. Individual bands were then cut out and purified using Qiagen's QIAquick Gel Extraction Kit (Section 2.2.3.3). The purified PCR products were then ligated into pGEM®-T Easy Vector (Section 4.2.11.3.2).

5.2.3. Functional Comparison of FOXE1 Allelic Variants

5.2.3.1. The pcDNA3-FOXE1(14-Ala) Construct

The FOXE1 construct consisted of a 1.3 kb BamHI-XbaI fragment, encompassing the entire FOXE1 coding region, cloned into a pcDNA3 vector [Invitrogen] (Clifton-Bligh *et al.*, 1998). Direct sequencing (Section 2.2.3.4) of the insert was performed using primers complementary to the T7 (5'-TAATACGACTCACTATAGGG-3') and SP6 (5'-GATTTAGGTGACACTATAG-3') promoters [Invitrogen], and this revealed the FOXE1 polyAla tract to consist of 14-Ala residues.

5.2.3.2. Generation of the pcDNA3-FOXE1(16-Ala) Construct

FOXE1-A (5'-AGC CTG GGC CGC TGG GCT CTC GG-3') and FOXE1-B (5'-GGA AAA GAC CGA GCA GGC CTC TAG A-3') primers (annealing temp = 55°C), flanking the entire FOXE1 coding region, were used to amplify a patient's gDNA. As the patient cohort did not contain any individuals homozygous 16/16, the gDNA from a patient heterozygous 14/16 was used instead. The FOXE1-B primer incorporated an XbaI restriction enzyme site (5'-TCT AGA-3').

To ensure high amplification efficiency, PCR was performed using Takara's PrimeSTAR™ HS proofreading DNA polymerase that possesses a 3′→5′ exonuclease activity. The following components were added to a 500 µl nuclease-free tube: 10µl 5× PrimeSTAR™ buffer (Mg^{2+}plus), 4 µl 10 mM dNTP mix, 1 µl 10 µM FOXE1-A primer, 1 µl 10 µM FOXE1-B primer, 0.5 µl 2.5 U/µl DNA polymerase, 50 ng gDNA and the volume made up to 50 µl with nuclease-free water [Promega]. The reaction mixture was mixed gently by vortexing, briefly spun in a microcentrifuge before being transferred to the PE Applied Biosystems 9700 thermocycler.

Thermocycler protocol:

- Initial denaturation: 1 min at 96°C
- 25 cycles of Denaturation: 10 sec at 98°C

Annealing: 5 sec at 55°C

Extension: 1.5 mins at 72°C

The PCR products were run on a 4% gel (3% Nusieve, 1% agarose) and the two alleles separated from each other using the gel extraction method (Section 2.2.3.3). A BamHI-XbaI digestion was then performed on each FOXE1-16Ala amplicon. For undetermined reasons a double digestion performed in the same tube did not work, and so digestions were performed sequentially.

BamHI digestion: The following components were added to a 100 µl nuclease-free tube: 4 µl 10× buffer, 0.4 µl 10 µg/µl BSA, 5 µl 380 ng/µl DNA, 2 µl 10 U/µl BamHI [all reagents from Promega]. The reaction was incubated in a waterbath at 37°C for 2 hrs.

Ethanol precipitation: 4 µl 3 M NaAcetate and 100 µl ice-cold 100% ethanol were added to the reaction mixture and the tube incubated on dry ice for 30 mins. The tube was then centrifuged, the supernatant removed and the pellet washed in 200 µl ice-cold 70% ethanol. The pellet was allowed to air-dry and then resuspended in 33.6 µl nuclease-free water. The solution was incubated on ice for 20 mins, vortexed and briefly spun down before being transferred to a clean tube.

XbaI digest: To the resuspended DNA the following were added: 4 µl 10× buffer D, 0.4 µl 10 µg/µl BSA and 2 µl 12 U/µl XbaI [all reagents from Promega]. The reaction was incubated in a waterbath at 37°C for 2 hrs.

The FOXE1 BamHI-XbaI fragment was ligated into the empty pcDNA3 vector using T4 DNA ligase [Promega]. A vector:insert ratio of 3:1 was used. Briefly, the following components were added to a nuclease-free 200 µl microtube: 5 µl 2× rapid ligation buffer, 100 ng linearised-pcDNA3, 7 ng FOXE1 BamHI-XbaI fragment and the reaction made up to 10 µl with nuclease-free water [Promega]. The reaction was then incubated overnight at 4°C.

5µl ligation product was used to transform One Shot® TOP10 Competent Cells [Invitrogen] (Section 4.2.11.3.3). Blue/white colony screening was used to determine successful cloning and small-scale mini-prep isolation of plasmid constructs was performed on single selected colonies (Section 2.2.3.1).

The length of the polyAla tract was determined by direct sequencing using the T7 and SP6 primers (Section 5.2.3.1).

5.2.4. HEK293 Cells

All previous studies had used the human embryonic kidney-293 (HEK293) cell-line to measure FOXE1 transcriptional activity (Clifton-Bligh *et al.*, 1998; Castenet *et al.*, 2002 and Barış *et al.*, 2006). The HEK293 cell-line was generated by the transformation of human embryonic kidney cells with adenovirus type 5 DNA (Graham *et al.*, 1977). Recent evidence suggests that the cell-line is actually derived from a neuronal cell lineage present in the developing kidney (Shaw *et al.*, 2002). The cells were kindly provided by Dr. G. Wilkinson (Cardiff, Wales).

5.2.4.1. Maintaining HEK293 Cells

5.2.4.2. Culture Conditions

HEK293 cells were grown in T75 Nunclon delta surface flasks [Nunc] containing 10 ml of culture medium. The medium consisted of DMEM (with 4.5 g/L Glucose, L-Glutamine and without Na Pyruvate) supplemented with 10% heat-inactivated FCS (EU approved), 50 U/ml penicillin, 50 µg/ml streptomycin, and 2.5 µg/ml fungizone (amphotericin B) [all reagents from Cambrex]. The cells were kept in a humidified 5% CO_2 atmosphere at 37°C, and the culture medium was routinely replaced every 2 days. The HEK293 cells did not adhere well to the tissue culture flask so extra care had to be taken when replacing the culture medium not to dislodge the cells.

5.2.4.3. Cell Passaging

The cells were passaged every time they reached 80% confluence. As these cells were loosely attached they could be detached simply by pipetting culture medium over the surface of the flask. Once all the cells had been detached an appropriate volume of the cell suspension was transferred to a fresh flask (if split 1:10 they were ready to passage again within 7 days).

5.2.4.4. Cryopreservation of Cells

To produce stocks of cells for storage, cells were detached as above but rather than aliquotting into fresh flasks cells they were centrifuged at 1000 rpm for 5 mins at RT. The frozen stock was then prepared as described in Section 4.2.2.3.

5.2.4.5. Transient Transfection of HEK293

Twenty-four hours prior to transfection HEK293 cells were plated in 24-wells in DMEM with 10% heat-inactivated FCS (EU approved) [all reagents from Cambrex].

For each transfection, 1 μg Z16TKLUC reporter, 100 ng psV-β-Gal [Promega UK Ltd, Hampshire, UK], 1-100 ng pcDNA3-FOXE1 expression vector and Transfast™ reagent [Promega] (Transfast:DNA ratio = 3:1) were added to 200 μl DMEM. The reagent/DNA mixture was vortexed briefly, spun down and incubated at RT for 15 mins. The culture medium was aspirated and the cells washed with 400 μl sterile PBS. The transfection mixture was added dropwise to the well and the plate returned to the incubator for 1 hr. At the end of the incubation period, 200 μl complete medium was added to the well and the plate returned to the incubator for a 48 hr period.

After 36-48 hrs cells were harvested by adding 120 μl of passive lysis buffer [Promega] to each well and shaking the plates for 20 mins on an automatic shaker. Luciferase and β-galactosidase assays were performed with normalization of luciferase values to β-galactosidase activity.

5.2.4.6. β-Galactosidase Assay

For each transfection, 50 µl of cell lysate was transferred to a clear 96-well plate and incubated with an equal volume of ice-cold assay buffer (120 mM $Na_2HPO_4.12H_2O$, 80 mM NaH_2PO_4, 2 mM $MgCl_2.6H_2O$, 100 mM β-mercaptoethanol, 1.33 mg/ml ONPG [o-nitrophenyl-β-D-galactopyranoside], pH 7.5) at RT for 30 mins. The reaction was stopped by the addition of 150 µl 1 M Na_2CO_3 and the absorbance read at 420 nm using an ELISA plate reader.

5.2.4.7. Luciferase Assay

The luciferase activity in 50 µl of cell lysate was determined using Promega's Dual-Luciferase Reporter Assay System according to the manufacture's instructions and was measured on an automatic luminometer [Perkin Elmer TR717] set to inject 50 µl of the luciferase assay reagent and wait for 2 secs before reading the light output of each sample for 10 secs.

5.2.5. Statistical Analyses

Pairwise comparisons were made using Student's T test (one-tailed).

5.3. Results

5.3.1. Genotyping of Individuals with Suboptimal Thyroid Function

5.3.1.1. Determining the Concentration of gDNA Samples

The concentration of the gDNA was determined by measuring the absorbance of the samples at 260 nm using a spectrophotometer. Also, the purity of the gDNA samples was determined by calculating the ratio of absorbance at 260 nm to the absorbance at 280 nm (pure DNA should have an absorbance ratio of 1.7-1.9). The DNA concentration and ratio values for each sample are shown in Table 5.5. The low ratio value for some of the samples was indicative of protein contamination in the sample.

Table 5.5. The Concentration and Purity of the gDNA Samples was Assessed by Spectrophotometric Measurement of the Absorbance at 260 nm and 280 nm

Patient	Concentration (ng/µl)	Ratio
HN	40.0	2.105
HC	68.0	1.581
VN	62.0	1.879
TA	38.0	1.510
RR	28.0	1.647
JR	64.0	1.524

5.3.1.2. Determining Length of the Polyalanine Tract

Genotyping of the 12 patients was performed by conventional PCR and then by direct sequencing of the PCR products. FOXE1 F8+R8 PCR primers were used to amplify a portion of the FOXE1 coding sequence that encompasses the polyAla tract (producing a 146 bp amplicon when the polyAla tract consists of 16-Ala residues). In addition, sequencing of the entire FOXE1 coding sequence was performed using FOXE1 A+B primers. The results of the genotyping are shown in Figure 5.5.

Genotyping of the 12 subjects revealed that they all possess previously described FOXE1 polyAla allelic variants: 14-Ala, 16-Ala and 17-Ala. Both the normal controls were homozygous 14/14. Among those subjects diagnosed with autoimmune SH, HN

was found to be heterozygous for 14/17, HC was homozygous 14/14 and VN was heterozygous 14/16. Among those individuals with non-autoimmune SH, TA and JR were found to be homozygous 14/14 and RR to be heterozygous 14/16. Of those individuals who had familial SH, IS A and B were heterozygous 14/16.

Figure 5.5. Agarose Gel Analysis of FOXE1 Polyalanine Tract PCR Products in Patients with Sub-optimal Thyroid Function. 1) pcDNA3-FOXE1 containing FOXE1-14Ala (size = 146 bp), **2)** SH patient homozygous 14/14, **3)** Patient VL heterozygous 14/16, **4)** SH patient heterozygous 14/17.

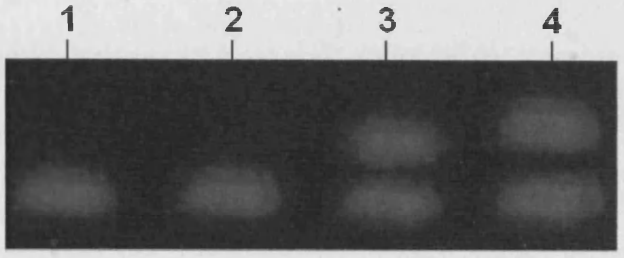

5.3.1.3. Identifying Single Nucleotide Polymorphisms

As well as variations in the length of the polyAla tract, the FOXE1 coding sequence of each patient was further analysed for the presence of additional polymorphisms such as SNPs (single nucleotide polymorphisms). The twelve sequences were compared with the online sequence for FOXE1 [March 2006 human reference sequence (NCBI build 36.1) via UCSC Genome Browser]. In total, four SNPs were identified: two had previously been reported, a third represented a novel nucleotide at a previously reported polymorphic site (720G/C/T), and a fourth was at a position (743C/G) not previously known as polymorphic (Table 5.6). All SNPs were silent except for 743C/G that leads to a conservative amino acid change from an alanine to a glycine residue.

Table 5.6. Single Nucleotide Polymorphisms in the FOXE1 Coding Region. The polymorphic variants possessed by subjects within the patient and control groups are shown.

SNP		Normal		Sporadic SH						Familial SH		
Nucleotide	Amino Acid	NI	MA	HN	HC	VN	TA	RR	JR	IS	A	B
388 C/T^†*	Leu 129 Leu	C/C	C/C	C/C	C/C	C/T	C/T	C/T	C/C	C/C	C/T	C/T
720 G§/C/T†*	Pro 240 Pro	G/G	G/G	G/G	G/G	G/G	G/G	G/G	G/G	G/G	G/G	G/G
743 C/G§	Ala 248 Gly	C/C	C/C	C/C	C/C	C/C	C/C	C/C	C/C	C/C	C/C	C/C
825 C/T^†*	Ser 271 Ser	T/T	C/T	T/T	C/T	T/T	C/T	T/T	C/T	T/T	T/T	T/T

^ Macchia *et al.*, 1999
† Hishinuma *et al.*, 2001
* Watkins *et al.*, 2006
§ Not previously reported

5.3.2. Confirming the identity of the pcDNA3-FOXE1(14-Ala) construct

A pcDNA3 vector containing the FOXE1 coding sequence with a polyAla tract consisting of 14-Ala residues had been prepared previously (Clifton-Bligh *et al.*, 1998). Restriction enzyme analysis (Figure 5.6) and direct sequencing were performed to confirm the identity of the construct.

Figure 5.6. Restriction Enzyme Analysis of pcDNA3-FOXE1(14-Ala). 1) 1 kb DNA ladder, **2)** Single digest with BamHI to linearise the plasmid, thus determining the size of the entire construct (5.4 kb), **3)** Sequential digestion with BamHI and XbaI to excise the insert, thus determining the inserts size (1.3 kb).

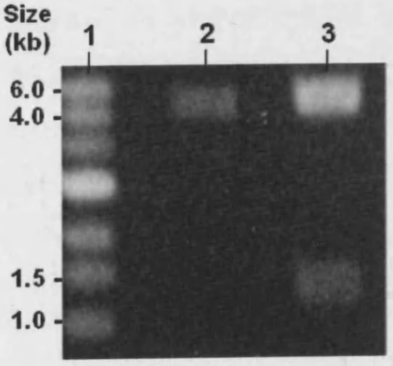

5.3.3. Creation of pcDNA3-FOXE1(16-Ala) construct

As there were no individuals homozygous 16/16 it was decided to amplify the FOXE1-AB fragment from the gDNA of patient RR who was heterozygous 14/16 (Figure 5.7), and then isolate the 16-Ala allele using a cloning strategy similar to that employed earlier to sequence heterozygous individuals. A comparison of the sequencing data from subject RR and pcDNA3-FOXE1(14-Ala) revealed that, apart from the insertion of the six nucleotides that encode the additional two Ala residues, the two sequences were identical.

Figure 5.7. Amplification of the FOXE1 Coding Sequence from Patient RR who was heterozygous 14/16. 1) 1 kb DNA ladder, **2)** FOXE1-AB amplicon.

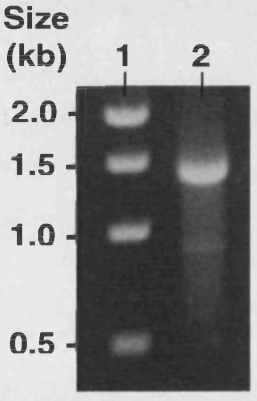

The PCR amplicon was cut with BamHI and XbaI restriction enzymes and then ligated into an empty pcDNA3 expression vector that had been linearised using the same enzymes. Several clones were picked and successful ligations determined by restriction enzyme analysis with BamHI and XbaI (Figure 5.8). Those constructs containing the 16-Ala variant were identified by PCR using FOXE1 F8+R8 PCR primers and analysis of the products on 4% agarose gel (Figure 5.9). The length of the polyAla tract was confirmed by direct sequencing using FOXE1 A+B primers.

Figure 5.8. Restriction Enzyme Analysis of Minipreps to Identify Successful Ligations. 1) 1 kb DNA ladder, **2-5)** BamHI-XbaI digests to excise the 1.3 kb insert from the 5.4 kb pcDNA3 vector

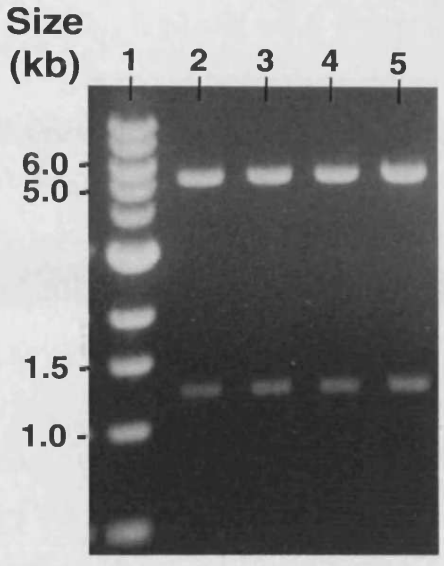

Figure 5.9. Identification of a Clone Containing pcDNA3-FOXE1(16-Ala). 1) 100 bp DNA ladder, **2)** pcDNA3-FOXE1(14-Ala), **3)** gDNA from patient VL (heterozygous 14/16), **4-9)** minipreps

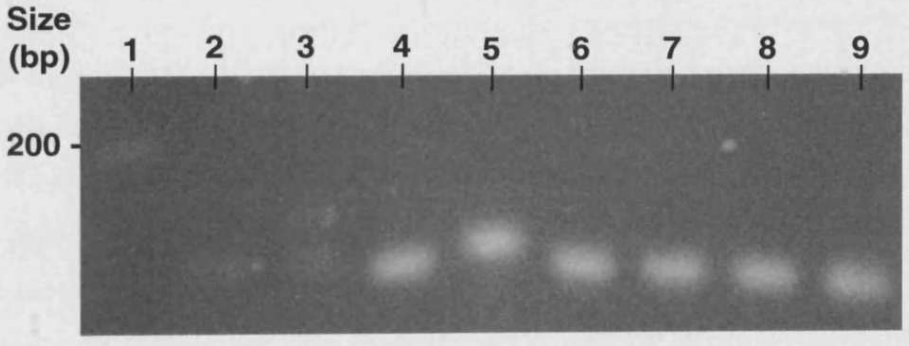

5.3.4. FOXE1-14Ala is More Transcriptionally Active than FOXE1-16Ala

As FOXE1-14Ala and FOXE1-16Ala were the two most commonly occurring variants we decided to compare their transcriptional activity using an *in vitro* reporter assay. The results of a representative experiment are shown in Table 5.7 and Figure 5.10. The results are the mean average of three technical replicates, each normalised by β-Gal to correct for transfection efficiency. They show that the FOXE1-14Ala variant had an approximately two-fold increase in transcriptional activity across the concentration range, when compared with the FOXE1-16Ala variant. This difference in activity was statistically significant ($p<0.01$ between 5 and 50 ng, $p<0.05$ at 1, 3 and 100 ng). Similar results were obtained in three further experiments, in which fresh reporter and expression constructs were prepared, to ensure the results were not attributable to sample degradation, contamination etc.

5.3.5. FOXE1-14/FOXE1-16 Heterozygotes Display Reduced Transcriptional Activity Compared with FOXE1-14/FOXE1-14 Homozygotes

The first experiments effectively provided an *in vitro* comparison of the activity of individuals who were homozygous 14/14 and 16/16. However, as 14/16 was the second most common genotype, we sought to investigate the transcriptional potential of the heterozygous state. Table 5.8 and Figure 5.11 shows the results of a representative experiment in which transfected DNA concentration was investigated using equal quantities of the FOXE1-14Ala and FOXE1-16Ala variants, both contributing half the amount, so that the total amount was the same as in the equivalent wells containing FOXE1-14Ala or FOXE1-16Ala alone.

The transcriptional activity of the FOXE1-14Ala was significantly greater than that of the FOXE1-16Ala and FOXE1-14/16Ala ($p<0.01$ between 3-5 ng, $p<0.05$ at 1, 10, 50 and 100 ng). There was no significant difference, at any concentration, when comparing FOXE1-16Ala with FOXE1-14/16Ala. Similar results were obtained in three further experiments.

Table 5.7. Relative Light Units (RLU) and β-Gal Values for Each Transfection. The β-Gal values were used to normalise the luciferase values for transfection efficiency (RLU = relative light units). Statistical analysis used student's T test.

Amount of DNA (ng)	FOXE1-14Ala					FOXE1-16Ala					P-Value
	Luciferase	β-Gal	Normalised	Mean	S.D	Luciferase	β-Gal	Normalised	Mean	S.D	
0	545,803	811	673	531	131	545,803	811	673	531	131	
	427,230	846	505			427,230	846	505			
	329,056	791	416			329,056	791	416			
1	6,734,160	846	7,960	7,052	1,736	2,285,360	616	3,710	3,094	616	1.62E-02
	4,009,700	794	5,050			1,746,990	705	2,478			
	6,483,420	796	8,145			1,893,528	612	3,094			
3	7,588,869	907	8,367	8,390	1,352	2,581,935	645	4,003	4,526	518	2.82E-02
	5,830,350	827	7,050			4,524,124	898	5,038			
	7,920,248	812	9,754			4,070,586	897	4,538			
5	6,695,630	695	9,634	10,518	1,189	5,484,016	848	6,467	6,727	722	3.92E-03
	7,125,450	709	10,050			5,504,532	892	6,171			
	8,225,910	693	11,870			6,494,523	861	7,543			
10	8,971,480	895	10,024	10,305	652	4,001,697	837	4,781	4,923	270	8.37E-04
	8,298,550	751	11,050			4,480,304	856	5,234			
	5,963,040	606	9,840			3,807,954	801	4,754			
50	7,957,600	725	10,976	11,567	545	4,211,200	896	4,700	3,616	957	5.81E-03
	9,025,450	749	12,050			2,349,570	813	2,890			
	6,410,124	549	11,676			2,661,786	817	3,258			
100	4,788,798	798	6,001	5,293	623	2,464,424	856	2,879	3,191	706	3.62E-02
	4,772,250	945	5,050			3,364,000	841	4,000			
	3,755,406	778	4,827			2,217,985	823	2,695			

Figure 5.10. Comparison of Transcriptional Activity of FOXE1-14Ala and FOXE1-16Ala. 0-100ng of pcDNA3-FOXE1 expression vectors were cotransfected with 1 μg Z16TKLUC reporter and 100 ng psV-β-Gal internal control plasmid into HEK293 cells. Values are the mean (±SD) of a single experiment performed in triplicate, expressed as normalised relative light units i.e. light output from the luciferase reporter assay/β-Gal $O.D_{420}$. Statistical analysis used Student's T test (* represents $P<0.05$, ** represents $P<0.01$).

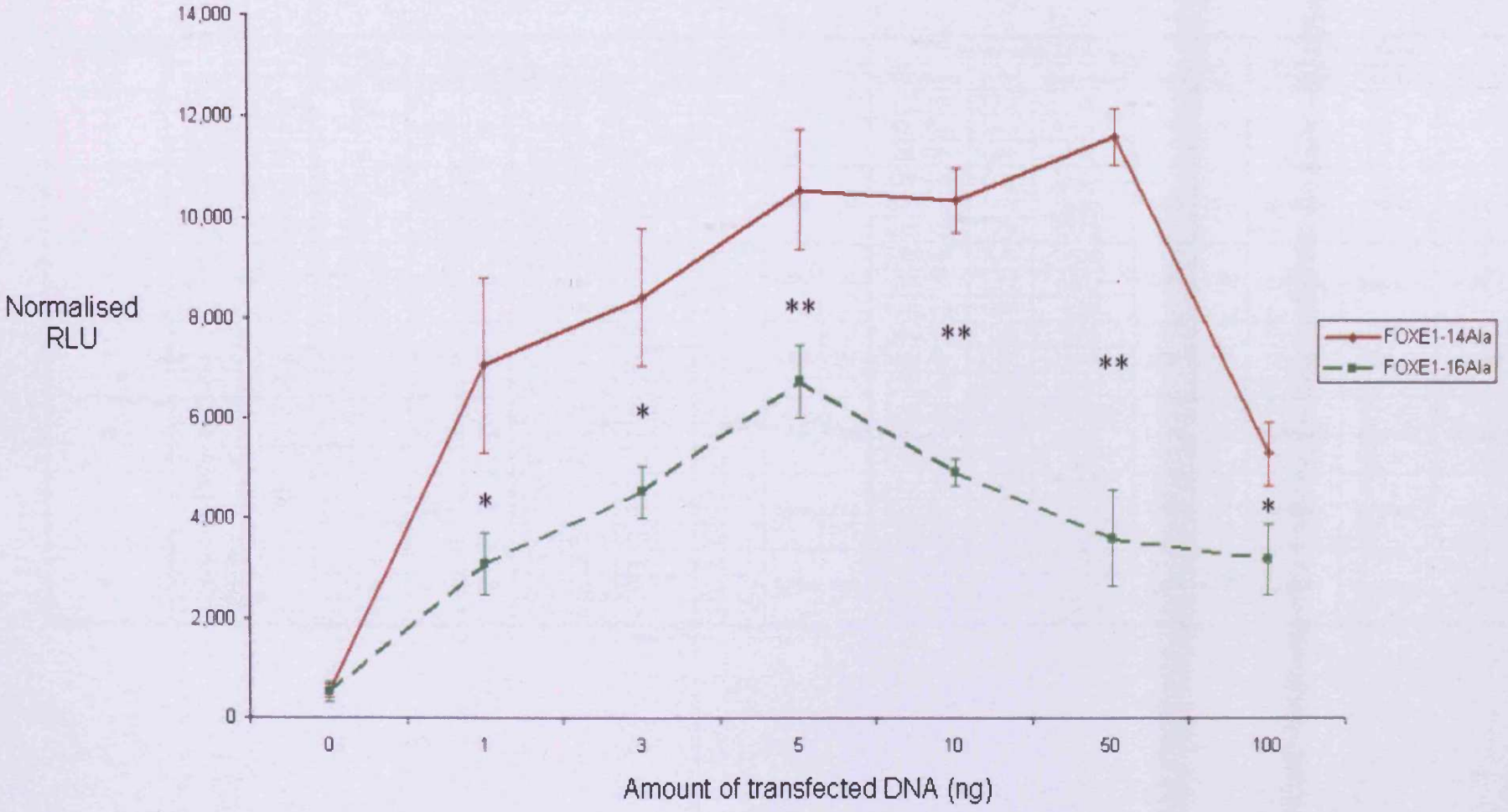

Table 5.8. Relative Light Units (RLU) and β-Gal Values for each Transfection. The β-Gal values were used to normalise the luciferase values for transfection efficiency (RLU = relative light units). Statistical analysis used Student's T test.

Amount of DHA	FOXE1-14Ala					FOXE1-16Ala					FOXE1-14Ala + FOXE1-16Ala					P-Values		
(ng)	Luciferase	β-Gal	Normalised	Mean	S.D	Luciferase	β-Gal	Normalised	Mean	S.D	Luciferase	β-Gal	Normalised	Mean	S.D	14/14+16/16	14/14+14/16	14/16+16/16
0	127,092	1428	89	116	24	127,092	1,428	89	116	24	127,092	1,428	89	116	24			
	179,056	1444	124			179,056	1,444	124			179,056	1,444	124					
	208,624	1534	136			208,624	1,534	136			208,624	1,534	136					
1	12,620,800	1450	8,704	9,723	1,246	5,033,037	1,411	3,567	4,035	443	2,263,141	1,397	1,620	2,443	1,049	6.78E-03	1.28E-04	5.47E-02
	12,983,352	1388	9,354			6,230,247	1,401	4,447			3,077,460	1,476	2,085					
	16,045,728	1444	11,112			5,732,892	1,401	4,092			5,151,125	1,421	3,625					
3	35,773,586	1429	25,034	25,860	908	6,966,520	1,420	4,906	5,072	764	6,308,940	1,331	4,740	5,011	1,168	7.86E-04	2.19E-04	4.80E-01
	34,249,716	1332	25,713			8,392,426	1,421	5,906			5,215,909	1,303	4,003					
	36,129,693	1421	26,833			6,268,315	1,423	4,405			8,172,009	1,299	6,291					
5	33,743,085	1401	24,085	24,446	921	4,963,190	1,490	3,331	3,484	737	2,862,825	1,425	2,009	2,760	653	1.71E-05	3.34E-04	1.56E-01
	40,686,678	1596	25,493			6,088,985	1,421	4,285			4,381,417	1,423	3,079					
	32,717,520	1377	23,760			3,978,908	1,403	2,836			4,767,354	1,494	3,191					
10	18,973,746	1422	13,343	12,705	720	4,274,250	1,390	3,075	3,441	1,032	6,803,256	1,401	4,856	5,716	1,405	5.40E-03	1.44E-02	7.14E-03
	17,086,510	1330	12,847			3,758,346	1,422	2,643			7,426,046	1,499	4,954					
	14,321,925	1201	11,925			5,711,440	1,240	4,606			10,961,478	1,494	7,337					
50	8,062,110	1337	6,030	6,665	948	4,386,624	1,474	2,976	2,189	733	4,536,496	1,264	3,589	4,164	571	2.03E-02	2.72E-02	5.06E-02
	7,879,221	1269	6,209			2,937,207	1,421	2,067			6,722,751	1,421	4,731					
	10,236,600	1320	7,755			2,096,875	1,375	1,525			5,861,660	1,405	4,172					
100	8,746,050	1465	5,970	5,537	753	3,643,695	1,299	2,805	2,448	908	3,861,816	1,267	3,048	2,924	1,127	7.15E-04	6.96E-03	6.73E-02
	6,539,868	1401	4,668			2,010,555	1,421	1,415			2,550,840	1,466	1,740					
	7,234,514	1211	5,974			4,437,531	1,421	3,123			5,472,642	1,374	3,983					

Figure 5.11. Comparison of Transcriptional Activity in FOXE1 Homozygotes and Heterozygotes. HEK293 cells were cotransfected with 1 μg Z16TKLUC reporter, 100 ng psV-β-Gal internal control plasmid and 0-100 ng of pcDNA3 expression vector containing the two FOXE1 variants alone or combined. Values are the mean (±SD) of a single experiment performed in triplicate, expressed as normalised relative light units i.e. light output from the luciferase reporter assay/β-Gal $O.D_{420}$. Statistical analysis used student's T test (* represents $P<0.05$, ** represents $P<0.01$).

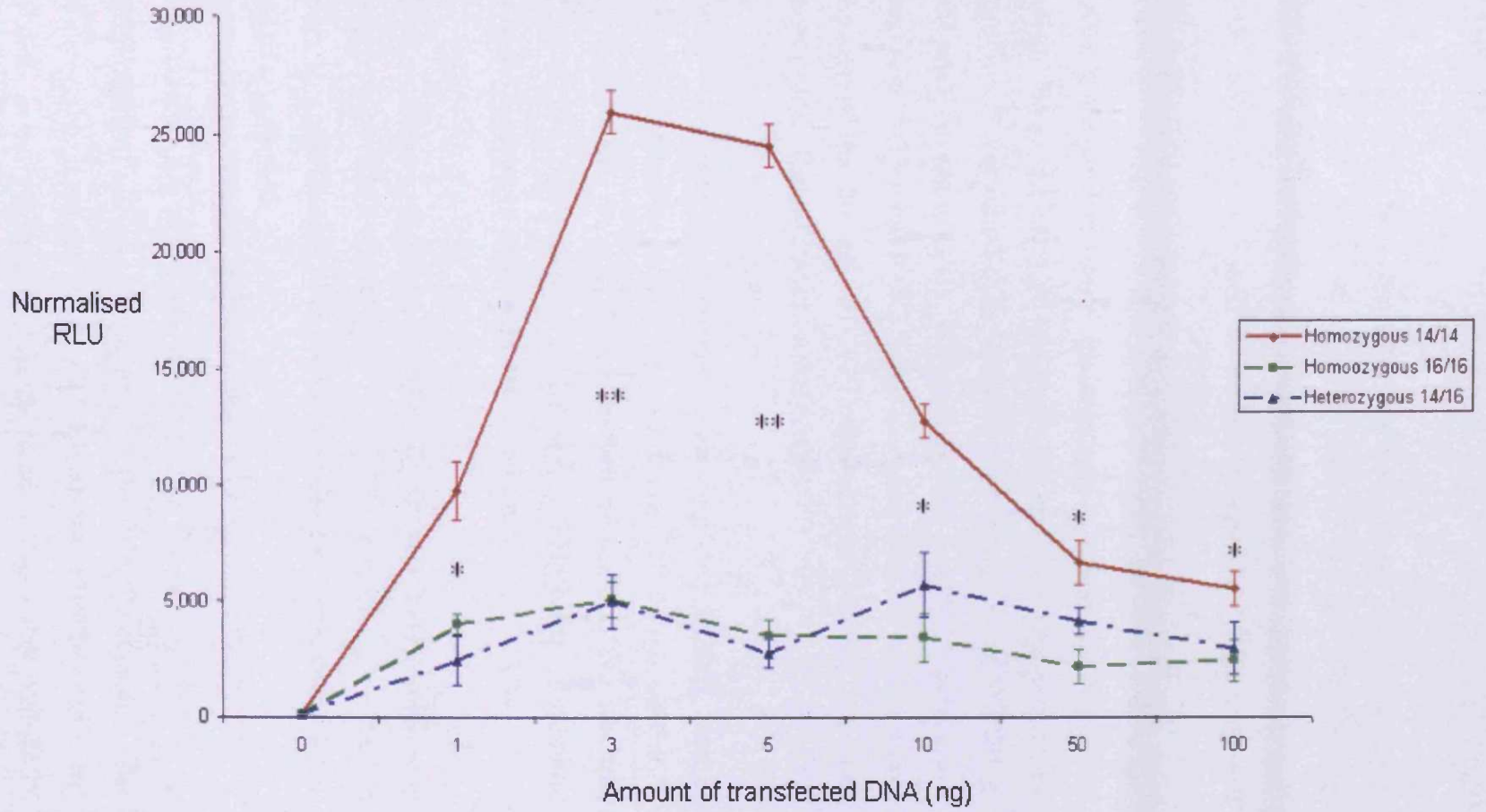

5.3.6. Investigation into the Difference in Reporter Activity Observed in HEK293 and HaCaT

As well as HEK293, functional analysis of the FOXE1 variants was also attempted in two additional cell-lines: HaCaT and COS (Cells of Simian). However, despite the successful transfection (as indicated by β-Gal levels, data not shown) of both cell-types, the Z16TKLUC reporter was found to be non-responsive to cotransfected FOXE1.

The ability of a FOXE1 responsive reporter to function only in specific cell-types was also observed by Hishinuma *et al* (2001). In this study the luciferase reporter (driven by the human TG promoter) was found to be responsive to cotransfected FOXE1 in VMR-LCD (lung cell-line), but not in G401 (kidney cell-line). As FOXE1 was known to functionally interact with TITF1 and PAX8 in the modulation of TG transcriptional activity, the authors proposed that the lack of TITF1 expression in G401 could explain their result (the authors did not look at PAX8 expression).

Although, our reporter was a synthetic construct, containing only FOXE1 binding sites, it is still possible that PAX8 and/or TITF1 were required for transactivation (possibly interacting with FOXE1 in a DNA-independent manner). If this was true and HaCaT and COS lacked expression of PAX8 and/or TITF1 then this could explain the inability of the reporter to function in these cell-lines.

RT-PCR analysis was performed to detect FOXE1, PAX8 and TITF1 mRNA in HEK293 and differentiating HaCaT cell (Figure 5.12). The integrity of the cDNA samples was confirmed by amplification of the APRT housekeeper gene, which found to be at similar levels in all samples.

In agreement with the QPCR data of Chapter 4 FOXE1 mRNA was detected at all stages of HaCaT differentiation, and was also detected in the HEK293 cells at similar levels. However, no detectable level of PAX8 or TITF1 mRNA could be seen in the HEK293 or HaCaT cells at early stages of differentiation (up to 1 day post-shift). Unexpectedly, the expression of PAX8 and TITF1 was found to 'switched on' at 3

and 6 days post-shift respectively. This represents the first time that the expression of these two genes has been observed in keratinocytes. Furthermore, it is the first time that coexpression of PAX8, TITF1 and FOXE1 has been observed in a non-thyrocyte cell-type.

Figure 5.12. RT-PCR Analysis of APRT, FOXE1, PAX8 and TITF1 mRNA Levels in HEK293 and Differentiating HaCaT. 1) 100 bp DNA ladder, **2)** HEK293 replicate 1, **3)** HEK293 replicate 2, **4)** HaCaT 30-40% confluent, **5)** HaCaT 70-80% confluent, **6)** HaCaT 1 day post-shift, **7)** HaCaT 3 days post-shift, **8)** HaCaT 6 days post-shift, **9)** HaCaT 6 days no-shift control, **10)** no template control.

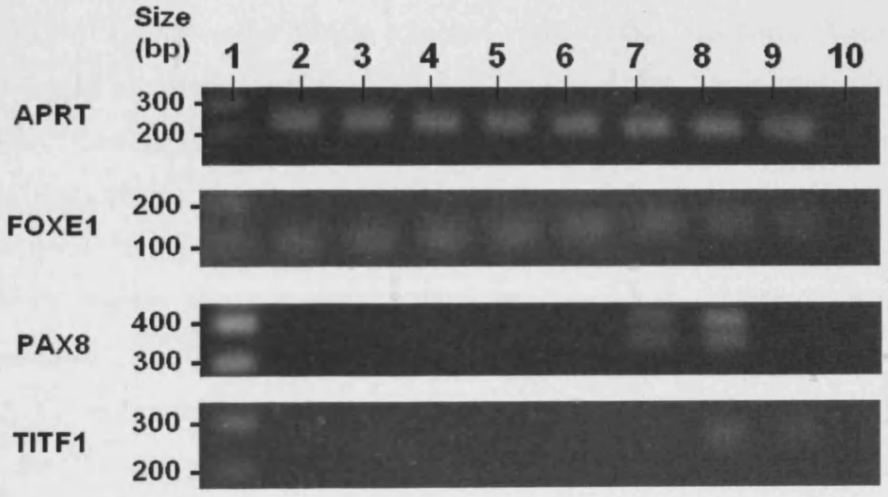

5.4. Discussion

The main achievements of this chapter were: (1) The genotyping of FOXE1 in a cohort of patients with sub-optimal thyroid function; (2) The construction of an expression plasmid to allow the expression of the FOXE1-14Ala variant (3) The performance of a series of luciferase reporter assays that compare the transcriptional activity of the FOXE1-14Ala and 16Ala variants; (4) Preliminary investigations of the expression of thyroid transcription factors in different cell-lines.

Three previous studies have reported that FOXE1-14Ala homozygotes are underrepresented in patients with CH (Hishinuma *et al*, 2001; Tonacchera *et al.*, 2004; Santarpia *et al.*, 2007). Despite considerable efforts to identify the causative genes, only a small proportion of CH cases can be explained by mutations in e.g. FOXE1, TITF-1, PAX8 or the TSHR (Gruters *et al.*, 2004). Recently, Amendola *et al* (2005) presented evidence for the multigenic nature of CH. The authors showed that mice doubly heterozygous for pax8 and titf1 null mutations display thyroid dysgenesis (hypoplasia or hemiagenesis), provided the mutations are present on a specific genetic background (C57BL/6). However, when the same mutations are introduced in another background (129/Sv), the mice are completely wild-type. A simple backcross experiment allowed the authors to propose that the strain differences were likely to be due to the influence of two modifier genes. Could variations in the length of the FOXE1 polyAla tract have been a contributory factor to multigenic thyroid dysgenesis?

Reduced incidence of the FOXE1-14Ala variant has also been reported in patients with premature ovarian failure (POF), a condition that is often associated with hypothyroidism (Watkins *et al.*, 2006). Although it is not known if FOXE1 is expressed in the ovaries, FOXE1 protein has been detected in the seminiferous tubules of the testes. Therefore, FOXE1 may play an important role in functioning of these organs, which could have implications for fertility.

In the mature thyroid gland, the main role of FOXE1 is to mediate the control of thyroid hormone synthesis by the TSH and IGF-1 signaling pathways. In combination

with PAX8 and TITF1 it modulates the expression of two key genes involved in thyroid hormone synthesis, TG and TPO. Therefore, the transcriptional activity of FOXE1 may directly influence the thyroid gland's ability to produce adequate amounts of thyroid hormone. Several studies have shown that thyroid hormone levels can vary considerably between people, and this is due at least in part to genetic factors. The symptoms of subclinical hyper- and hypothyroidism show that these minor changes can have important consequences for a whole range of physiological parameters e.g. heart rate, cholesterol metabolism and bone mineral density. These observations could be explained by polymorphisms that have subtle effects on the functional activity of proteins involved in thyroid hormone metabolism. Presently, only the TSHR and iodothyronine deiodinases have been analysed for an association between polymorphisms and serum thyroid hormone levels (Peeters *et al.*, 2006). Could polymorphic variation in the FOXE1 gene also be a contributing factor here?

In this study, we examined a cohort of twelve patients with SH, and found that half of them were heterozygous 14/16, 5 were homozygous 14/14 and one was heterozygous 14/17. Although such a small cohort cannot produce statistically meaningful data, it does not contradict previous studies, which have shown that the 16-Ala variant is more common in patients with CH.

Using an *in-vitro* luciferase reporter assay, we determined that the 14-Ala variant had an approximately 2-fold greater transcriptional activity than the 16-Ala variant. This was an unexpected result, as we did not think that a two amino acid difference would have such a large impact on the functional activity of the protein. However, previous studies have shown the addition of one amino acid in the polyalanine tract of PABPN1 can cause oculopharyngeal muscular dystrophy.

As the most common genotype in our patient cohort was heterozygous 14/16, we set out to compare the functional activity of the heterozygous state with the two homozygous states. We expected the activity of the heterozygous state to be approximately half way in between 14/14 and 16/16. However, we found that the activity was lower than expected being at a level similar to that found in the homozygous 16/16. This suggests that the 16-Ala variant was able to suppress the activity of the wild type acting in a dominant negative manner. Another forkhead

gene FOXL2 (also containing a polymorphic polyAla tract expansions of which have been linked to human disease), also acts in a dominant negative manner.

The variation in FOXE1 transcriptional activity attributable to the differing polyAla tract length is very subtle, and would be expected to cause a very mild phenotype, such as that found in people with SH. Such individuals are largely asymptomatic and tend to be identified in the course of investigation for other conditions. There is some controversy as to whether SH, which can be associated with increased cardio-vascular risk, should be treated (Owen & Lazarus, 2003). If the underlying mechanism responsible for the SH was known it might be possible to analyse the results by subgroup and achieve some resolution of the conflict. We, and others, have found that expressing a single functional TSHR accounts for some cases of SH, with TSH being elevated in compensation (Locantore *et al.*, 2007). The response of these patients to thyroxine treatment may differ to other SH patients (e.g. patients with autoimmune SH). In light of our present findings, it would be informative to genotype FOXE1 in a cohort of normal individuals, in whom thyroid function tests are well within the limits of the normal ranges, and compare the results with a group of clearly defined SH patients.

An unexpected outcome of the functional studies was the observation that our Z16TKLUC reporter was only responsive to FOXE1 in certain cell-lines. As HEK293 cells (used in previous studies) were not immediately available in the lab, preliminary experiments attempted to use alternative cell-lines, these being HaCaT and COS. However, in both cases the reporter was found to be non-responsive to FOXE1, with the light output from the luciferase assay remaining at background levels, even when the cells were transfected with 1 μg FOXE1 expression vector. This was not due to poor transfection efficiency, as the transfected cells were found to contain high levels of β-Galactosidase. Also, the result could not be explained by inhibition of the luciferase enzyme, as lysates from cells transfected with a cAMP responsive luciferase reporter, and stimulated with forskolin (an adenyl cyclase activator) produced a high light output. Indeed, the fault seemed to lie at the transcriptional level. In Chapter 4, real-time QPCR analysis of the HaCaT-LUC cell-line revealed a 3-fold increase in the level of luciferase transcripts, correlating with a similar increase

in the level of FOXE1 transcripts. However, despite this increase the luciferase transcripts were still expressed at very low levels (Ct values > 35).

A likely possibilty was that the cell-lines differed in their expression of additional genes that were able to influence the ability of FOXE1 to induce transcription e.g. cofactors. Two explanations could explain our results:

1. HEK293 express a coactivator(s) that HaCaT and COS do not
2. HaCaT and COS express a corepressor(s) that HEK293 do not

Our results were similar to the observations made by Hishinuma *et al* (2001), who observed that their own luciferase reporter (driven by the human TG promoter – containing FOXE1, PAX8 and TITF1 binding sites) was responsive to cotransfected FOXE1 in VMR-LCD (lung cell-line) but not in G401 (kidney cell-line). The authors suggested that this was because transactivation of the native promoter required the additional binding of TITF1 (expressed by VMR-LCD, but not G401). Unfortunately, the authors did not examine whether PAX8 expression differed between the two cell-lines, but as PAX8 functionally cooperates with TITF1 in TG promoter activation (Di Palma *et al.*, 2003), this too may have contributed to the differences observed in reporter function.

The situation in our case was slightly different to that described by Hishinuma *et al* (2001), as the reporter we used was a synthetic construct that contained only FOXE1 binding sites. However, FOXE1 has previously been shown to functionally interact with both PAX8 and TITF1 in a DNA independent manner (Zannini *et al.*, 1997). This led to the hypothesis that PAX8 and/or TITF1 could play a role as cofactors, interacting with FOXE1 and modulating its ability to transactivate the reporter construct. Thus, if HEK293 differed from HaCaT and COS in the expression levels of PAX8 and/or TITF1 then this could potentially explain the differences observed between these cell-lines.

RT-PCR analysis revealed that HEK293 cells, cultured under similar conditions to when they were transfected, contained no detectable levels of PAX8 or TITF1 mRNA. The same was also true for undifferentiated HaCaT cells (up to 1 day post-shift). However, both PAX8 and TITF1 expression was found to be 'switched on' as

HaCaT differentiation proceeded. Firstly, this represents the first time that the expression of these genes has been detected in a keratinocyte cell-line. Secondly, this also represents the first reported instance of coexpression of FOXE1, PAX8 and TITF1 in a non-thyroidal cell-line. Finally, the presence of PAX8 and TITF1 expression in differentiated HaCaT (see below for applicability to transfected HaCaT) and their absence from HEK293 supported the idea one or both may function as a corepressor of FOXE1.

Prior to transfection, HaCaT cells were seeded in DMEM + 10% FCS (>1.8mM Ca^{2+}) culture medium at a sufficient density so that the cells would be 80% confluent the following day. This combination of high cell density and exposure to a high extracellular Ca^{2+} concentration would have greatly increased the rate of differentiation. And so, the cells were likely to be at a fairly advanced stage of differentiation at the time of the luciferase assay. Although there is no ICC data to confirm this, the morphology of the cells at the time seemed to suggest that this was the case. Thus, it is not unlikely that PAX8 and TITF1 expression was switched on by this time. RT-PCR analysis of total RNA extracted from HaCaT cell grown under these conditions would confirm this.

In conclusion, the results indicate that individuals homozygous for the FOXE1-14Ala variant display optimal transcription and hence thyroid function. Deviations from this genotype may be a contributory factor sufficient to account for some cases of SH and/or contribute to multigenic CH. We believe that the FOXE1 polyAla tract may provide a genetic marker for identifying individuals predisposed to developing suboptimal thyroid function.

Coexpression of FOXE1, PAX8 and TITF1 has only been previously reported in thyrocytes and is a defining feature of this cell-type. And so, detecting the expression of all three transcription factors in a keratinocyte cell-line was a surprising result. Of course, in order to determine if this has real biological implications western blot analysis will have to be performed to confirm that PAX8 and TITF1 proteins are present. Recently, another group have shown that cultured keratinocytes express functionally active TSHR as well as NIS and TG genes (Slominski *et al.*, 2006). This begs the question as to why keratinocytes are expressing so many components, which

were previously though to be thyroid-specific. As skin is commonly affected by thyroid disease, does this suggest that the skin has a more direct involvement than previously thought?

Chapter 6.

General Discussion

When I commenced my PhD research, the title of the project was 'Regulation of Hair Follicle Development and Cycling by Thyroid Transcription Factor 2 (TTF2)'. The following specific aims were identified:

1. Examining expression of TTF2 transcripts and protein in different hair follicle regions and assessing co-localisation with known keratin genes, which define specific hair follicle cell-lineages.
2. Assessing which hair keratin genes contain TTF2 consensus binding sites and whether TTF2 alters their transcription *in vitro* and *in vivo*, thus defining a role for TTF2 in regulating these genes.
3. Defining which other hair genes are regulated by TTF2, if hair keratin genes are not targeted.

Since then the nomenclature of forkhead transcription factors has been standardised, as outlined in Chapter 1, thus TTF2 became FOXE1, a name that better reflects the extent of its biological activities. The combination of initial technical difficulties, combined with advances in the field, resulted in a change in the direction of the project.

In the first experimental chapter I used the pAb to full-length FOXE1 fusion protein which had been developed by Sequeira *et al* (2003). The antibody was produced in response to the requirement of confirming FOXE1 transcript expression data obtained using northern blots and RT-PCR. These studies had revealed FOXE1 expression in adult thyroid gland and testis (Clifton-Bligh *et al.*, 1998) and then in benign and malignant thyroid lesions (Sequeira *et al.*, 2001). The 2003 study reported FOXE1 protein in normal and Graves' thyroid tissue, and was also the first to demonstrate expression of the protein in the outer root sheath (ORS) of the hair follicle, as would be expected from the hair phenotype which persists in patients with loss-of-function mutations in the FOXE1 forkhead binding domain, the first two of whom were from the Cardiff area.

Examination of the patients' notes revealed a wide range of defects including:
'Four days after birth, wiring of the hair which has a strange distribution and extends to nape of neck and forehead. Hair on both forearms.' The Professor of Dermatology

wrote 'The length and profusion of hair over the limbs, forehead and eyebrows is remarkable. The scalp is covered with curling black hair.'

Other defects, not previously reported in the literature, include hydrocoele right testis in one brother and in the left testis in his sibling; eruption of teeth in the soft palate in both brothers, receding chin in one boy and absence of both sets of lower lid lashes and septic areas covering the hands and feet. Some of these abnormalities are found in other children with mid-line defects, but they indicate the wide spectrum of tissues that can be affected by mutations in FOXE1. Of interest the mother, heterozygous WT/A65V for FOXE1, has choanal atresia.

In Chapter 2, our aim to perform co-localization studies to identify the cells within the hair follicle that express FOXE1 and assess the stage of differentiation, as determined by the type of keratin present in those cells. Although it was possible to confirm the specificity of the antibody for FOXE1, on both human thyroid and skin sections using immunohistochemistry, the antibody did not work well in an immunofluorescence protocol. Extended attempts to produce sufficient fusion protein to couple to CnBr-sepharose and perform affinity purification were not successful. The yield was too low and the only induced protein did not migrate at the predicted molecular weight. Subsequent experiments revealed that this was probably due to aggregation of the protein, and could be avoided by low temperature treatment of samples for SDS-PAGE.

In 2004, Brancaccio and colleagues, using a combination of *in vivo* and *in vitro* techniques, reported their findings of FOXE1 in the context of hair follicle development. They found that the apparent differentiation programme of skin from FOXE1$^{-/-}$ mice was normal and that it was the alignment and migration of the hair follicles within the skin that was significantly disrupted. Therefore, we decided to direct our attention to the role that FOXE1 plays in cell-migration.

In Chapter 4, we present data generated using a combination of QPCR-based expression profiling and siRNA-based gene knockdown, which strongly suggests that FOXE1 is a direct transcriptional regulator of TIMP3 expression in human keratinocytes. On the basis of these findings we propose a model for the mechanism

by which FOXE1 is able to control the orientation of growing hair follicles. We believe that by inducing the expression of TIMP3 in the ORS keratinocytes that surround the sides of the follicle, the ECM is maintained and the follicles are prevented from growing sideways. This work may have implications for the treatment of skin tumours such as BCCs (the most commonly occurring tumour in caucasions) that are believed use a similar mechanism to hair follicles to invade local tissues. Interestingly, Eichberger *et al* (2004) have shown that FOXE1 is highly upregulated in BCCs. Could upregulation of FOXE1 be responsible for the invasive nature of these tumours? Although BCCs are rarely life-threatening are easily removed by surgery, there are a variety of more serious skin tumours e.g. squamous cell carcinomas and malignant melanomas which also may require FOXE1 for their invasive properties. If so, then this knowledge may lead to new forms of treatment. Gene therapy as proved to be more successful in dermatology than in other fields due easy accessible nature of the tissue. Maybe a treatment could be developed based on knocking-down the expression of FOXE1 or one of its target genes.

We also provide the first reported detection of DREAM in human keratinocytes. We also preliminary data that, as has been shown to be the case in the thyroid, DREAM acts as a transcriptional repressor of FOXE1 in skin. As calcium signalling is one of the main regulators of epidermal homeostasis, it is not surprising that DREAM is present in this tissue. Future work will elucidate the precise role(s) this transcription factor plays in skin.

In Chapter 5, we used an *in vitro* reporter assay to show for that variations in the length of the FOXE1 polyAla tract have a subtle but significant influence on the transcriptional activity of the protein. We show that the 16-Ala variant, which several studies have shown to be over-represented in patients with CH, has a 2-fold lower activity than the 14-Ala variant (the wild-type variant). A recent study by Amendola *et al* (2005) provided evidence of the multigenic nature of thyroid dysgenesis (the most common cause of CH). We propose that expansions in the FOXE1 polyAla tract, whilst by themselves are not sufficient to cause thyroid dysgenesis, are a contributory factor in the pathogenesis of the disease.

We also provide preliminary results that show the 16-Ala variant to be over-represented in patients with SH. However, at this stage we have examined too few patients too produce statistically meaningful results (we are currently in the process of obtaining gDNA samples from a much larger cohort). However, if our initial observations are true, then the small reduction we observed in the transcriptional activity of the 16-Ala variant may explain the very mild phenotype displayed by these individuals. Therefore, the FOXE1 polyAla tract may provide a genetic marker for identifying individuals predisposed to developing suboptimal thyroid function.

An unexpected outcome of this chapter, is the detection of all three thyroid transcription factors (FOXE1, PAX8 and TITF1) in a keratinocyte cell-line. The expression of PAX8 and TITF1 still has to be confirmed at the protein level before we can be confident that their presence is of biological significance. However, the recent detection of TSHR, TG and NIS (downstream targets of the thyroid transcription factors) by Slominski *et al* (2002) expression in human skin suggests that this will be the case. The coexpression of these genes has only previously been seen in the thyroid gland itself, where they are all involved in thyroid hormone synthesis. This begs the question, does the skin produce thyroid hormones. And if it does, for what purpose? At present, this remains a complete mystery.

References

Abramowicz, M. J., Targovnik, H. M., Varela, V., Cochaux, P., Krawiec, L., Pisarev, M. A., Propato, F. V., Juvenal, G., Chester, H. A., Vassart, G. (1992). Identification of a mutation in the coding sequence of the human thyroid peroxidase gene causing congenital goiter. *J Clin Invest.* **90(4):** 1200-4.

Airola, K., Ahonen, M., Johansson, N., Heikkilä, P., Kere, J., Kähäri, V. M., Saarialho-Kere, U. K. (1998). Human TIMP-3 is expressed during fetal development, hair growth cycle, and cancer progression. *J Histochem Cytochem.* **46(4):** 437-47.

Alberti, L., Proverbio, M. C., Costagliola, S., Romoli, R., Boldrighini, B., Vigone, M. C., Weber, G., Chiumello, G., Beck-Peccoz, P., Persani, L. (2002). Germline mutations of TSH receptor gene as cause of nonautoimmune subclinical hypothyroidism. *J Clin Endocrinol Metab.* **87(6):** 2549-55.

Albrecht, A. N., Kornak, U., Böddrich, A., Süring, K., Robinson, P. N., Stiege, A. C., Lurz, R., Stricker, S., Wanker, E. E., Mundlos. S. (2004). A molecular pathogenesis for transcription factor associated poly-alanine tract expansions. *Hum Mol Genet.* **13(20):** 2351-9.

Ambrugger, P., Stoeva, I., Biebermann, H., Torresani, T., Leitner, C., Grüters, A. (2001). Novel mutations of the thyroid peroxidase gene in patients with permanent congenital hypothyroidism. *Eur J Endocrinol.* **145(1):** 19-24.

Amendola, E., De Luca, P., Macchia, P. E., Terracciano, D., Rosica, A., Chiappetta, G., Kimura, S., Mansouri, A., Affuso, A., Arra, C., Macchia, V., Di Lauro, R., De Felice, M. (2005). A mouse model demonstrates a multigenic origin of congenital hypothyroidism. *Endocrinology.* **146(12):** 5038-47.

Andersen, S., Pedersen. K. M., Bruun, N. H., Laurberg, P. (2006). Narrow individual variations in serum T(4) and T(3) in normal subjects: a clue to the understanding of subclinical thyroid disease. *J Clin Endocrinol Metab.* **87(3):** 1068-72.

Bakker, B., Bikker, H., Vulsma, T., de Randamie, J. S., Wiedijk, B. M., De Vijlder, J. J. (2000). Two decades of screening for congenital hypothyroidism in The Netherlands: TPO gene mutations in total iodide organification defects (an update). *J Clin Endocrinol Metab.* **85(10):** 3708-12.

Ball, S., Bella, J., Kielty, C., Shuttleworth, A. (2003). Stuctural basis of type VI collagen dimer formation. *J Biol Chem.* **278(17):** 15326-32.

Bamforth, J. S., Hughes, I. A., Lazarus, J. H., Weaver, C. M., Harper, P. S. (1989). Congenital hypothyroidism, spiky hair, and cleft palate. *J Med Genet.* **26(1):** 49-51.

Baris, I., Arisoy, A. E., Smith, A., Agostini, M., Mitchell, C. S., Park, S. M., Halefoglu, A. M., Zengin, E., Chatterjee, V. K., Battaloglu, E. (2006). A novel missense mutation in human TTF-2 (FKHL15) gene associated with congenital hypothyroidism but not athyreosis. *J Clin Endocrinol Metab.* **91(10):** 4183-7.

Barker, J. N., Palmer, C. N., Zhao, Y., Liao, H., Hull, P. R., Lee, S. P., Allen, M. H., Meggitt, S. J., Reynolds, N. J., Trembath, R. C., McLean, W. H. (2007). Null mutations in the filaggrin gene (FLG) determine major susceptibility to early-onset atopic dermatitis that persists into adulthood. *J Invest Dermatol.* **127(3):** 564-7.

Bedford, F. K., Ashworth, A., Enver, T., Wiedemann, L. M. (1993). HEX: a novel homeobox gene expressed during haematopoiesis and conserved between mouse and human. *Nucleic Acids Res.* **21(5):** 1245-9.

Bikker, H., den Hartog, M. T., Baas, F., Gons, M. H., Vulsma, T., de Vijlder, J. J. (1994). 20-basepair duplication in the human thyroid peroxidase gene results in a total iodide organification defect and congenital hypothyroidism. *J Clin Endocrinol Metab.* **79(1):** 248-52.

Bikker, H., Vulsma, T., Baas, F., de Vijlder, J. J. (1995). Identification of five novel inactivating mutations in the human thyroid peroxidase gene by denaturing gradient gel electrophoresis. *Hum Mutat.* **6(1):** 9-16.

Bikker, H., Waelkens, J. J., Bravenboer, B., de Vijlder, J. J. (1996). Congenital hypothyroidism caused by a premature termination signal in exon 10 of the human thyroid peroxidase gene. *J Clin Endocrinol Metab.* **81(6):** 2076-9.

Bikle, D. D., Ratnam, A., Mauro, T., Harris, J., Pillai, S. (1996). Changes in calcium responsiveness and handling during keratinocyte differentiation. Potential role of the calcium receptor. *J Clin Invest.* **97(4):** 1085-93.

Bogue, C. W., Ganea, G. R., Sturm, E., Ianucci, R., Jacobs, H. C. (2000). Hex expression suggests a role in the development and function of organs derived from foregut endoderm. *Dev Dyn.* **219(1):** 84-9.

Boukamp, P., Petrussevska, R. T., Breitkreutz, D., Hornung, J., Markham, A., Fusenig, N. E. (1988) Normal keratinization in a spontaneously immortalized aneuploid human keratinocyte cell line. *J Cell Biol.* **106(3):** 761-71.

Bowden, P. E. (1993). Keratins and Other Epidermal Proteins in Molecular Aspects of Dermatology. Editor G.C. Priestly. **Chapter 2**, 19-54. John Wiley & Sons Ltd.

Bowden, P. E., Hainey, S., Parker, G., Jones D., O., Zimonjic, D., Popescu, N. C., Hodgins, M. B. (1998). Characterization and Chromosomal Localisation of Human Hair-Specific Keratin Genes and Comparative Expression during the Hair Growth Cycle. *J Invest Dermatol.* **110:** 158-164.

Bowden, P. E., Quinlan, R., Breitkreutz, D., Fusenig, N. E. (1984). Proteolytic modification of acidic and basic keratins during terminal differentiation of mouse and human epidermis. *Europ J Biochem.* **142:** 29-36.

Bowden, P. E., Stark, H. J., Breitkreutz, D., Fusenig, N. E. (1987). Expression and modification of keratins during terminal differentiation of mammalian epidermis. Current Topics in Developmental Biology. *The Molecular and Developmental Biology of Keratins.* **Chapter 22:** 35-68. Academic Press, Orlando, Florida, USA.

Brancaccio, A., Minichiello, A., Grachtchouk, M., Antonini, D., Sheng, H., Parlato, R., Dathan, N., Dlugosz, A. A., Missero, C. (2004). Requirement of the forkhead gene Foxe1, a target of sonic hedgehog signaling, in hair follicle morphogenesis. *Hum Mol Genet.* **13(21):** 2595-606.

Braverman, L. E., Utiger, R. D. (2005). Werner & Ingbar's The Thyroid: A Fundamental and Clinical Text (9th edition). Lippincott, Williams & Wilkins.

Breitkreutz, D., Schoop, V. M., Mirancea, N., Baur, M., Stark, H. J., Fusenig, N. E. (1998). Epidermal differentiation and basement membrane formation by HaCaT cells in surface transplants. *Eur J Cell Biol.* **75(3):** 273-86.

Brewster, R., Mullor, J. L., Ruiz i Altaba, A. (2000). Gli2 functions in FGF signaling during antero-posterior patterning. *Development.* **127(20):** 4395-405.

Brown, L. Y., Brown, S. A. (2004). Alanine tracts: the expanding story of human illness and trinucleotide repeats. *Trends Genet.* **20(1):** 51-8.

Buntincx, I. M., Van Overmeire, B., Desager, K., Van Hauwaert, J. (1993). Syndromic association of cleft palate, bilateral choanal atresia, curly hair, and congenital hypothyroidism. *J Med Genet.* **30(5):** 427-8.

Burgeson, R. E. (1993). Type VII collagen, anchoring fibrils, and epidermolysis bullosa. *J Invest Dermatol.* **101(3):** 252-5.

Buzzio, O. L., Lu, Z., Miller, C. D., Unterman, T. G., Kim, J. J. (2006). FOXO1A differentially regulates genes of decidualization. *Endocrinology.* **147(8):** 3870-6.

Caburet, S., Demarez, A., Moumné, L., Fellous, M., De Baere, E., Veitia, R. A. (2004). A recurrent polyalanine expansion in the transcription factor FOXL2 induces extensive nuclear and cytoplasmic protein aggregation. *J Med Genet.* **41(12):** 932-6.

Caillou, B., Dupuy, C., Lacroix, L., Nocera, M., Talbot, M., Ohayon, R., Dème, D., Bidart, J. M., Schlumberger, M., Virion, A. (2001). Expression of reduced nicotinamide adenine dinucleotide phosphate oxidase (ThoX, LNOX, Duox) genes and proteins in human thyroid tissues. *J Clin Endocrinol Metab.* **86(7):** 3351-8.

Candi, E., Oddi, S., Terrinoni, A., Paradisi, A., Ranalli, M., Finazzi-Agró, A., Melino, G. (2001). Transglutaminase 5 cross-links loricrin, involucrin, and small proline-rich proteins in vitro. *J Biol Chem.* **14;276(37):** 35014-23.

Candi, E., Tarcsa, E., Idler, W. W., Kartasova, T., Marekov, L. N., Steinert, P. M. (1999). Transglutaminase cross-linking properties of the small proline-rich 1 family of cornified cell envelope proteins. Integration with loricrin. *J Biol Chem.* **12;274(11):** 7226-37.

Carroll, J. S., Liu, X. S., Brodsky, A. S., Li, W., Meyer, C. A., Szary, A. J., Eeckhoute, J., Shao, W., Hestermann, E. V., Geistlinger, T. R., Fox, E. A., Silver, P. A., Brown, M. (2005). Chromosome-wide mapping of estrogen receptor binding reveals long-range regulation requiring the forkhead protein FoxA1. *Cell.* **122(1):** 33-43.

Castanet, M., Lyonnet, S., Bonaïti-Pellié, C., Polak, M., Czernichow, P., Léger, J. (2000). Familial forms of thyroid dysgenesis among infants with congenital hypothyroidism. *N Engl J Med.* **343(6):** 441-2.

Castanet, M., Park, S. M., Smith, A., Bost, M., Léger, J., Lyonnet, S., Pelet, A., Czernichow, P., Chatterjee, K., Polak, M. (2002). A novel loss-of-function mutation in TTF-2 is associated with congenital hypothyroidism, thyroid agenesis and cleft palate. *Hum Mol Genet.* **11(17):** 2051-9.

Castanet, M., Polak, M., Bonaïti-Pellié, C., Lyonnet, S., Czernichow, P., Léger, J., On behalf of AFDPHE (Association Française pour le Dépistage et la Prévention des Handicaps de l'Enfant. (2001). Nineteen years of national screening for congenital hypothyroidism: familial cases with thyroid dysgenesis suggest the involvement of genetic factors. *J Clin Endocrinol Metab.* **86(5):** 2009-14.

Caubet, C., Jonca, N., Brattsand, M., Guerrin, M., Bernard, D., Schmidt, R., Egelrud, T., Simon, M., Serre, G. (2004). Degradation of corneodesmosome proteins by two serine proteases of the kallikrein family, SCTE/KLK5/hK5 and SCCE/KLK7/hK7. *J Invest Dermatol.* **122(5):** 1235-44.

Chen, J. M., Chuzhanova, N., Stenson, P. D., Férec, C., Cooper, D. N. (2005) Meta-analysis of gross insertions causing human genetic disease: novel mutational mechanisms and the role of replication slippage. *Hum Mutat.* **25(2):** 207-21.

Cirillo, L. A., Lin, F. R., Cuesta, I., Friedman, D., Jarnik, M., Zaret, K. S. (2002). Opening of compacted chromatin by early developmental transcription factors HNF3 (FoxA) and GATA-4. *Mol Cell.* **9(2):** 279-89.

Cirillo, L. A., McPherson, C. E., Bossard, P., Stevens, K., Cherian, S., Shim, E. Y., Clark, K. L., Burley, S. K., Zaret, K. S. (1998). Binding of the winged-helix transcription factor HNF3 to a linker histone site on the nucleosome. *EMBO J.* **17(1):** 244-54.

Civitareale, D., Lonigro, R., Sinclair, A. J., Di Lauro, R. (1989). A thyroid-specific nuclear protein essential for tissue-specific expression of the thyroglobulin promoter. *EMBO J.* **8(9):** 2537-42.

Clark, K. L., Halay, E. D., Lai, E., Burley, S. K. (1993). Co-crystal structure of the HNF-3/fork head DNA-recognition motif resembles histone H5. *Nature.* **364(6436):** 412-20.

Clifton-Bligh, R. J., Wentworth, J. M., Heinz, P., Crisp, M. S., John, R., Lazarus, J. H., Ludgate, M., Chatterjee, V. K. (1998). Mutation of the gene encoding human TTF-2 associated with thyroid agenesis, cleft palate and choanal atresia. *Nat Genet.* **19(4):** 399-401.

Clubb, B. H., Chou, Y. H., Herrmann, H., Svitkina, T. M., Borisy, G. G., Goldman, R. D. (2000). The 300-kDa intermediate filament-associated protein (IFAP300) is a hamster plectin ortholog. *Biochem Biophys Res Commun* **24;273(1):** 183-7.

Cocquet, J., De Baere, E., Gareil, M., Pannetier, M., Xia, X., Fellous, M., Veitia, R. A. (2003) Structure, evolution and expression of the FOXL2 transcription unit. *Cytogenet Genome Res.* **101(3-4):** 206-11.

Cocquet, J., Pailhoux, E., Jaubert, F., Servel, N., Xia, X., Pannetier, M., De Baere, E., Messiaen, L., Cotinot, C., Fellous, M., Veitia, R. A. (2002). Evolution and expression of FOXL2. *J Med Genet.* **39(12):** 916-21.

Congdon, T., Nguyen, L. Q., Nogueira, C. R., Habiby, R. L., Medeiros-Neto, G., Kopp P. (2001). A novel mutation (Q40P) in PAX8 associated with congenital hypothyroidism and thyroid hypoplasia: evidence for phenotypic variability in mother and child. *J Clin Endocrinol Metab.* **86(8):** 3962-7.

Conway, G. S. (1997). Clinical manifestations of genetic defects affecting gonadotrophins and their receptors. *Clin Endocrinol (Oxf).* **45(6):** 657-63.

Crompton, M. R., Bartlett, T. J., MacGregor, A. D., Manfioletti, G., Buratti, E., Giancotti, V., Goodwin, G. H. (1992). Identification of a novel vertebrate homeobox gene expressed in haematopoietic cells. *Nucleic Acids Res.* **20(21):** 5661-7.

Cullen, B. R. (2004). Derivation and function of small interfering RNAs and microRNAs. *Virus Res.* **102(1):** 3-9.

Daftary, G. S., Taylor, H. S. (2006). Endocrine regulation of HOX genes. *Endocr Rev.* **27(4):** 331-55.

D'Andrea, B., Di Palma, T., Mascia, A., Motti, M. L., Viglietto, G., Nitsch, L., Zannini, M. (2005). The transcriptional repressor DREAM is involved in thyroid gene expression. *Exp Cell Res.* **305(1):** 166-78.

Dathan, N., Parlato, R., Rosica, A., De Felice, M., Di Lauro, R. (2002). Distribution of the titf2/foxe1 gene product is consistent with an important role in the development of foregut endoderm, palate, and hair. *Dev Dyn.* **224(4):** 450-6.

De Felice, M., Damante, G., Zannini, M., Francis-Lang, H., Di Lauro, R. (1995). Redundant domains contribute to the transcriptional activity of the thyroid transcription factor 1. *J Biol Chem.* **270(44):** 26649-56.

De Felice, M., Di Lauro, R. (2004). Thyroid development and its disorders: genetics and molecular mechanisms. *Endocr Rev.* **25(5):** 722-46.

De Felice, M., Ovitt, C., Biffali, E., Rodriguez-Mallon, A., Arra, C., Anastassiadis, K., Macchia, P. E., Mattei, M. G., Mariano, A., Schöler, H., Macchia, V., Di Lauro, R. (1998). A mouse model for hereditary thyroid dysgenesis and cleft palate. *Nat Genet.* **19(4):** 395-8.

De Leo, R., Miccadei, S., Zammarchi, E., Civitareale, D. (2000). Role for p300 in Pax 8 induction of thyroperoxidase gene expression. *J Biol Chem.* **275(44):** 34100-5.

Di Palma, T., Nitsch, R., Mascia, A., Nitsch, L., Di Lauro, R., Zannini, M. (2003). The paired domain-containing factor Pax8 and the homeodomain-containing factor TTF-1 directly interact and synergistically activate transcription. *J Biol Chem.* **278(5):** 3395-402.

Dohán, O., Carrasco, N. (2003). Advances in Na(+)/I(-) symporter (NIS) research in the thyroid and beyond. *Mol Cell Endocrinol.* **213(1):** 59-70.

Eckert, R. L. (1989) Structure, Function and differentiation of the keratinocyte. *Physiol Rev.* **69(4):** 1316-46.

Eckert, R. L., Yaffe, M. B., Crish, J. F., Murthy, S., Rorke, E. A., Welter, J. F. (1993). Involucrin--structure and role in envelope assembly. *J Invest Dermatol.* **100(5):** 613-7.

Eichberger, T., Regl, G., Ikram, M. S., Neill, G. W., Philpott, M. P., Aberger, F., Frischauf, A. M. (2004). FOXE1, a new transcriptional target of GLI2 is expressed in human epidermis and basal cell carcinoma. *J Invest Dermatol.* **122(5):** 1180-7.

Eichberger, T., Sander, V., Schnidar, H., Regl, G., Kasper, M., Schmid, C., Plamberger, S., Kaser, A., Aberger, F., Frischauf, A. M. (2006). Overlapping and distinct transcriptional regulator properties of the GLI1 and GLI2 oncogenes. *Genomics.* **87(5):** 616-32.

Elbashir, S. M., Lendeckel, W., Tuschl, T. (2001). RNA interference is mediated by 21- and 22-nucleotide RNAs. *Genes Dev.* **15;15(2):** 188-200.

Francis-Lang, H., Price, M., Polycarpou-Schwarz, M., Di Lauro, R. (1992). Cell-type-specific expression of the rat thyroperoxidase promoter indicates common mechanisms for thyroid-specific gene expression. *Mol Cell Biol.* **12(2):** 576-88.

Fuchs, E. (1990) Epidermal differentiation: the bare essentials. *J Cell Biol.* 111 **(6):** 2807-14.

Fujiwara, H., Tatsumi, K., Miki, K., Harada, T., Okada, S., Nose, O., Kodama, S., Amino, N. (1998). Recurrent T354P mutation of the Na+/I- symporter in patients with iodide transport defect. *J Clin Endocrinol Metab.* **83(8):** 2940-3.

Gajiwala, K. S., Burley, S. K. (2000). Winged helix proteins. *Curr Opin Struct Biol.* **10(1):** 110-6.

Gersak, K., Harris, S. E., Smale, W. J., Shelling, A. N. (2004). A novel 30 bp deletion in the FOXL2 gene in a phenotypically normal woman with primary amenorrhoea: case report. *Hum Reprod.* **19(12):** 2767-70.

Goldman, R. D., Gruenbaum, Y., Moir, R. D., Shumaker, D. K., Spann, T. P. (2002). Nuclear Lamins: building blocks of nuclear architecture. *Genes & Development.* **16:** 533-547.

Goodman, F. R., Mundlos, S., Muragaki, Y., Donnai, D., Giovannucci-Uzielli, M. L., Lapi, E., Majewski, F., McGaughran, J., McKeown, C., Reardon, W., Upton, J., Winter, R. M., Olsen, B. R., Scambler, P. J. (1997). Synpolydactyly phenotypes correlate with size of expansions in HOXD13 polyalanine tract. *Proc Natl Acad Sci U S A.* **94(14):** 7458-63.

Graham, F. L., Smiley, J., Russell, W. C., Nairn, R. (1977). Characteristics of a human cell line transformed by DNA from human adenovirus type 5. *J Gen Virol.* **36(1):** 59-74.

Grapin-Botton, A., Melton, D. A. (2000). Endoderm development: from patterning to organogenesis. *Trends Genet.* **16(3):** 124-30.

Grinius, L., Kessler, C., Schroeder, J., Handwerger, S. (2006). Forkhead transcription factor FOXO1A is critical for induction of human decidualization. *J Endocrinol.* **189(1):** 179-87.

Gu, J., Stephenson, C. G., Iadarola, M. J. (1994). Recombinant proteins attached to a nickel-NTA column: use in affinity purification of antibodies. *Biotechniques.* **17(2):** 257, 260, 262.

Grüters, A., Krude, H., Biebermann, H. (2004). Molecular genetic defects in congenital hypothyroidism. *Eur J Endocrinol.* **151 Suppl 3:** U39-44.

Guazzi, S., Price, M., De Felice, M., Damante, G., Mattei, M. G., Di Lauro, R. (1990). Thyroid nuclear factor 1 (TTF-1) contains a homeodomain and displays a novel DNA binding specificity. *EMBO J.* **9(11):** 3631-9.

Han, K., Manley, J. L. (1993) Transcriptional repression by the Drosophila even-skipped protein: definition of a minimal repression domain. *Genes Dev.* **7(3):** 491-503.

Hansen, L. A., Alexander, N., Hogan, M. E., Sundberg, J. P., Dlugosz, A., Threadgill, D. W., Magnuson, T., Yuspa, S. H. (1997). Genetically null mice reveal a central role for epidermal growth factor receptor in the differentiation of the hair follicle and normal hair development. *Am J Pathol.* **150(6):** 1959-75.

Hansen, P. S., Brix, T. H., Bennedbaek, F. N., Bonnema, S. J., Kyvik, K. O., Hegedüs, L. (2004). Genetic and environmental causes of individual differences in thyroid size: a study of healthy Danish twins. *J Clin Endocrinol Metab.* **89(5):** 2071-7.

Harris, S. E., Chand, A. L., Winship, I. M., Gersak, K., Aittomäki, K., Shelling, A. N. (2002). Identification of novel mutations in FOXL2 associated with premature ovarian failure. *Mol Hum Reprod.* **8(8):** 729-33.

Heinemeyer, T., Wingender, E., Reuter, I., Hermjakob, H., Kel, A. E., Kel, O. V., Ignatieva, E. V., Ananko, E. A., Podkolodnaya, O. A., Kolpakov, F. A., Podkolodny, N. L., Kolchanov, N. A. (1998). Databases on transcriptional regulation: TRANSFAC, TRRD and COMPEL, *Nucleic Acids Res.* **26(1):** 362-7.

Hellqvist, M., Mahlapuu, M., Blixt, A., Enerbäck, S., Carlsson, P. (1998). The human forkhead protein FREAC-2 contains two functionally redundant activation domains and interacts with TBP and TFIIB. *J Biol Chem.* **273(36):** 23335-43.

Hertz, G. Z., Stormo, G. D. (1999). Identifying DNA and protein patterns with statistically significant alignments of multiple sequences. *Bioinformatics.* **15(7-8):** 563-77.

Hesse, M., Zimek, A., Weber, K., Magin, T. M. (2004) Comrehensive analysis of keratin gene clusters in humans and rodents. *Eur J Cell Biol.* **83:** 19-26.

Hishinuma, A., Ohyama, Y., Kuribayashi, T., Nagakubo, N., Namatame, T., Shibayama, K., Arisaka, O., Matsuura, N., Ieiri, T. (2001). Polymorphism of the polyalanine tract of thyroid transcription factor-2 gene in patients with thyroid dysgenesis. *Eur J Endocrinol.* **145(4):** 385-9.

Hishinuma, A., Takamatsu, J., Ohyama, Y., Yokozawa, T., Kanno, Y., Kuma, K., Yoshida, S., Matsuura, N., Ieiri, T. (1999). Two novel cysteine substitutions (C1263R and C1995S) of thyroglobulin cause a defect in intracellular transport of thyroglobulin in patients with congenital goiter and the variant type of adenomatous goiter. *J Clin Endocrinol Metab.* **84(4):** 1438-44.

Huebner, A., Thorwarth, A., Biebermann, H., Birke, I., Renault, N., Aust, D., Müller, D., Grueters, A., Kreuz, F., Schwarze, R., Krude, H. (2004). Congenital Hypothyroidism Due to Thyroid Agenesis and Cleft Palate Resulting from a Novel Homozygous Mutation in *FOXE1* (*TTF2*). Abstract.

Irvine, A. D., McLean, W. H., (1999) Human keratin disease: the increasing sprectrum of disease and a phenotype-genotype correlation. *Brit J. Dermatol.* **140:** 815-828.

Irvine, A. D., McLean, W. H. (2006). Breaking the (un)sound barrier: filaggrin is a major gene for atopic dermatitis. *J Invest Dermatol.* **126(6):** 1200-2.

Ishida-Yamamoto, A., McGrath, J. A., Lam, H., Iizuka, H., Friedman, R. A., Christiano, A. M. (1997). The molecular pathology of progressive symmetric erythrokeratoderma: a frameshift mutation in the loricrin gene and perturbations in the cornified cell envelope. *Am J Hum Genet.* **61(3):** 581-9.

Ishida-Yamamoto, A., Senshu, T., Eady, R. A., Takahashi, H., Shimizu, H., Akiyama, M., Iizuka, H. (2002). Sequential reorganization of cornified cell keratin filaments involving filaggrin-mediated compaction and keratin 1 deimination. *J Invest Dermatol.* **118(2):** 282-7.

Jäkel, S., Görlich, D. (1998). Importin beta, transportin, RanBP5 and RanBP7 mediate nuclear import of ribosomal proteins in mammalian cells. *EMBO J.* **17(15):** 4491-502.

Jin, C., Marsden, I., Chen, X., Liao, X. (1999). Dynamic DNA contacts observed in the NMR structure of winged helix protein-DNA complex. *J Mol Biol.* **289(4):** 683-90.

Jolly, E. R., Chin, C. S., Herskowitz, I., Li, H. (2005). Genome-wide identification of the regulatory targets of a transcription factor using biochemical characterization and computational genomic analysis. *BMC Bioinformatics* **18;6:** 275.

Jones, K. T., Sharpe, G. R. (1994). Thapsigargin raises intracellular free calcium levels in human keratinocytes and inhibits the coordinated expression of differentiation markers. *Exp Cell Res.* **210(1):** 71-6.

Kaestner, K. H., Knochel, W., Martinez, D. E. (2000). Unified nomenclature for the winged helix/forkhead transcription factors. *Genes Dev.* **14(2):** 142-6.

Karlin, S., Brocchieri, L., Bergman, A., Mrazek, J., Gentles, A. J. (2002). Amino acid runs in eukaryotic proteomes and disease associations. *Proc Natl Acad Sci U S A.* **99(1):** 333-8.

Kasper, M., Schnidar, H., Neill, G. W., Hanneder, M., Klingler, S., Blaas, L., Schmid, C., Hauser-Kronberger, C., Regl, G., Philpott, M. P., Aberger, F. (2006). Selective modulation of Hedgehog/GLI target gene expression by epidermal growth factor signaling in human keratinocytes. *Mol Cell Biol.* **26(16):** 6283-98.

Katoh, M., Katoh, M. (2004). Human FOX gene family (Review). *Int J Oncol.* **25(5):** 1495-500.

Kim, S. S., Chen, Y. M., O'Leary, E., Witzgall, R., Vidal, M., Bonventre, J. V. A novel member of the RING finger family, KRIP-1, associates with the KRAB-A transcriptional repressor domain of zinc finger proteins. *Proc Natl Acad Sci U S A.* **93(26):** 15299-304.

Kimura, S., Hara, Y., Pineau, T., Fernandez-Salguero, P., Fox, C. H., Ward, J. M., Gonzalez, F. J. (1996). The T/ebp null mouse: thyroid-specific enhancer-binding protein is essential for the organogenesis of the thyroid, lung, ventral forebrain, and pituitary. *Genes Dev.* **10(1):** 60-9.

Kotani, T., Umeki, K., Yamamoto, I., Maesaka, H., Tachibana, K., Ohtaki, S. (1999). A novel mutation in the human thyroid peroxidase gene resulting in a total iodide organification defect. *J Endocrinol.* **160(2):** 267-73.

Kotani, T., Umeki, K., Yamamoto, I., Ohtaki, S., Adachi, M., Tachibana, K. (2001). Iodide organification defects resulting from cosegregation of mutated and null thyroid peroxidase alleles. *Mol Cell Endocrinol.* **182(1):** 61-8.

Kuechle, M. K., Thulin, C. D., Presland, R. B., Dale, B. A. (1999). Profilaggrin requires both linker and filaggrin peptide sequences to form granules: implications for profilaggrin processing in vivo. *J Invest Dermatol.* **112(6):** 843-52.

Lai, E., Prezioso, V. R., Smith, E., Litvin, O., Costa, R. H., Darnell, J. E., (1990). HNF-3A, a hepatocyte-enriched transcription factor of novel structure is regulated transcriptionally. *Genes Dev.* **4(8):** 1427-36.

Lai, E., Prezioso, V. R., Tao, W. F., Chen, W. S., Darnell, J. E. (1991). Hepatocyte nuclear factor 3 alpha belongs to a gene family in mammals that is homologous to the *Drosophila* homeotic gene fork head. *Genes Dev.* **5(3):** 416-27.

Lam, E. W., Francis, R. E., Petkovic, M. FOXO transcription factors: key regulators of cell fate. *Biochem Soc Trans.* **34(5):** 722-6.

Lang, D., Powell, S. K., Plummer, R. S. Young, K. P., Ruggeri, B. A. (2006). PAX genes: Roles in development, pathophysiology, and cancer. *Biochem Pharmacol.* **73(1):** 1-14.

Lania, A., Mantovani, G., Spada, A. (2001). G protein mutations in endocrine diseases. *Eur J Endocrinol.* **145(5):** 543-59.

Langbein, L., Rogers, M. A., Praetzel-Wunder S., Boeckler, D., Schirmacher, P., Schweizer, J. (2007). Novel type I hair keratins K39 and K40 are the last to be expressed in differentiation of the hair: Completion of the human hair keratin catalog. *J Invest Dermatol.* **127:** 1532-5.

Laoukili, J., Stahl, M., Medema, R. H. (2007). FoxM1: at the crossroads of ageing and cancer. *Biochim Biophys Acta.* **1775(1):** 92-102.

Lavoie, H., Debeane, F., Trinh, Q. D., Turcotte, J. F., Corbeil-Girard, L. P., Dicaire, M. J., Saint-Denis, A., Pagé, M., Rouleau, G. A., Brais, B. (2003). Polymorphism, shared functions and convergent evolution of genes with sequences coding for polyalanine domains. *Hum Mol Genet.* **12(22):** 2967-79.

Lawrence, C. E., Altschul, S. F., Boguski, M. S., Liu, J. S., Neuwald, A. F., Wootton, J. C. (1993). Detecting subtle sequence signals: a Gibbs sampling strategy for multiple alignment. *Science.* **8;262(5131):** 208-14.

Lee, Y., Ahn, C., Han, J., Choi, H., Kim, J., Yim, J., Lee, J., Provost, P., Rådmark, O., Kim, S., Kim, V. N. (2003) The nuclear RNase III Drosha initiates microRNA processing. *Nature.* **425(6956):** 415-9.

Leuschner, P. J., Ameres, S. L., Kueng, S., Martinez, J. (2006). Cleavage of the siRNA passenger strand during RISC assembly in human cells. *EMBO Rep.* **7(3):** 314-20.

Licht, J. D, Grossel, M. J., Figge, J., Hansen, U. M. (1990). Drosophila Krüppel protein is a transcriptional repressor. *Nature.* **346(6279):** 76-9.

Locantore, P., Evans, C., Zhang, L., Warner, J., Gregory, J. W., John, R., Lazarus, J. H., Ludgate, M. (2007). W546X mutation of the thyrotropin receptor causes subclinical hypothyroidism in various clinical settings. *Clin Endocrinol (Oxf).*

López, O., Cócera, M., Wertz, P. W., López-Iglesias, C., de la Maza, A. (2007). New arrangement of proteins and lipids in the stratum corneum cornified envelope. *Biochim Biophys Acta* **1768(3):** 521-9.

Maas-Szabowski, N., Stärker, A., Fusenig, N. E. (2003). Epidermal tissue regeneration and stromal interaction in HaCaT cells is initiated by TGF-alpha. *J Cell Sci.* **116(14):** 2937-48.

Macchia, P. E., Lapi, P., Krude, H., Pirro, M. T., Missero, C., Chiovato, L., Souabni, A., Baserga, M., Tassi, V., Pinchera, A., Fenzi, G., Grüters, A., Busslinger, M., Di Lauro, R. (1998). PAX8 mutations associated with congenital hypothyroidism caused by thyroid dysgenesis. *Nat Genet.* **19(1):** 83-6.

Macchia, P. E., Mattei, M. G., Lapi, P., Fenzi, G., Di Lauro, R. (1999). Cloning, chromosomal localization and identification of polymorphisms in the human thyroid transcription factor 2 gene (TITF2). *Biochimie.* **81(5):** 433-40.

Mansouri, A., Chowdhury, K., Gruss, P. (1998). Follicular cells of the thyroid gland require Pax8 gene function. *Nat Genet.* **19(1):** 87-90.

Martinez Barbera, J. P., Clements, M., Thomas, P., Rodriguez, T., Meloy, D., Kioussis, D., Beddington, R. S. (2000). The homeobox gene Hex is required in definitive endodermal tissues for normal forebrain, liver and thyroid formation. *Development.* **127(11):** 2433-45.

Maxwell, I. H., Harrison, G. S., Wood, W. M., Maxwell, F. (1989). A DNA cassette containing a trimerized SV40 polyadenylation signal which efficiently blocks spurious plasmid-initiated transcription. *Biotechniques.* **7(3):** 276-80.

Medeiros-Neto, G., Gil-Da-Costa, M. J., Santos, C. L., Medina, A. M., Silva, J. C., Tsou, R. M., Sobrinho-Simões, M. (1998). Metastatic thyroid carcinoma arising from congenital goiter due to mutation in the thyroperoxidase gene. *J Clin Endocrinol Metab.* **83(11):** 4162-6.

Meeus, L., Gilbert, B., Rydlewski, C., Parma, J., Roussie, A. L., Abramowicz, M., Vilain, C., Christophe, D., Costagliola, S., Vassart, G. (2004). Characterization of a novel loss of function mutation of PAX8 in a familial case of congenital hypothyroidism with in-place, normal-sized thyroid. *J Clin Endocrinol Metab.* **89(9):** 4285-91.

Miccadei, S., De Leo, R., Zammarchi, E., Natali, P. G., Civitareale, D. (2002). The synergistic activity of thyroid transcription factor 1 and Pax 8 relies on the promoter/enhancer interplay. *Mol Endocrinol.* **16(4):** 837-46.

Miccadei, S., Provenzano, C., Mojzisek, M., Natali, P. G., Civitareale, D. (2005). Retinoblastoma protein acts as Pax 8 transcriptional coactivator. *Oncogene.* **24(47):** 6993-7001.

Miettinen, P. J., Berger, J. E., Meneses, J., Phung, Y., Pedersen, R. A., Werb, Z., Derynck, R. (1995). Epithelial immaturity and multiorgan failure in mice lacking epidermal growth factor receptor. *Nature.* **376(6538):** 337-41.

Mill, P., Mo, R., Fu, H., Grachtchouk, M., Kim, P. C., Dlugosz, A. A., Hui, C. C. (2003). Sonic hedgehog-dependent activation of Gli2 is essential for embryonic hair follicle development. *Genes Dev.* **17(2):** 282-94.

Milligan, J. F., Groebe, D. R., Witherell, G. W., Uhlenbeck, O. C. (1987). Oligoribonucleotide synthesis using T7 RNA polymerase and synthetic DNA templates. *Nucleic Acids Res.* **15(21):** 8783-98.

Minoo, P., Hu, L., Xing, Y., Zhu, N. L., Chen, H., Li, M., Borok, Z., Li, C. (2006). Physical and functional interactions between homeodomain NKX2.1 and winged helix/forkhead FOXA1 in lung epithelial cells. *Mol Cell Biol.* **27(6):** 2155-65.

Missero, C., Di Cunto, F., Kiyokawa, H., Koff, A., Dotto, G. P. (1996). The absence of p21Cip1/WAF1 alters keratinocyte growth and differentiation and promotes ras-tumor progression. *Genes Dev.* **1;10(23):** 3065-75.

Moll, R., Franke, W. W., Schiller, D. L., Geiger, B., Krepler, R. (1982) The catalog of human cytokeratins: Patterns of expression in normal epithelia, tumors and cultured cells. *Cell.* **31:** 11-24.

Moreno, J. C., Bikker, H., Kempers, M. J., van Trotsenburg, A. S., Baas, F., de Vijlder, J. J., Vulsma, T., Ris-Stalpers, C. (2002). Inactivating mutations in the gene for thyroid oxidase 2 (THOX2) and congenital hypothyroidism. *N Engl J Med.* **347(2):** 95-102.

Moumné, L., Fellous, M., Veitia, R. A. (2005). Deletions in the polyAlanine-containing transcription factor FOXL2 lead to intranuclear aggregation. *Hum Mol Genet.* **14(23):** 3557-64.

Mularoni, L., Guigó, R., Albà, M. M. (2006). Mutation patterns of amino acid tandem repeats in the human proteome. *Genome Biol.* **7(4):** R33.

Nag, D. K. (2003). Trinucleotide repeat expansions: timing is everything. *Trends Mol Med.* **9(11):** 455-7.

Nallathambi, J., Moumné, L., De Baere, E., Beysen, D., Usha, K., Sundaresan, P., Veitia, R. A. (2007). A novel polyalanine expansion in FOXL2: the first evidence for a recessive form of the blepharophimosis syndrome (BPES) associated with ovarian dysfunction. *Hum Genet.* **121(1):** 107-12.

O'Guin, W. M., Manabe, M., Sun, T. T. (1989). Association of a basic 25K protein with membrane coating granules of human epidermis. *J Cell Biol.* **109(5):** 2313-21.

Ortiz, L., Aza-Blanc, P., Zannini, M., Cato, A. C., Santisteban, P. (1999). The interaction between the forkhead thyroid transcription factor TTF-2 and the constitutive factor CTF/NF-1 is required for efficient hormonal regulation of the thyroperoxidase gene transcription. *J Biol Chem.* **274(21):** 15213-21.

Ortiz, L., Zannini, M., Di Lauro, R., Santisteban, P. (1997). Transcriptional control of the forkhead thyroid transcription factor TTF-2 by thyrotropin, insulin, and insulin-like growth factor I. *J Biol Chem.* **272(37):** 23334-9.

Overdier, D. G., Porcella, A., Costa, R. H. (1994). The DNA-binding specificity of the hepatocyte nuclear factor 3/forkhead domain is influenced by amino-acid residues adjacent to the recognition helix. *Mol Cell Biol.* **14(4):** 2755-66.

Owen, P. J., Lazarus, J. H. (2003). Subclinical hypothyroidism: the case for treatment. *Trends Endocrinol Metab.* **14(6):** 257-61.

Pannain, S., Weiss, R. E., Jackson, C. E., Dian, D., Beck, J. C., Sheffield, V. C., Cox, N., Refetoff, S. (1999). Two different mutations in the thyroid peroxidase gene of a large inbred Amish kindred: power and limits of homozygosity mapping. *J Clin Endocrinol Metab.* **84(3):** 1061-71.

Paramio, J. M., Segrelles, C., Ruiz, S., Martin-Caballero, J., Page, A., Martinez, J., Serrano, M., Jorcano, J. L. (2001). The ink4a/arf tumor suppressors cooperate with p21cip1/waf in the processes of mouse epidermal differentiation, senescence, and carcinogenesis. *J Biol Chem.* **23;276(47):** 44203-11.

Park, S. M., Chatterjee, V. K. (2005). Genetics of congenital hypothyroidism. *J Med Genet.* **42(5):** 379-89.

Parlato, R., Rosica, A., Rodriguez-Mallon, A., Affuso, A., Postiglione, M. P., Arra, C., Mansouri, A., Kimura, S., Di Lauro, R., De Felice, M. (2000). An integrated regulatory network controlling survival and migration in thyroid organogenesis. *Dev Biol.* **276(2):** 464-75.

Paschke, R., Ludgate, M. (1997). The thyrotropin receptor in thyroid diseases. *N Engl J Med.* **337(23):** 1675-81.

Pedersen, J. T., Moult, J. (1996). Genetic algorithms for protein structure prediction. *Curr Opin Struct Biol.* **6(2):** 227-31.

Peeters, R. P., van der Deure, W. M., Visser, T. J. (2006). Genetic variation in thyroid hormone pathway genes; polymorphisms in the TSH receptor and the iodothyronine deiodinases. *Eur J Endocrinol.* **155(5):** 655-62.

Perrone, L., Pasca di Magliano, M., Zannini, M., Di Lauro, R. (2000). The thyroid transcription factor 2 (TTF-2) is a promoter-specific DNA-binding independent transcriptional repressor. *Biochem Biophys Res Commun.* **275(1):** 203-8.

Peus, D., Pittelkow, M. R. (1996). Growth factors in hair organ development and the hair growth cycle. *Dermatol Clin.* **14(4):** 559-72.

Philpott, M. P., Green, M. R., Kealey., T. (1990) Human hair growth in vitro. *J Cell Sci.* **97(3):** 463-71.

Pierrou, S., Hellqvist, M., Samuelsson, L., Enerbäck, S., Carlsson, P. (1994). Cloning and characterization of seven human forkhead proteins: binding site specificity and DNA bending. *EMBO J.* **13(20):** 5002-12.

Plachov, D., Chowdhury, K., Walther, C., Simon, D., Guenet, J. L., Gruss, P. (1990). Pax8, a murine paired box gene expressed in the developing excretory system and thyroid gland. *Development.* **110(2):** 643-51.

Pohlenz, J., Duprez, L., Weiss, R. E., Vassart, G., Refetoff, S., Costagliola, S. (2000). Failure of membrane targeting causes the functional defect of two mutant sodium iodide symporters. *J Clin Endocrinol Metab.* **85(7):** 2366-9.

Popescu, N., Bowden, P. E., DiPaolo, J. A. (1989). Two type II keratin genes are localised on human chromosome 12. *Human Genetics.* 82: 109-112.

Porter, R. M., Corden, L. D., Lunny, D. P., Smith, F. J, Lane, E. B., McLean W. H. (2001). Keratin K6irs is specific to the inner root sheath of hair follicles in mice and humans. *Br J Dermatol.* **145 (4):** 558-68.

Rand, T. A., Petersen, S., Du, F., Wang, X. (2005). Argonaute2 cleaves the anti-guide strand of siRNA during RISC activation. *Cell.* **18;123(4):** 621-9.

Randall, V. A., Sundberg, J. P., Philpott, M. P. (2003). Animal and in vitro models for the study of hair follicles. *J Investig Dermatol Symp Proc.* **8(1):** 39-45.

Rapoport, B. (1991). Pathophysiology of Hashimoto's thyroiditis and hypothyroidism. *Annu Rev Med.* **42:** 91-6.

Reardon, W., Trembath, R. C. (1996). Pendred syndrome. *J Med Genet.* **33:**1037–40.

Ren, Y., Gong, W., Xu, Q., Zheng, X., Lin, D., Wang, Y., Li, T. (2006). siRecords: an extensive database of mammalian siRNAs with efficacy ratings. *Bioinformatics* **15;22(8):** 1027-8.

Reynolds, A., Anderson, E. M., Vermeulen, A., Fedorov, Y., Robinson, K., Leake, D., Karpilow, J., Marshall, W. S., Khvorova, A. (2006) Induction of the interferon response by siRNA is cell type- and duplex length-dependent. *RNA.* **12(6):** 988-93.

Robinson, D. O., Hammans, S. R., Read, S. P., Sillibourne, J. (2005). Oculopharyngeal muscular dystrophy (OPMD): analysis of the PABPN1 gene expansion sequence in 86 patients reveals 13 different expansion types and further evidence for unequal recombination as the mutational mechanism. *Hum Genet.* **116(4):** 267-71.

Rogers, M. A., Elder, H., Winter, H., Langbein, L., Beckman, I., Schweizer, J. (2005) Characterisation of new members of the human type II hair keratin gene family and a general evaluation of the keratin gene domain on chromosome 12q13.13. *J Invest Dermatol.* **124:** 536-544.

Rogers, M. A., Winter, H., Langbein, L., Bleiler, R., Schweizer, J. (2004) The human type I keratin gene family: characterization of new hair follicle specific members and evaluation of the chromosome 17q21.2 gene domain. *Differentiation.* **72 (9-10):** 527-40.

Rogers, M. A., Winter, H., Langbein, L., Schweizer, J. (2000). Characterisation of a 300 kbp region of human DNA containing the type II hair keratin gene locus. *J Invest Dermatol.* **114:** 464-472.

Romanelli, M. G., Tato', L., Lorenzi, P., Morandi, C. (2003). Nuclear localization domains in human thyroid transcription factor 2. *Biochim Biophys Acta.* **1643(1-3):** 55-64.

Roulet, E., Fisch, I., Junier, T., Bucher, P., Mermod, N. (1998). Evaluation of computer tools for the prediction of transcription factor binding sites on genomic DNA. *In Silico Biol.* **1(1):** 21-8.

Royaux, I. E., Suzuki, K., Mori, A., Katoh, R., Everett, L. A., Kohn, L. D., Green, E. D. (2000). Pendrin, the protein encoded by the Pendred syndrome gene (PDS), is an apical porter of iodide in the thyroid and is regulated by thyroglobulin in FRTL-5 cells. *Endocrinology.* **141(2):** 839-45.

Russo, D., Betterle, C., Arturi, F., Chiefari, E., Girelli, M. E., Filetti, S. (2000). A novel mutation in the thyrotropin (TSH) receptor gene causing loss of TSH binding but constitutive receptor activation in a family with resistance to TSH. *J Clin Endocrinol Metab.* **85(11):** 4238-42.

Samollow, P. B., Perez, G., Kammerer, C. M., Finegold, D., Zwartjes, P. W., Havill, L. M., Comuzzie, A. G., Mahaney, M. C., Göring, H. H., Blangero, J., Foley, T. P., Barmada, M. M. (2004). Genetic and environmental influences on thyroid hormone variation in Mexican Americans. *J Clin Endocrinol Metab.* **89(7):** 3276-84.

Sanger, F., Nicklen, S., Coulson, A. R. (1977). DNA sequencing with chain-terminating inhibitors. *Proc Natl Acad Sci USA.* **74(12):** 5463-7.

Santarpia, L., Valenzise, M., Di Pasquale, G., Arrigo, T., San Martino, G., Cicciò, M. P., Trimarchi, F., De Luca, F., Benvenga, S. (2007). TTF-2/FOXE1 gene polymorphisms in Sicilian patients with permanent primary congenital hypothyroidism. *J Endocrinol Invest.* **30(1):** 13-9.

Santos, C. L., Bikker, H., Rego, K. G., Nascimento, A. C., Tambascia, M., De Vijlder, J. J, Medeiros-Neto, G. (1999). A novel mutation in the TPO gene in goitrous hypothyroid patients with iodide organification defect. *Clin Endocrinol (Oxf).* **51(2):** 165-72.

Sato, K., Di Lauro, R. (1996). Hepatocyte nuclear factor 3beta participates in the transcriptional regulation of the thyroperoxidase promoter. *Biochem Biophys Res Commun.* **220(1):** 86-93.

Schweizer, J., Bowden, P. E., Coulombe, P. A., Langbein, L., Lane, E. B., Magin, T. M., Maltais, L., Omary, M. B., Parry, D. A. D., Rogers, M. A., Wright M. W. (2006) New consensus nomenclature for mammalian keratins: *J Cell Biol.* **174:** 169-174.

Schoop, V. M., Mirancea, N., Fusenig, N. E. (1999) Epidermal organization and differentiation of HaCaT keratinocytes in organotypic coculture with human dermal fibroblasts. *J Invest Dermatol.* **112(3):** 343-53.

Scott, K. L., Plon, S. E. (2005). CHES1/FOXN3 interacts with Ski-interacting protein and acts as a transcriptional repressor. *Gene.* **359:** 119-26.

Semizarov, D., Frost, L., Sarthy, A., Kroeger, P., Halbert, D. N., Fesik, S. W. (2003). Specificity of short interfering RNA determined through gene expression signatures. *Proc Natl Acad Sci U S A.* **100(11):** 6347-52.

Sequeira, M., Al-Khafaji, F., Park, S., Lewis, M. D., Wheeler, M. H., Chatterjee, V. K., Jasani, B., Ludgate, M. (2003). Production and application of polyclonal antibody to human thyroid transcription factor 2 reveals thyroid transcription factor 2 protein expression in adult thyroid and hair follicles and prepubertal testis. *Thyroid.* **13(10):** 927-32.

Sequeira, M. J., Morgan, J. M., Fuhrer, D., Wheeler, M. H., Jasani, B., Ludgate, M. (2001). Thyroid transcription factor-2 gene expression in benign and malignant thyroid lesions. *Thyroid.* **11(11):** 995-1001.

Shaw, G., Morse, S., Ararat, M., Graham, F. L. (2002). Preferential transformation of human neuronal cells by human adenoviruses and the origin of HEK 293 cells. *FASEB J.* **16(8):** 869-71.

Shim, E. Y., Woodcock, C., Zaret, K. S. (1998). Nucleosome positioning by the winged helix transcription factor HNF3. *Genes Dev.* **12(1):** 5-10.

Sibilia, M., Wagner, E. F. (1995). Strain-dependent epithelial defects in mice lacking the EGF receptor. *Science.* **269(5221):** 234-8.

Sinclair, A. J., Lonigro, R., Civitareale, D., Ghibelli, L., Di Lauro, R. (1990). The tissue-specific expression of the thyroglobulin gene requires interaction between thyroid-specific and ubiquitous factors. *Eur J Biochem.* **193(2):** 311-8.

Sledz, C. A., Holko, M., de Veer, M. J., Silverman, R. H., Williams, B. R. (2003). Activation of the interferon system by short-interfering RNAs. *Nat Cell Biol.* **5(9):** 834-9.

Slominski, A., Wortsman, J., Kohn, L., Ain, K. B., Venkataraman, G. M., Pisarchik, A., Chung, J. H., Giuliani, C., Thornton, M., Slugocki, G., Tobin, D. J. (2002). Expression of hypothalamic-pituitary-thyroid axis related genes in the human skin. *J Invest Dermatol.* **119(6):** 1449-55.

Smith, F. J., Irvine, A. D., Terron-Kwiatkowski, A., Sandilands, A., Campbell, L. E., Zhao, Y., Liao, H., Evans, A. T., Goudie, D. R., Lewis-Jones, S., Arseculeratne, G., Munro, C. S., Sergeant, A., O'Regan, G., Bale, S. J., Compton, J. G., DiGiovanna, J. J., Presland, R. B., Fleckman, P., McLean, W. H. (2006). Loss-of-function mutations in the gene encoding filaggrin cause ichthyosis vulgaris. *Nat Genet.* **38(3):** 337-42.

Sontheimer, E. J. (2005). Assembly and function of RNA silencing complexes. *Nat Rev Mol Cell Biol.* **6(2):** 127-38.

Stark, H. J., Breitkreutz, D., Limat, A., Bowden, P. E., Ryle, C., Fusenig, N. E. (1987) Keratins of the human hair follicle. "Hyperproliferative" keratins consistently expressed in outer root sheath cells in vivo and in vitro. *Differentiation.* **35:** 236-248.

Steinböck, F. A., Wiche, G. (1999). Plectin: a cytolinker by design. *Biol Chem.* **380(2):** 151-8.

Steinert, P. M., Parry, D. A. D. (1993) The conserved H1 domain of the type II keratin 1 chain plays an essential role in the alignment of nearest neighbour molecules in mouse and human keratin 1/keratin 10 intermediate filaments as the two- to four-molecule level of structure. *J Biol Chem.* **268 (4):** 2878-2887.

Stratagene (2005). Method and Application Guide Introduction to Quantitative PCR.

Stroud, J. C., Wu, Y., Bates, D. L., Han, A., Nowick, K., Paabo, S., Tong, H., Chen, L. (2006). Structure of the forkhead domain of FOXP2 bound to DNA. *Structure.* **14(1):** 159-66.

Sunthornthepvarakui, T., Gottschalk, M. E., Hayashi, Y., Refetoff, S. (1995). Brief report: resistance to thyrotropin caused by mutations in the thyrotropin-receptor gene. *N Engl J Med.* **332(3):** 155-60.

Surks, M. I., Ortiz, E., Daniels, G. H., Sawin, C. T., Col, N. F., Cobin, R. H., Franklyn, J. A., Hershman, J. M., Burman, K. D., Denke, M. A., Gorman, C., Cooper, R. S., Weissman, N. J. (2004). Subclinical thyroid disease: scientific review and guidelines for diagnosis and management. *JAMA.* **291(2):** 228-38.

Thomas, P. Q., Brown, A., Beddington, R. S. (1998). Hex: a homeobox gene revealing peri-implantation asymmetry in the mouse embryo and an early transient marker of endothelial cell precursors. *Development.* **125(1):** 85-94.

Tomari, Y., Zamore, P. D. (2005). Perspective: machines for RNAi. *Genes Dev.* **1;19(5):** 517-29.

Tompa, M., Li, N., Bailey, T. L., Church, G. M., De Moor, B., Eskin, E., Favorov, A. V., Frith, M. C., Fu, Y., Kent, W. J., Makeev, V. J., Mironov, A. A., Noble, W. S., Pavesi, G., Pesole, G., Régnier, M., Simonis, N., Sinha, S., Thijs, G., van Helden, J., Vandenbogaert, M., Weng, Z., Workman, C., Ye, C., Zhu, Z. (2005). Assessing computational tools for the discovery of transcription factor binding sites *Nat Biotechnol.* **23(1):** 137-44.

Tonacchera, M., Agretti, P., De Marco, G., Perri, A., Pinchera, A., Vitti, P., Chiovato, L. (2001). Thyroid resistance to TSH complicated by autoimmune thyroiditis. *J Clin Endocrinol Metab.* **86(9):** 4543-6.

Tonacchera, M., Banco, M., Lapi, P., Di Cosmo, C., Perri, A., Montanelli, L., Moschini, L., Gatti, G., Gandini, D., Massei, A., Agretti, P., De Marco, G., Vitti, P., Chiovato, L., Pinchera, A. (2004). Genetic analysis of TTF-2 gene in children with congenital hypothyroidism and cleft palate, congenital hypothyroidism, or isolated cleft palate. *Thyroid.* **14(8):** 584-8.

Toublanc, J. E. (1992). Comparison of epidemiological data on congenital hypothyroidism in Europe with those of other parts in the world. *Horm Res.* **38(5-6):** 230-5.

Truss, M., Swat, M., Kielbasa, S. M., Schäfer, R., Herzel, H., Hagemeier, C. (2005), HuSiDa--the human siRNA database: an open-access database for published functional siRNA sequences and technical details of efficient transfer into recipient cells. *Nucleic Acids Res.* **1:** 33

Tsai, K. L., Huang, C. Y., Chang, C. H., Sun, Y. J., Chuang, W. J., Hsiao, C. D. (2001). Crystal structure of the human FOXK1a-DNA complex and its implications on the diverse binding specificity of winged helix/forkhead proteins. *J Biol Chem.* **281(25):** 17400-9.

Uitto, J., Chung-Honet, L. C., Christiano, A. M. (1992). Molecular biology and pathology of type VII collagen. *Exp Dermatol.* **1(1):** 2-11.

Van den Bergh, F., Giudice, G. J. (2003). BP180 (type XVII collagen) and its role in cutaneous biology and disease. *Adv Dermatol.* **19:** 37-71.

Van Dongen, M. J., Cederberg, A., Carlsson, P., Enerbäck, S., Wikström, M. (2000). Solution structure and dynamics of the DNA-binding domain of the adipocyte-transcription factor FREAC-11. *J Mol Biol.* **296(2):** 351-9.

Van Helden, J. (2003). Regulatory sequence analysis tools. *Nucleic Acids Res* **1;31(13):** 3593-6.

Varela, V., Rivolta, C. M., Esperante, S. A., Gruñeiro-Papendieck, L., Chiesa, A., Targovnik, H. M. (2006). Three mutations (p.Q36H, p.G418fsX482, and g.IVS19-2A>C) in the dual oxidase 2 gene responsible for congenital goiter and iodide organification defect. *Clin Chem.* **52(2):** 182-91.

Vigone, M. C., Fugazzola, L., Zamproni, I., Passoni, A., Di Candia, S., Chiumello, G., Persani, L., Weber, G. (2005). Persistent mild hypothyroidism associated with novel sequence variants of the DUOX2 gene in two siblings. *Hum Mutat.* **26(4):** 395.

Vilain, C., Rydlewski, C., Duprez, L., Heinrichs, C., Abramowicz, M., Malvaux, P., Renneboog, B., Parma, J., Costagliola, S., Vassart, G. (2001). Autosomal dominant transmission of congenital thyroid hypoplasia due to loss-of-function mutation of PAX8. *J Clin Endocrinol Metab.* **86(1):** 234-8.

Watkins, W. J., Harris, S. E., Craven, M. J., Vincent, A. L., Winship, I. M., Gersak, K., Shelling, A. N. (2006). An investigation into FOXE1 polyalanine tract length in premature ovarian failure. *Mol Hum Reprod.* **12(3):** 145-9.

Watt, F. M. (1983). Involucrin and other markers of keratinocyte terminal differentiation. *J Invest Dermatol.* **81(1 Suppl):** 100s-3s.

Watt, F. M. (1989). Terminal differentiation of epidermal keratinocytes. *Curr Opin Cell Biol.* **1 (6):** 1107-15.

Watson, R. E., Ball, S. G., Craven, N. M., Boorsma, J., East, C. L., Shuttleworth, C. A., Kielty, C. M., Griffiths, C. E. (2001). Distribution and expression of type VI collagen in photoaged skin. *Br J Dermatol.* **144(4):** 751-9.

Weigel, D., Jäckle, H. (1990). The *fork head* domain: A novel DNA binding motif of eukaryotic transcription factors? *Cell.* **63(3):** 455-56.

Weigel, D., Jürgens, G., Küttner, F., Seifert, E., Jäckle, H. (1989). The homeotic gene *fork head* encodes a nuclear protein and is expressed in the terminal regions of the Drosophila embryo. *Cell.* **57(4):** 645-58.

Weigelt, J., Climent, I., Dahlman-Wright, K., Wikström, M. (2001). Solution structure of the DNA binding domain of the human forkhead transcription factor AFX (FOXO4). *Biochemistry.* **40(20):** 5861-9.

Wiche, G. (1998). Role of plectin in cytoskeleton organization and dynamics. *J Cell Sci.* **111:** 2477-86.

Wijchers, P. J., Burbach, J. P., Smidt, M. P. (2006). In control of biology: of mice, men and Foxes. *Biochem J.* **397(2):** 233-46.

Winter, H., Langbein, L., Praetzel, S., Jacobs, M., Rogers, M. A., Leigh, I. M., Tidman, N., Schweizer, J. (1998). A Novel Human Type II Cytokeratin, K6hf, Specifically Expressed In The Companion Layer Of The Hair Follicle. *J Invest Derm* **111(6):** 955-62.

Yang, Q., Kong, Y., Rothermel, B., Garry, D. J., Bassel-Duby, R., Williams, R., S. (2000). The winged-helix/forkhead protein myocyte nuclear factor beta (MNF-beta) forms a co-repressor complex with mammalian sin3B. *Biochem J.* **345(2):** 335-43.

Zannini, M., Avantaggiato, V., Biffali, E., Arnone, M. I., Sato, K., Pischetola, M., Taylor, B. A., Phillips, S. J., Simeone, A., Di Lauro, R. (1997). TTF-2, a new forkhead protein, shows a temporal expression in the developing thyroid which is consistent with a role in controlling the onset of differentiation. *EMBO J.* **16(11):** 3185-97.

Zannini, M., Avantaggiato, V., Biffali, E., Arnone, M. I., Sato, K., Pischetola, M., Taylor, B. A., Phillips, S. J., Simeone, A., Di Lauro, R. (2001). Corrigendum. TTF-2, a new forkhead protein, shows a temporal expression in the developing thyroid which is consistent with a role in controlling the onset of differentiation. *EMBO J.* **20(8):** 2108.

Zeng, Y., Rosborough, R. C., Li, Y., Gupta, A. R., Bennett, J. (1998). Temporal and spatial regulation of gene expression mediated by the promoter for the human tissue inhibitor of metalloproteinases-3 (TIMP-3)-encoding gene. *Dev Dyn.* **211(3):** 228-37.

Zeiger, S. F. (2006). FOXP3: of mice and men. *Annu Rev Immunol.* **24:** 209-26.